**UNIVERSITY OF
MODENA AND REGGIO EMILIA**

Ph.D. Course “Enzo Ferrari”
in Industrial and Environmental Engineering

Cycle: XXXVI

Exploring innovative uses of high temperature biochar to improve the environmental sustainability of agroindustrial frameworks.

Ph.D. Candidate: Eng. Filippo Ottani

Tutor: Prof. Eng. Giulio Allesina

Co-Tutor: Dr. Eng. Simone Pedrazzi

Coordinator of the Ph.D. Course: Prof. Eng. Alberto Muscio

Biochar through ESEM, magnified 1200x

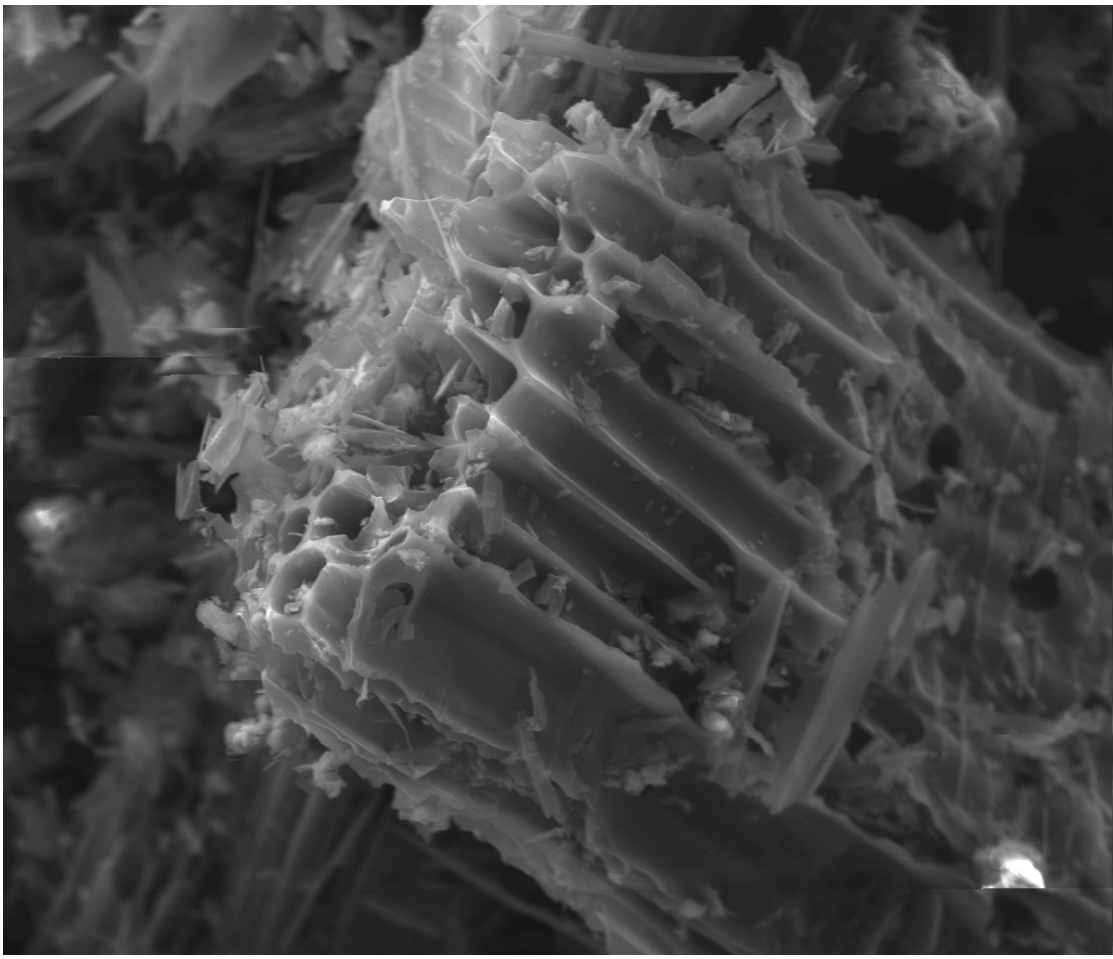

Alla mia famiglia.

Quella
che c'è sempre stata
che c'è
e che ci sarà

TABLE OF CONTENT

1 Overture

This thesis has a highly experimental character.

Before getting to the experimental side of the thesis, however, some theoretical backgrounds are developed. Understanding the role of biochar in climate change mitigation, guides the entire discussion. By fusing small and preliminary parts of theory and longer and more detailed parts of experimental results, the thesis wants to provide additional elements to elucidate the potential of biochar in mitigating climate change and promoting sustainability.

With growing concerns about climate change, the exploration of innovative solutions has become essential to mitigate its negative effects. Among these solutions, biochar stands out as a promising technology in the field of carbon capture and, consequently, in climate change fight. This thesis places biochar at its core, focusing on its carbon storage capacity, on the use of gasification as a carbon-negative technology, and on the biochar implications for advancing global sustainability. Biochar derived from the gasification or slow pyrolysis of biomass offers a pathway towards carbon storage by capturing carbon and sequestering it when it is buried into the soil. Biochar contributes to subtract the carbon dioxide (CO_2) since the carbon in it was atmospheric CO_2 that, during the process of sub-stoichiometric thermal conversion, are not reconverted into carbon dioxide, unlike combustion processes.

Leading this exploration is the urgent need to address climate change through scientifically informed efforts. The global nature of the challenge requires a comprehensive understanding of its causes and potential solutions. "Philosophical" pillars of this thesis are the concepts of sustainability and reducing human pressure on the environment. The goal of higher environmental sustainability must necessarily consider the social/technological context and the boundary conditions, whether local or global. For this reason, no innovations are proposed in this paper that are difficult to apply in real cases. Therefore, this thesis pursues both 1) to investigate the potential of biochar as a sustainable solution in mitigation of the climate change and 2) to investigate if the applications of it in agro-industrial scenarios are "sustainable" from economic, technological, executive, and practical perspectives. Furthermore, as it is crucial to ground the conclusions of the research to scientific and experimental investigations (empirical evidence rather than mathematical models) and to avoid drawing conclusions merely from initial impressions or perceptions, many experimental campaigns have been conducted and will be presented here.

Therefore, recognizing climate change as an urgent global problem that requires attention, the **Chapter 1** of this thesis is intended to be an exploration of the scientific basis of global warming and its consequences. Motivated by the

need for an accurate starting point, the chapter summaries the physics of global warming allowing for a better comprehension of its effects on planet Earth. The Chapter 1 might appear simple and "concise": this is intentional.

The fight against global warming is the primary driver behind research on biochar, which promises to elevate its relevance beyond academia. This thesis is driven by the necessity of combating climate change, validating the importance of biochar research and its practical implications.

Concluding, this chapter speak of **rise in the Earth's average temperature** (the most perceptible consequence of climate change to humans) and the **main quantifiable impacts**. Readers please feel free to ignore the chapter 1 and proceed to read the following.

The **Chapter 2** delves into the historical, technical, and practical aspects of biochar. From its origins as *mere byproduct of gasification* processes to its emergence as a *leading carbon sequestration technique*, biochar offers multifaceted benefits across environmental, agricultural, and industrial domains.

Chapter 2 goes into an accurate description of biochar: the "well-known" characteristics; the unstudied proprieties; the improvements that biochar brings to biological systems and their motivations. It then goes into detail about the concept of carbon storage and explains why biochar falls under carbon subtraction and storage techniques. Beyond its role in carbon storage, biochar holds promise in renewable energy co-production, in the exploitation of residual biomass and the renovation of marginal lands, in the creation of innovative porous building materials, as solution for GHGs mitigation in farms or in waste treatment processes, etc.

Summarizing the chapter here would be complex and reductive; it is left to the reader to choose the paragraphs most interesting to him or her from the Table of Content.

Thanks to the intrinsic properties of high-quality biochar and integrating scientific insights into everyday practices, biochar truly represents a practical solution to address the complexities of fighting climate change. **Chapter 3** goes into detail about the scientific works on the biochar developed during the doctoral years: the results obtained, the deductions, the still open questions, and the possible future developments. Chapter 3 is, in fact, the chapter of findings. The most significant research that has led to concrete and consistent results has been included here. The sections range from the investigation on the thermal-physical properties of biochar (water retention, specific heat, electrical conductivity, …), passing through the emissions reduction effect in biological systems, coming up to present an innovative use for improving the energy efficiency of low-enthalpy geothermal systems. Various experimental campaign carried out in external facilities or in laboratory are presented. As the reader will certify, all research shares a specific focus: enhancing sustainability.

The next few paragraphs are intended to give the reader a quick overview of the research in this thesis.

Section 8 – Introducing and exploring the "high temperature biochar"

This research investigates biochars produced at relatively high temperatures through slow pyrolysis, produced via a laboratory apparatus. Using a screw-type pyrolizer, this research aims to examine chemical composition and electrical conductivity of four different biochars, focusing on the (eventually) enhanced conversion and reorganization of the biomass structure in graphitic-like carbon structure. The biochars, produced under different conditions, exhibit varied properties. T30, biochar sample produced at 589 °C for a 30-minute residence time, demonstrates exceptional electrical conductivity values, despite not exhibiting the highest carbon content compared to the other samples. Conversely, T15 (517 °C for 15-minute residence time) behaves as a dielectric material due to reduced biomass conversion. T30EC (487 °C for 30-min) in which pyrolysis gases flowed "co-current" through the biomass, displays lower carbon content and low electrical conductivity. T30CC (481 °C for 30-min) in which pyrolysis gases flowed "countercurrent" through the biomass exhibits slightly higher conductivity.

Results highlight a threshold around 600°C for molecular structure reorganization and confirms that the C content is not sufficient to understand the electrical conductivity of a biochar sample (consequently, the C content alone is not an index of the quality of the biochar).

The study underscores the complex interplay between pyrolysis parameters and biochar properties, essential for optimizing the production processes for obtaining a high-quality biochar.

a)

b)

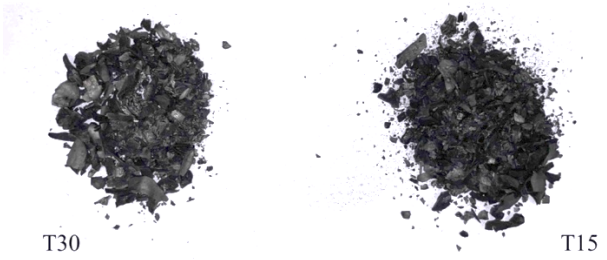

c)

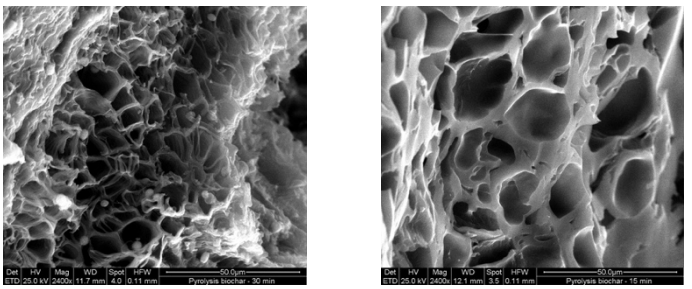

d)

Figure 1-1. a) the screw-type pyrolizer used to produce biochars. Thermal energy is supplied by a LPG-fueled Bunsen burner; b) experimental set-up for the temperature recording and measure of the extracted pyrolysis gases (when it is necessary); c) comparison between T30 and T15 as-it-is biochar, after extraction from the pyrolizer; d) comparison between T30 (on the right) and T15 (on the left) biochar by scanning electron microscope (SEM) images, the difference of the porosity level can be seen.

Section 9 – Water retention capacity of biochar-aided-soil

This section explores the impact of biochar on soil water retention, crucial for agricultural productivity and/or other innovative application. Investigating various biochar types, the study employs a controlled cultivation of Cannabis Sativa in an indoor greenhouse, during a six-weeks experimental campaign in which moisture level of the soil was periodically measured. Three blends of biochar and substrate, along with a control (coconut fiber and perlite substrate), are tested for understanding the water retention capabilities. The gasification biochar tested derived both from pine woodchips and wood pellets.

The experiments span two tests: one measuring moisture during plant growth and another assessing soil water content in empty pots with focus on the roots water retention.

The final value of SWC are: 33.9 % for 10% wood-chips biochar; 25.9 % for 5% wood pellets biochar; 26 % for 5% wood-chips biochar; 22.1 % for standard substrate. These results underline how the addition of biochar effectively change the soil physical characteristics. The highest water retention capacity is reached by the 10% wood-chips biochar blend.

a)

b)

c)

Figure 1-2. a) coconut+perlite standard soil; b) ferti-irrigation system and pots with "grated" walls; c) a plant on the day1 of the experimental campaign.

Section 10 – Biochar thermo-physical proprieties investigation

The research explores improving heat transfer efficiency in geothermal systems by focusing on the backfill material (BM) used to bury Horizontal Shallow Ground Heat Exchangers. Traditional BMs, like bentonite, sand or the same excavation material, impact heat transfer based on their properties. Novelty is the use of biochar as a BM, due to its high water retention and porosity, for improving soil thermal proprieties and moisture retention. Research studies thermal conductivity, specific heat, and the enhanced capillary rise capacity of water. Experimental tests were performed on soil, on biochar, and on various matrices composed by their combination, to quantify the improvements, especially under different moisture conditions.

Results show that while biochar inclusion may not drastically alter thermal conductivity under dry conditions, when biochar is wet the impacts really change.

Soil aided with 10% of biochar w/w passes from 1132.24×10^{-3} W (m K)$^{-1}$ at 30% w/w of humidity, to 1867.93×10^{-3} W (m K)$^{-1}$ at 36 % w/w of humidity: an increase of 64% with a rise on of 6% of humidity. The measured specific heat is 930 J kg^{-1} °C^{-1} for soil and 1310 J kg^{-1} °C^{-1} for biochar. Specific heat calculations suggest biochar inclusion may elevate the mixture specific heat, especially in high-moisture scenarios.

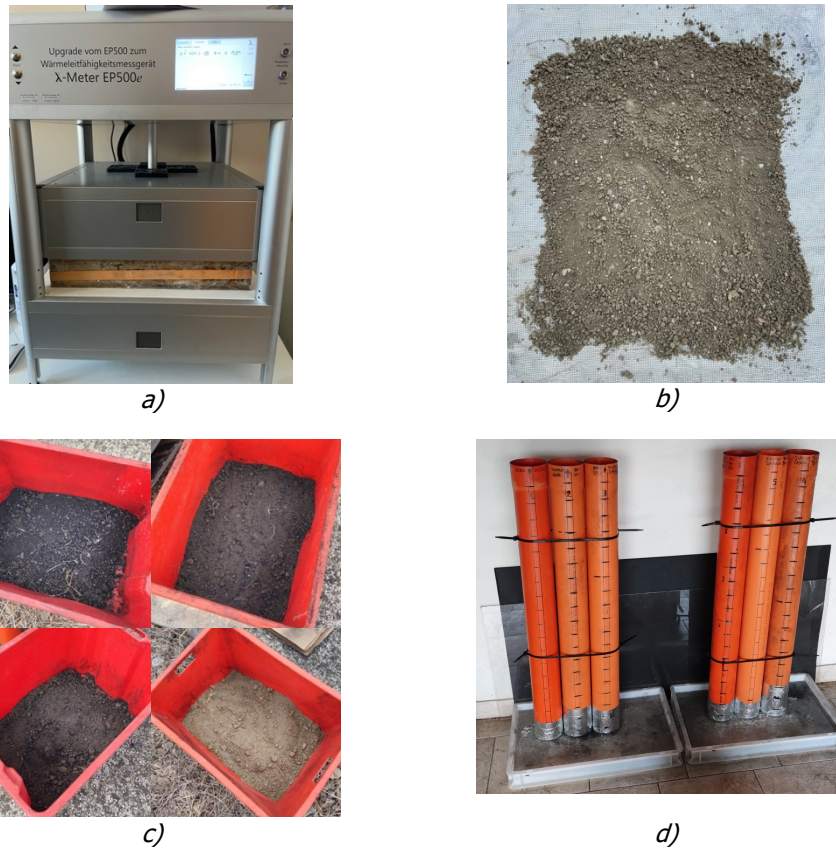

Figure 1-3. a) the hot plate apparatus (for measuring the thermal conductivity) during a test; b) pretreatment of soil part of the tested mixtures; c) some "soil + biochar" mixtures tested during the experimental campaign; c) experimental system for measuring water capillarity rising potential.

Further experiments demonstrate that biochar-containing mixtures exhibit superior water capillary rise potential compared to controls, also maintaining higher moisture levels in the long term. In the samples containing biochar, the minimum moisture level recorded at a height of 0.25 m over water level is 43.5%, significantly higher than the 6.5% measured in the control group. Even in the long term, mixtures with biochar maintained high moisture content,

ranging from 36% to 57%, compared to the control's 8% (at heights near 0.5 m over the free surface of the water).

In addition, biochar allows geothermal energy to be even more sustainable, since leads to the storage of up to 0.7 tons of CO_2eq m^{-2} of geothermal field.

Section 11 – Electrical conductivity of gasification biochar

The research in this Section studies the electrical conductivity (EC) of biochar, crucial for its interaction with soil microorganisms. The compression method for measuring the conductivity of carbon powders is used and the limitations are examined. Findings reveal significant variations in conductivity measurements, up to 85%, attributable mainly to the measurement mechanism and different testing conditions. Grinding or sifting alters conductivity by 41% and 85%, respectively, highlighting morphology's impact. Additionally, the composition of biochar affects conductivity: higher ash content corresponds to lower EC values.

Conductivity increases with pressure and carbon content, reaching 97.79 S m^{-1} @25 bar. However, biochar grinding disrupts this trend, affecting conductivity strongly and lowering the EC values even up to 43.04 S m^{-1} @25 bar.

The compression method's limitations emphasize the need for a methodology aligning with soil (or electric/electronic) applications. Further research are necessary to redefine EC measurement to accurately reflect biochar-microorganism interactions, challenging existing testing standard.

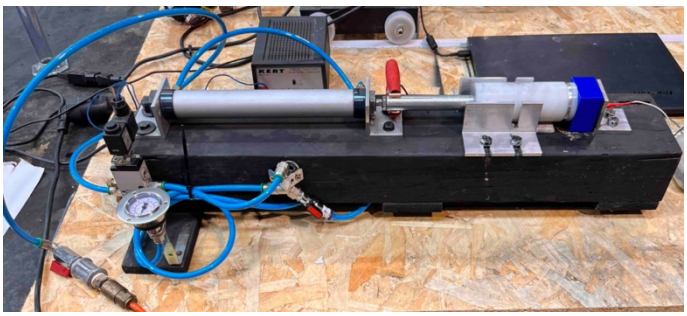

a)

c)

Figure 1-4. a) the apparatus used for measuring the EC under compression; b) two of the samples tested: on the right the biochar as-it-is after the gasification process, on the left the same biochar after grinding treatment.

Section 12 – Gasification biochar in organic waste composting

The effects of gasification biochar on the thermal behavior and on the greenhouse gas emissions during a composting process of organic fraction of municipal waste composting are investigated. A long experimental campaign, on nine compost bins is carried out: six bins are aided with two different biochar granulometries at 3% w/w (theses); other three bins are dedicated to a standard composting process, without biochar (control).

From the thermal point of view, biochar addition brings to a 4°C temperature increase and improves the stability of the process, compared to controls. The addition of fine biochar increases thermal energy production by 0.5 MJ kg^{-1}, while coarse biochar increases it by 0.4 MJ kg^{-1}. The standard composting process yields 2.5 MJ kg^{-1}. These findings suggest potential reductions both in composting time and in process-related issues (aeration, stability, quality of the final product, …)

a) b) c)

d)

e)

Figure 1-5. a) Facility in which the experimental campaign was carried out; b) compost bins used for the tests, before the filling operation, ; c) organic mix used during the composting process; d) aeration control and temperatures recording system (before the test); e) system for measuring the emissions.

From the emission point of view, results show a reduction of emitted greenhouse gases, in terms of equivalent carbon dioxide (CO_2eq), by 36% and 45% respectively for fine and coarse biochars aided processes, compared to the process without biochar. While CH_4 and N_2O emissions decrease, NH_3 emissions are not significantly reduced. Overall, both biochar types improve bio-oxidative processes and can reduce emissions, however the low biochar-to-organic waste application rate. These findings underscore the potential of biochar in mitigating greenhouse gas emissions in composting processes.

Section 13 – Feasibility of biochar application in composting facilities

This feasibility study delves into the technological, economic, and environmental aspects of integrating biochar into a municipal composting facility, exploring both commercial biochar purchase from the market and in situ biochar production through gasification. Different scenarios are examined, varying the gasification size and the subsequent biochar supplement rates.

Economic analysis reveals that, in general, self-production of biochar through gasification is more feasible than purchasing biochar. The 1.7 MW gasifier proves most cost-effective, but it requires a very high initial investment.

From technological point of view the integration of biochar is simple as it does not require new practices or complex procedures.

Furthermore, the study quantifies carbon dioxide equivalent storage and methane emission reductions (in term of CO_2eq), highlighting the environmental benefits of biochar utilization in composting industrial processes.

Integrating biochar into composting operations offers a promising avenue for waste management optimization, blending economic viability with environmental sustainability, and transform the composting facilities into pioneers of the circular economy.

Section 14 – Application of high temperature biochar to swine slurry for the emission abatement

This experimental research explores the reduction of greenhouse gases and ammonia emission from swine slurry storage through gasification biochar application. The efficacy of biochar and the most effective methodology for biochar application are investigated through an experimental campaign of several months. To do this, three methodologies were tested: a floating biochar layer on swine surface, a filter with biochar cartridge, and a nitrifying-denitrifying system in which biochar was used as substrate for micro-organism. The storages were simulated with 1000l tanks. Twelve replicas were realized: three for each methodology and three as control. Emissions were monitored over winter, spring, and summer seasons.

Results identify biochar as effective in reducing emissions: when used as a substrate for microbial colonies biochar can significantly reduce methane and nitrous oxide, when it is applied on the surface, biochar can significantly reduce ammonia emission. Biochar, traditionally used as soil improver, exhibits enhanced agronomic characteristics after the contact with slurry. Chemical analysis confirms biochar's potential as a nutrient-rich soil amendment.

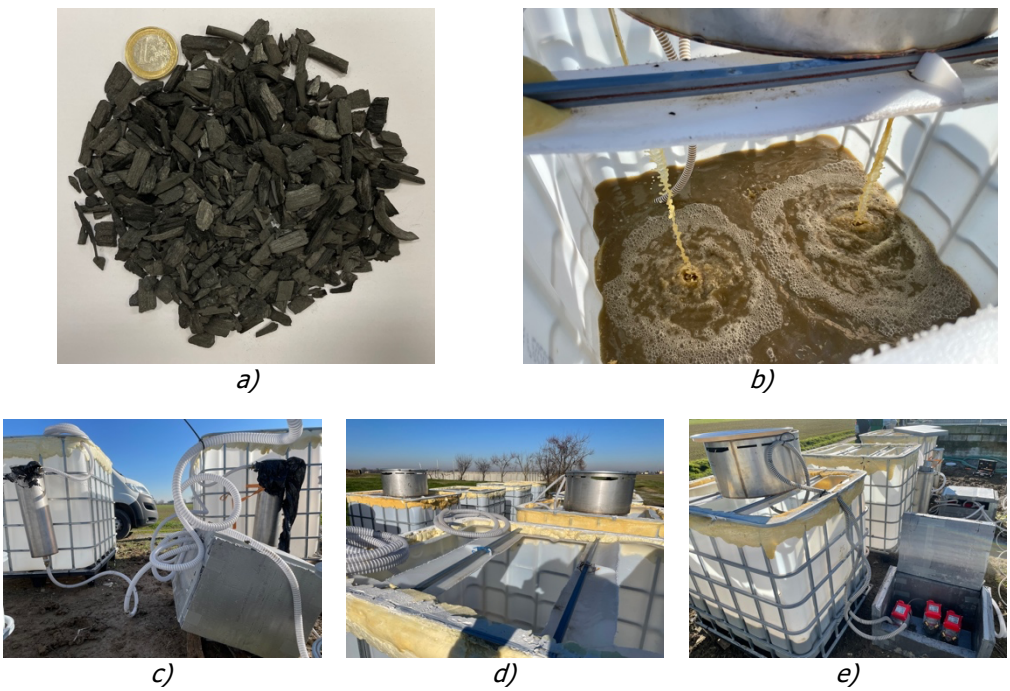

Figure 1-6. a) biochar used in the experimental setup; b) swine slurry recirculation during an initial test of the experimental setup; c) biochar filters; d) a "control" storage in the foreground and a general view of the field in which the experiment was carried out; e) nitrifying-denitrifying system and some pumps for swine recirculation.

Section 15 – Pyroweeding as sustainable alternative to weeds treatment

Weed control is essential for managing green spaces and agricultural crops. People still rely to herbicides, for efficacy, cost-effectiveness and speed but they are not environmentally sustainable, and to mechanical methods, which are more sustainable but less efficient.

In this scenario, thermal weeding promises to be a sustainable alternative. In this research, a prototype of thermal weeding system fueled by syngas, a gas from biomass gasification, is presented with the goal of reducing costs and improving environmental sustainability. The biochar produced through gasification, during the weeding treatment, can be re-used to improve soil quality. Thanks to the biochar, the gasification-based flame weeding machines emerges as a carbon-negative solution. In a prototype test conducted on vineyards and pomegranate fields, gasification-based pyroweeding demonstrated its effectiveness on weeds, without causing damage to crops.

a) *b)* *c)* *d)*

Figure 1-7. a) the pyroweeding prototype tractor-mounted; pyroweeding flare positioned toward the field to be treated; c) "premixed-air combustion mode" that bring the flame inside the flare during an initial test; d) "diffusive-flame combustion mode" with outer flame during a treatment in the vineyard.

From the environmental point of view, pyroweeding emits four times less CO_2 than the chemical methods. Moreover, biochar can offset the emissions of the weeding treatment. An LCA analysis showed that greenhouse gases emissions can be reduced by about 25%, potentially making pyroweeding a carbon-neutral and even a negative-technology, when biochar yield (kg biochar/kg biomass) respectively reaches or exceeds the 20%.

Introduction

1st chapter

2 Scientific exploration of the urgency of global warming.

2.1 Physical principles of greenhouse effect.

The sun is the only external energy contributor to planet Earth, transmitting radiation mostly in the visible spectrum. The second source of energy is geothermal energy from the Earth's core which is about 10 000 times less than solar energy.

A black body is ideal body that absorbs all incident electromagnetic radiation, regardless of frequency and angle of incidence, re-emitting it at all frequencies. Considering a point source of energy, the following quantities can be defined:

- energy emitted by the source Q [J]
- radiant flux $\phi = dQ/dt$ [W]
- solid angle ω [sr^{-1}]
  defined as a portion of space bounded by infinite half-lines leaving from a point (vertex) and passing through the points of a closed curve plotted on a surface that does not contain the vertex. It is the equivalent in 3-dimensions of the planar angle.
- intensity $I = d\Phi /d\omega$ [W sr^{-1}]
- irradiance $E = d\Phi/dA$ [W m^{-2}]
- exitance $M = d\Phi/dA$ [W m^{-2}]
- radiance, that is the radiant flux per unit of solid angle per unit area in the direction of theta angle of incidence,
  $B = dE/(d\omega\, cos\theta)$ [W m^{-2} sr^{-1}].

All these quantities can be expressed as a function of wavelength λ.

Planck radiation law, Equation (2-1) explains how all bodies emit electromagnetic radiation according to their temperature. At higher temperatures, the total radiated energy increases, with the peak of radiation in the spectrum shifting to shorter wavelengths (higher frequencies).

$$B(\lambda, T) = \frac{c_1}{\lambda^5 \cdot \left(e^{\frac{c_2}{\lambda \cdot T}} - 1\right)} \qquad [W\, m^{-2}\, \mu m^{-1}] \qquad (2\text{-}1)$$

Considering the sun as a black body, it is possible to define the spectral density of energy emitted at thermal equilibrium at a given temperature T, when there is no net flux of matter or energy with surrounding elements. If the sun would have a temperature of about 26 °C (300 K) the radiation would be mainly infrared radiation, in the non-visible spectrum. As the temperature increases, the wavelength decreases, and the emitted radiation would be part of the visible

spectrum. At this point the sun would start to assume a bright red color and at the same time heat would also be perceived. With a further temperature increase, to around 6000 K, the sun would become bright yellow since the radiation wavelength would be shorter. This phenomenon is explained by *Wien's displacement law*, Eq. (2-2), which states that the peak of radiation is inversely proportional to temperature T, through the Wien's Constant: $b = 2.898 \cdot 10^3\ [\mu m \cdot K]$.

$$\lambda_{peak} = \frac{b}{T} \qquad [\mu m] \qquad (2\text{-}2)$$

The sun's emissive spectrum is very large and only a fraction of emitted spectrum is visible, as reported in Figure 2-1: shaded area represents all the emitted spectrum.

To define the energy transported by solar radiation, the Stefan-Boltzmann Law is used, Equation (2-3). For a black body, it is possible to link the radiated energy (*Black Body exitance*) to the temperature of the body using the Stefan-Boltzmann Constant: $\sigma = 5.67 \cdot 10^{-8}\ [W\ m^{-2}\ K^{-4}]$.

$$B(T) = \int_0^\infty B(\lambda, T)\, d\lambda = \sigma \cdot T^4 \qquad [W\ m^{-2}] \qquad (2\text{-}3)$$

Considering the sun as a black body with surface's temperature of $T_{sun} = 5777\ K$, using Eq. (2-4) is possible to calculate the radiant flux from the sun's external surface (starting from the definition of radiance as $B = dE/(d\omega\ cos\theta)$) emitted in all direction.

$$\Phi_{sun} = B \cdot d\omega\ cos\theta = \sigma \cdot T_{sun}^4 \cdot (4 \cdot \pi \cdot R_{sun}^2) \qquad [W] \qquad (2\text{-}4)$$

where $R_{sun} = 6.96 \cdot 10^8\ [m]$, the radiant flux is $\Phi_{sun} = 3.84 \cdot 10^{26}\ [W]$.

Similarly, if also the Earth is considered a black body irradiated by the sun, it possible to calculate the received energy at the *top of the Earth's atmosphere* (upper layer of the atmosphere, see next paragraph) following Eq. (2-5).

$$E_{received} = \frac{\Phi_{sun}}{4 \cdot \pi \cdot R_{sun-Earth}^2} \qquad [W\ m^{-2}] \qquad (2\text{-}5)$$

Since the flux irradiated by the sun impact the top of atmosphere at a certain distance from the point of emission, using the average distance between sun an Earth $R_{sun-Earth} = 1.50 \cdot 10^{11}\ [m]$, the irradiance per square meter is obtained: $E_{received} = \sim 1360\ [W\ m^{-2}]$. This is the power of solar irradiance per-unit-area that cross the spherical surface centered in the Sun and with a radius equal to

the sun-Earth distance. Since this distance is large, the solar rays are among parallels. Therefore, it is possible to approximate the Earth, when viewed from the Sun, as a circular disk that receives at each instant $\sim 1360\ W\ m^{-2}$. The area of the disk is $\pi \cdot R_{Earth}^2$, while the impacted area of the Earth (considered circular) is $4 \cdot \pi \cdot R_{Earth}^2$. Based on this observation, it's possible to calculate the average irradiance at the top of the atmosphere over the day and over the year, using Eq. (2-6): $E_{average} = \sim 340\ [W\ m^{-2}]$.

$$E_{average} = E_{received}\ \frac{\pi \cdot R_{Earth}^2}{4 \cdot \pi \cdot R_{Earth}^2} = \frac{E_{received}}{4} \qquad [W\ m^{-2}] \qquad (2\text{-}6)$$

Following the previous calculations and evaluating a solar rays reflection from the Earth surface of 31% ("albedo", see the next paragraph), the Earth surface temperature can be calculated, at the thermodynamic equilibrium and as a black body, through Eq. (2-7) - derived from Eq. (2-3).

$$T_{Earth} = \sqrt[4]{\frac{E_{average} \cdot (1 - 0.31)}{\sigma}} = 254\ K = -18\ °C \qquad [W\ m^{-2}] \qquad (2\text{-}7)$$

These calculations give an Earth surface temperature of $T_{Earth} = -18\ °C$. It is easy to understand that this result cannot be true since the *measured average surface temperature* of the Earth is $T = 15\ °C$.

The difference between the theoretical blackbody temperature and the real temperature is attributed to the Earth's atmosphere and the phenomenon known as **Greenhouse Effect**. This effect contributes positively to the maintenance of temperatures on Earth. It is clear, therefore, that the Greenhouse Effect was fundamental to the development of living species, and it has still a positive effect for life on Earth.

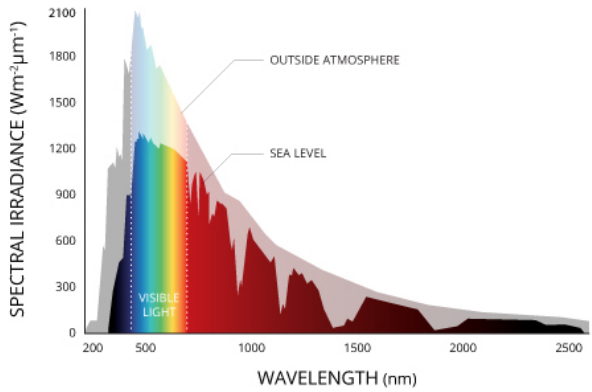

Figure 2-1. Spectrum of solar radiation. The colored-marked area is the solar radiation at sea level, the shaded area is the radiation reaching the top of the atmosphere and absorbed by the gases.

2.2 Contribution of the atmosphere of Greenhouse Effect.

To comprehend why the term "Greenhouse Effect" has become commonly associated with a negative connotation in recent decades, it is necessary to understand the interaction between the atmosphere and solar radiation.

The troposphere - the lowest layer of the Earth's atmosphere that extends from the Earth's surface to a height where the temperature is stable around -55 °C, up to about 120 km above ground level - is composed mainly of dry air, water vapor and other minor components and it plays a crucial role in absorbing and scattering solar radiation from the sun.

Dry air is composed mainly of nitrogen at 78.08%, oxygen at 20.95% and argon at 0.93%. The other part includes among others carbon dioxide CO_2 at 0.05%, hydrogen H_2 at 0.000055%, methane CH_4 at 0.00018%, and helium He at 0.00052% [1]. In addition to dry air, the troposphere contains water vapor and elements such as ozone (O_3), nitrous oxide (N_2O), suspended droplets of water, and fine and coarse particulate matter (PM2.5 and PM10). This composition is a key factor to understand the attenuation given by the troposphere. Two phenomena coexist: *continuous attenuation*, caused by atmospheric scattering of the sun's rays, and *selective attenuation*, due to the specific absorption of each component. As reported in Figure 2-1, at sea level the intensity of solar irradiance is lower than the intensity at the top of the atmosphere: the curve shows a decrease over the entire spectrum and some negative peaks are evident in the wavelengths corresponding to specific absorptions.

Assuming that, in general, (1) solar radiation reaching the Earth's atmosphere can be directly reflected, transmitted or absorbed and (2) at thermodynamic equilibrium the absorbed energy is totally re-emitted, it is necessary to analyze some consequences of these phenomena on planet Earth.

- The atmosphere in some intervals of the near-infrared spectrum is almost transparent. These intervals are called "*atmospheric windows*".
  As can be seen from Figure 2-1 in the near-infrared region, although it does not fall in the visible spectrum, a non-negligible fraction of energy (in the form of solar radiation) reaches the atmosphere. In general, in the infrared range (0.7 μm - 1000 μm) the atmosphere has low absorption capacity, also shown by the small attenuation of the colored area compared to the shaded area of Figure 2-1. Therefore, a substantial fraction of solar radiation reaches the Earth's surface (white area in Figure 2-2.a).
  Focusing on the *Thermal InfraRed* (TIR) region, range 0.75 μm - 15 μm, high atmospheric transmittance is measured, and up to 80% of the radiation hits the Earth's surface, Figure 2-2.b. This is called *TIR windows*.
  These *atmospheric windows* are related both to the elements that compose the atmosphere and to their concentration.
  The phenomenon of transparency of atmospheric windows occurs in both directions, inbound to Earth and outbound to the universe.
- A fraction of the incident solar energy $E_0(\lambda)$ at the top of atmosphere, accounting for 31%, is reflected directly, $E_R(\lambda)$. This phenomenon is called Earth albedo and is related to various components: water vapor, clouds, reflecting surfaces, snow and ice, water, and vegetation. As these components change, the albedo can vary.
- Considering that
  - transmittance is defined as the ratio of the impacting solar radiation $E_0(\lambda)$ and the transmitted radiation E_τ: $\tau(\lambda) = \frac{E_\tau(\lambda)}{E_0(\lambda)}$
  - transmittance affects the amount of absorbed radiation (for the same albedo, if transmittance is reduced, absorbance increases)
  - an arbitrary volume of atmosphere irradiated by the sun, following Stefan-Boltzmann's Law, Eq. (2-3), re-emits in function of its temperature, at different wavelengths. Moreover, in that according to Planck's Law (2-1) this volume emits more energy when the wavelength increases.

  it can be stated that the emissivity of the atmosphere air near the Earth's surface is greater than the emissivity at the top of atmosphere (since the temperature of the atmosphere near the ground is higher) and therefore the re-emitted radiations are in the frequency range of the TIR region. In addition, radiations are re-emitted in a distributed manner: the phenomenon from local (point radiation) being global (distributed radiation).

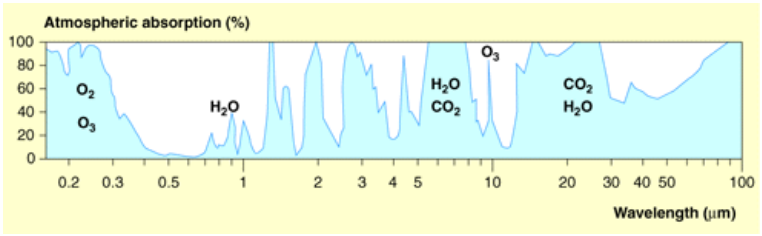

a)

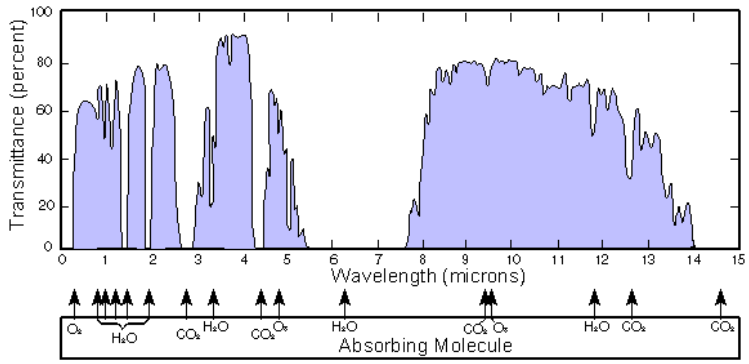

b)

Figure 2-2. a) Atmospheric adsorption of the solar radiation in 0 to 100μ m range. The compounds in black are the main responsible of the absorption phenomena - light-blue area [2]*. b) transmittance of the atmosphere of the near infrared radiation. In the frequency corresponding to the violet area the passage of radiation is close to 80% [*3].

The above phenomena describe the positive greenhouse effect and explain why the Earth's surface has an average temperature of 15°C.

Considering now the Earth's energy balance, a 31% of energy is reflected thanks to the Earth albedo, while remaining 69% is absorbed by the Earth and re-emitted to preserve thermodynamic equilibrium. The energy absorbed by the Earth's surface, at an average temperature of 15°C, is re-emitted through convective phenomena, e.g. evapotranspiration and "surface radiation", following the same mechanism of the atmosphere. For this reason and because Earth surface is relatively cold, the radiations are emitted with longer wavelengths than the radiations received. Earth, in fact, emits in the TIR region. Thanks to the TIR window (and other atmospheric windows) a fraction of this re-emitted radiation is transmitted directly into the atmosphere. The other fraction is instead absorbed and subsequently re-emitted both towards the atmosphere and towards the Earth's surface (the so-called "back radiation").

A key role in this *absorption* mechanism is played by the elements that constitute the atmosphere and that absorb radiations. The main absorbers are, in order of importance: H_20, CO_2, CH_4, O_3, N_2O and the Chlorofluorocarbons (CFCs). For example, water vapor and CO_2 absorb radiations in the range of wavelengths of 4 μm - 8 μm and 12 μm - 80 μm, while O_3 absorbs wavelengths

in 9 μm - 10 μm. As the percentage of these gases in the atmosphere changes, the atmospheric windows also change: if the concentration increases, the absorption capacity and energy stored by the molecules (in the form of heat) increases and the atmospheric windows frequency range shrinks. Direct consequences are the increase in back radiation and the increase in the Earth's surface temperature.

2.3 Greenhouse effect. Greenhouse gases and their impact.

The initially "positive" greenhouse effect, as the concentration of the above cited responsible gases increases in recent decades, has caused an increase in temperature, compared to last century, with strong impacts on the life of the planet and living species. These gases are called Greenhouse gases (GHGs).

Although the main actor in the greenhouse effect is water vapor, its concentration in the atmosphere remained almost constant over the years, and its permanence in the atmosphere is on the order of days. Therefore, the impact on the Earth's temperature increase is negligible.

CO_2, on the other hand, persists in atmosphere for up to 1000 years because of its high stability [1]. CO_2 has always been in balance with the Earth's ecosystem, as the main removal mechanisms are ocean-absorption and storage and biomass's chlorophyll photosynthesis. The emission of CO_2 into the atmosphere due to human activities (mainly related to the combustion of fossil fuels) and the inability of natural systems to absorb the massive amount of CO_2 emitted, has led to a significant concentration increase in recent centuries: in 1750 the concentration was 280 ppm, in October 2023 it is 418.82 ppm, Figure 2-3.a [4]. The increase in CO_2 concentration leads to an increase in back-radiation and increase in Earth's temperature.

Other increasingly important GHGs are methane and nitrous oxide.

CH_4 originates from industrial or transportation-related activities, but mostly comes from the agricultural sector (anaerobic fermentations or decompositions), livestock farming (enteric CH_4 emissions), and bad waste management (unwanted anaerobic decompositions). CH_4 in 1750 has a concentration of 770 ppb, in July 2023 of 1915.25 ppb [4].

N_2O comes mainly from the agricultural sector. Intensification of crop and livestock farming has led to increased use of nitrogen fertilizers and livestock manure with high nitrogen content. When there is not complete exploitation of the nitrogen content or if it overdosed, substantial emissions of N_2O occur. In 1750 the concentration was 270 ppb, in July 2023 it is 336.66 ppb. This increase is the least significant among the three GHGs, but with high impact (see below).

CFCs are not discussed in this thesis because awareness actions and programs to replace them with more sustainable gases and fluids have been active for several years.

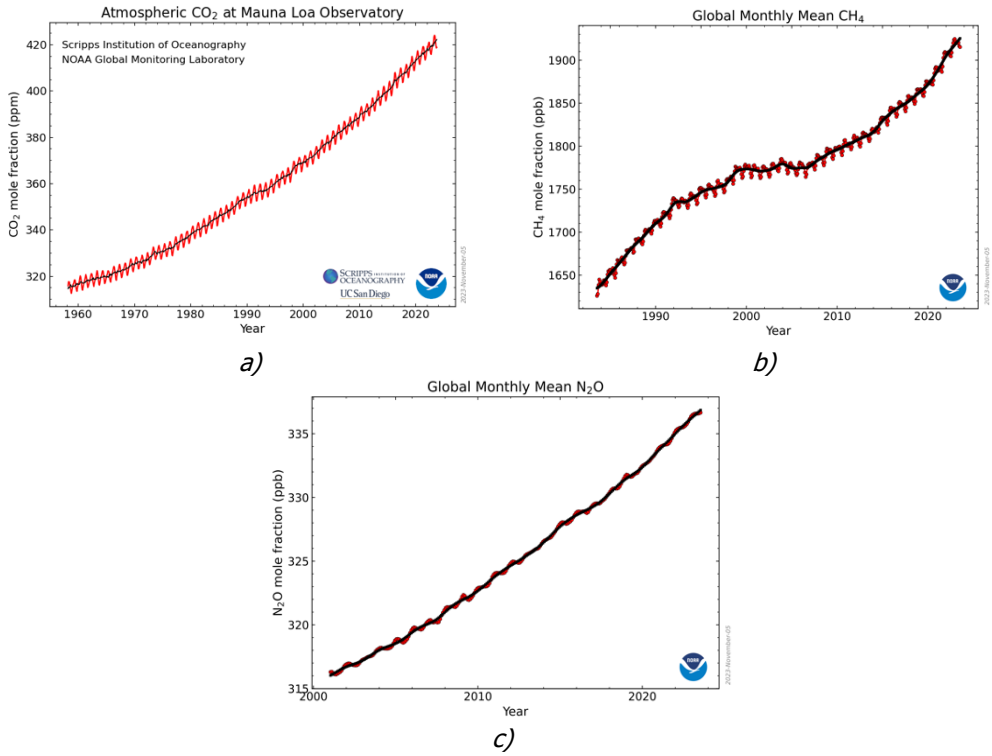

Figure 2-3. Increase in a) CO_2 , b) CH_4 and c) N_2 O concentrations in recent decades [5]*. The red lines are the experimental data, the black lines are the interpolation curves.*

The phenomenon of Earth's temperatures rising is called Global Warming. To compare the impact of different GHGs on Global Warming, a few conversion indices are issued periodically by the Intergovernmental Panel on Climate Change (IPCC). These indices are called **Global Warming Potential (GWP)** and are the result of research that quantifies the Radiative Forcing[1] both direct and indirect effects, over a given time horizon (e.g., 100 years), related to the emission of a unit mass of gas. CO_2 is considered as reference gas [6]. Direct effects consider the impact of the gas alone; indirect effects consider additional gases and particulate matter production or change in the formation of other gases caused by the initial gas. The most recent IPCC AR6 report publishes GWPs in Table 1.

[1] Radiative Forcing quantifies the influence an element has in changing the balance of incoming and outgoing energy in the Earth-atmosphere system. A high radiative forcing value for a compound indicates that it is responsible for letting out less energy than the energy that had previously entered. It is expressed in $W\,m^{-2}$ and refers to values in 1750 (preindustrial era) [403].

Table 1. GWP in IPCC AR6 [7].

	100 years time-period	**20 years time-period**
CH_4 - fossil origin	29.8	82.5
CH_4 - non-fossil origin	27.2	80.8
N_2O	273	273

The direct and indirect effects of global warming are now tangible in everyday life and touch areas that were hardly imaginable in the past. The term **climate change** to refer to the impacts and to the frame of evidence of the rising of Earth's temperatures, has come into common usage, moving out of purely scientific language.

In the AR6 report, the IPCC formalizes the increase in temperature over the past century and bluntly blames human activity for Global Warming:

> *Human activities, principally through emissions of greenhouse gases, have unequivocally caused global warming, with global surface temperature reaching 1.1°C above 1850-1900 in 2011-2020. Global greenhouse gas emissions have continued to increase, with unequal historical and ongoing contributions arising from unsustainable energy use, land use and land-use change, lifestyles and patterns of consumption and production across regions, between and within countries, and among individuals (high confidence)* [7].

2.4 Temperature increase

The United Nations IPCC is the most authoritative source on climate change, global warming and related impacts on planet Earth. Through the periodic publication of scientific reports (based on peer review) it raises awareness and provides fundamental data for the study of climate change.

For many years these reports presented future scenarios based on GHGs concentration. From the report *Sixth Assessment Report* (2021) [8] this type of scenario was superseded, and more complex scenarios of temperature evolution and related climate consequences were introduced, based both on environmental data and on policy and action choices: the "X-Y.y SPPs." The *Shared Socioeconomic Pathways* (SSP) are the backbone of these scenarios. Proposed by Nakicenovic et al. (2014) [9], they make climate change research multidisciplinary. They combine qualitative and narrative plots to describe the evolution of society, with quantifiable and geographically defined parameters of development [10]. IPCC reports considers five climate narratives correlated to five different situations of global warming, socioeconomic context (urbanization,

technological development, population growth, education, ...) and adaptive capacity. The SSPs are matched with some "carbon emission curves" called Representative Concentration Pathway (RCPs) creating a matrix of possible future scenarios. Previously, the scenarios were based only on the forecast of GHGs emission, now by considering the different SSPs it is possible to include socioeconomic and climate policies in the forecasts. Indeed, the intent of this matrix is to represent how current choices will strongly influence temperatures and climate in the next century, starting from what they have already modified in the past.

Table 2. Scenarios used in the IPCC Sixth Assessment Report. Adapted from O'Neill B. et al. (2014) [11].

Name	Classification	Description
SSP 1	Low for mitigation and adaptation	• Sustainable development with lower carbon energy sources. • Reducing social inequality. • Fast evolution toward environmentally friendly technologies.
SSP2	Moderate	• SSP intermediate between SSP1 and SSP2 • Continuity with historical data
SSP 3	High for mitigation and adaptation	• Moderate economic and population growth • High unmitigated emissions due to slow technological development in the energy sector. • Nationalisms policy. • Persistent social inequalities and vulnerability to climate change.
SSP 4	High for adaptation, low for mitigation	• High-emissive regions: excellent development of carbon neutral energy sources. High climate change mitigation. • Remaining regions: low technological development. High vulnerability and low resilience. • High global social inequality and economic nationalism.
SSP 5	High for mitigation, low for adaptation	• Absence of climate policies and high demand for energy produced mainly from fossil fuels.

		• Low development of energy technologies. Absence of mitigation solutions. • But rapid economic development. Consequent equitable distribution of resources. • Less vulnerable and more technologically resilient world.

SSP1 and SSP5 are the most optimistic scenarios for humans, with high societal development and high economic growth. While SSP1 is based on sustainable growth and increased efforts, SSP5 is based on progress driven by a growing economy and high fossil energy consumption. SSP3 and SSP4 are pessimistic pathways with no socioeconomic developments and high inequality. SSP2 is in continuity with the past reports: it uses historical data from the 20th century to create future projections.

A Representative Concentration Pathway (RCP) is a forecast curve of the concentration of GHGs in the atmosphere, not a forecast of emissions. Four different possible scenarios are presented and used in the IPCC Fifth Assessment Report (AR5): RCP2.6, RCP4.5, RCP6, and RCP8.5. The scenarios are based on the amount of GHGs emitted into the atmosphere and were labeled as a function Radiative Forcing reached to the year 2100 (respectively: $2.6;\ 4.5;\ 6\ e\ 8.5\ W\ m^{-2}$).

Table 3. Representative Concentration Pathway (RCP) from the Fifth Assessment reports of 2014. Adapted from Van Vuuren D. et Al. (2011) [12].

Name	Emission reduction	Goals
RCP2.6	CO_2 emission reduction already before 2020. No emissions by 2100. Reduction of 40% of CH_4 and 10% of sulfur dioxide, compared to 1990, by 2100. It requires the subtraction of environmental CO_2.	Maintain temperature rise below 2 °C by 2100.
RCP4.5	CO_2 emission reduction from 2045 to reach in 2100 the half of 2050 emission level. Stop CH_4 emissions in 2050 to reach in 2100 the 75% less emission than 2040 levels.	Limiting temperature rise to between 2 and 3 °C by 2100. Raising seas by 35% more than RCP2.6. This is identified among the most likely scenarios [13].

	It requires the subtraction of environmental CO_2.	
RCP6	Peak emissions in 2080. From 2100 need for implementation of GHGs abatement strategies.	Temperature rise within 4°C by 2100.
RCP8.5	Uncontrolled increase in emissions until 2100.	The temperature increase exceeds 4°C. RCP8.5 is unlikely since it overestimates the availability of fossil fuels.

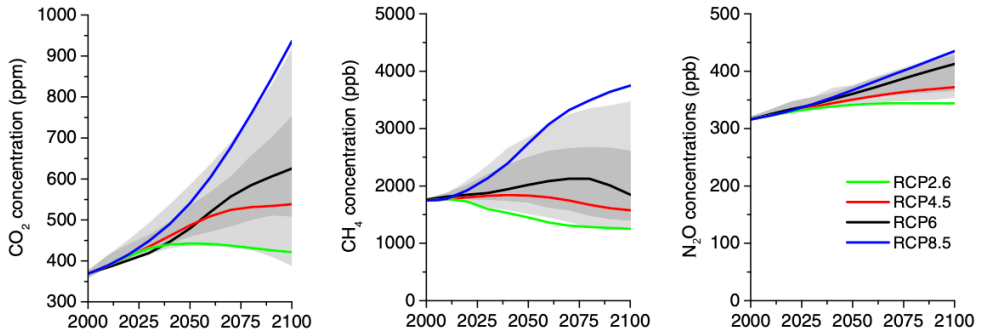

Figure 2-4. Evolution of the concentration of the main GHGs from 2000 to 2100 (forecast) used in the IPCC Fifth ASSESSment report [12].

With the Sixth Assessment Report, the IPCC combined SSPs and RCPs to create a matrix of scenarios, seeking to address the complexity of the future in a scientific and comprehensive way. The RCPs used try to be close to those presented in the previous report versions, with the addition of a scenario that keep the temperature increase below 1.5 °C by 2100, in according to the goals of the Paris agreements [14]. The PPSs used as backbones are those shown in Table 2.

Five are the final scenarios which the report focused on. Two optimistic scenarios: SSP1-1.9 and SSP1-2.6, both based on SSP1 and with Radiative Forcing at 2100 of, respectively, $1.9\ e\ 2.6\ W\ m^{-2}$; an intermediate scenario: SSP2-4.5; a pessimistic forecast without mitigation actions, SSP3-7.0; and an extreme scenario, SSP5-8.5, maintained to give continuity to RCP8.5.

Table 4. SPP X-Y.y scenarios proposed in the IPCC Sixth Assessment Report (2021) for presenting and forecasting the climate change until 2100. Name of actual scenarios are flanked by the name of concentration forecast models (RCPs) used in the past reports.

Name	Emission reduction	Goals
SSP1-1.9 **(no similar RCP)**	Net zero CO_2 emissions around 2050.	Temperature rise below 1.5°C in 2100 compared to 1850-1900 in 2100.
SSP1-2.6 **(~ RCP2.6)**	Achieving net zero CO_2 emissions from 2050 to 2100.	Temperature increase of maximum 2.0°C in 2100, relative to 1850-1900 level.
SSP2-4.5 **(~ RCP4.5 & RCP6)**	Scenario in line with the UN Agenda 2030. CO_2 emission rates are maintained unchanged to 2050.	Temperature increase between 2.7°C and 3.4°C by 2100. If more countries adopt 2050 net zero targets, a temperature around 2.7°C will be the most probable.
SSP3-7.0 **(~ RCP7)**	CO2 emissions in 2100 doubled, compared to 2021 level. High particulate matter and aerosol emissions are also included.	-
SSP5-8.5 **(~ RCP8.5)**	No climate policy. CO_2 emissions double by 2050. It is achieved only considering an evolution of society based totally on fossil fuels.	Higher temperatures than the old RCP8.5 (4 °C)

Figure 2-5.a, .b and .c reports the emissions trends of the major GHGs, according to different scenarios. Emissions are estimated on the scenarios and are not to be confused with concentrations or cumulative concentration of gases in the atmosphere. Projections of CO_2 concentrations in the five different scenarios are instead reported in Figure 2-5.d. These projections are obtained according to specific emulators and input data, please refer to *IPCC Technical Summary in Climate Change* 2021 [15] for details.

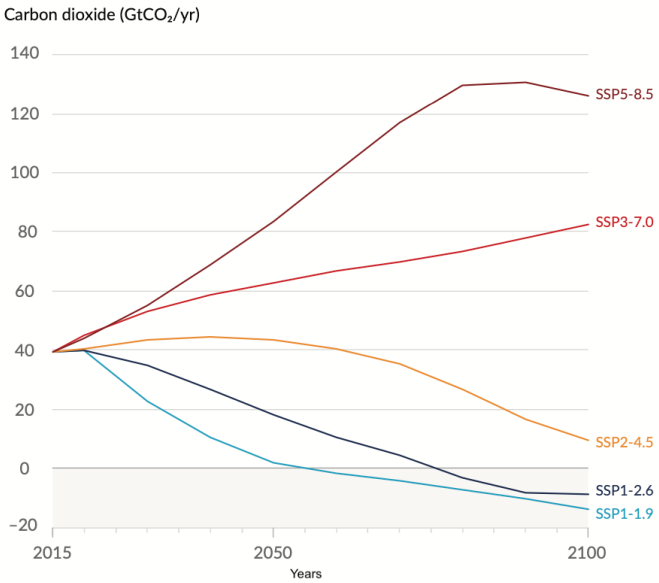

a) CO_2 trend forecasts of different scenarios

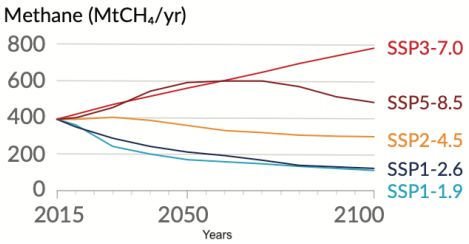

b) CH_4 trend forecasts of different scenarios.

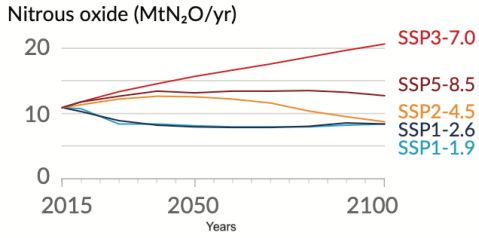

c) N_2O trend forecasts of different scenarios.

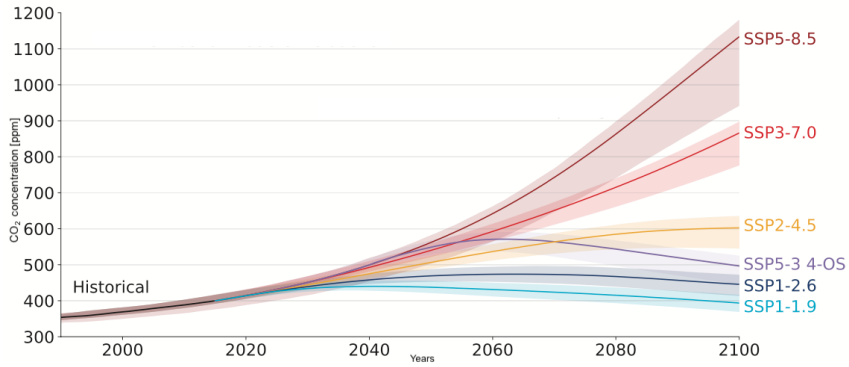

d) CO_2 concentration in atmosphere: historical data before 2020 and projection after 2020 based on SSP scenario. Shaded are are the tolerances of the model. Adapted from [15].
SSP5-3 4-OS is not considered in this discussion.

Figure 2-5. Forecast of the anthropogenic emissions (not concentration) of main GHGs for the five IPCC AR6 scenarios [10].

For each SPP X-Y.y scenario, the increase in the global average temperature of the Earth's surface is estimated, compared with the period 1850-1900. Temperatures are estimated in the short-term, 2021 to 2040; in the medium-term, 2040-2060; and in the long-term, with reference period 2081-2100, Table 5. The long-term time range is the one used to set targets in the largest number of environmental and climate change mitigation policies. Keeping the temperature below the 1.5°C increase is the goal of the Paris Agreements negotiated in the context of the XXI Conference of Parties (COP) and the basis for proposed policies in successive COPs. This goal has always been much discussed. It originates from proposals and policy spaces to which the scientific community has been forced to respond with its research, effectively entering into a science-policy compromise [16]. To this day it is considered by many to be unfeasible [17,18].

Table 5. Changes of the global temperature based on the IPCC scenario. Adapted from [15].

Scenario	**Most optimistic value**	**Most possible range**	**Most optimistic value**	**Most possible range**	**Most optimistic value**	**Most possible range**
	2021-2040		2041-2060		2081-2100	
SSP1-1.9	1.5	1.2-1.7	1.6	1.2-2.0	1.4	1.0-1.8
SSP1-2.6	1.5	1.2-1.8	1.7	1.3-2.2	1.8	1.3-2.4
SSP2-4.5	1.5	1.2-1.8	2.0	1.6-2.5	2.7	2.1-3.5
SSP3-7.0	1.5	1.2-1.8	2.1	1.7-2.6	3.6	2.8-4.6
SSP5-8.5	1.6	1.3-1.9	2.4	1.9-3.0	4.4	3.3-5.7

All data are in °C.

From Table 5 it is evident how the IPCC reports indicate, unless there are revolutions in climate policies and technologies, that the global temperature increase of 1.5°C will be reached around 2030. Thereafter, the temperature could then exceed this value in the following years, reaching 1.6°C by 2050 (also in the SSP1-1.9 scenario). Mitigation policy efforts are needed to be able to bring it back below 1.5°C before 2100 [19].

Climate data published by the U.S. National Oceanic and Atmospheric Administration (NOOA) reports that the rate of temperature increase since 1981 is 0.18°C per decade, reaching an increase of 1.06°C in 2022 compared to the period 1880-1900. 2023 reached an increase of 1.13°C [20]*. 2023 was the hottest year since temperatures have been recorded* [21]*.*

Measurements are in line with the IPCC forecast scenarios. The Figure 2-6 extracted from the *IPCC Sixth Assessment Report (2021)*, summarizes what is reported in this section (different scenarios and relative temperature increases) through a high-impact graphic mode: warming stripes. This type of graph, firstly proposed in 2018 by Prof. Ed Hawkins [22], indicate the temperature increase (related to the 1850-1900 period) using blue (little gap) and red (high gap) vertical lines. Warming stripes clearly explain the strong variation that occurred over the past 150 years.

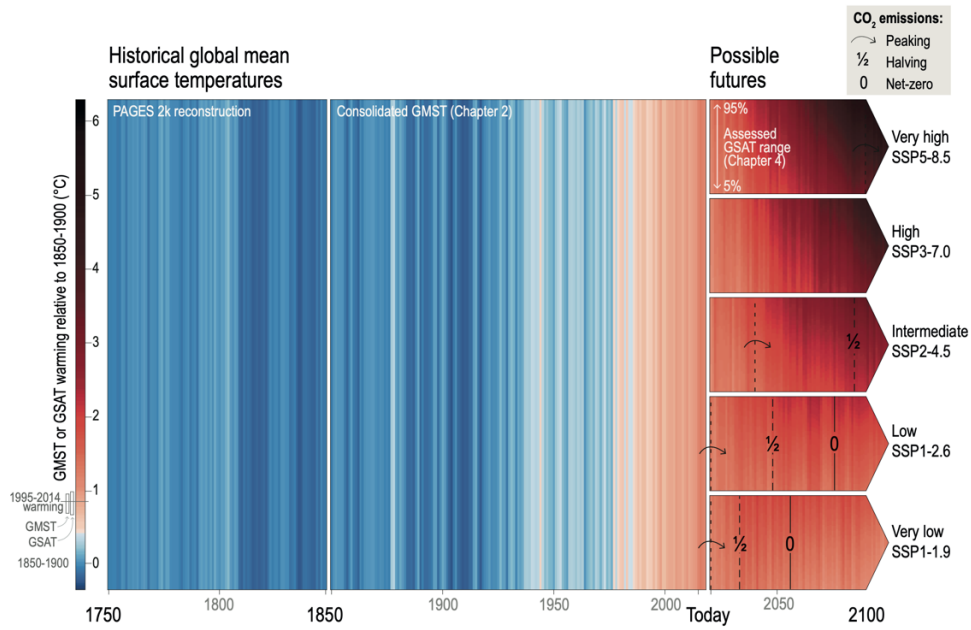

Figure 2-6. Global warming temperature represented through warming stripes. Temperature forecasts for the different scenarios are also reported in relation to the CO2 peak.

2.5 Impacts on planet Earth and its inhabitants.

This section aims to briefly outline the **effects**, in many cases already visible, **of global warming**. Climate change has a big impact on the life of humans and now more and more overwhelmingly influencing economies (national, regional, family, ...), choices (national, regional, personal, ..), migration and new human settlements, and the evolution of society.

The most remote impacts for the European continent and less perceptible to its habitants are certainly:

- the melting of arctic ice;
- the melting of mountain ice and snow;
- the reduction of snow-covered areas. Spring snow is often taken as seasonal reference;

- the temperature of the oceans. They have high thermal inertia and store up to 91% of the heat related to global warming. As temperature rises, the ability to dissolve CO_2 in water decreases and the ability to storage carbon is reduced;
- the rise of the sea level.

Significantly closer impacts to which society is gradually becoming more sensitive include:

- increased rainfall in some geographic areas (poles and equator for example) and reduced rainfall in area that historically are not subject to droughts (southern Europe for example);
- increase in extreme events such as thunderstorms and cloudbursts, hail, tornadoes, and "tropical" storms. Increased conditions for the formation of such phenomena in historically non-predisposed areas;
- drought. Resulting in a major reduction in crop yields and food availability;
- difficulty of water absorption by the soil, due to extreme events and soil aridity, and consequent hydrogeological damage
- increase in the Earth's global temperature;
- urban heat island phenomenon, which further increases the temperature in the cities.

In Italy, 122 extreme events were measured in the January-May 2023 period, compared to 52 in the same period in 2022: +134%. The most frequent extreme event is flooding from heavy rains, with 30 occurrences in the period 01-05/2023 compared to 16 events in 2022, +87%. The region most affected was Emilia-Romagna. Other types of extreme events considered in the statistics include river flooding, tornadoes, landslides from heavy rains, storm surges, hail damage, and tornado damage [23].

Globally, the IPCC report assumes strong environmental effects and significant human impacts. Some of these impacts are depicted in the synoptic diagram, Figure 2-7.

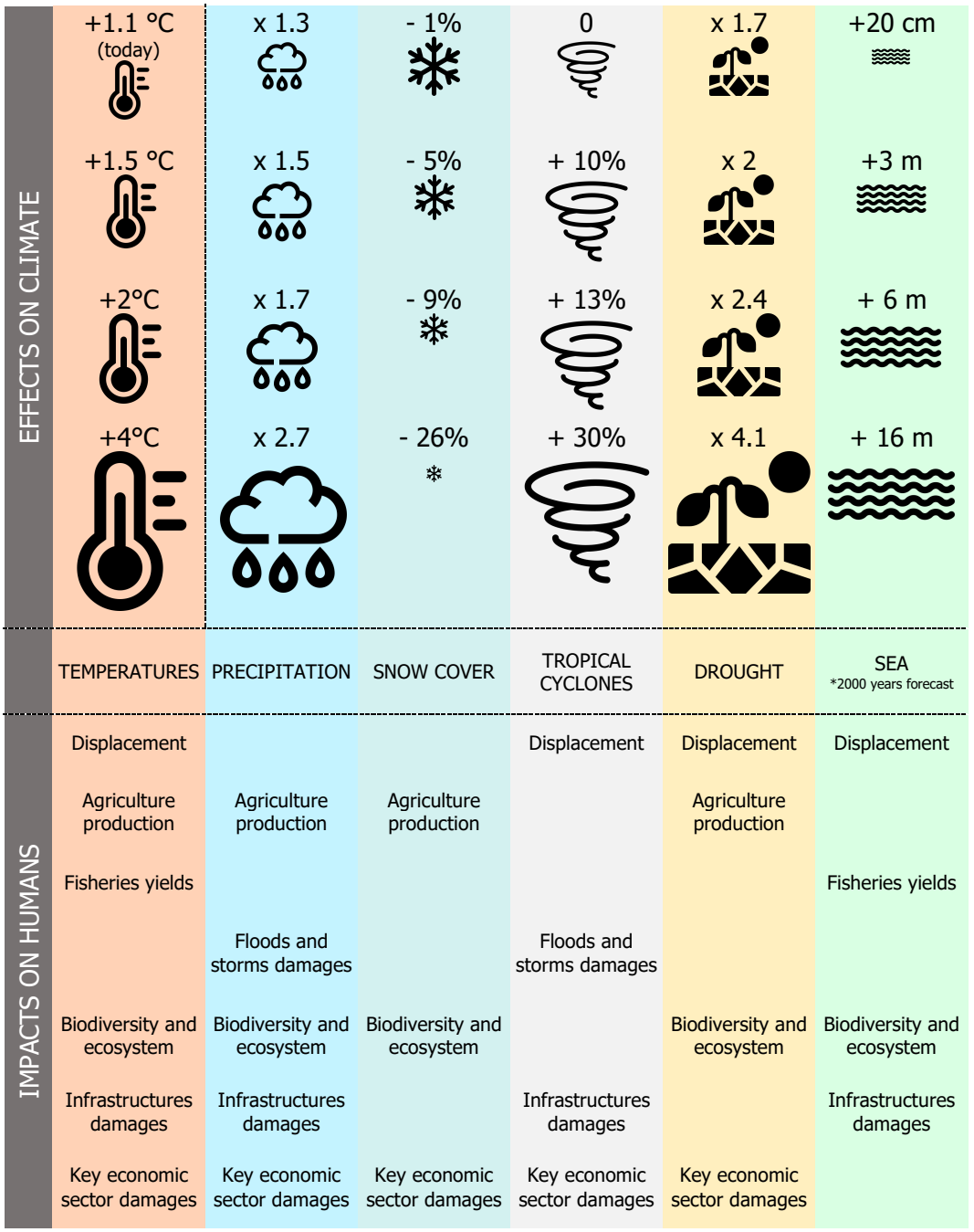

Figure 2-7. Synoptic diagram of effects and impacts of climate change. The orange column shows the increase in temperature, which is used in this diagram as an identifier of the different possible scenarios. Though, temperature is also an effect itself, an effect of the increase in GHGs concentration. At the bottom of the diagram are the impacts that the different effects have (and increasingly will have) on human life [24].
All data are average values and are referred to the 1850-1900 mean value.

3 Take Action

3.1 United Nations 2030 Agenda

The United Nations (UN) 2030 Agenda, approved on September 25, 2015, and signed by 193 countries of the United Nations, is already considered a milestone in the history of global efforts to address the most preeminent challenges threatening planet Earth. The goals of the 2030 Agenda are general and ambitious and embrace a variety of issues. The Agenda was created to bring together the efforts of signatory countries, for the first time united in a universal political and social action, in a work that starts from the present and aims to give a better future to Planet Earth and its 8.75 billion inhabitants [25]. In an interconnected world, where the actions of each nation can have consequences on a global scale, the need for a collective and shared approach had never been more evident; this reason encouraged the UNs to write a shared agreement.

In Agenda 2030, the proposed 17 Sustainable Development Goals (SDGs) interpret this vision, serving as a guide for building a more equitable, sustainable and inclusive future by 2030. The Goals are then broken down into 169 Targets, representing a "compass" to direct toward sustainability everyday choices. The core concepts of the Agenda are [26]:

- people: end poverty and hunger; ensure dignity, equality, and a healthy environment for all;
- planet: protecting the planet through sustainable practices, addressing climate change for future generations;
- prosperity: harmonize progress with nature, ensuring meaningful and enjoyable lives for everyone;
- peace: promoting inclusive, fair, and inclusive societies, free from violence. Recognizing the double connection of sustainable world and peace;
- partnership: mobilize global efforts for sustainable development, emphasizing solidarity and addressing the needs of the most vulnerable people.

An integrated action across goals will transform the world positively.

Although it may seem that the SDGs are primarily geared toward policymakers, social-decision stakeholders and justice actors, the reality is that the Agenda touches many aspects of everyday life and professional contexts, calling for a noticeable change in approach from all people. The link between the SDGs and engineering research is close and critical for achieving the goals.

The SDGs touch a lot of areas: include both ending poverty and hunger (Goals 1 and 2) and combating energy poverty (Goal 7), promoting peaceful and just communities (Goal 16) and building an inclusive and sustainable industry

(Goal 9), protecting the planet, aquatic and terrestrial species (Goals 13, 14 and 15) and promoting technological innovation to make cities resilient and resource efficient (Goal 11 and Goal 8) [27]. Technological innovations and engineering solutions are therefore necessary to achieve all the Goals, and engineering research plays a crucial role in providing the answers to many of these global challenges.

The paradigm shifts for an "engineering brain" is fundamental, and letting social issues permeate scientific works must be considered a mission. Innovation toward sustainable technologies, energy efficiency, the "from cradle to grave" product design of the circular economy concept, smart management of agricultural and water resources, and the study of smart infrastructure in the cities of the future, are just some of the areas where engineering research can make tangible contributions.

The connection between scientific progress, engineering, and the social goals of the 2030 Agenda translates into the need to innovate using clean technologies able to reduce the environmental impact of human actions, solutions that can reduce pollution, promoting sustainable production models for preserving natural resources, and ensuring that innovations are really feasible and sustainable.

3.1.1 Insight into the Sustainable Development Goals

This section will discuss some of the goals of the 2030 Agenda that are ambitious from an engineering perspective and closely related to the research presented later during this thesis. These Goals are not simply abstract objectives; they are the bases on which the collective directions of the global scientific community should stand. The following paragraphs will set out some premises and some targets to be transformed into concrete actions.

3.1.2 Goal 2: Zero Hunger

By 2030, some 600 million people are expected will suffer from hunger. Today 1/3 of the world's people fight with food insecurity and severe malnutrition problems, especially among children. Central to this goal is doubling both the agricultural productivity and the revenue of small-scale producers (Target 2.3). The target then extends to sustainability of production systems and implementation of agricultural practices to increase soil quality to improve both crop production and productivity. Some innovative methodologies must strengthen the ability of crops to adapt to climate change and extreme weather events (Target 2.4).

3.1.3 Goal 7: Affordable and Clean Energy

Energy emerges as both a challenge and an opportunity in the near future, since it is crucial in all everyday areas. Its role turns out to be fundamental to

global progress and a key-factor in the fight against climate change. To date, still one over five people are without modern electrical system and three billion people depend on traditional sources. Energy production impacts 60% of total GHGs emissions, underlining the urgency of the transition to energy renewable sources.

Agenda 2030 aims to ensure access to modern and sustainable energy services (Target 7.1), to significantly increase the share of energy from renewable sources (Target 7.2), and to double the energy efficiency of systems and infrastructure (Target 7.3) by 2030, for ensuring a resilient and sustainable energy future.

3.1.4 Goal 12: Responsible Production and Consumption

Statistics regarding food waste and global consumption of primary goods, bring to attention the current unsustainability of resource management. Every year

- about one-third of food produced globally becomes waste due to consumer waste and the production-transportation chain [28];
- the agri-food sector accounts for 30% of total energy consumption and 31 % of GHGs [29];
- energy demand will continue to grow by about 24% by 2030, compared to 2020 [30];
- by 2022 residential consumption accounts for 29% of global energy, and contributes for 21% to the CO_2 emissions;
- production from renewable energy (in 2021) was 22% of the total, as shown in Figure 3-1.

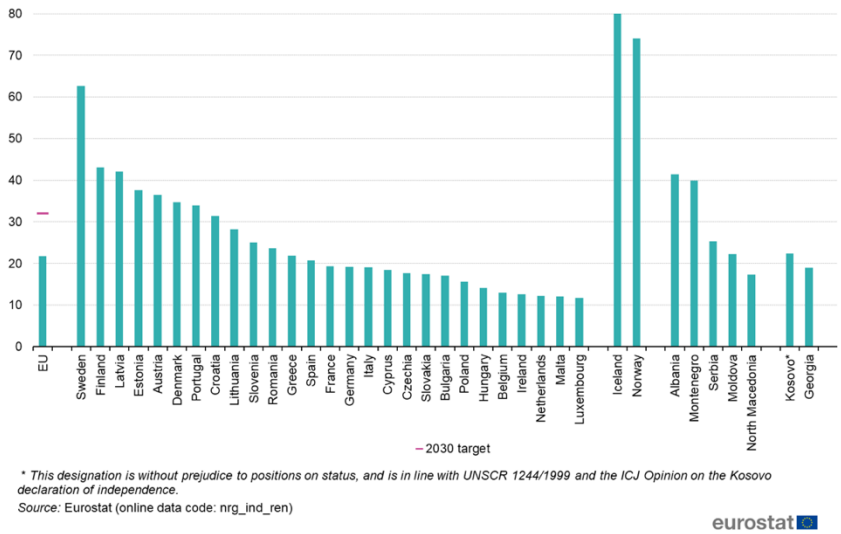

Figure 3-1. Share of energy from renewable sources in 2021 - % of gross final energy consumption [31].

Due to intensive exploitation of resources, from the agricultural point of view, soil degradation and withering, massive water use, …, are no longer negligible. Natural resources, o date, are no longer able to provide the balance.

According to WWF, in 2023, "Earth overshoot day" was August 2. This means that in eight months, the renewable resources that the Earth provides in a year have been exhausted, and since August 3, the consumed resources are a debt to future years [32]. It is estimated that in 2050, with current consumption, three planets will be needed to cover a one-year demand.

Agenda 2030 aims to achieve the efficient management and use of natural resources (Target 12.2), to halve the total food waste (Target 12.3), to significantly reduce waste generation through the "rule of three R: reduce, recycle and reuse" (Target 12.5), and to adopt innovative sustainable waste management practices in addition to promoting the theme of prevention (Target 12.6).

3.1.5 Goal 13: Climate Action

By 2035, global temperature will exceed the limit considered critical of 1.5°C, which will proceed in an increase of 2.5°C by 2100. The acceleration of global warming, compared to the last decades of the last century, is evident: the global average temperature increases of about 0.85°C from 1880 to 2012, the sea rises of 19 cm during 1901-2010 period and the warmest ever documented decade is the 2010-2019 period.

The 2030 Agenda gets a boost from the 2015 Paris Agreement, which aims to limit temperature increase to 2°C above pre-industrial levels. It is crucial to take measures such as integrating climate change strategies into national policies (Target 13.2), acting in terms of adaptation to the new climate and natural disasters (Target 13.1), and making people conscious through education on climate change (Target 13.3).

3.2 European Green Deal

The European Green Deal (EGB), launched by the European Commission in December 2019, is yet a milestone in addressing important environmental challenges. The EGD primary objective is ambitious: achieving **climate neutrality by 2050**. This goal translates into efforts to balance GHG emissions through a combination of reduction and absorption strategies.

EGD is a priority for the European Commission since it wants to be the basis for sustainable future for the European Union from 2030 onward. The EGD objectives are several including increasing energy efficiency, promoting renewable energy, revisiting production and consumption models. Scientific approach will guide the decision-making process, based mainly on collection and analysis of environmental data. Study on greenhouse gas emissions, climate

changes in European region, human activity impacts on the ecosystem are key aspects in the EGD.

Technological innovations (particularly the widespread adoption of renewable energy sources) and their adoption and integration are necessary for reducing dependence on fossil fuels and mitigating GHG. For this reason, great importance is also given to the social aspects: dissemination to the population, educational activities and training, and measurement of the achievement of the minimum goals are fundamental for change European countries.

The policies adopted to achieve climate neutrality by 2050 require collective commitment and an evidence-based approach. The path outlined by the EGD its hard and ambitious but provides a solid framework for addressing environmental challenges and shaping a resilient future for next generations.

3.3 Circular Economy Action Plan

The Circular Economy Action Plan is a framework that aims to transform the European linear economy into a sustainable and circular economy. The plan sets out a series of interrelated initiatives that will establish a strong and coherent product policy framework, making sustainable products, services, and business models the norm. The plan seeks to transform consumption patterns so that no waste is produced in the first place, and waste is seen as a valuable resource. The plan sets ambitious targets, such as ensuring that all plastic packaging on the EU market is reusable or recyclable by 2030 and reducing the waste generation. The plan also aims to provide incentives and support to circular materials and innovative production processes. The plan pursues to fortify the capacity of the EU to take responsibility for its waste and to create an EU market for high-quality secondary raw materials.

From consumers and public buyers' point of view, this action plan aims to raise awareness on sustainable products and on reuse and repair services, providing guidance to achieve high levels of separate collection of waste.

The Circular Economy Action Plan is a future-oriented agenda for achieving a cleaner and more competitive Europe in co-creation with economic actors, consumers, citizens, and civil society organizations, where high-quality products are designed for long-lasting life and reuse/repair/recycling concept. This plan is a crucial step toward achieving a cleaner, more competitive, and sustainable Europe by 2050.

3.4 Fit for 55%

The Fit for 55 (FF55) package is a set of proposals of the European Commission to generate policies on climate change fights, aiming for a 55% reduction (compared to the 1990 level) in net greenhouse gas emissions by 2030. It includes legislative revisions for a just transition, industry

competitiveness, and global climate leadership of Europe. The package is composed of twelve regulations and implications, including: new trading system for carbon credits, land use and forestry, alternative fuels, "Social Climate Fund," CO_2 emissions for cars sector, energy taxation, renewable energy, energy efficiency and buildings performance.

The reform of the EU Emissions Trading System (EU ETS), which has already reduced EU emissions by 41%, involves the inclusion of shipping and aviation sectors and the phases out of free allowances. The final target is emission reduction of 62% by 2030.

FF55 change the regulation of land use, land use change, and silviculture and forest management, including reducing new areas that may become sealed and innovative solutions to increase CO2 removed by exploiting uncultivated and marginal lands.

The package also addresses emissions from cars and trucks, responsible for 15 % of EU CO_2 emissions. The new rules set progressive emission reduction targets, embracing the much-discussed goal of banning endothermic engines for new cars in 2035. Moreover, in the energy sector, a reduction of methane consumption is imposed, aiming for greater electrification of systems. In parallel, new regulations on sustainable and decarbonized fuels, from 2023 onward, are also imposed on the aviation and shipping sectors.

The revision of the directive on renewable energy sets at least 40% the level of energy production through renewable energy sources, by 2030. And contemporary the energy efficiency program aims to reduce energy consumption by 12%, always by 2030. Increased energy savings and decreased energy consumption in public sector (and households) buildings will be the standards for the next years. The energy performance of buildings directive focuses on making EU buildings more energy-efficient: new buildings will be zero-emission by 2030, for existing buildings the target is 2050. About gas for heating and energy production, the FF55 aims to shift from natural gas to renewable and low-carbon gases and large electrification of the systems.

The FF55 plan is a set of several regulations, approved in recent years by the European Commission, which composed a "community path" toward a more sustainable and resilient Europe, together with other plans, agendas, deals, ... Many action actions must be supported by political choices and forward-looking policy makers, as many points inevitably have raised and will raise some controversies. The role of research is certainly to support technological innovation, but also to make it simple and understandable, to be usable and "accepted" by the people.

The biochar

2nd chapter

4 Carbon removal concept and biomass thermochemical conversion

IPCC scenarios predict a reduction in global GHGs emissions of about 60% from current levels by 2035, to limit the global warming. Countries' collective political commitments, though undertaken with great efforts and discussed policy choices, fall far short of that goal. Current policies are still insufficient to meet countries' signed commitments. Scientific results calculate that by adopting the 2030 Agenda, the most probable scenarios are the SSP1-2.6 and the SSP2-4.5, associated with an increase of 1.8 °C and 2.7 °C, respectively: far from the 2 °C required by the Paris agreements (scenario SSP1-1.9).

To be able to keep the temperature increase target below 1.5°C (same for the 2°C target), the IPCC has introduced, in the AR5 of 2014, an important innovation for fighting climate change: the **atmospheric carbon removals**. This innovation is fundamental mainly for the SSP1-1.9 and SSP1-2.6 scenarios.

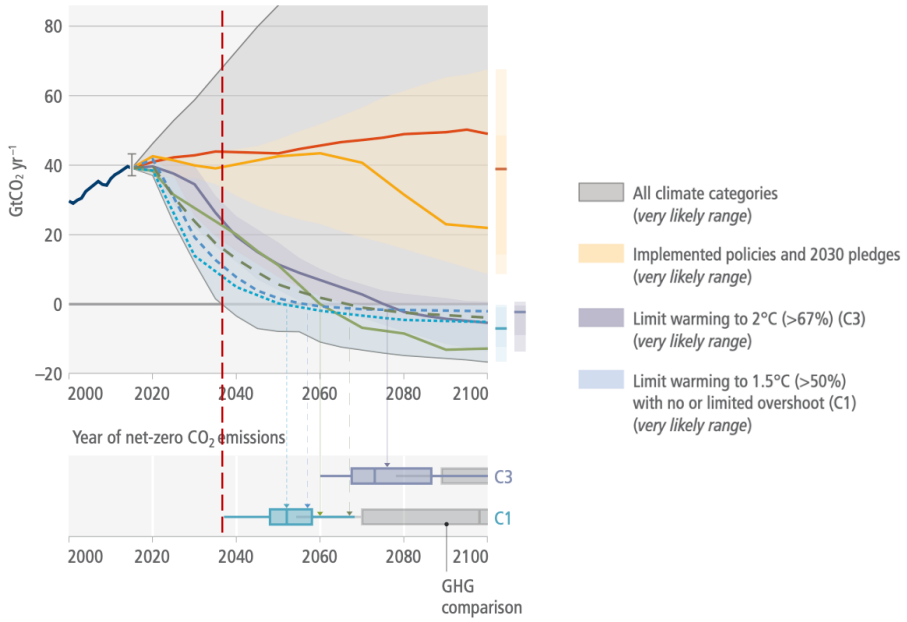

Figure 4-1. Simulations of CO2 emissions over the next 80 years. The simulations are linked to mitigation works to limit warming to 1.5°C or 2°C. Significant, rapid and continuous emission reductions, coupled with systematic abstraction of atmospheric CO2 through different methods and technologies, are needed to keep these reduction targets valid. global greenhouse gas and CO_2 emissions in global pathways. Figure is adapted from WGIII - Technical report [33]*. The colored intervals indicate the 5th-95th percentile of various pathway simulations. C1 corresponds to the SSP1-1.9 scenario with no exceedance of the 1.5°C goal; C2 corresponds to the SSP1-1.9 scenario with time-limited exceedance of 1.5°C, not shown here; C3 corresponds to the SSP1-2.6 scenario.*

Figure 4-1 shows net CO_2 emissions over the next century. The trends shown are not predictions, but simulations of emission trends in the case of non-application of climate policies (gray color) and application of climate policies: agenda 2030 (yellow color) and additional policies to limit temperature increase to 1.5°C or 2°C (light blue and purple color, respectively). It can be seen that **carbon capture**, through various methods and/or technologies, plays a hey-role, already by now, in order to reach the next decade (red vertical bar) with "negative " emissions. This means that the amount of carbon removed from the atmosphere is greater than the amount of carbon injected by anthropogenic activities.

4.1 Net zero CO_2 emissions

The goal set by the Paris Agreements, which is to keep the global average temperature increase below 2 °C compared to pre-industrial levels, and preferably limit the increase to 1.5 °C, can only be achieved by reducing emissions of about 50% by 2030 and reach net-zero emissions by 2050. The IPCC glossary defines net zero as follows:

> *Net zero carbon dioxide (CO_2) emissions are achieved when anthropogenic CO_2 emissions are balanced globally by anthropogenic CO_2 removals over a specified period. Net zero CO_2 emissions are also referred to as carbon neutrality* [34].

In discussions of *net-zero emission*, the focus is often only on the CO_2, since it is the gas most emitted by anthropogenic activities and it is an index of the greenhouse effect. Other greenhouse gases such as CH_4 and N_2O are also getting more attention, which is why increasingly stringent regulations on their emission into the atmosphere are emerging. In the documents describing the climate policy actions and goals, there is no mention of **zero emissions** but of **net-zero emissions** to give the possibility for gradual actions in the future years. Net-zero, in fact, allows for "virtually zeroing" even emissions that to date are difficult to control or for which a transition period is needed.

The need for actions that can reduce atmospheric CO_2 concentration through carbon removal is evident. This process is known as Carbon Dioxide Removal (CDR).

4.2 Carbon Dioxide Removal (CDR) Methodologies.

In the CDR concept, CO_2 is removed from the atmosphere by extending the potential of natural carbon sinks whether they are physical, biological or geochemical. Carbon storage methods involve several, very different methods: a) removal of CO_2 directly from the atmosphere and subsequent immobilization

through natural systems (seas and oceans, soils, ...) and/or engineered systems (conversion of CO_2 into stable substances, subtraction through membranes, ...); b) conversion of CO_2 through the process of chlorophyll photosynthesis; c) transformation through external catalyzed reactions; d) pump and storage in Carbon Sinks (CS) identified in specific suitable underground environments; e) exploitation as CS of agricultural or marginal lands. Some of these mechanisms enters in the field of engineering because to their technical characteristics, while other systems fall in the field of agricultural and forestry policies.

Carbon storage can be used firstly to offset the emissions from hard-to-abate sectors, and after can be expanded to offset global emissions for reaching negative CO_2 emissions. Assessing the amount of carbon dioxide stored is not easy since, as occurs in natural systems, even in "forced" systems some of the stored CO_2 returns, over time, in the atmosphere. The amount inserted into the CS does not correspond to long-term immobilized amount but there is a storage "efficiency".

In addition, the abatement of the greenhouse effect (and consequently of the temperature rise) is not immediate but there is a temporal latency, which is why implementing CO_2 removal actions is like offsetting future emissions. However, since temperature reduction follows a semi-linear correlation with CO_2 concentration, CS results are visible immediately: there is no minimum amount after which changes begin to be noticed. Some of the proposed methods of carbon storage are collected in Table 6.

Table 6. Compilation of some proposed methods considered viable for long-term carbon storage to cope with temperature increase above 1.5°C.

Methods	Description	Storage form	Time Scale	Problematics
Afforestation, reforestation and forest management	New and restored forest	Biomass (Organic)	Decades to centuries	Fires, drought, ...
Soil carbon sequestration	Improve agricultural and land management	Soil organic carbon (Organic)	Decades to Centuries	Mismanagement
Biochar	Sub stoichiometric thermo-conversion of biomass	Stable carbon (Organic)	Decades to centuries	Fire, leakage, decomposition
Bioenergy with carbon capture and storage - BECCS	Energy from woody biomass and biochar production	Usually as biochar (organic). Or in other carbon sink (inorganic).	Potentially permanent. As DACCS	Decomposition & Leakage
Ocean fertilization	Fertilize ocean with micro and macro nutrients (Fe, N, P) for enhancing the	Biomass and dissolution in water	Decades to millennials	Stratification of water

	photosynthesis and biomass of phytoplankton			
Restoration of vegetated coastal ecosystems	Manage coastal ecosystems to store carbon in sediments	Sediments	Decades to centuries	Coastal-use change, sea level
Ocean alkalinization	Adding alkaline minerals to increase alkalinity	Increased CO_2 ocean uptake	Up to 100 000 years	Chemistry and stratification of water
Direct air carbon capture with storage - DACCS	Direct removal of CO2 from the atmosphere through chemical adsorption, absorption or mineralization	Carbon sink* (inorganic)	Potentially permanent. As BECCS	Leakage

* Storage in underground, deep ocean or in lasting materials

4.3 Bioenergy with carbon capture and storage

The "**Bioenergy with carbon capture and storage**" (BECCS) methodology is considered among the most important and promising carbon storage systems, alongside reforestation and afforestation systems [8]. It is relatively easy to integrate into environmental economies and policies and it is a cost-effective solution. The potential impact on carbon storage for BECCS is estimated up to 22 Gton y^{-1} of CO_2 [35]

BECCS exploit biomass as fuel to produce electricity and heat. The CO_2 that is produced during biomass combustion is captured and temporary stored. In a second stage the CO_2 is transported, if necessary, and stored in suitable sites identified as CS.

The main advantage of BECCS is that it is the only CO_2 removal technique that simultaneously produces electricity. Similar technologies are the "**Direct air carbon capture with storage**" (DACCS). DACCS, however, require high electricity consumption for the suction of CO_2 from the atmospheric air, CO_2 separation by filtering and pumping of the removed CO_2 in the CS.

Considering BECCS technologies, different starting biomasses (waste, woody biomass, paper, ...) can be used, different thermal conversion methodologies can be exploited (combustion, co-firing, gasification, ...) and different techniques of storage can be implemented. Main steps of BECCS are shown in Figure 4-2.

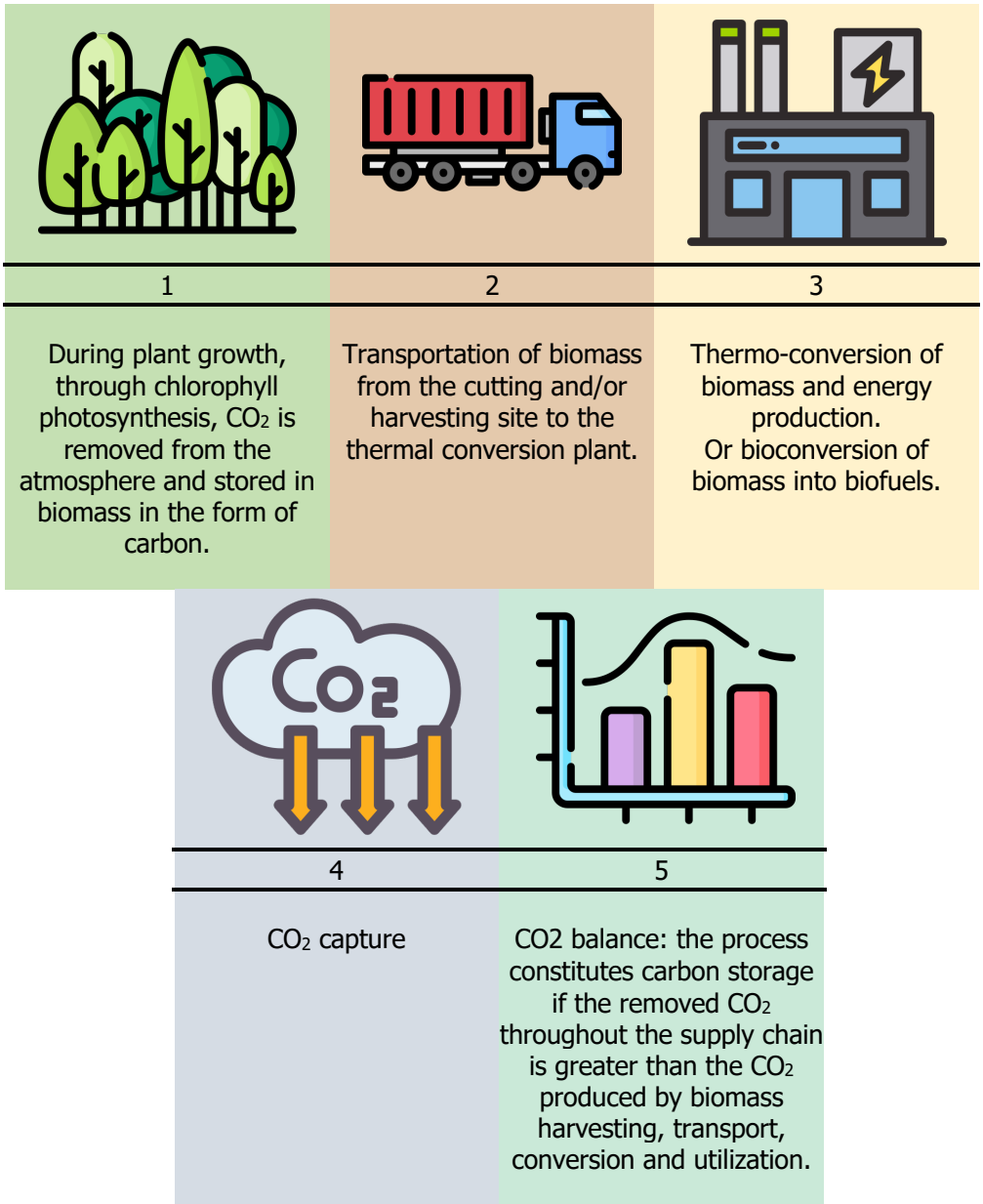

Figure 4-2. Graphical representation of the key stages of BECCS

The most used technologies are combustion, gasification, and biochemical conversion. While in combustion and gasification woody biomass a fuel brought to high temperatures to produce heat or to generate gas, respectively. Biochemical conversion, instead, through digestion or fermentation, processes the biomass to produce biofuels (e.g., ethanol).

Problems of BECCS are the constant demand of biomass and the related cost [36]. It is also necessary to specify that the biomass used in these plants is generally waste biomass or it comes from necessary maintenance and management of forests and woodlands. Other biomasses that can be used are agricultural biomass, to date often not reused, and the organic fraction of municipal organic waste (OFMSW). Important area are also algae cultivation [37] and energy crops, the latter much-debated because it is considered a low-ethic process. It should be noted that not all types of biomasses are suitable for all processes: for example, OFMSW cannot be used, efficiently, in thermal conversion processes.

4.4 Gasification and pyrolysis

One technology that has occupied an important role in the energy sector (and beyond) in an up-and-down manner for a century now is gasification [38].

Gasification cannot be properly classified as BECCS since it does not couple energy production and the removal and storage of CO_2 produced during the process. Often, gasification systems are a "simple" energy production plant for easiness, convenience of operation and maintenance, and cost-effectiveness. Gasification converts biomass to fuel gas (and employing it for power generation) and to carbonaceous by-product. It's thanks to this by-product, called **char**, that gasification falls under the concept of "**carbon negative**" technology. Gasification, in fact, winks at carbon storage through char. Char is a vegetable coal, produced at high temperatures (Section 5), high in carbon content - up to 90 % - and stable over time. Gasification is a carbon negative technology for these just mentioned properties of char. Negative carbon balance means that the amount of carbon emitted, usually in the form of CO_2 originated from the combustion of the synthesis gas, is less than the amount of CO_2 initially absorbed by the plant through chlorophyll photosynthesis. The difference, negative, is the amount stored in the char and it is considered carbon storage.

"Stand-alone" gasification, therefore, can be seen as a subset between BECCS and Carbon Negative process since there is no technological system proper for voluntary CO_2 subtraction, but there is carbon storage thanks to the intrinsic characteristics of the gasification process. The Figure 4-3 shows, recalling Figure 4-2, how gasification fits into the context of carbon storage even without CO_2 capture.

As also reported in Table 6, to date, char is considered a viable mode for carbon storage even by the IPCC, even when it is not produced through gasification. In fact, there are other types of biochar production processes: pyrolysis [39] and hydrothermal carbonization (HTC) [40]. HTC is not considered in this discussion. Pyrolysis, on the other hand, will be mentioned often during next Parts as a promising technology for carbon storage but, compared to

gasification, it provides fewer overall benefits and, because of different process conditions, it produces a char with some different characteristics.

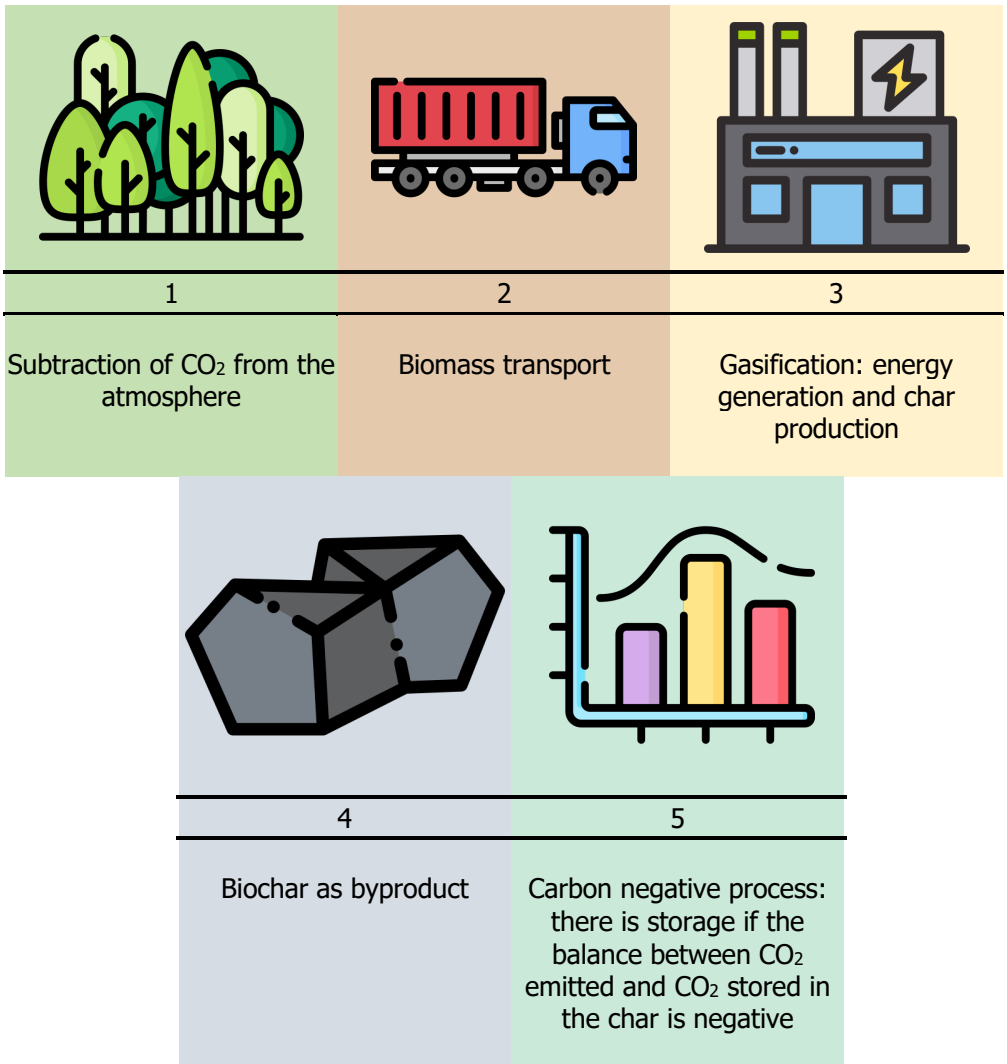

Figure 4-3. Changes for gasification systems as a carbon storage method in analogy with BECCS systems (Figure 4-2).

This work will explore char as important player in the ecological transition. Char and its production methods combine several benefits and different thematic areas precious for the fight against climate change:

- method among the most promising in carbon storage sector
- simultaneous production of electricity and thermal energy through renewable sources

- new soil conditioners and fertilizers to improve agriculture and depleted lands;
- contribution to the growth of the circular economy: emergence of new supply chains; exploitation of materials to date not used; creation of new, more sustainable markets.
- char as an innovative material in construction, electronics, other materials.

According to the IPCC, char produced at global scale, potentially store up to 3 Gt CO_2 yr^{-1}. The char, to make carbon storage, must be buried into the soil during the crop-sowing process [41]. The char has an immediate removal effect and therefore is thought to have a rapid expansion in the short future, 13.2% between 2022 and 2031 [42]. Char gives a positive impact to agricultural field since it enhances crop yields [41].

4.5 Carbon credits

Alongside the concept of carbon storage, it is necessary to introduce the mechanism of **carbon credits** (CCs). CCs are increasingly becoming a key tool in the fight against climate change since they allow to quantify the removal of CO_2 and monetize it on a dedicated market.

One carbon credit is equal to one metric ton of carbon dioxide, or in some markets, carbon dioxide equivalent gases (CO_2eq), and are bought and sold through international brokers, online retailers, and trading platforms [43].

CCs were formalized with the adoption of the 1997 Kyoto Protocol [44], which included the Emission Trading System (ETS), or carbon credit trading market, among the instruments for reduce the climate change. A CC represents the reduction of one ton of GHGs emissions or the absorption of one ton of CO_2eq by a project/activity/methodology that contributes to reducing overall emissions, such as biochar production or land afforestation.

The basis of the CC exchange is the concept that companies, nations or private citizens who emit more CO_2 than the target fixed by the climate policies can purchase CCs from who emit less CO_2 than the targets. Another possibility is to purchase CCs from entities that store CO_2 and generates certified CCs. The certification of CCs occurs through standard methodologies, now internationally recognized, that estimate through experimental analysis and specific algorithms the carbon removal. Puro.Earth [45] and Verra [46] are dedicated to char, while "Reducing Emissions from Deforestation and Forest Degradation" (REDD+) are dedicated to afforestation/reforestation [47].

The creation of a regulated market is an incentive solution for reducing emissions, for increasing energy efficiency and for transitioning to cleaner energy sources. The European emissions trading market EU ETS is the first and largest emissions trading system and was started in 2005. The EU ETS has passed through four different phases. The last phase is currently ongoing: it started in 2021 and will end in 2030. The ETS Directive requires that, in Europe, high-emitting facilities must obtain a permit to emit into atmosphere. Following that permit, each facility must monitor its emissions annually and compensate them by purchasing CCs on EU ETS [48]. These facilities usually belong to emission-intensive sectors (power and heat production; refineries, steel mills, metals, cement, glass, ceramics, paper, chemicals; civil aviation). At the same time, other smaller companies can participate in trading on a voluntary basis to buy or sell CCs. The EU ETS contributes to achieving the "**net zero emission**" goal by 2050.

In this context, char becomes a tool to obtain CCs and to participate in the EU ETS. In fact, after an analysis conducted by independent entities (e.g.: VERRA) if a char production chain demonstrates an effective carbon sequestration, it can be recognized a certain value of CO_2eq stored in a char mass unit and, consequently, a fraction of carbon credit can be associated.

5 Production and characteristics of biochar

This section briefly presents two of the principal modes of biochar production: pyrolysis and gasification. Hydrothermal carbonization is excluded from the discussion. There are various characteristics and parameters that differentiate gasification and pyrolysis: the main one is in the equivalence ratio (ER). The ER is defined as the ratio the oxygen used during the process and the oxygen required for the total combustion of biomass in stoichiometric conditions, Eq (5-1). Depending on the ER, the end-products differs to each other. These will be discussed in detail in the following sections. As ER increases, the process changes from pyrolysis, to gasification, and finally to combustion, Figure 5-1.

$$ER = \frac{Oxigen\ used}{Stoichiometric\ oxygen\ for\ total\ combustion} \quad \% \qquad (5\text{-}1)$$

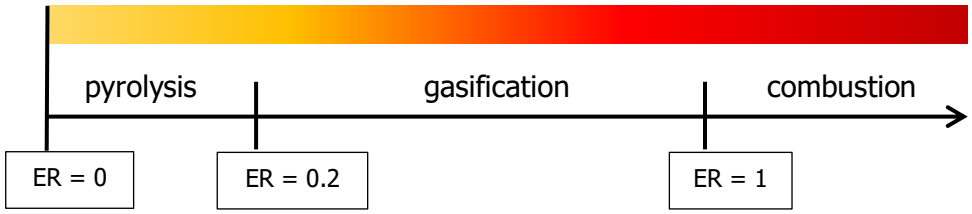

Figure 5-1. Equivalence ratio of thermochemical conversion. Adapted from [49].

5.1 Biomass gasification

Gasification is a thermochemical conversion process with the aim to maximize gas production starting from biomass, hence the name "Gas-ification". The other products that result from this thermo-conversion are by-products often undesired.

Gasification is the conversion of solid or liquid feedstock into useful and convenient ***gaseous fuel*** *or* ***chemical feedstock*** *that can be burned to release energy or used for production of value-added chemicals. [...]* Gasification packs energy into chemical bonds in the product gas; combustion breaks those bonds to release the energy [38].

Combustion converts the total energy from breaking the chemical bonds of biomass into thermal energy, with production of CO_2 and particulate matter suspended in the fumes. Gasification, on the other hand, produces a combustible and high-calorific gas whose chemical bonds can be "broken," releasing energy,

at a later stage. The gas that is generated has a high hydrogen-carbon (H/C) ratio: these elements are taken from the biomass and are recombined into the gaseous final product.

Initial biomass passes through four different stages: a) drying; b) pyrolysis; c) combustion (of some biomass, gases, vapors, and char); and d) gasification (also of previous obtained products). In Figure 5-2, adapted from [38], the gasification process is shown graphically, starting from biomass, going through intermediate products, and finally generating the final products.

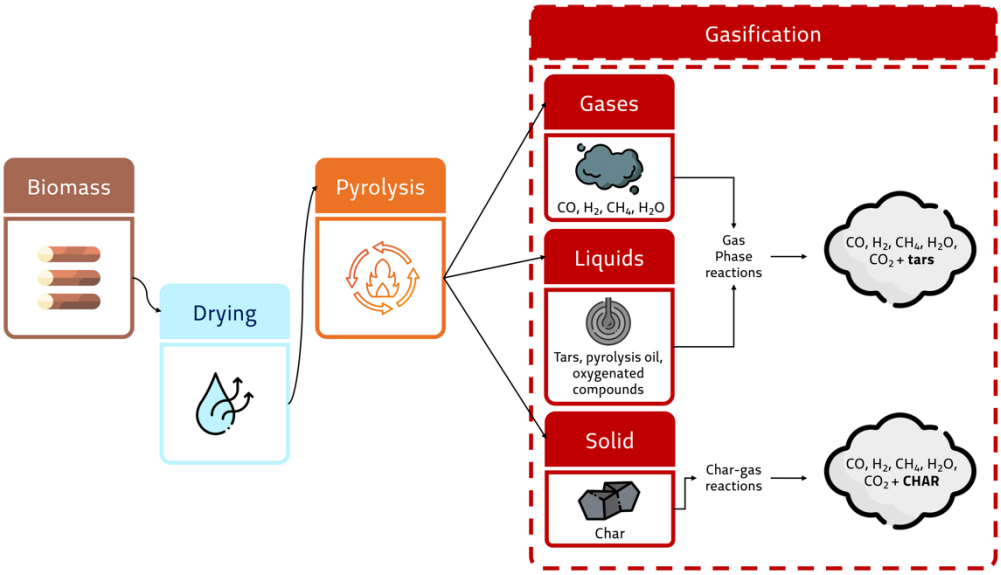

Figure 5-2. Steps of gasification process, from biomass to the final products. The different stages with the related (intermediate and final) products are reported.

Gasification takes place in a gasifier, typically a tank (which can vary in shape and size), adapted to resist to high temperatures and to high pressure/vacuum condition. Through a controlled injection of a gasifying agent (oxidizer), the process converts biomass into gas. This gas in the literature has taken on several names: wood gas, city gas, producer gas, synthesis gas and syngas. The term "syngas" comes from the contraction of synthesis gas. Historically, syngas has found multiple applications: 1) around the first decade of the 1800s it was used to light the cities (in fact, the gas was called "city gas" and it was stored in gasometers, still visible today in many metropolises); 2) in the second half of the 1800s it was used in the steel industry, and in the early 1900s it found application on heavy vehicles, such as trucks and tractors; 3) later, with technological and industrial evolutions (e.g., Germany's *Deutz* [50]) it was used to power internal combustion engines in automobiles, especially during the fuel crisis of World War II [51]. To date, gasification has evolved, and syngas is mainly used in static applications: in burners and/or heat boilers to

produce heat and thermal energy, in internal combustion engines to produce electricity, in gas turbines and in fuel cells. The construction of co-generative plants, even big ones, has gradually become an increasingly viable option. The "Vaasa Bio-gasification Plant" is an example of a very large gasification power plant, with a nominal capacity of 140 MW [52].

The upgrade of syngas into biomethane, hydrogen, or other chemical compounds to produce biofuels have also been receiving increasing attention in recent years [53]. Other innovative applications are mainly related to permutations of the above-mentioned uses.

Energy production through gasification offers several advantages over simple combustion: a) higher thermal conversion efficiency [38]; b) better combustion of syngas since it is a gaseous vector; c) lower production of exhaust gas due to reduced air excesses; d) possibility of utilizing syngas in many different type of power generation systems.

Often the focus in evaluating these systems rests on energy production, neglecting the main by-product of gasification: the char. For a long time considered a residue, char is now gradually assuming a role of primary importance, as already discussed. A key component in innovative materials, it has major impacts in industrial and agricultural sectors by promoting soil fertility and offers a safe technology for carbon storage.

5.1.1 Classification of gasification processes

The classification of gasification processes can follow different patterns. A brief discussion of the main parameters is given in the following paragraphs.

5.1.1.1 Direct and indirect methods.

In indirect gasification - allothermic process - an inert material, usually sand, is used as an energy carrier to transfer heat from the heat generation system to the biomass. The process is not self-sustaining.

In direct gasification - autothermal process - the heat required for thermo-conversion comes from the combustion of a fraction of the biomass or of the intermediate products (pyrolytic oil, gas, tars, ...) providing energy for the endothermic gasification reactions. The process is **self-sustaining**.

5.1.1.2 Gasification agent.

The gasifying agent is the comburent that is fed into the gasifier during the thermal conversion process. Ambient air, oxygen and steam are the most used agents. Air is the cheapest and easiest agent to use, but it produces gas with the lowest Lower Heating Value (LHV): 4 to 7 MJ Nm^{-3} . Steam is used when the gas must contain a high fraction of hydrogen (H_2). Steam requires energy to be produced, reducing the overall efficiency of the system, but generates gas having 10 - 18 MJ Nm^{-3} of LHV. Finally, oxygen has the highest cost but produces

a gas with a higher fraction of carbon monoxide (CO) reaching an LHV of 12 - 28 MJ Nm^{-3} .

The choice of gasifying agent is also based on the final application of the syngas: co-generation, thermal/electrical power generation or upgrading into pure gas (e.g., H_2 or CH_4).

5.1.1.3 Architecture of the gasification reactor.

There are different types of reactors: entrained flow gasifier, fluidized bed and fixed bed.

Entrained flow gasifiers are used in large combined cycle gasification power plants or refineries. The reactor operates at high temperatures and high pressures, up to 1900°C and up to 70 bar. Often the fuels are petroleum by-products or pulverized biomass, and they are fed into the gasifier via gasifying agent. Oxygen is commonly used for optimization of the end products [54]. Reactor feeding is from the top with gas extraction from the bottom, or side feeding with gas extraction from the top.

Fluidized bed gasifiers are suitable for medium-sized plants, from 1 MW to 100 MW [38], fed with shredded biomass of 6-10 mm dimension and with reactor core temperatures up to 1000°C. The temperature distribution is more uniform than other types of gasifiers [38,55]. In this type of reactor, fuel is mixed with an inert granular material and are kept in suspension through the gasifying agent that is injected at high velocities. The production of tars is not high since the uniformity of the process stimulates high efficiency of carbon conversion in gaseous products. Ashes are extracted from the bottom. Due to size flexibility and the ability to work at both low and high pressure, fluidized bed are often the most popular systems used in gasification power plants. Two architectures are most used: *bubbling fluidized-bed* and *Circulating Fluidized-Bed*. In both types, the biomass is inserted laterally at the level of the bubbling bed.

In Bubbling Fluidized-Beds (BFBs) the fluidized bed remains limited to the lower part of the reactor where the combustion phase occurs. Gasification and cracking of carbonaceous substances and volatile compounds happens thanks to the contact with the hot fluidized bed. The residence time of the fuel and gases is relatively low.

In Circulating Fluidized-Beds (CFBs), on the other hand, the residence time in the reactor of the fuel and gases is longer and for that reason it is more suitable for woody biomass [38]. This is done by adding a recirculation branch and using high injection velocities of gasifying agent. Biomass conversion involves the entire height of the reactor, and the recirculating branch permits to recover both the inert medium and the not-converted biomass. A variation of CFBs are the *Twin reactors* in which the recirculating branch acts as a second reactor thanks to secondary nozzles inserted in the branch.

The last types of reactors are **fixed-bed (FB) gasifiers**.

Fixed-bed gasifiers are the oldest and most commonly employed reactors for the gasification of biomass feedstocks on account of their simple design, easy operation, high thermal efficiency along with minimum pretreatment of raw materials. [...] These gasifiers are considered the first choice for small-scale gasification for local power generation [56].

FB reactors are known for their simplicity: if the previous architectures require several auxiliary plants, high construction complexity, safeties to operate under high pressure conditions, ..., in FB gasifiers there are no special needs since it is the biomass that proceeds "by gravity" inside the reactor (for this reason they are also called *moving beds*). FBs, on the other hand, are not known for their versatility. They can work with coarsely shredded biomass, up to 50 mm, but due to the high compactness of the fuel in the reactor, little mixing and low gas mobility, the heat transfer in the reactor is not optimal. Therefore, the conversion efficiency is not high, and the creation of tarry agglomerates or reactor clogging is common. Temperatures in the gasification zone reach 900 °C but the tar content in the syngas is the lowest of the architectures presented so far [57]. Usually used for power plants up to 10 MW, they do not accept all types of biomasses and require stages of syngas cleaning if it is applied in internal combustion engines.

There are three main architectures by which FBs are made: updraft, downdraft and crossdraft.

Downdrafts are co-current reactors: the biomass, the gasifying agent and the produced syngas travel in the same direction: from the top to down. Biomass is fed from the top and initially encounters a drying stage and later a pyrolysis stage. At the gasifying agent introduction nozzles, a portion of biomass or pyrolysis products (char and pyrolysis oil) are combusted, generating energy (heat) and mainly two gases: CO_2 and H_20. This heat allows the entire process to be self-sustaining. The solid (char), liquid (pyrolytic vapors, tars, ...) and gaseous (CO, H_2, H_20) products, generated in the previous stages, finally enter the gasification stage where the final conversion into gaseous products, mainly CO and H_2, takes place. Due to the passage of the intermediate products through the hot char bed, a very efficient gasification stage occurs in downdraft architectures: tars are sensibly converted to gas and there is a residue of 0.015 to 3 g Nm^{-3}, while the char is "washed" by the high-temperature syngas, which then leaves it free of residual tars or other condensate products.

The two realizations of the downdraft type are the *throated gasifier* (also known as the *Imbert gasifier*) and the *throatless gasifier* (also known as the *stratified gasifier*). The throated has a narrowing-throat-that begins at the

gasifying agent nozzles. The throat allows to a more efficient combustion and to an easier control of the gasifying agent dosage. Moreover, throat forcing the passage of pyrolysis vapors thorough the gasification zone.

In contrast, *throatless gasifiers* design is simpler. They have a cylindrical shape in which biomass is fed from the top and it goes down, through the four zones, by gravity. It is suitable for light biomass.

In both types, a grid at the bottom of the reactor separates the gasification zone from the char collection zone. This grid also allows the passage of syngas for the extraction, which always occurs from the bottom.

Updrafts have the simplest architecture. They are countercurrent gasifiers in which the biomass is fed in from above and proceeds to the bottom of the reactor, passing through the four thermo-conversion zones, while the syngas produced is drawn from the top of the gasifier. A grid separates the gasifier body from the char collection zone. The gasifying agent is introduced from the bottom and rises to the top through the grate. The biomass first encounters the drying zone and then the pyrolysis zone. The heavier products of pyrolysis, which takes the heat from combustion zone, flow downward while the vapors rise, passing through the virgin biomass, and condensing on its cooler surfaces. The char and pyrolysis products meet the warmer gasification zone, where conversion to gases (mainly CO and H_2) occurs. Energy to the gasification zone is provided by combustion that occurs near the bottom grate. Here the gasifying agent passes through the burning char bed and converts a fraction of char in gases (mainly CO_2). The combustion zone is far from the pyrolysis and drying zones compared to the downdraft, which is why a lower fraction of pyrolysis vapors, tars or gases (through cracking and reforming reactions) are converted into gas. The final syngas has a higher tars content, from 30 to 150 g Nm^{-3} [57]. These gasifiers are preferred for thermal applications, and they work well with light biomass also with high moisture content. The char in the updraft architecture is not "washed" by hot gases since the gas is extracted from the bottom. Due to high heat diffusion, there is good conversion of the carbon contained in the char into gaseous products.

Crossdraft gasifiers have a cylindrical structure like updrafts, have no constrictions, and biomass flows from the top to the bottom. A grate at the bottom separates the ash zone while a special internal architecture allows the syngas extraction from the side. Opposite to the gas outlet there is the nozzle for injecting the gasifying agent (at high velocity). A small combustion zone is created around the nozzle, at temperatures close to 1500 °C: char and other pyrolytic products are converted to gas, mainly CO_2 and H_2O. The gasification zone is between combustion zone and the syngas outlet section: H_2 and CO are formed here. The pyrolysis and drying zones are placed in the upper section of the reactor. The gases are extracted very hot since are withdrawn quickly after

their formation: this results in less heat diffusion and less conversion of solid molecules to gas (cracking and reforming are penalized). For this reason, crossdraft are not often used with woody biomass. Since the syngas is taken very hot, tars cannot condense and get trapped in the flow: the tars content in gas is low, 0.01 to 0.1 g Nm^{-3}. Crossdraft are suitable for small stand-alone applications, up to 10 kW, and are economical since the reactor core is kept confined to the center of the reactor and the wall materials do not have to withstand high temperatures [57].

To complete this discussion in Table 7, Figure 5-4 and Figure 5-3 are given some comparisons and some insights into the different types of gasification reactors, as well as schematic representations of some architectures.

Table 7. Summary and comparison of gasification reactors mentioned in the paragraph 5.1.1.

Gasifier reactor	Gasification zone temperature	Combustion zone temperature	Last zone seen by char	Char production
Downdraft	700-900 °C	1000 - 1400 °C	Gasification	4 to 7 % w/w of char not converted
Updraft	700-900 °C	1200 - 1800 °C	Combustion	High carbon conversion
Crossdraft	900 °C	> 1500 °C	Gasification	-
BFBs	800 - 900 *	-	Uniform temperature	High carbon conversion
CFBs	800 - 900 *	-	Uniform temperature	High carbon conversion

* One temperature, there are no well-defined zones in this architecture.

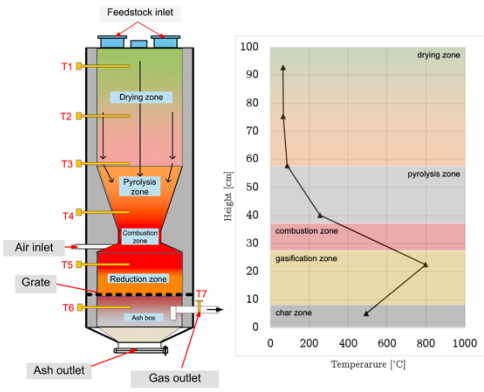

a) throated downdraft gasifier temperature profile. Modified from [58].

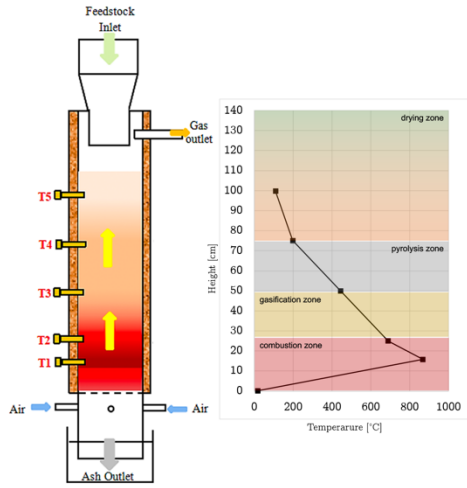

b) updraft gasifier temperature profile. Modified from [59].

Figure 5-3. Comparison of vertical temperature profiles of a downdraft throated gasifier and an updraft gasifier. The temperature profiles, on the right, are recreated from thermocouple measurements and are aligned with the reactor zones shown in the sketches, on the left. Temperatures are high in the updraft oxidation zone, in the downdraft no thermocouple was inserted in the throat and the precise temperature is not known. The reduction zone reaches little higher temperatures in the downdraft than in the updraft. The two zones of oxidation and reduction are reversed in the two architectures.

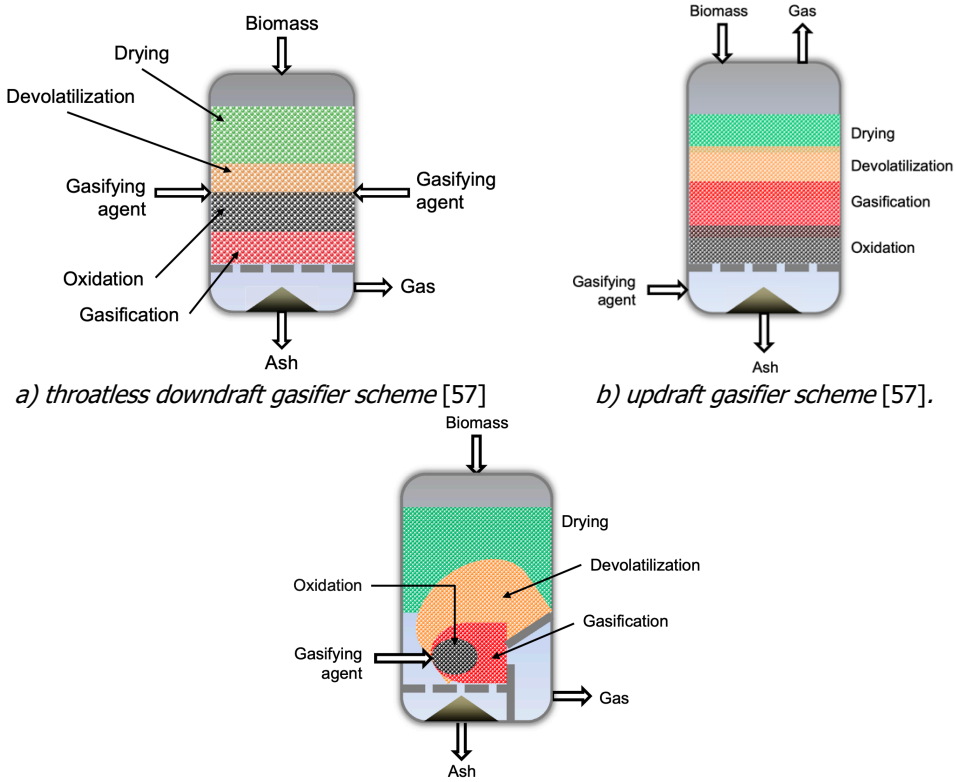

a) throatless downdraft gasifier scheme [57] *b) updraft gasifier scheme* [57].

c) Crossdraft gasifier scheme [57]

Figure 5-4. Schematics of the architectures of the most popular fixed-bed gasifiers.

Concluding, fixed-bed gasifiers applied in small-scale settings demonstrate cost-effectiveness and versatility. On the other hand, medium-scale and large-scale gasifiers are predominantly fluidized-bed reactors, which are advantageous in terms of performance, but associated with higher costs (both initial and operating) and complexity than fixed-bed gasifiers.

Gasification is certainly a versatile and fascinating technology that can be exploited to produce electricity and thermal energy and in parallel generates a **"positive" environmental impact** in terms of carbon storage. However, there are still significant challenges to be addressed. Gasifiers architecture require precise design, and reactors need careful management. The cost of equipment maintaining and cleaning represents a cost in terms of materials and labor hours. A fraction of gasification by-products (tars, tarry water, agglomerated products, ash, ...) remain in the pipes and require periodic interventions. Also, the disposal of waste demand special attention.

Moreover, gasification is a process that requires a) continuous biomass supply chain, b) possible biomass pretreatment steps, and c) continuous reactor

feed for continuous power generation. These operations hide expertise and costs. Finally, filtering of syngas need filtering to comply with generators acceptance limits (internal combustion engine, turbine, ..) and the exhaust gas need treatment to stay below the air emission regulations limits.

5.1.2 Theory of gasification: drying phase

Biomass just harvested has high moisture content (usually from 30% to 60%, sometimes exceeding 90%). Biomass requires about 2242 kJ of energy to vaporize each kg of moisture. Moisture in the cellular structure can hardly be eliminated, but it is essential to remove the moisture contained in the more superficial layers through a "drying" stage until 10-20%. Therefore, an external dryer is sometimes necessary. The drying stage inside the reactor takes place by exploiting the combustion heat.

5.1.3 Gasification theory: pyrolysis phase

Pyrolysis is the first step in the conversion of biomass (lignin, cellulose and hemicellulose) to its by-products (char, tars, pyrolytic oil and gas). It is a key step in gasification. It occurs at ER = 0 or very low ER, and temperatures should remain in the 300-800°C range. The pyrolysis temperature, which is the temperature at which decomposition begins, is typical of pyrolyzed biomass. Two consecutive steps are identified in the pyrolysis stage: primary pyrolysis and secondary pyrolysis.

- Primary or "volatilization" pyrolysis: primary char, primary gas and pyrolytic vapors are obtained as intermediate products.
- Secondary pyrolysis or "cracking" pyrolysis is the breakdown of pyrolytic vapors into secondary combustible gases and secondary char.

During pyrolysis starts the formation of tar products (tars) due to the condensation of water vapor and of some less volatile molecules. Please refer to Sec. 5.2 for the complete discussion of the pyrolysis process.

Since pyrolysis is an endothermic process, a key factor is the energy contribution from outside, in the form of heat. In gasification, this energy is provided by the gasification reactions.

5.1.4 Gasification theory: combustion phase (or oxidation)

It is the heart of the whole process since it is the main step that give energy to the gasification and pyrolysis reactions. In gasification reactors, combustion occurs at the injection of the gasifying agent (see Figure 5-4). A fraction of biomass burns and provide sufficient energy for the other endothermic reactions of the gasification stage. The main products are CO_2 and water vapor.

The most important reactions are given below, Eqs. (5-2) - (5-5). The energy developed in single reaction (indicated by the "-" sign) may be different

depending on the author. For a self-sustaining process, the total energy produced must balance the energy required by the endothermic reactions.

$C + \frac{1}{2} O_2 \rightarrow CO - 111 \frac{kJ}{mol}$	Carbon (from char) combustion/oxidation	[60]	*(5-2)*
$C + O_2 \rightarrow CO_2 - 394 \frac{kJ}{mol}$	Carbon (from char) combustion/oxidation	[60]	*(5-3)*
$CO + \frac{1}{2} O_2 \rightarrow CO_2 - 283 \frac{kJ}{mol}$	Carbon monoxide combustion/oxidation	[60]	*(5-4)*
$H_2 + \frac{1}{2} O_2 \rightarrow H_2O - 242 \frac{kJ}{mol}$	Hydrogen combustion/oxidation	[61]	*(5-5)*

5.1.5 Gasification theory: gasification or reduction phase

The reduction zone is the area of the reactor where syngas formation takes place. Some of the reactions that generate the gas are endothermic and therefore require energy from the surrounding environment. Other reactions are exothermic: the free energy (see section 5.1.4), through the conversion of intermediates into final products, is "stored" in the syngas in the form of chemical energy. The gasification reactions are listed below, Eqs: (5-6) - (5-14).

$C + CO_2 \leftrightarrow 2\,CO + 172 \frac{kJ}{mol}$	Boudouard reaction	[60]	*(5-6)*
$C + H_2O \leftrightarrow CO + H_2 + 131 \frac{kJ}{mol}$	Water-gas reaction[1]	[62]	*(5-7)*
$C + H_2 \leftrightarrow CH_4 - 74 \frac{kJ}{mol}$	Hydrogasification reaction[2]	[62]	*(5-8)*
$2CO + 2\,H_2 \leftrightarrow CH_4 + CO_2 - 247 \frac{kJ}{mol}$	Methanation reaction n.1[3]	[63]	*(5-9)*

$CO + 3\,H_2 \leftrightarrow CH_4 + H_2O - 206\,\frac{kJ}{mol}$	Methanation reaction n.2[3]	[63]	*(5-10)*
$CO_2 + 4\,H_2 \leftrightarrow CH_4 + 2\,H_2O - 165\,\frac{kJ}{mol}$	Methanation reaction n.3[3]	[62]	*(5-11)*
$CO + H_2O \leftrightarrow CO_2 + H_2 - 41.2\,\frac{kJ}{mol}$	Water-gas shift reaction[4]	[63]	*(5-12)*
$CH_4 + H_2O \leftrightarrow CO + 3\,H_2 - 206\,\frac{kJ}{mol}$	Steam reforming n.1[5]	[60]	*(5-13)*
$CH_4 + \frac{1}{2}\,O_2 \leftrightarrow CO + 2\,H_2 - 36\,\frac{kJ}{mol}$	Steam reforming n.2[5]	[60]	*(5-14)*

[1] Reaction between solid char and water vapor. [2] Hydrogen from water-gas reaction is a reactant for hydrogasification reactions, generating methane and giving energy to the whole process. [3] All the methanation reactions gives energy to the process: this energy is stored into the gases. [4] The water-gas shift reaction eliminates water vapor using CO, it is strictly linked to the process temperature: if temperature increase, there is a lower products yield, but an increase in the kinetics of the reaction. [5] During the process there is a continuous equilibrium of products and reactants. Steam reforming reactions regulate water vapor: low temperature facilitates production of CO and H_2, high temperature goes back to CH_4 and water vapor formation.

5.1.6 Theory of gasification: end products, advantages and disadvantages.

The goal of gasification is the maximum conversion of biomass into gaseous products. Syngas is a mixture of the following gases (in varying percentages)

- methane (CH_4)
- carbon monoxide (CO)
- carbon dioxide (CO_2)
- hydrogen (H_2)
- water in the form of vapor (H_2O)
- nitrogen (N_2)

Nitrogen is present both in biomass and in air. High percentages of N_2 are present in syngas when air is used as the gasifying agent. For syngas for upgrading (e.g.: bio-methane and bio-hydrogen) it is preferred to use other gasifying agents to simplify the syngas refining process.

As also often reported in the previous paragraphs, the advantage of gasification lies in the production of a combustible gas, with high energy content (the energy developed during reactions is "stored" as chemical energy in

molecular bonds), easy to transport and to use in different end applications. However, suspended in the syngas or mixed with it in a gaseous state there are various impurities. These **impurities** consist of fine particulate matter (carbon dust and ash) and tar compounds (mainly PAHs). Filtration, dry or wet, is a necessary stage for the use of syngas in certain applications and involves significant costs.

Finally, char is the least noble gasification by-product. It must be extracted from the reactor to avoid clogging and represent, in reality, an *inefficiency* of the thermal conversion process. A complete gasification process, in fact, involves the total conversion of carbon into gas with no residual of solid material. This also highlights the complexity of the technology. However, it is precisely the char that, unexpectedly, allows this technology to be classified as "carbon negative," since net carbon emissions are negative thanks to the carbon stored in the char.

This thesis investigates char in detail, focusing on its characteristics and possible applications in which the char-donated improvement is combined with positive impact on the environment.

Figure 5-5. Biomass and biochar samples taken at different heights on the vertical of an All Power Labs Inc downdraft gasifier located in laboratory [64]*. The conversion stages, from virgin biomass (in this case A1 pellets) to biochar, firstly through pyrolysis and after through gasification, are clearly visible. (The four samples on the left continues with the four samples on the right).*

5.2 Biomass pyrolysis

A second process of great importance in biomass thermal conversion is pyrolysis. Unlike gasification whose goal is to optimize gas production, pyrolysis maximizes the production of solid and liquid. Depending on the technology used, different amount of products and different production yields are obtained .

> *Pyrolysis is a thermochemical decomposition of biomass into a range of useful products, either in the total absence of oxidizing agents or with a limited supply that does not permit gasification to an appreciable extent. [...] During pyrolysis, large complex hydrocarbon molecules of biomass break down into relatively smaller and simpler molecules of gas, liquid, and char* [38].

Pyrolysis is a thermochemical process that involves the decomposition of organic materials, such as biomass, in the absence of oxygen or with a limited supply of oxygen. The process is used to convert biomass into a range of useful products: pyrolysis oils, combustible gases and char. Pyrolysis is an important technology for converting waste biomass into new product, reducing GHGs emissions and producing renewable energy (mainly thermal). Pyrolysis has historically been used to produce charcoal needed by the industrial sector. Before that, charcoal furnaces were used to reduce the volume of wood used in domestic fireplaces. Through the pyrolysis of coal, *kerosene,* the first liquid energy carrier, was also ideated bringing revolution in houses and cities lighting all over the world. To date, pyrolysis is a promising alternative to traditional fossil fuels and has the potential to play a significant role in the transition to a more sustainable biofuel [65,66].

Pyrolysis of biomass typically reach the temperature range of 300-650 °C instead of the 800 to 1000 °C of gasification. Pyrolysis is very similar to other biomass thermal conversion processes (such as carbonization or torrefaction, which reaches a maximum of 300°C), but it is very different from gasification both in terms of products and energy balance.

5.2.1 Phases of pyrolysis.

Biomass pyrolysis process can be divided into three phases: drying of biomass, devolatilization, and tar cracking. All three stages require energy, in the form of heat, supplied by a system outside the pyrolysis reactor. During the *drying* stage, moisture is removed from the biomass. High moisture content of biomass affects the efficiency of the process and the yield of final products, but it is a less impactful parameter than on gasification.

The *devolatilization* stage involves the release of volatile organic compounds: this is the earth of the process. During this step, large complex hydrocarbon molecules (cellulose, lignin, hemicellulose) of biomass break down into smaller and simpler molecules of condensable gas (e.g. benzene, toluene, xylene, ...) and solid product (char).

The *tar cracking* stage involves the previous condensable gases and part of the carbon in the char, for producing the final product of the pyrolysis: gases (CO, CO_2 , H_2 , CH_4), liquid (condensable), semi-liquid products (tars) and a large amount of char. The reactions involve both gaseous products, whose molecules are reduced into simpler molecules of noncondensable gases (gas-phase reaction), and solid products since some endothermic reactions occur between gas and char (gas-solid-phase reaction).

A high fraction of the complex condensable molecules is not converted and forms **tars**. This fraction is a complex mixture of organic compounds that can be further processed into biofuels or chemicals. The gaseous products, composed of a mix of inflammable gas, can be used as a fuel or burned to generate heat.

The pyrolysis process can be summarized by the simplified reaction Eq. (5-15).

$$\underset{biomass}{C_nH_mO_p} + \underset{heat}{ENERGY} \rightarrow \sum_{liquid} C_zH_yO_z + \sum_{gas} C_aH_bO_c + H_2O + \underset{char}{C} \qquad (5\text{-}15)$$

Figure 5-6 shows in graphical form all the steps of pyrolysis and describes the end products.

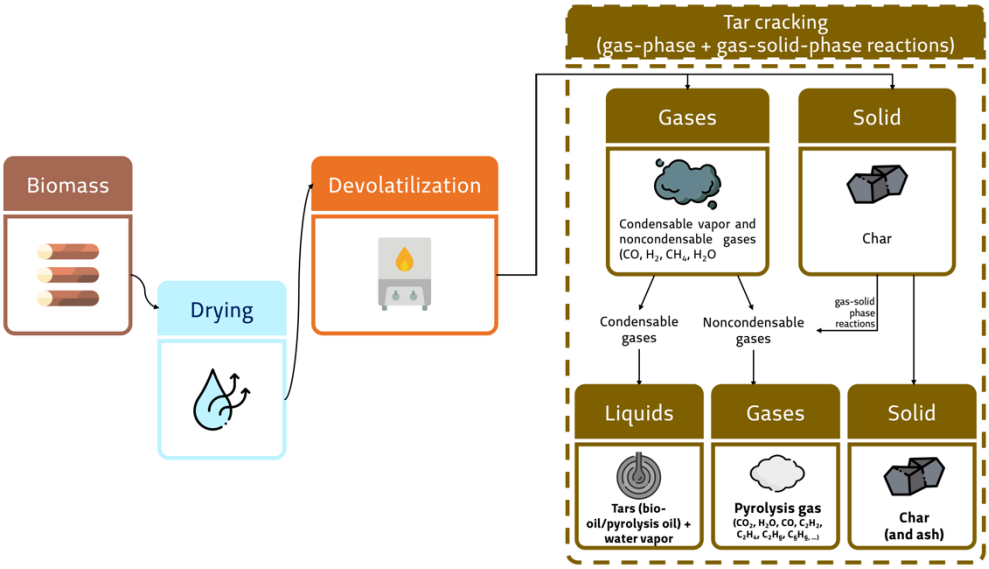

Figure 5-6. Steps of pyrolysis process, from biomass to the final products. During volatilization stage the primary products are generated. During the tar cracking stage, gas-phase and gas-solid-phase reactions occurs and generated the final product. The yields of the different products and the final amounts depends on the process parameters.

5.2.2 Pyrolysis products and their maximization.

Different final targets of the pyrolysis process require different products yields to achieve the right amount of the desired end-product. Therefore, control of the process and its parameters becomes essential to maximize liquid, gaseous or solid products.

Tar is a black, tarry fluid containing up to 20 % water. It consists mainly of phenolic compounds[2] (hydrocarbons) bound to oxygen and water. They are an emulsion in an aqueous solution, composed of 1) water, 2) products from the cellulose and hemicellulose decomposition and 3) long-chain hydrocarbon molecules from lignin [67]. The lower heating value (LHV) in this transformation goes from about 19 MJ kg^{-1} of biomass to about 13 MJ kg^{-1} of tar [68].
To maximize tars production, biomass is subjected to a rapid temperature rise, 1000 to 10000 °C s^{-1}, to a maximum of 650 °C, in an oxygen-free reactor vessel.

---

[2] Phenolic compounds are composed of one or more hydroxyl groups (-OH) linked to an aromatic hydrocarbon, that is a benzene-like organic compound.
In the figure: the phenol molecule, C_6H_5-OH, the simplest phenolic compound.

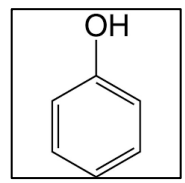

Fast cooling is then necessary to limit further conversion of liquid products to gas. This pyrolysis type is called *fast pyrolysis.*

Short-chain noncondensable gases, mainly CO_2, CO, CH_4, ethane (C_2H_6) and ethylene (C_2H_4) are called **pyrolysis gases**. These are combustible gases that can be used for thermal energy production or can be burned in the reactor for self-sustaining pyrolysis. Noncondensable gases are generated both during the first stage of devolatilization (primary gases) and during the second stage (secondary gases). Secondary gases originate from the further cracking of condensable vapors composed of long-chain molecules under high temperature conditions. The LHV of primary gases is near 11 MJ $(Nm^3)^{-1}$; after a severe secondary cracking of the vapor, gases reach 20 MJ $(Nm^3)^{-1}$ [68]. To maximize the gaseous products, therefore, high temperatures and high conversion times are required: the process is very different from *fast* pyrolysis. Pyrolysis is hardly used for syngas production since dirty gases are produced and the energy balance is often inconvenient. The most suitable technologies for this purpose are *flash pyrolysis* and *ultrafast pyrolysis.*

Finally, the solid product is **char**. For char production, the most suitable technology is *slow pyrolysis*, which is very similar to the "historical" carbonization of wood. The conversion time is the longest among all types of pyrolysis. The goal is to obtain a pure char, consisting mainly of carbon, giving the time needed to convert most of the condensable pyrolysis vapors into secondary gas or char. The char obtained has low residual of polycyclic aromatic hydrocarbon (PAH). *Slow pyrolysis* takes place in total absence of oxygen, the heating of biomass is slow, and the temperature are about 400/600 °C. The LHV of char from *slow pyrolysis* is about 32 MJ kg^{-1} [68].

5.2.3 Parameters of pyrolysis processes

Pyrolysis can be carried out using different types of reactors, including fixed-bed and fluidized-bed, similarly to gasifier reactors [69]. Fixed-bed reactors are the simplest and most common type of reactor used for pyrolysis: the stationary bed of biomass is heated from below. Fluidized-bed reactors are more complex and involve the use of a fluidizing medium, such as sand or ash, to suspend the biomass particles in the reactor and convert it.

As mentioned above, an initially classification of the pyrolysis process is *slow pyrolysis* and *fast pyrolysis*. *Slow pyrolysis* involves heating the biomass at a relatively low temperature, typically between 300°C and 500°C, for a long period of time, up to several hours. This process produces a high yield of char and a low yield of liquid and gas products. *Fast pyrolysis* involves heating the biomass at a high temperature, between 400°C and 600°C, for a short period of time, usually in the order of seconds/minutes. This process produces high yields of liquid products and a low yield of char and gas. Other types of pyrolysis for bio-oil production (up to tars yield of 75% of total products) are *Flash pyrolysis* and *Ultrarapid pyrolysis*.

Since the pyrolysis process and its products yields depend on several factors, further potentially classification is:

- the type of biomass
- the heating rate
- the residence time
- the final temperature reached.

The type of biomass affects the yield of final products. The content of cellulose, hemicellulose and lignin is the main parameter, along with the hydrogen to carbon (H/C) ratio. Cellulose and hemicellulose are the two components that generate the greatest amount of condensable vapors and, therefore, tars. Hemicellulose also originates a fraction of noncondensable gases. Decomposition of these fractions begins around 200°C for hemicellulose and from 300°C for cellulose. Lignin decomposes from 280°C to 500 °C. Since it consists mainly of aromatic compounds, it is the fraction that generates char.

Heating rate is an important parameter for selecting the type of final product. High heating rates shift production to large amounts of liquids; low heating rates shift production to large amounts of solids (char). However, the heating rate must be coupled with both the resident time and the achieved temperature [70].

Residence time, i.e. the time during which the biomass stay in the reactor, allows greater conversion of the condensable vapors (generated during the first stage) into final gaseous. Therefore, to maximize char low heating rates, maximum 2°C s^{-1}, and high residence times are required. To maximize bio-oil production, high heating rates and maximum temperatures of 600°C are required. To maximize gas production, an intermediate heating rates can be used but with very high final temperature, around 800°C [71].

Finally, the last control parameter is the maximum temperature reached by the biomass. Some pyrolysis temperatures are yet given above, reflecting the fact that all these parameters are interconnected. High temperatures lead to higher production of pyrolysis gas. This happens because the fixed carbon of the char combines with condensable products (due to high residence temps) and produces noncondensable gases. Low pyrolysis temperature produces high liquids [70,72].

Char products at different temperatures show different properties [73]. Char produced at high temperature, compared to a low-temperature char, has greater surface area, greater porosity, higher purity, greater crystallization of molecular structure, etc. Scientific research has shown that the benefits to the systems to which high-temperature char is applied (agriculture, industries, electronics, ...) are significantly greater, than the low-temperature char [74,75]. This issue is widely debated, and it is part of the discussion of this thesis. Therefore, please refer to the next Part for further discussion.

In Table 8 the parameters seen in this paragraph have been summarized. The last column reassumes the main product that is obtained using the conditions contained in the row.

Finally, it is important to underline, as also previously mentioned, that pyrolysis has the potential to play a significant role in the transition to a more sustainable future, but further research and development are needed to adapt the process to the needed of this century (renewable energy, carbon storage, fight against climate change, …) and overcome the challenges associated with the technology.

Table 8. Comparison of parameters governing biomass pyrolysis according to the technology typology. Adapted from [38].

Pyrolysis typology	**Max temperature**	**Heating rate**	**Residence time**	**Principal products**
Slow pyrolysis	> 400 °C	Very low (~ 2/3 °C s)$^{-1}$	~ hours	Char
Fast pyrolysis	~ 500 °C	Very high	< 2 seconds	Bio-oil
Flash pyrolysis	< 650 °C	High	< 1 second	Bio-oil, tars and gas
Ultrarapid pyrolysis	~ 1000 °C	Very high	< 0.5 second	Tars and gas

Figure 5-7. Evolution of cork subjected to pyrolysis in the absence of oxygen, processed through a small vessel laboratory pyrolizer. The progress of biomass conversion, from the left to the right, can be observed.

6 Biochar

Char produced by both pyrolysis and gasification has used for several centuries for different application (see Chapter 1). In recent years, due to a growing interest, hydrothermal carbonization (HTC) has also been added to the investigated technologies for char production. In this work HTC will not be considered. Char from gasification and pyrolysis, instead, will be treated in depth. From this point on the term "pyrolysis" will refer exclusively to slow pyrolysis.

Slow pyrolysis, thermal conversion of biomass in the absence of oxygen at moderate temperatures and long residence times, has been identified as the most effective for high char yields: moderate temperatures and long residence times allow for good, but not complete, biomass conversion. However, in the pyrolysis process, the char yields are more important than the char quality [76]. Gasification, on the contrary, was born for syngas production and char is therefore only a by-product. The yield of char from gasification may vary depending on operating conditions, but the product has high stable carbon content, low impurities or residues and particular molecular structure. Gasification char is important for the quality, leaving the yields in second place [77].

6.1 Introducing biochar

Char is known in scientific literature both in the field of soil sciences and in the field of carbon storage as **biochar**. Since *coal* or *charcoal* refers purely to the material used as fuel (for energy production, in industry, for cooking purposes, in iron production, ...) and *char* is often related to combustion residues (e.g.: forest wildfires), The scientific community wanted to assign a specific term to carbon products that are voluntarily applied to the soil to improve characteristics. The term chosen was *biochar* to combine the well-known term *char* with the term *bio*, from the Greek βίος meaning "life." Among the first to ascribe this name to char were Lehmann, Gaunt and Rondon in the early 2000s [78].

Biochar is a fine-grained charcoal high in organic carbon and largely resistant to decomposition. It is produced from pyrolysis of plant and waste feedstocks. As a soil amendment, biochar creates a recalcitrant soil carbon pool that is carbon-negative, serving as a net withdrawal of atmospheric carbon dioxide stored in highly recalcitrant soil carbon stocks. The enhanced nutrient retention capacity of biochar-amended soil not only reduces the total fertilizer requirements, but also the climate and environmental impact of croplands. IBI definition, [79].

Figure 6-1. A famous and important photos comparison from the study of Glaser et Al. (2001) showing the profile of the "terra preta" and the profile of a nearby soil (oxisol soil). The depth of the hole is the same [80]

Application of biochar to soils is not a 21st century idea. In fact, the most important research on biochar concerns Amazonian dark soils, known as "terra preta de índio". "Terra preta" refers to soils that were mixed with high amounts of carbonaceous materials by the Indigenous peoples of the Americas before the discovery of America. These peoples probably, initially noticing an increase in vegetation growth in the area where fires residuals were disposed, began intentionally adding charcoal to the soils to make fertile the poor soils. Depth of application, Figure 6-1, and the wide area in which "terra preta" was finding, allow us to affirm the intentionality of this practice [81]. High amounts of carbon (which is too much higher to be explained only by plant carbon fixation potential) applied in the form of biochar before the 1500 A.D. persist today, testifying the stability of this carbon type over many years.

Over time, the term biochar has been slowly extended to all char used in applications with environmental benefits. Today the term biochar is also used for materials (of pyrolytic or gasification origin) that are used for new purposes: filtration, electrical and electronic applications, new building materials, insulation materials, etc.

The real innovative idea of this century is the integration of biochar into environmental issues. First, the coupling of biochar (capable of maintaining its stable carbon molecular structure for a minimum period of one hundred years [82]) to the concept of carbon sink. This coupling has been proposed since the earliest discussions of biochar in the scientific literature. Research immediately followed in parallel two important issues: a) verification (experimental and theoretical) of the benefits brought by biochar to soils and to agricultural crops; b) the potential of carbon capture and storage in soils or other long-term applications, for the fight against climate change [83,84]. In addition, c) biochar has always been seen as a "tool" for the recovery of waste biomass, that to date are still little exploited. Innovative research are paving the way for new possibilities for waste treatment and management with biochar. Finally, d) biochar is linked (even if only with certain technologies) to the production of energy from renewable sources.

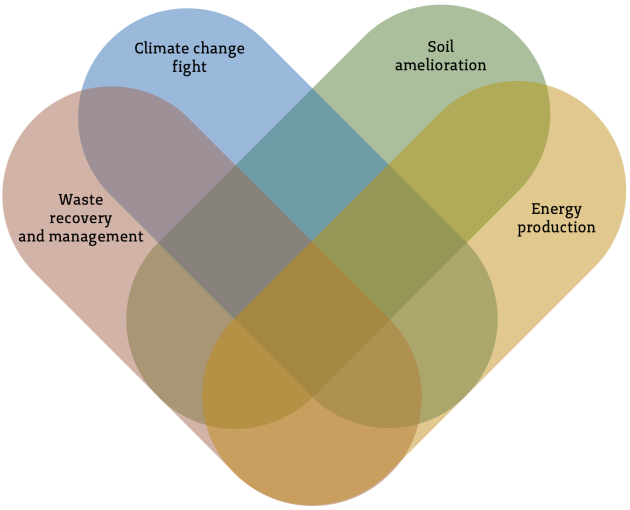

Figure 6-2. All the areas that the biochar links. Areas that are called upon again and again in the 21st century: from IPCC reports, through UN 2030 Agenda, to the national policies. Adapted from [84]

Biochar is as a charcoal composed of small grains whose shape is similar to the shape of the original piece of wood, with smaller volume. Since the biomass is usually chipped or shredded, also biochar has small size and wide grain size distribution (from a few μm to a few cm). Furthermore, the extraction method from the reactor may change the size and shape of biochar grains, often reducing the grain size. Three different grain sizes of biochar are shown in Figure 6-3.

a) Fine biochar

b) Biochar as it leaves the gasifier

c) Coarse biochar

Figure 6-3. Some samples of biochar with different grains dimensions and different particle size distribution: from fine grains, a), to coarse grains, c).

6.2 Composition of biochar

Biochar can be composed of up to 90 % carbon depending on the starting biomass, production methodology and temperature. In Table 9 a summary of the characteristics of some biochar.

Table 9. Summary of some biochar from the scientific literature: the different technologies used, and different carbon contents are reported. Adapted from [85].

Feedstock	Temperatures	Type of technology	Residence time	Carbon content	Source
Bamboo	500 °C	Pyrolysis	-	84%	[86]
Pinus taeda	1000 °C	Pyrolysis	15 minutes	92%	[87]
Straw	700-750 °C	Gasification	-	48%	[88]
Pine sawdust	650 °C	Pyrolysis	-	87%	[89]
Pine wood	1200 °C	Gasification	-	65%	[88]
Wood chips	1200 °C	Gasification	up to 90 minutes	81%	[90]
Papermill waste	550 °C	Pyrolysis	-	52%	[91]
Prune residues	500 °C	Pyrolysis	-	23%	[92]

The carbon (C) in biochar is predominantly present in its **aromatic form**, that is compounds in which six C atoms are bonded together in a ring form, called "aromatic rings". However, some C atoms can be bonded to other atoms, usually oxygen (O) and hydrogen (H), forming the so-called aromatic

compounds. *Benzene*[3] is the simplest aromatic compound. If C atoms are bonded only to other C (not to H or O) and the rings are arranged in a layered structure, graphite emerges.

During formation, biochar does not reach sufficiently high temperatures or adequate pressures to reach the graphitic structure, but it stabilizes in an intermediate structure. In this structure C atoms have failed to fully re-order themselves and some aromatic rings are bound to other elements. These compounds are called polycyclic aromatic hydrocarbons (PAHs). PAHs are molecules of C-O-H (hydrocarbons) composed of two or more aromatic rings bound together (polycyclic aromatics) in a flat structure.

6.2.1 Biochar formation process

During pyrolysis of biomass, the following processes take place [84,93]:

1) C is present in woody biomass in the form of **aliphatic** chains**. Aliphatic chains** are molecular chains, sometimes long chains, in which C atoms are bound to H atoms both in linear and branched structure, but not in rings. Alkanes, alkenes, and alkynes are among the most famous compounds: CH_4 is the simplest one. As the temperature of the pyrolysis process increases, **aliphatic** carbon chains are broken and converted to **aromatic** C rings**.** During this conversion some **intermediate products** are created, the PAHs (e.g., acetone, benzene, and toluene): some of PAHs will be converted during the process, others remain as-it-is until the process end.
2) With further increase in temperature, > 270°C, and in function of the residence time, part of the aromatic C combines with each into aromatic carbon portions, originating **aromatic planes**. These aromatic planes of different sizes are connected by aromatic rings or aliphatic chains and originates **interconnected carbon planes.** The complex structure of interconnected carbon planes is called ***fixed carbon***.
3) **Intermediate products** that do not convert and remains trapped between the planes of the fixed carbon, take the generic name of volatile organic compounds (VOCs). These **VOCs** (including PAHs) are considered the ***labile carbon*** fraction [94].

---

[3] Benzene is composed of 6 C atoms bonded to 6 H atoms, with the brute formula C_6H_6 . The bonds are equidistant from each other. Benzene at room temperature is liquid.
In the left figure: benzene ring. In the right figure: benzene ring in the most commonly used representation (proposed by Kekulé):

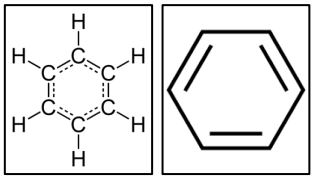

Figure 6-4.b graphically explain the process described in the previous bulleted list.

The proportion of ***fixed carbon and labile carbon*** depends on pyrolysis or gasification conditions, heating rate, maximum temperature reached, and residence time. The quality of the feedstock and its proportions of lignin, cellulose and hemicellulose, as well as the inorganic compounds in the biomass (ashes) are also not negligible. In general, biochar produced at high temperature contains a low proportion of **aliphatic carbon and VOCs** and a high proportion of **aromatic carbon** due to the higher energy received during conversion.

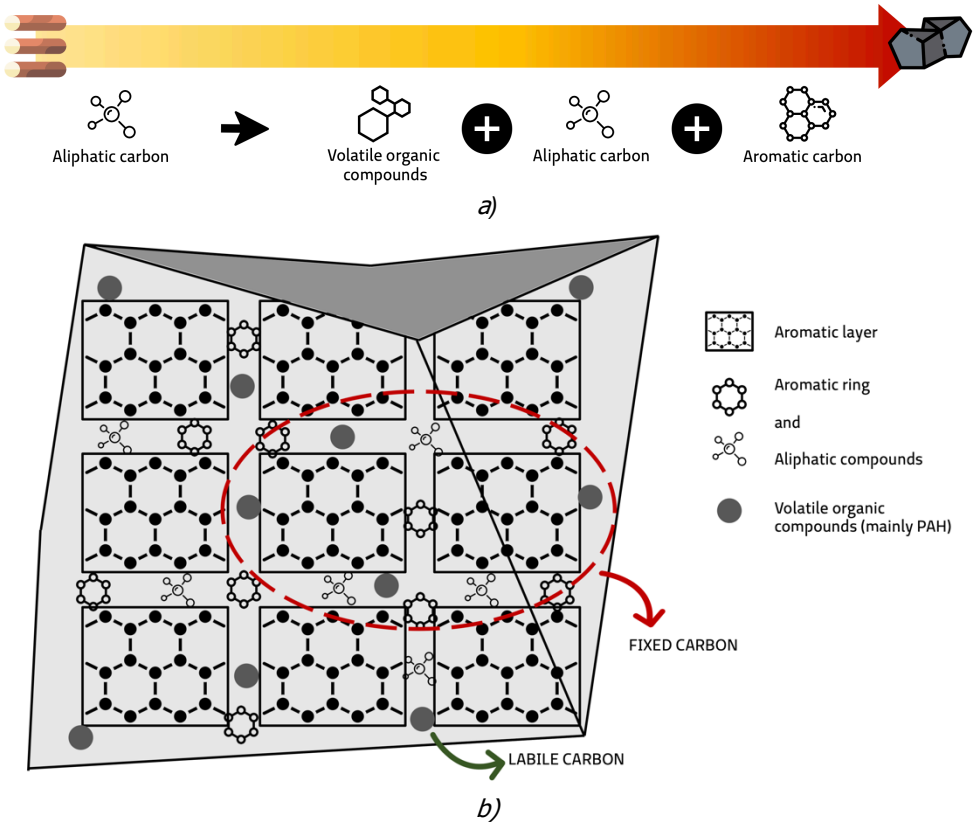

Figure 6-4. Steps of biochar formation, at the atomic and molecular level, as a function of temperature (a). Schematization of the molecular structure of biochar in which the infeasibility of total conversion to carbon layer is highlighted (b).

Therefore, it is possible to identify two types of carbon in biochar: **stable or fixed carbon** (i.e., aromatic carbon) that hardly decays or degrades; and **labile carbon** (i.e., aliphatic carbon or others volatile compounds) that degrading or being subject to leaching. Compared to the carbon in woody biomass, the carbon in biochar is present in high percentages in the aromatic fraction. Reason why it does not degrade as biomass degrades. Quantifying the **aromatic fraction** present in biochar identifies the amount of fixed carbon.

The nature of the different C structures and the proportion of stable-labile C establishes the stability of biochar [95].

6.2.2 Aromatic fraction (fixed carbon) of biochar

To understand how biochar can be a carbon storage tool, it's necessary understand why the fixed carbon fraction remains stored in biochar for a long time. During the conversion from lignocellulosic to carbonaceous structure, several transformations take place and atoms re-organize into new molecules. The Figure 6-5 is probably the most famous figure in the scientific literature related to the molecular structure of biochar [96].

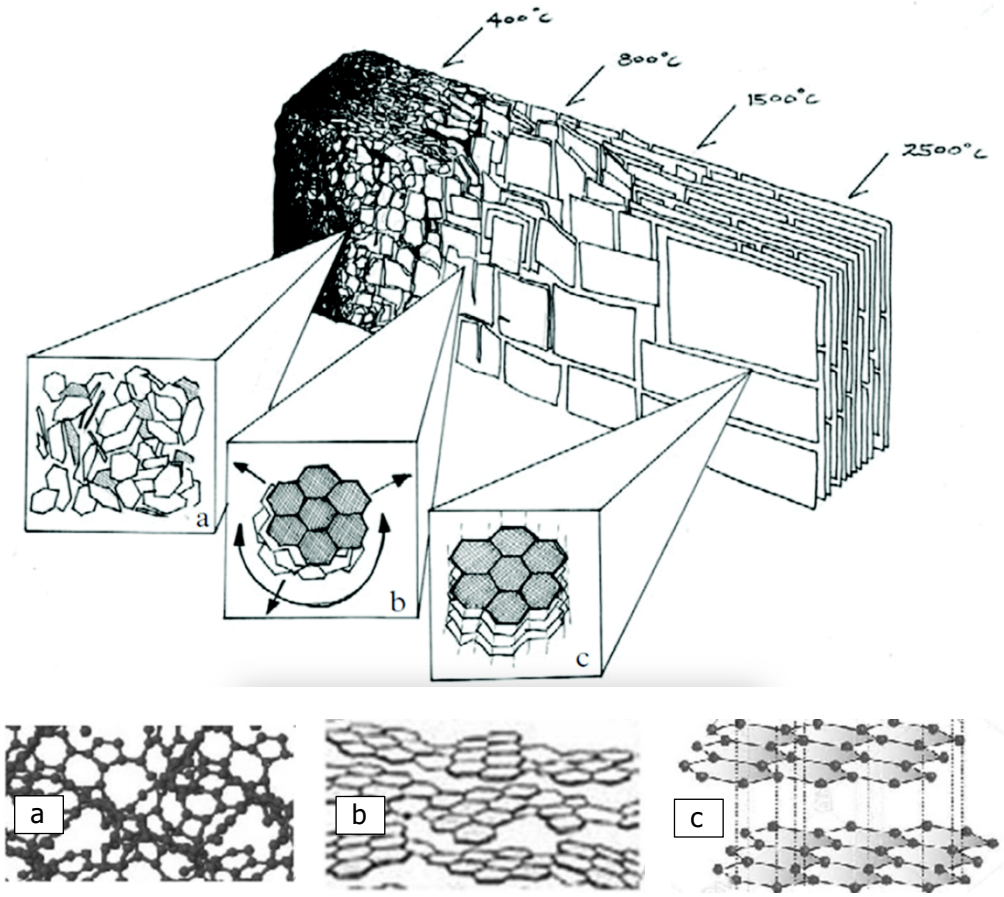

Figure 6-5. Ideal structure of biomass-to-biochar, from low temperature treatment to high temperature treatment. a) low temperature: large fraction of aromatic C, but high disordered in amorphous mass; b) layers/sheets of aromatic carbon connected each other's, but turbostratically arranged, c) graphitic like structure with good order in all the three dimensions [73,96].

The aromatic C in biochar is present in two structures: amorphous and crystalline. Biochar, because it is produced at relatively low temperatures, has a predominantly amorphous structure, meaning there is no long-range order in the positions of the atoms/molecules of C and of the other elements in biochar, Figure 6-5.a.

At the same time, however, the biochar has locally crystalline spots. In these crystalline spots, the re-organization of atoms has originated a rigid structure with a well-defined spatial shape. The spots are composed of stacked aromatic layers. Each layer is **graphene** since it is formed of aromatic rings bound together in planar structures. These layers are arranged turbostratically. Turbostratic structures layers not aligned with each other, but they are rotated, randomly, with each other, Figure 6-5.b. Some examples of turbostratic structures are shown in Figure 6-6.a. Generally, turbostratic structures can be defined as amorphous solid structures that exhibit spots of crystal of graphene.

Figure 6-6.a and Figure 6-6.b compare graphene in turbostratic structures and graphitic-like structure.

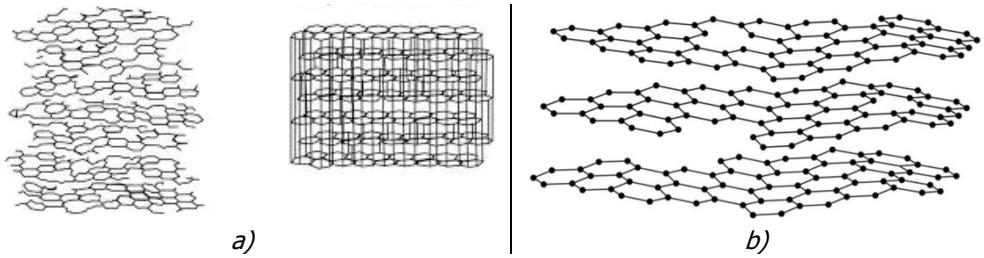

Figure 6-6. a) comparison between a turbostratic structure on the left and a graphitic-like structure on the right; b) another representation of an amorphous turbostratic structure [97]

These crystalline spots are also called **clusters or nanoclusters** and they are the structures that make biochar electrically conductive.

The other elements that complete the composition of biochar are aliphatic compounds and "isolated" aromatic compounds not organized into complex structures. As the temperature increases, new carbon atoms or aromatic rings are included in the clusters, enlarging the graphene layers and the crystal structures, bringing the biochar closer and closer to a graphite structure. The necessary energy to reach a graphite structure, however, is very high: only at high temperatures (over 3500 °C) could total conversion of biochar in graphite be achieved, Figure 6-6.c [84]. Therefore, the structure of biochar is often defined **graphitic-like structure**.

The increase of the crystal fraction in biochar leads to an increase in biochar pores (both open and closed; at the micro/meso/macro scale) since more and more C atoms reorganize itself in solid structures and the more and more volatile compounds are released (e.g., O and H).

6.3 Stability of biochar

It is known in the literature that the molecular structure of biochar explains its carbon storage capacity. In recent years, however, attention has shifted to the long-term stability of biochar, especially when it is applied to soil. Low erosion, low leaching and low degradation by the external environment results in prolonged time storage [98,99]. Since biochar was historically applied to soil and the soil is "living matter", the discussion of biochar stability most often is referred to the degradation by the soil microbiota [100,101].

Chemical stability of biochar means low willingness to release the chemical elements. C is a source of energy for microorganisms, as well as other organic and inorganic elements. If these elements are not readily exploitable, biochar degradation does not occur. However, the more labile fractions of biochar can undergo fracturing or leaching, becoming usable by soil biota: this operation is called mineralization [84,102]The phenomenon of biochar degradation is also known as biochar aging. By applying biochar to soil, **aliphatic carbon and VOCs** (labile C fractions) are gradually mineralized by microorganisms. Since the **aliphatic fractions** connect the **aromatic layers** (see Figure 6-4), this natural decomposition causes the separation of the **fixed C aromatic fractions** from the frame. This phenomenon leads to grain disintegration [94]. The surface of these **disconnected fractions**, in contact with the soil, tends to oxidize and develop functional groups (e.g., carboxyl and hydroxyl groups) in the break points. Functional groups facilitates both interaction with microorganisms and formation of links with minerals, nutrients and soil contaminants. A "biofilm" is slowly created on the surface, while the inner part of the biochar remains stable. Oxidation and biofilm formation are relatively slow at room temperature, but they are facilitated by high temperatures [103].

As the fraction of fixed C in biochar (crystals, aromatic layers, ...) increases, the degradation and consequent fracturing decreases. And the stability of biochar increases. To evaluate this ability of biochar to non-degrade, called **recalcitrance**, some parameters have been identified.

1. O:C ratio. The higher is the C content over O content, the greater is the stability in soil.
   In terms of numbers, a molar ratio of O:C < 0.2 ensures a 1000-year of biochar half-life[4] [101].
2. R50 (Recalcitrant Index). Designed to determine the quality of biochar in terms of carbon sequestration, it expresses the stability of biochar

[4] Half-life time is the time required for a quantity to reduce to the half of its initial value. The mass of biochar is the factor here considered.

compared to stability of graphite. It assumes that more recalcitrant biochar requires more energy to be oxidized or mineralized. Therefore, the greater this energy, the greater the potential storage of CO_2. By comparing the amount of energy required to oxidize a known mass of different biochar, normalized to the energy to oxidize the same mass of graphite, a scale was defined to quantify the storage capacity of CO_2. In R50, soil contact is not considered, only oxidation energies are evaluated.

Evaluation of the stability-recalcitrance of biochar in soils is also of primary importance in calculating the stored equivalent carbon dioxide (CO_2eq) and the resultant carbon credits. The reference for recalcitrance and permanence in soils is normally considered to be 100 years. This value, initially fixed by the Kyoto Protocol, corresponds to the time frame in which policymakers have influence on the living population and it is an appropriate period to observe the effects of actions taken at "time 0" [104,105]. Biochar respects this time horizon since the fixed-C remaining in the soil for even longer periods (up to 1000 years) [106,107].

Methods for evaluation of stability, devoted to the topic of carbon removal, have emerged over time. In this work, VERRA standard will be used for quantification of C storage. The main formulas on which the calculation is based are given in Appendix F.8. Carbon footprint and carbon credit revenue (VERRA standard) [46]. Below is a brief preview of the simple ideas on which it is based.

3. Adjustment Factor. The factor used by VERRA, PR_{de}, evaluates the decay of biochar and estimates the amount of fixed C that remains in the soil. In general, 0.74 is considered a conservative value. It is otherwise possible to choose from some tabulated values depending on the production methodology used:
   - 0.89 - pyrolysis or gasification at high temperature, > 600 °C
   - 0.80 - for medium temperature pyrolysis, 450 - 600 °C
   - 0.65 - low-temperature pyrolysis, < 450 °C
   - 0.56 - pyrolysis at unknown temperature.

   The PR_{de} factor multiplies the mass of biochar $M_{y,t}$ [kg] and the C content [w/w or %] FC_p (from CHNS(O) analysis or tabulated values). The computation returns the total stored carbon in mass, (6-1):

$$CC_{y,t} = M_{y,t} \cdot FC_p \cdot PR_{de} \qquad \text{[kg]} \qquad (6\text{-}1)$$

6.3.1 Role of temperature: "high temperature" and "low temperature" biochar

As seen in paragraph 6.2.1 and 6.2.2 the temperature at which the biomass is treated plays a key role in the formation of the biochar structure. In paragraph

6.3 the recalcitrance of biochar was analyzed, identifying a direct dependence with temperature. Indeed, the higher is the process temperature, the more C is re-organized into amorphous or crystalline structures and the higher is the recalcitrance of biochar [108]. As proof of this, the VERRA standard proposes maximum values of its Adjustment Factor for processes (pyrolysis or gasification) at high temperatures, > 600 °C.

It is therefore possible to assume that biochar can be classified into two categories, **high temperature biochar** and **low temperature biochar**, identifying 600°C as the separation temperature [109]. At about 400°C nanoclusters begin to be created, although they are still dispersed in the biochar mass and integrated into the amorphous carbon. At 600°C, however, the nanoclusters begin to enlarge. At this stage the biochar also begins to be **electrically conductive** due to a high crystalline fraction. This new characteristic is also considered an important parameter for evaluating the recalcitrance. Between 610 °C and 1000 °C, there is a noticeable increase in electrical conductivity, reflecting the fact that the clusters have increased in volume and got closer reaching high degrees of crystallinity [110]. The production of biochar at high temperatures makes biochar a **stable graphitic-like carbon material**.

In addition to generating biochar with high porosity and high surface area, the crystalline structure makes biochar electrically conductive and thus able to transfer electrons at high rates [111,112].

Confirming that temperature is one of the key parameters (perhaps "The parameter") for producing biochar of high quality, high temperatures reduce the risk of condensation of tars both on the surface and inside the porosity, producing a char with low PAH content. In contrast, this phenomenon is very common in the low temperature biochar.

In the following paragraphs, the characteristics of biochar will be explained in detail, giving attention to the difference between low temperature biochar and high temperature biochar, referring to the latter as gasification product. This choice is justified by two factors:

- biochar from gasification is produced at temperatures much higher than 600 °C (close to 1000 °C, see 5.1.1.3) and it is traversed by hot syngas that extract the tars
- gasification is an auto-thermal and self-sustaining process. Alongside the production of biochar, there is thermal and electrical energy production that can generate economic profits.
  In pyrolysis, on the other hand, heat must be supplied from outside: the higher the temperatures requested, the higher the energy (and economic) cost of the process.

7 Characteristics, applications and improvement of biochar

7.1 Characteristics of biochar

Biochar, in addition to its elemental composition - the most important element is C - has many different and highly interesting intrinsic characteristics: from porosity to water retention capacity, from cation exchange capacity to electrical conductivity, from bulk density to pH value. Each type of biochar may have some characteristics that are more marked than others, depending mainly on the starting biomass and the production process.

In the following paragraphs, some of these characteristics will be explored in more detail. Much research has been carried out on the properties of biochar, and there are still many unknown and under-investigated aspects: some studies contradict each other; other studies attribute the same effect or characteristic to two different reasons; other research investigates biochemical interactions between biochar and the external environment, while others stop at the macroscopic level. Biochar is a complex topic. Therefore, it is not intended to carry out a review of the characteristics of biochar, but merely to provide the main notions necessary for understanding this work.

There are other extrinsic characteristics, such as grains size, grain size distribution, or spatial distribution of grains in soil after biochar applications, which influence the intrinsic characteristics or add new properties to the complete system.

7.1.1 Ultimate composition and carbon content

Total C, O and H contents in the biochar are probably the first information to know about a type of biochar. The stable and labile fraction of C is then equally important to study its recalcitrance. The O and H contents are necessary since these are the elements that make up the labile part of the biochar.

The most common analyses are the so-called "ultimate analysis" that identify C, N, H, S and O according to the standard ASTM D1762-84. Quantification by gravimetric methodology of ash (inorganic elements, e.g.: calcium and potassium) and moisture content also follows this standard. N and S are elements usable by soil biota, but they are not interesting for biochar classification.

The fraction of labile C and stable C is often difficult to measure. Some tests proposed to calculate labile C are based on thermal extraction or dissolution methods, and do not integrate biological decomposition. Therefore, it is common to use total C content as parameter to compare different biochars, see Table 9.

The C content also depends on the temperature at which the biochar is produced. Figure 7-1.a shows the classification based on total C proposed by

Lehmann and Joseph (2009): the higher the process temperature, the higher the content of total C in the biochar. In Figure 7-1.b and Figure 7-1.c, instead, some biochars are classified by the H/C and O/C molar ratio. Both studies report that high temperature biochar present low H/C and low O/C ratio: higher is the process temperature, lower are these ratios. Since O/C < 0.2 implies biochar stability (as reported in paragraph 6.3), and H/C < 0.7 means a greater fused aromatic ring structures [79], high temperature biochars are more recalcitrant and more suitable for carbon storage than low temperature biochars.

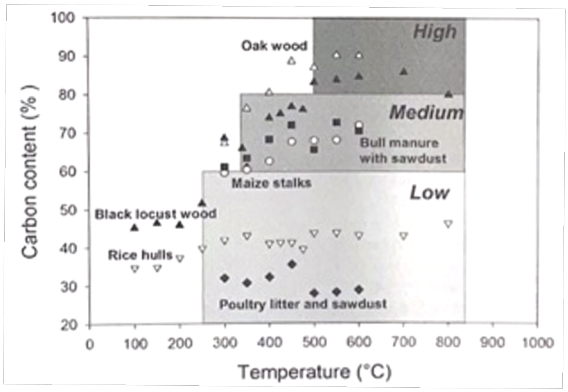

a)

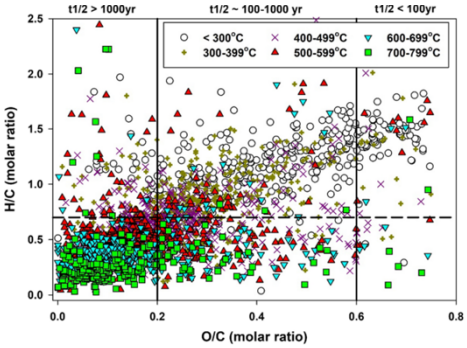

b) [113]

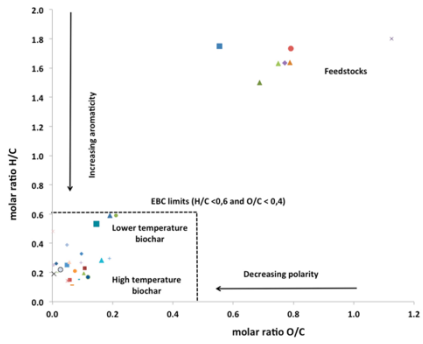

c) [114]

Figure 7-1. Classification prosed in Lehmann and Joseph (2009). It is evident the correlation between high temperature and high total C content in biochar. Data are from [115]*. Interesting data from a review study (a) and a research study (b) on different biochar produced at different temperatures. The correlation between high temperature and low and very-low H/C and O/C ratios is clearly identified. Low ratio values mean high total C and high biochar recalcitrance.*

7.1.2 Porosity

Porosity is probably the most well-known characteristic of biochar. As also repeated in previous paragraphs, the internal molecular structure of biochar, and its formation process, determines the porosity and surface area [78]. The porosity of biochar is formed for two reasons: a) the initial dehydration of

biomass and the release of volatile components from cellulose and hemicellulose contribute to create a fraction of pores [116], b) the subsequent development of the graphitic-like structure of the C atoms [117]. High temperature, therefore, plays a key role.

Pores can be classified into three groups (IUPAC classification): micropores: <2 nm; mesopores: 2 - 50 nm; macropores: >50 nm. Leng et Al. (2001) [118] reports that the total pores volume for biochar are commonly $0.016 - 0.083\ cm^3\ g^{-1}$, reaching $0.25\ cm^3\ g^{-1}$ when quality biomass is used [119]. With chemical post-treatment, biochar becomes similar to activated carbon, having up to $1.772\ cm^3\ g^{-1}$ of total pore volume. However, this latter fabrication is not a self-sustaining process since require energy-intensive industrial processes.

Generally, micropores (around $0.012 - 0.060\ m^3\ g^{-1}$) and mesopore (around $0.007 - 0.020\ cm^3\ g^{-1}$) are predominant in biochar. Figure 7-2 shows the results of a review of many biochar samples, from different biomasses and from different temperatures. First, biomasses with high lignin-cellulosic content - Figure 7-2.a and Figure 7-2.b - achieve higher porosity than lower quality biomasses - Figure 7-2.c. Moreover, the trends clearly show that porosity (total pore volume) increases significantly as temperature increase. Biochar produced from nobler biomass (e.g., poplar wood, maple wood, bamboo and the palm kernel shell) at low temperature has low porosity, which then increases with rising of the temperatures. There are some exceptional cases: some types of biomasses, for example pine sawdust and cotton stalk, produce low porosity biochar both at low and at high temperatures. Other biomasses are not suitable for pyrolysis or gasification.

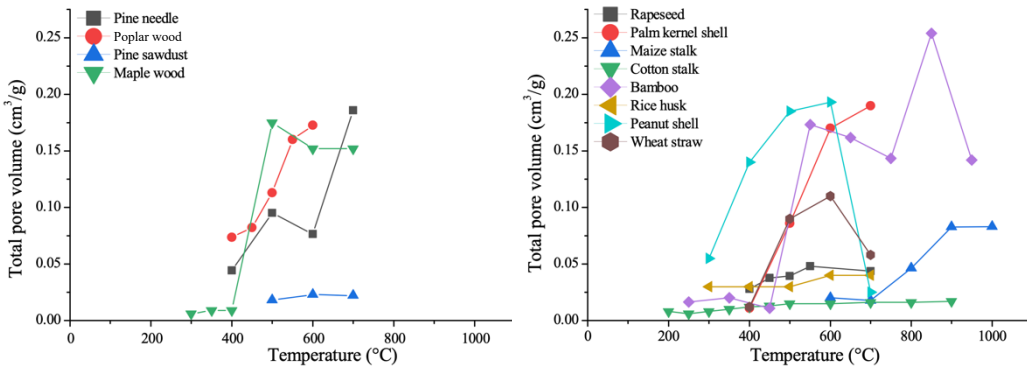

a) *b)*

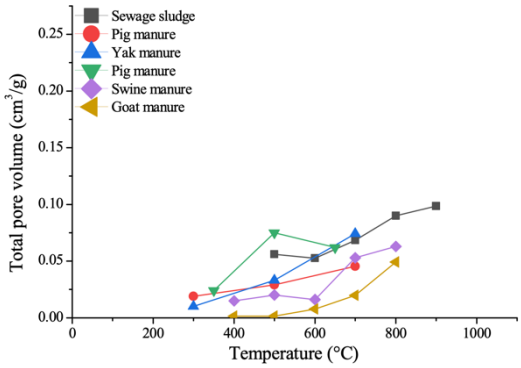

c)

Figure 7-2. Porosity - production temperature relationship of some biochar from (a) woody biomasses, (b) agricultural wastes and (c) manures. Graphs are from [118].

Generally, biochar from gasification exhibits high total pores volume. In the work of Fryda et Al. (2015) [114] some biochars are produced using greenhouse pruning through two fluidized bed gasifiers. They showed increasing porosity with increasing temperature: $0.069\ cm^3\ g^{-1}$ at 600 °C, $0.129\ cm^3\ g^{-1}$ at 750 °C (using a small gasifier); $0.140\ cm^3\ g^{-1}$ at 600 °C and $0.143\ cm^3\ g^{-1}$ at 750 °C (using a large-scale gasifier).

7.1.3 Specific Surface Area (SSA)

The specific surface area (SSA) is defined as the total surface area of a material per unit mass (e.g.: $m^2\ g^{-1}$). SSA is strictly connected with the porosity of the biochar and for this reason the topics exposed in paragraph 7.1.2 are also applicable here. Higher is the porosity in terms of pores quantity and pores dimension, higher is the SSA.

Typical values of SSA in biochar are in the range of $8 - 132\ m^2\ g^{-1}$. The value can reach $491\ m^2\ g^{-1}$ when good biomass is selected and with specific treatments after biochar production it can get up to $3263\ m^2\ g^{-1}$ (in the range of activated carbons).

SSA is measured through BET methodology (Brunauer-Emmett-Teller method [120]) which uses an inert gas and evaluates the adsorption of the fluid to the biochar surface. The method is recommended by the International Biochar Initiative guideline [79].

7.1.3.1 SSA and porosity: correlation with the temperature

Process temperature is again the main parameter influencing SSA [118]:

1. Up to 400 °C, biochar does not show a noticeable increase in SSA values compared to the starting woody biomass.
2. Between 400 °C and 500 °C, when crystalline nanoclusters begin to form and the VOCs evaporate, the number of pores and consequently SSA

begins to significantly increase. The eventually fracturing of biochar grains also generates SSA increase.

3. Above 500 °C, two different behaviors appear, depending mainly on the initial biomass:
    a. constant increase of SSA and of the total pores volume as temperature increases. Biomass with high lignin content falls into this behavior.
    b. decrease in SSA but increase in total pores volume, as temperature increases. Due to the high energy provided, the micropores enlarge and the structure becomes organized, generating new pores. Some pores connect with each other, resulting in an increase of total pores volume, but the "available" surface area decreases, resulting in an SSA reduction. Low-quality biomass (e.g.: manure) falls into this category.

Surface area and porosity are correlated also to other biochar characteristic. SSA is responsible for the efficiency of contact between biochar and external environment, determining high or low cation exchange capacity or electron transfer. Porosity, in particular open pores, and their interconnection are key factors for the biochar water retention.

7.1.4 Cation Exchange Capacity (CEC)

Biochar is known to retain nutrients, ions and metals (e.g.: minerals as Calcium or Potassium; Iron, ...) over time. Among the main reasons is the cation exchange capacity (CEC) [121]. The CEC is the total capacity of biochar or other material (called "exchanger") to retain exchangeable cations on its surface. Biochar has a high cation exchange capacity and has many negative charges on its surface: these properties increase the CEC of the soil in which biochar is buried [122]. Therefore, biochar with high CEC facilitates the exchange of nutrients: nutrients are generally positively charged elements (ammonium ion NH^{4+}, Magnesium - Mg^{2+}, …) which bind to biochar, reducing their leaching and remaining available to plants and soil biota over time.

As char aging increases the oxygenated functional groups (which act as electron acceptors or donors) on the biochar surface, CEC also increase [94,123]. Thus, CEC is closely related not only to the type of virgin starting biomass but also to SSA and porosity: high contact surfaces between biochar and soil, in fact, increase the CEC potential (measured in $[cmol^{(+)}\ kg^{-1}]$) [124].

Low temperature biochar CEC is very low, but it increases with the rise of process temperature. However, there is not a linear increase: once a certain temperature is reached, the CEC drops. High pyrolysis temperatures (> 500 °C) produce low CEC biochar probably due to the loss of negatively charged functional groups [84,125,126]. Therefore, for high-temperature biochar, CEC is not the main governing principle of biochar-soil interaction. This property is

exploited for soil remediation in polluted soils where biochar is used as an immobilizing element [111].

7.1.5 Water holding (or retention) capacity (WHC)

Closely related to porosity, water holding capacity (WHC) is one of the most interesting macroscopic characteristics of biochar. WHC measures the total amount of water (in mass or volume) that can be absorbed per mass or volume unit from the biochar: a 50 % WHC means, for example, that 100 g of biochar can store 50 g of water. Some biochar can reach a 400 % w/w of WHC.

Responsible for water retention are both porosity, particularly micropores and mesopores, and the interstitial spaces formed between grains [127]. Biochar, in fact, has a low bulk density[5] (from 0.27 to 1.30 g l^{-1}, due mainly to the initial biomass) and once it is applied to the soil it also reduces the soil density. Observing the whole matrix soil-biochar, several are the parameters that influence the WHC: carbon content, agglomeration, biochar particle size and porosity, biochar bulk density and final mixture bulk density, texture of the soil-biochar mix [128]. Biochar composed of both fine and coarse fractions have higher WHC capacity than small size grains biochar. However, some studies have shown that also the CEC, the SSA and the biochar charge affect WHC due to the presence of negative potentials on the surfaces [129].

To the remaining characteristics of biochar such as pH (biochar tends to be alkaline [130]), particle size, bulk density, etc., are not dedicated specific paragraphs. However, they will be mentioned in the paragraphs related to biochar applications.

7.1.6 Electrical conductivity

When we talk about the electrical conductivity of biochar, we must specify which effect we are referring to. Certainly, important is the presence in the biochar of salts (in the form of ions) that, once the biochar is applied to the soil, make the substrate more conductive. However, this concept is very limited both in the field of application (agronomic) and in the biochar quality (composition)

In recent years, more and more studies explore the electrical conductivity (EC) in connection with the biochar structure and the electron transfer through the biochar grains. In this paper we refer to EC with this meaning.

From an agronomic perspective, the use of biochar as a soil conditioner improves soil quality: it increases crop productivity, increases soil organic carbon

---

[5] Bulk density (or apparent density) of some biochar grains is the total mass divided by the total volume that grains occupy: grains volume + void between grains + volume of internal pore.

(SOC), improves soil water and nutrient retention, decreases soil erosion and depletion, reduces the need for fertilizers, and, most importantly, increases soil biota microbial activity [78,131–133].

In addition to creating the optimal conditions of temperature and moisture in the soil, stimulating the proliferation of microbial activity and harboring microfauna in the pores [102], some literature studies argue that the electron transfer facilitated by biochar is fundamental to explain the positive effects of biochar in soil [134].

Soil electron exchange is a key-parameter for geochemical and biochemical transformations in soil or other biological systems and governs the exchange processes between biome and nutrients in soil [72,135,136]: a) the oxidation reactions between species involve the transfer of electrons between these chemical species; b) the microbial biochemistry of soil involves reactions which require the transfer of electrons to or from micro-organisms (including bacteria and fungi). In the absence of some external mediation, microbes exchange electrons via microbial protein wires called *pili*, in a process called *direct interspecies electron transfer* (DIET), with no intermediators. However, this DIET is limited in the volume, in velocity and the amount of transferred electrons, in addition to the restriction in terms of contacts number [136].

Recent literature identifies **biochar's electron transfer and absorptivity** as being primarily responsible for the increase of microbes' activities. Biochar, interposed and in contact with soil species, facilitates the transfer of electron (e^-) and increases the rate and number of activities.

There are two mechanisms by which biochar contributes to electron transfer in the soil: *geobattery* and *geoconductor* [112].

- *Geobattery*. In the *geobattery* mechanism, biochar acts as a "site" where electrons can be easily exchanged. The biochar can modify its electrical charge according to the charge of the species it touches, behaving as both a donor and an acceptor of e^-: if the species is negative, the biochar becomes neutral or negative, and vice versa. Responsible for this behavior are the quinone aromatic-compounds[6] (functional groups) present on the surface, especially in the organic biofilm.

[6] Quinone organic-compounds are a class of organic compounds, usually derived from aromatic compounds, that exhibit high reactivity and capable of participating in both oxidation and reduction reactions. In this discussion we do not go beyond this brief definition. Figure show a "1,2-Benzoquinone" a quinone derived from benzene.

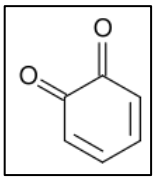

Geobattery is a moderately slow transfer mechanism: organisms receiving an e^-, must wait for "biochar recharge" before they can obtain a second electron from the biochar quinone.
This behavior occurs mainly in low-temperature biochar, see Figure 7-3.

- *Geoconductor.* In the *geoconductor* mechanism, the biochar acts as a "superconductor" for all the microbes and other species that are in contact with the grains. The biochar donates or receives e^-, significantly increasing both the number of pathways between microbes and the rate of e^- transfer. Also the DIET process benefits from this mechanism.
  Responsible for this behavior is the internal structure of the biochar, and not the external functional groups. The more ordered the structure, the more conductive the biochar is.
  This behavior occurs only in high-temperature biochar, see Figure 7-3, since the biomass structure has re-organized into graphitic-like structure (from 700 °C).

For a long time, biochar has been studied only in terms of *geobattery* (which can be associated with CEC), but cation/ion exchange alone does not explain the big improvements given to the biological system by biochar. Therefore, it is probably the high ability of biochar to easily transfer electrons, between different species, that is the real reason behind these evident improvements. With the theorization of the *geoconductor* mechanism more and more attention from the scientific community has been paid to the crystal structure of biochar and the relative electrical conductivity [112,137]. In the following section, the relationship between EC and biochar production temperature will be explored.

7.1.6.1 EC and High temperature biochar

The EC value is closely related to the atomic structure of the biochar and consequently to the thermal conversion process that transforms the biomass from dielectric wood to electrically conductive biochar. The reason is the re-organization of the structure into graphitic-like structures (graphene layers, nanoclusters and clusters). As the production temperature increases, the EC value of biochar will tend to the EC values of graphene, in the range of 103 S m^{-1} [138]. Thus, EC value allows to assess the quality of biochar in terms of stable carbon fraction [84,110].

The geoconductor mechanism occurs only for high temperature biochar thanks to the structural characteristics. As reported in Figure 7-3, adapted from Sun et al. (2017) [112], there is an increase in electron transfer as temperature increases. The three areas identify the three ranges in which the different mechanisms occur:

- at low temperatures, the main mechanism governing electron transfer is geobattery;

- in the 600-700 °C range, the first crystals begin to form in the biochar structure (see paragraph 6.2.1) and the electron transfer rate increases, facilitated by the co-presence of both mechanisms;
- at high temperatures (> 700°C) the geoconductor mechanism dominates and the electron transfer reaches very high level. This behavior occurs even though in high temperature biochar the functional groups are lesser than in low temperature biochar: this confirms that the conversion of C atoms into crystalline structures is more important than biochar aging processes. In addition to geoconductor behavior, at high temperature biochar acts like a "small capacitor" by storing electrons and balancing reactions, even when reactions are not balanced in terms of the number of exchanged e^-.

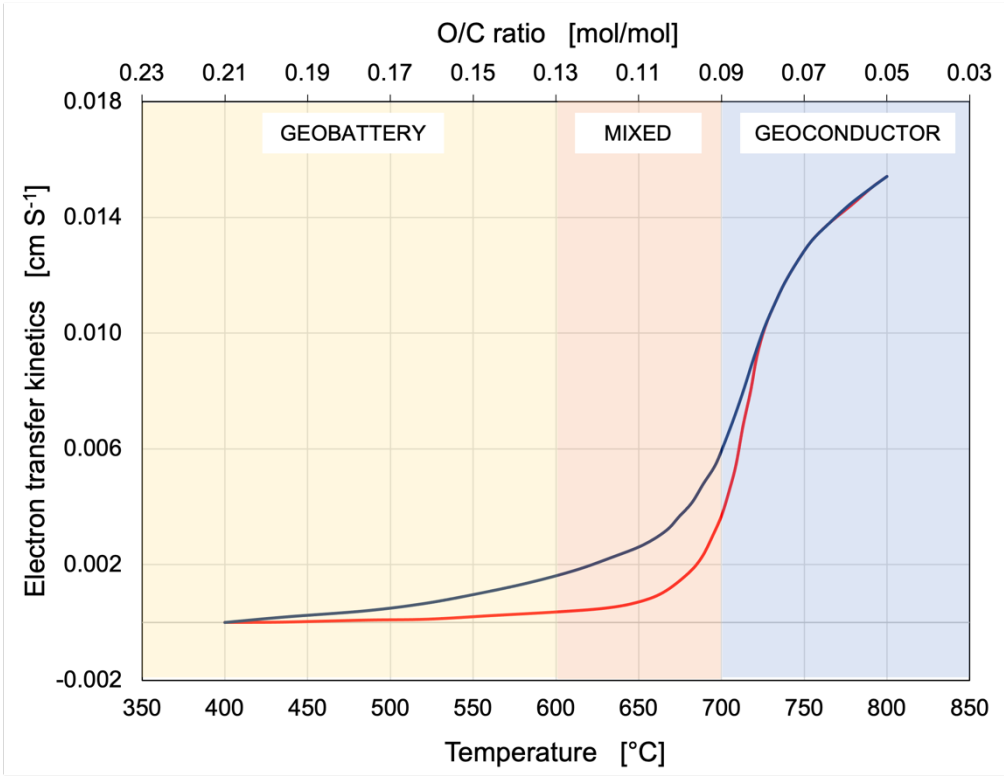

Figure 7-3. Electron transfer kinetics correlated to the temperature of biochar production. The three different areas represent the range of temperatures in which the geobattery and geoconductor mechanisms respectively handle the electron transfer. The two curves represent the upper limit of uncertainty (blue curve) and the lower limit of uncertainty (red curve) of the electron transfer value. Adapted from [112].

Consequently, the electron transport in soils thanks to biochar addition is radically enhanced only when the biochar is a high-temperature biochar. Thanks to the *geobattery* mechanism and especially thanks to the *geoconductor*

mechanism, biochar is a solution to make electron exchange more efficient in soil, making significant improvements and enhancements to the proliferation of soil microorganisms. As a result of the above, highly crystalline biochars are the ones that provide these improvements: biochars from gasification and high-temperature pyrolysis are therefore the most suitable for these applications.

"Microorganisms need electrons for everything they do. If they consume nutrients or spew out methane or expel carbon dioxide -- for any living, biological process -- they need electrons."

T. Sun

"Previously we thought there were only low-performing electron pathways in the soil - and now we've learned the electrons are channeled through soil very efficiently in a high-performing way,"
J. Lehmann

[139]

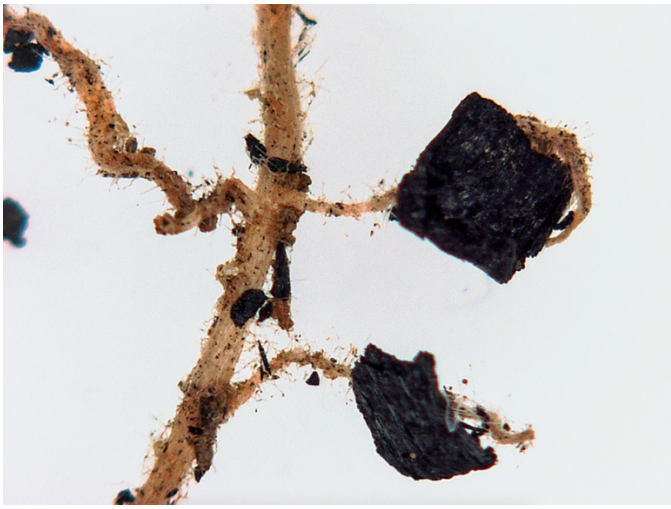

Figure 7-4. Plant roots and biochar on microscope. It is evident the preferential path of the roots that growth up toward biochar. This is a proof that the electron transfer is enhanced by biochar. (Kelly Hanley/Lehmann Lab - [139])

The excellent abilities to accept and donate high amounts of electrons, from and to the external environment, are still little explored by scientific research and it is probable that they are underestimated, having a much greater impact on soil biochemical processes than to date intuited [111].

To date, one of the great deficiencies in the characterization of biochar, is an unambiguous definition of the value of EC. Although EC has always been

considered an important parameter in the study of carbonaceous materials, the EC of biochar is still little investigated. EC measurement methods for carbonaceous materials have recently been applied to biochar to quantify the ability of biochar to be crossed by electrons.

In Section 11 a long experimental campaign on different types of biochar is carried out, for investigate the EC, but in which also doubts, gaps, and possible and necessary future developments for the unification of the EC measurement methodology are raised.

In Section 8 an exploration high-temperature biochar production via slow pyrolysis is presented. It examines chemical composition, conductivity and porosity. Goals include identifying if slow pyrolysis is suitable for a high-yield and a gasification-like biochar production.

7.2 Biochar's application to biological system

7.2.1 Improvements in soil

The first and most important application of biochar is its use as a soil conditioner in agriculture. There are several benefits that biochar brings to the soil, both at the macroscopic and microscopic levels. The reasons lie in what is listed in paragraph 7.1 at 7.1.6.1.

Benefits for the soil [140]:

- Porosity. Biochar changes the texture of the soil, increasing porosity and reducing the bulk density of the substrate.
- Water retention. Both through its own porosity and by increasing the total porosity of the soil, biochar improves soil water retention.
- Nutrient retention. Like water retention and thanks to CEC and to SSA, biochar retains nutrient elements contributing to the increased availability and reduction of fertilizer.

Benefits for the microorganisms [141]:

- Colonization. The porous structure of biochar provides a large surface area that offers a physical substrate for microbial colonization. This enhanced colonization leads to increased microbial diversity and abundance.
- Habitat. Biochar enhances soil structure and water retention. After colonization, biochar offers a stable habitat. This secure environment supports the survival and proliferation of more resilient microbial community.
- Nutrients. Biochar contains organic carbon and other nutrients that can be a source of energy and nutrition for microorganisms, increasing microbials growth and activity.
- Water retention. Biochar promotes water retention and improves soil drainage capacity, reducing the risk of toxic conditions (e.g., water stagnancy) for the microorganism community.

- pH. Since biochar for soil application is normally alkaline, it consequently modifies the pH of the whole soil in which it is applied. Biochar can also regulate the pH variation in time, creating conditions that are favorable to the growth of microorganisms.

Plant grows and soil fertility [142,143]:

- Fertility. Biochar improves soil fertility stimulating plant growth and promoting plant resilience to unfavorable conditions.
- Crop productivity. The biochar in soil promotes increased nutrient availability and promotes plant root development. It interacts synergistically with soil nutrients. Increased leaf surface area and plant photosynthesis activity are measured.
- Yield of agricultural products. In addition to the increase of total biomass, increases in yield of final products (grain, fruits, vegetables, ...) are measured up to 150/200 % in specific cases. A 20/30 % is an average value of yield increase [144].

Soil amelioration [145,146]:

- Erosion. Biochar enhances soil texture and stability, reducing the erosion phenomenon.
- Long effects. Biochar's effects on soil lasts in long-time, contributing to improves the soil for many decades. This long-term impact makes biochar a solution for sustainable agriculture.
- Humus. Biochar can indirectly contribute to humus formation by promoting microbial activity and community.
- TOC and SOC. The stable fraction of biochar contributes to increase the total organic carbon and the labile fraction contributes to increment the soil organic carbon. A high carbon content in soil has positive effects on soil fertility and microbial activity.
- Peat substitution. Biochar application to soil and consequent amelioration in terms of fertility and aeration is an effective alternative to the low-sustainable peat (that requires dig and extraction) [147].

The use of biochar in agriculture is a significant step toward more **sustainable agricultural systems**. Its multiple benefits (improvements in soil composition, increased soil fertility, high plants and roots interaction) make it a valuable and economic resource. Increasingly advanced production methods, e.g., high temperature pyrolysis or gasification, continue to improve the quality of biochar, creating a climate change-friendly product suitable for agricultural uses.

7.2.2 Advances in compost process

Observing the high interaction between biochar and biological systems, attributed to the intrinsic characteristics of biochar, such as porosity and SSA, alongside its high electron transfer capabilities and CEC toward external species,

it was hypothesized that biochar may serve as an ameliorative element not only in agricultural soils but also in various other biological environments. One of these environments is the aerobic composting. The addition of biochar to composting process is normally called **co-composted biochar**. Co-composting sees the application of biochar at the beginning of the composting process, so that it can interact with microorganisms present in the decomposable organic biomass throughout the degradation process.

Some contemporary research explored the effect on the biochar of co-composting, exploiting the composting activity as means for the *aging* of the biochar. It is known, in fact, that an aged biochar is charge of functional groups and microbes and it can interact better with the soil biota.

In contrast, this study introduces a novel perspective where biochar acts as a **catalyst**, initiating a cascade of reactions, interactions, and relationships among nutrients, microorganisms, bacteria that are present in the organic matter. The aim is to optimize the entire composting process in terms of quality, duration, and sustainability by leveraging the synergistic effects of biochar. Co-composted biochar process involves microbes, fungi and generally the soil zoology.

There are several benefits of biochar applied to composting process.:

- bulk density and aeration. The addition of biochar reduces the bulk density of the mass and consequently improves the oxygenation of decomposition. This results in less risks of anaerobiosis and of proliferation of anaerobic microorganisms [148].
- Moisture. Biochar, which possesses good WHC, also transfers this property to the mass under biodegradation, which remains more constant especially during the thermophilic phase [149,150].
- Macronutrients. Biochar retains nutrients (e.g.: potassium - K^+ , calcium - Ca^{2+} , magnesium - Mg^{2+} , ...) and prevents their dissolution and their leaching through soil water, producing a better-quality end-product [151].
- Temperature. Biochar raises the temperature reached during the thermophilic phase and extends its duration, compared to a standard composting process. This behavior is related to higher microbial activity and lower heat losses through latent heat [149,152].
- Emissions. The high electrons transfer capacity of biochar produces increased interaction of microorganisms with elements and species in the organic mass. This causes high fixation of elements which is why they are not transformed into gaseous products, effectively reducing GHGs emissions during whole composting process [153].

The final product of co-composting biochar process (often call COMBI) is a high-quality product. It is a) usable in agriculture as a partial substitute for chemical fertilizers, as it provides nutrients to the soil and increases their

bioavailability [154]; b) as a material for the metal-contaminated soils remediation since biochar retains pollutants [155]; c) as "rich soil" to replace the less-sustainable peat; d) as soil amelioration since COMBI is able to increase carbon, nitrogen and other elements soils [156].

7.2.2.1 Temperature increase

An increase in peak temperature and duration of thermophilic phase brings several benefits in organic degradation processes. Higher temperatures accelerate microbial activity and facilitate the proliferation of microbes' community, increasing the rate of degradation. Compost achieves high stabilities, with a higher fraction of degraded matter than standard compost. High temperatures reduce the risk of pathogens and bacteria, improving the health safety of the final product. Optimal thermal conditions promote mineralization of organic matter, generating a compost of higher quality also in terms of nutritional content and making compost a more effective fertilizer.

From a management perspective, higher temperatures allow maximizing the efficiency of aerobic degradation by significantly time reduction in complete the process [156].

A comprehensive analysis and detailed discussion on this issue is described in Section 12.

7.2.2.2 Emission reduction

Several studies in the literature show how biochar added to composting processes significantly reduces GHGs and ammonia emissions. However, much research does not consider the concept of *geobattery* (paragraph 7.1.6), but consider biochar only as bulk material, focusing on the "standard" characteristics such as porosity and CEC.

Several authors report significant reductions in major GHGs and other pollutant gases. Figure 7-5 shows the emission reductions from co-composting with biochar and zeolite. Data are compared to a non-aided composting process. The average emission abatement values and related uncertainties are the result of a review of many studies. Zeolite is commonly used as bulk-material to improve aeration of the decomposing mass. Biochars considered in the review are obtained from different feedstocks and are produced at both low and high temperatures. Despite this heterogeneity, emission abatement by biochar is still found to be effective. Moreover, biochar is more sustainable since zeolite coming from extraction process.

Some results and abatement mechanisms are quickly covered below, but please refer to Section 14 and Section 12 for a deeper investigation.

- CH_4. Methane abatement around 65% with low-temperature biochar [157]. The reason lies in the growth of methanotrophic bacteria communities and the reduction of methanogenic bacteria [158]. In addition to improved aeration, bacterial proliferation is also associated

with the increase of electron exchange, which is only possible in high temperature biochar [159].

- N_2O. Biochar pyrolyzed at 600°C lowered the production of N_2O, e.g.: by 25% [160] and by 14% [161]. In these study, the reason of the emission reduction is identified in an enhanced electron transfer. The abatement mechanism may lie in improved breakdown of N_2O into simpler species [162]. Therefore, high temperature biochar would play an important role in this conversion, making the electron transport more efficient for the denitrifies bacteria that converts N_2O, usually, into N_2 or ions [163].
- Regarding CO_2, the debate is still open. Since the "environmental" decomposition of organic masses produces CO_2, also in controlled composting processes it is considered "biogenic", that means no climate change impact. Some studies, however, show an increase in emissions due to an enhanced and faster process and a more active microbial community [164]. Thus, the debatable question is whether this increase should be considered impacting on greenhouse effect.
- NH_3. Ammonia emissions are mainly reduced thanks to the absorption capacity of biochar [157]. This allows us to hypothesize that the high temperature biochar, which is like activated carbon, may have a better impact on reducing ammonia emissions [165].

The reduction of GHGs and other climate-altering emission (e.g.: ammonia or particulate emissions), the reuse of waste and of the end-of-life materials in a more sustainable circular economy concept, the focus on soil depletion and the reduction of impactful agricultural practices, the reduction of the chemical fertilizers, the electrification of activities and the local energy production through renewable energy sources, are few of the ambitious goals of the UN Agenda 2030.

Biochar, from its production through gasification processes in which renewable electric and thermal energy is produced, passing through its applications in agriculture system, environmental management (waste, contaminated soils, ...) and creation of new soil conditioners or fertilizers (such as COMBI), alongside the environmental benefits and climate change impacts (GHGs emissions reduction, long-term carbon storage, …) combines many of these goals.

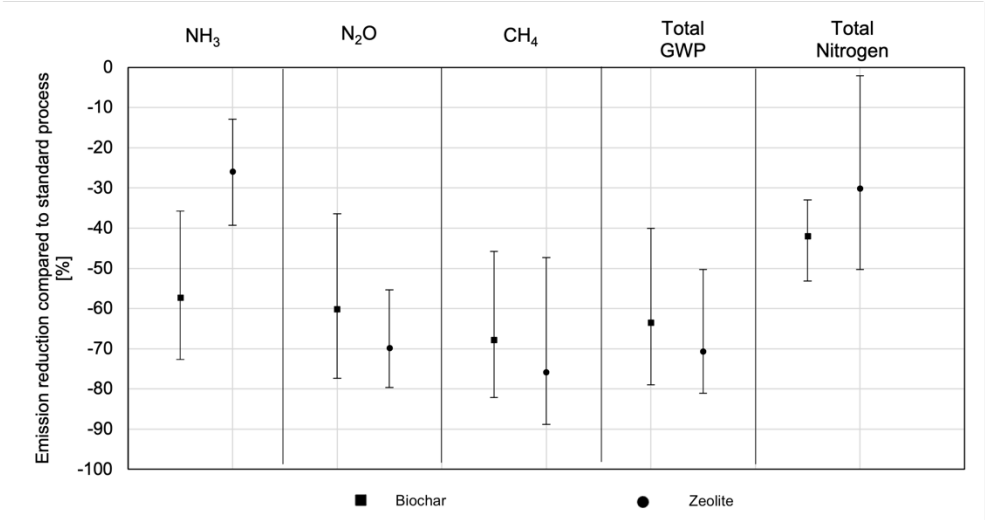

Figure 7-5. Emission reduction percentage thanks to the addition of biochar and zeolite at the beginning of composting processes. "Standard" means a without-additives process. GWP are calculated with the conversion factor reported in Table 1. Adapted from [157].

Undoubtedly, biochar is not a single *"magic bullet"*, but it stands out as one of numerous solutions that, when integrated together, can bring significant improvements for the planet Earth and for the living species that inhabit it.

Sections 12 and Section 13 contain a long and complex experimental campaign on biochar applied to a solid waste composting process. Gasification biochar was used to study a) the effects of high electron transfer offered by high-temperature thermal conversion and b) to explore biochar produced from a sustainable method. It was chosen to use the organic fraction of municipal waste (OFMSW) as degradable material. Since the OFMSW collected and processed in Italy is very high, with problems of management and emissions, the investigation of a sector where the application of co-composting can significantly improve the process and final products, as well as reduce environmental impact, is doubly useful. The study investigated a) process efficiency by monitoring **temperatures** reached by co-composting, humidity, aeration, etc.; b) **GHGs emissions** for a comparison with standard process emissions; and c) an economic, technical and environmental **feasibility study** to analyze in detail the real convenience and feasibility of applying biochar in high quantities to waste treatment plants. The research has produced important results, both in scientific and industrial terms.

7.2.3 Cascading effect and negative priming effect

Besides the direct benefit on emission reduction and carbon storage of biochar, there are some indirect effects: cascading effects and negative priming.

These will not explore in this work, but some insights are reported for the sake of knowledge and to confirm that high temperature biochar is the best biochar.

Cascading effects is referred to the positive indirect effects of adding biochar in terms of carbon storage in the soil. By burying biochar, biomass production increases (stem, leaves, roots, ...) and the amount of carbon removed from the atmosphere by chlorophyll photosynthesis, stored in biomass and partly transferred to the soil, increases. For each fraction of carbon added to the soil, microbic activity then increases and with it the number of bacteria and fungi: since they are made of carbon, they in turn participate in the C storage [166,167]. However, it is still complex to quantify this effect and the relative carbon stored.

Other studies show a long-term benefit through increased stabilization of organic matter content when biochar (or COMBI) is applied into soil. The amount of SOC stored in the soil and its decomposition rate significantly affect the balance of CO_2 emitted and C sequestered. For this reason, increasing the SOC means storing C [168]. However, the addition of biochar appears to increase the SOC decomposition compared to soil without biochar, resulting in higher CO_2 emissions. This effect is called "positive priming." [169]. Despite this, in the long-term biochar instead promotes "**negative priming**", that is greater stabilization of SOC [170]. In fact, biochar can donate electrons with an order of magnitude higher than the number of accepted electrons, thanks to the *geoconductor* mechanism. In this way, biochar promotes the reaction of reduction of soil C, stabilizing (mineralizing) the carbon. At the same time, oxidation reactions are disfavored and therefore there is less formation of CO_2 [111]. In addition, biochar physically binds to SOC making it less available to soil microorganisms.

For both of above indirect effects, high temperature biochar plays a privileged role over the other types of biochar. Temperature is again one of the main factors governing the priming effect due to its high porosity and high electron transfer capacity [171].

7.3 Sustainable systems to produce high temperature biochar

High temperature biochar appears to be the biochar with the best qualities for land application and carbon storage. Among high temperature biochar, biochar from gasification has a major advantage over biochar from slow pyrolysis: the gasification process is **self-sustaining** and produces **thermal and electrical energy** that can be sold. On the other hand, the yield of biochar from gasification is lower than from pyrolysis. As technology has evolved, some pyrolysis systems can produce biochar through self-sustaining system, exploiting pyrolysis gas and producing higher biochar yield.

In Figure 7-6 a further and final comparison between **high temperature biochar** and **low temperature biochar** is shown. According to quality criteria,

different aspects are evaluated with rating from 1 to 10. It is interesting to note that economic sustainability is rated better for low temperature biochar thanks to the higher production-yield, while the durability of low temperature biochar is the half of high temperature biochar. Side impacts and effects are rated similarly, but many innovative findings are not considered since still poorly verified.

	Feasibility			Climate change effectiveness			Side impact
	Technical	Economic	Governance	Effect	Timeliness	Durability	Environmental
LOW TEMPERATURE BIOCHAR	7.2	9	6	5	10	3	6.7
HIGH TEMPERATURE BIOCHAR	7.2	6	6	6	10	6	6.7

Governance feasibility: a measure of incentives and barriers to diffusion, including consideration of public acceptance, policy choices and other practical obstacles.
Timeliness: represents how ready the technology is for large-scale application.
Environmental side impact: excludes direct climate change mitigation, but includes impacts related to land use change and improvement that may affect biodiversity and biomass growth (both positively and negatively).

Figure 7-6. Comparison between high temperature biochar and low temperature biochar under various aspects. The evaluation is based on qualitative and quantitative aspects. Adapted from [172].

Only self-sustaining processes were considered in this work to combine both the sustainability of biochar application and the sustainability of production. This approach is more consistent in the overall assessment of environmental sustainability and feasibility. Some examples of both gasifiers and "sustainable" pyrolizers (self-sustainable system) are given below.

7.3.1 SynCraft gasifier

SynCraft power plants use a patented floating bed reactor. In classic floating bed reactors biomass and the gas flow act downwards causing compaction, in the SynCraft reactor these two forces act in the opposite direction leaving biomass sparse in the volume and generating a high porosity biochar. The product line includes the CW700-200+, CW1200-400, CW1800-500, and CW1800x2-1000 models, each generating electrical and thermal power. For example, CW700-200+ produces 220 kW electrical and 328 kW thermal power (water at 90°C). The models are modular and adaptable, allowing power scalability. Operating with 0.70 to 0.73 kg of biomass per kWh, achieving a remarkable 16% w/w biochar output on dry biomass, wood power plants operate standalone, requiring no additional electrical energy sources, Figure 7-7.a).

7.3.2 Pyreg Pyrolizer

PYREG offer customized solutions with fuel combustion capacities ranging from 500 to 6000 kW. The plants are compact and can be easily integrated into

existing infrastructures and facilities. Biomass is pyrolyzed at 500-750 °C in an oxygen-limited process. PYREG plants produce only thermal energy. Containerized for easy transport and installation, PYREG's process accommodates various biomass inputs like digestate, manure, wood chips, paper, and more.

The PYREG process is autothermal, thus no external thermal energy is needed. While it operates as a self-sustaining process, PYREG plants require electrical energy for the auxiliary systems (pumps, augers, blowers, ...) . Three are the models, with varying fuel capacities: 500 kW, 1500 kW, and 6000 kW. The 500 kW model processes 1100 tons of biomass annually, generating 200 kWt and an energy consumption of up to 12 kWe. Biochar production yields range from 27-28% (at 20% moisture content) of initial gasified biomass, Figure 7-7.b).

7.3.3 Carbofex Pyrolizer

The operational Carbofex demo plant efficiently carbonizes 500 kg of wood chips hourly at 600-700 °C, yielding 140 kg of biochar and 1 MW of renewable thermal energy. The biomass undergoes to high temperature pyrolysis thanks to the combustion of pyrolysis gas at 1000 °C, minimizing emissions. Carbofex works continuously and the precise control of temperature and residence time guarantee uniform and high-quality biochar quality: EBC certification ensure a 92% carbon content and 420 m^2 g^{-1} surface area. For 100o tons of virgin biomass, Carbofex system generates 286 tons of biochar (yield = 28/29%), 2.2 MWh of thermal energy (autothermal process), for an equivalent storing of 920 tons of CO_2eq, Figure 7-7.c).

7.3.4 Glock Gasifier

The GLOCK Ecotech is a combined heat and power (CHP) plant. It is mainly a cost-effective energy solution for exploiting locally available biomass, and secondly for producing biochar. Two variants are available: the 18 kW electrical - 44 kW thermal power rating consumes 18 kg h^{-1} of wood chips, yielding approximately 5% biochar production; the 50 kW electrical - 110 kW thermal power rating consumes 50 kg h^{-1} of wood chips, with a production yield of approximately 9% biochar (considering an operativity of 8000 h y^{-1}). The two variants are relatively small since the interesting aspect of GLOCK is the systems are specially designed to be modular: in fact, gasifiers can be installed in parallel and therefore high electrical and thermal powers can be achieved, Figure 7-7.d).

7.3.5 CharTainer Pyrolizer

The ALL Power Labs CharTainer is a compact pyrolizer enclosed in a standard 20-foot shipping container. It is a fully automated system for producing heat and biochar. It is composed of a biomass hopper and pyrolyzing auger, a

gasifier-heart, a clean-burning flare with heat exchangers for exploiting syngas and providing heat to the whole system. The reactor is a scaled-up version of APL's latest Swirl Hearth architecture which accepts a high feedstock typology and size range. CharTainer is an autothermal system with a little electrical need for auxiliary. The system uses 250 kg h^{-1} of biomass and generates about 500 kWht. Biochar, produced at high temperature (> 600 °C) is extracted at the bottom of the reactor with a yield of about 16% w/w, Figure 7-7.e).

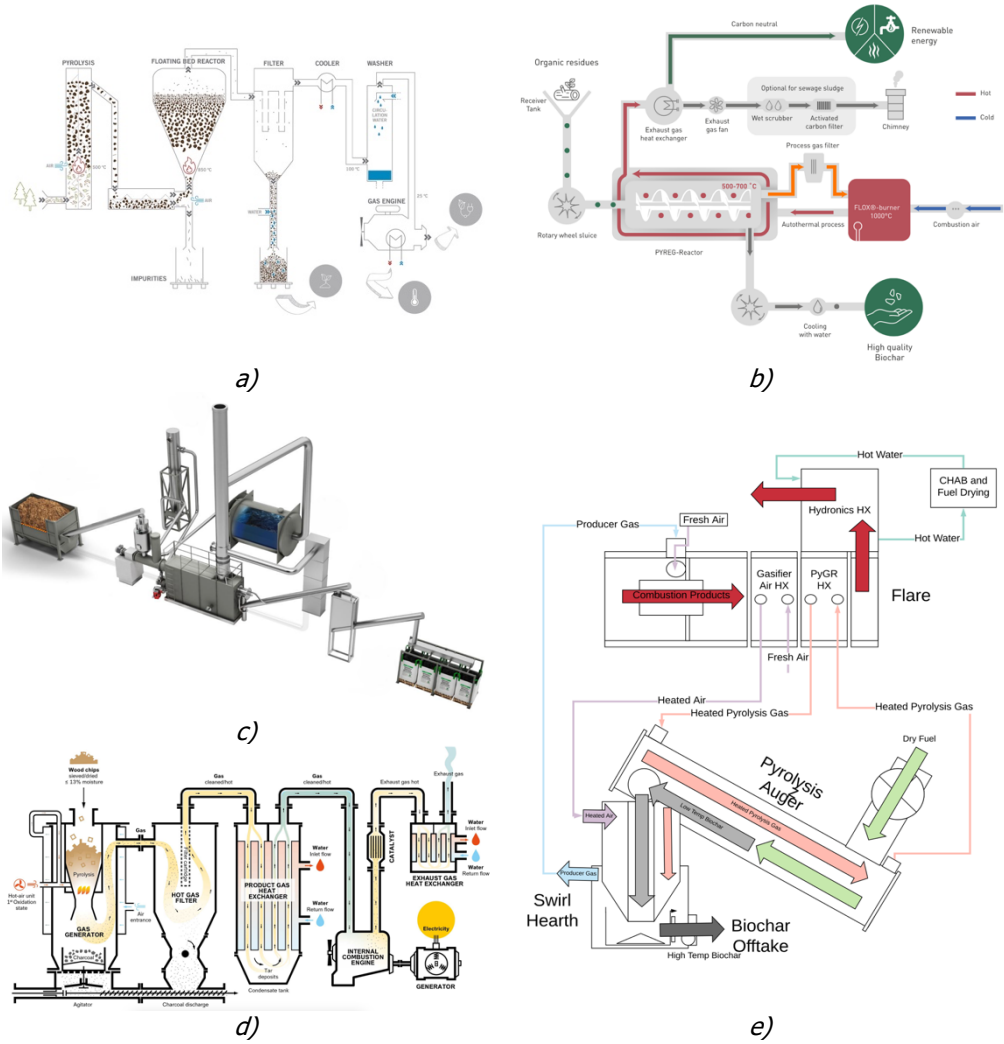

Figure 7-7. Schemes, diagrams or processes flow of different gasifier and pyrolizer: a) SynCraft gasifier [173]*; b) Pyreg pyrolizer* [174]*; c) Carbofex pyrolizer* [175]*; d) GLOCK downdraft gasifier* [176]*; e) CharTainer* [177].

7.4 Thermal properties of biochar and geothermal application

Goal 7 of UN 2030 Agenda emphasizing "Affordable and Clean Energy," the scientific community and institutions are intensifying efforts to diminish energy consumption, enhance the efficiency of energy production systems, and explore novel technologies, materials, or their combinations to meet the important objectives outlined in this Agenda [26].

A target is the elevation of the renewable energy share in the global energy mix by 2030, coinciding with the European Union's ambitious aim to achieve net-carbon neutrality by 2050 [178]. It is essential to integrate technologies and new materials for facilitating the transition to the renewables and to substantially abate the GHGs emissions. In this context BECCS standing out as a particularly promising strategy. But BECCS are complex, and the capture and storage technologies are, currently, not easily applicable. However, one solution that, to date, is "ready" is biochar.

Initial scientific focus primarily concentrated on direct biochar application in soil. Recently the attention has moved toward more complex applications: water filtering, sludge treatments, electronic and electrical applications, building technologies, new materials, ... [179,180].

Scientific community has made significant strides in understanding the interactions between biochar and water retention capacity from the agricultural point of view [181]. In contrast, limited research has explored the water-holding capacity of biochar to enhance existing technological processes in the energy sector.

Starting from WHC, deeply discussed in 7.1.2, porosity (paragraph 7.1.2) and the well-known characteristics of the atomic structure of biochar (paragraph 7.1.6), An innovative field of research has been explored: the application of biochar to improve the efficiency of geothermal fields. To investigate this application, some study to characterized biochar, soil and biochar/soil mixtures from a thermal point of view and from water rise capacity are carried out. Section 9 and Section 10 investigate the water retention capacity, the thermal conductivity, the specific heat, and then the ability of the biochar to increase the water capillarity potential in soil.

Findings

3rd chapter

This chapter represents the culmination of my research activities, where a selection of the investigations conducted, and their relative results are exposed and reviewed. The basis for understanding the reason of the research and the relative results have been extensively addressed in Chapter 2: "The biochar".

Through this in-depth chapter, the goal is to provide a comprehensive perspective on my investigations, thus laying a solid foundation for possible further study in the research field of biochar as "fascinating" and "carbon negative" material.

8 INTRODUCTION ON HIGH TEMPERATURE AND LOW TEMPERATURE BIOCHAR. AN INVESTIGATION ON SAMPLES FROM CONTROLLED SLOW PYROLYSIS PROCESSES

The following research is realized to study biochar obtained through slow pyrolysis at different temperatures. Using a prototype screw pyrolizer, biochar is produced both at high and low temperatures for a comparative analysis. The aim is to start to investigate the properties of these different biochars in term of chemical composition and electrical conductivity, identifying (if any) the greater biomass conversion triggered by a higher temperature process.

Biochars are also observed by scanning electron microscopy (SEM) to investigate the "porosity grade", which can be associated with the efficiency of the conversion from biomass to biochar.

Since the examined biochars are produced using the same method and apparatus, comparison becomes meaningful and allows to evaluate the difference between the characteristics of the biochars.

Keywords: Electrical conductivity; High temperature biochar; Slow Pyrolysis; Process parameters.

This work was carried to investigate different type of biochar, from electric conductivity, porosity and internal structure, and chemical composition point of view. This research has never been presented to journals or conferences.

8.1 Pyrolysis apparatus and biochar samples

Starting from the discussion in paragraphs 7.1.6 and 7.3, this research wants to investigate biochar types produced at relatively high temperature through slow pyrolysis. The scarcity of commercially certified biochar produced through controlled pyrolysis process and under defined temperatures and parameters, has required the production of low temperature biochar in laboratory through a lab-scale system, to perform a coherent examination of the differences between some different biochars. A prototype screw-type pyrolizer was employed to produce biochars.

A goal of this research lies in examining the chemical composition and electrical conductivity of the produced biochars to demonstrate the enhanced conversion from biomass wood to carbon, as result of high temperature, and to identify the potential reorganization of the biochar molecular structure as the temperature increases.

Another goal of this investigation is to identify a possible *high-yield biochar production process* that does not use gasification. This target aligns with the broader goal of developing an efficient and environmentally sustainable method for biochar production to aspire to broaden the variety of biochar applications, including soil improvement and carbon sequestration.

For producing biochar, a screw-type pyrolizer is used to allows a controlled experimentation, for a deeper understanding of the interplay between pyrolysis process parameters and biochars final properties. The pyrolizer used is explained below. Referring to Figure 8-1, it consists of an opening on the top for the biomass loading (1), an auger (2) placed in a trapezoidal housing, a jacket (around the auger) for flushing external hot fumes (3), and a cylindrical container for the biochar collection (4). The outer surface of the jacket and of the biochar outlet branch, are covered with a 2 cm thick insulating material (rock wool) to reduce heat losses. The hot fumes outlet (5) has been lengthened with a 1.5 m long pipe to facilitate the natural extraction via the "chimney effect".

Inside the pyrolizer, biomass advances thanks to the revolving movement of the auger, driven by a 220V motor. The biomass path inside the reactor is shown in yellow, Figure 8-1.

The path of the hot fumes, that provide heat to pyrolyze the biomass, is illustrated in red, Figure 8-1. The biomass is not in direct contact with the hot fumes, but the heat exchange occurs through the trapezoidal body in which the biomass is housed. Hot fumes are produced through an external burner, placed under the "Hot Exhaust Gas" inlet. The burner is adjustable in power, and it is fed with liquid propane gas (LPG): in this research, the focus are the parameters of the biochar production process, leaving out the self-sustaining pyrolysis concept.

The parameters here investigated are:

- the residence time of biomass in the pyrolysis zone. The residence time is set through an ON-OFF control of the auger, controlled via an Arduino UNO board and an actuator.
- the pyrolysis temperature. The desired temperature is obtained by adjusting the LPG flow rates and waiting for a start-up time for reaching the chosen temperature. Temperature measurement is performed using two K-type thermocouples, one placed at the "Hot Exhaust Gas" inlet and one at the outlet (5). The average value between these two temperatures is assumed as temperature of the pyrolysis process. Data logging was performed via a Pico Technology's TC08 system.

Chestnut processing waste (husk and pomace) is used. The auger is activated only when the pyrolysis temperature is reached.

An experimental campaign involving four tests (Test I, Test II, Test III, Test IV) were performed. In Test I and Test II, pyrolysis gases are not extracted from the pyrolizer. In Test III the pyrolysis gases are extracted (non-forced extraction) through a socket on the top of the system, (a) in Figure 8-1, while in TEST IV gases are extracted from a bottom socket, (b) in Figure 8-1. In this way, in Test III the gases traveled through the reactor in the opposite direction of the biomass progress: "countercurrent mode"; in Test IV the gases advanced in the same direction of the biomass: "co-current mode".

Table 10. Tests details and pyrolysis parameters used for producing biochars.

Test	Name of biochar	Pyrolysis temperature	Residence time	Auger OFF-period	Auger ON-period	Pyrolysis gases extraction mode
I	T30	589.4 °C	30 min	69.18 s	0.83 s	Not-extracted
II	T15	517.3 °C	15 min	34.50 s	0.83 s	Not-extracted
III	T30CC	487.5 °C	30 min	69.18 s	0.83 s	Co-current
IV	T30EC	481.4 °C	30 min	69.18 s	0.83 s	Counter-current

The extracted pyrolysis gases, before being released into the atmosphere, are flushed inside a flask containing 100 ml of acetone and then flows into a G4 gas-meter for measuring the gas flow rate.

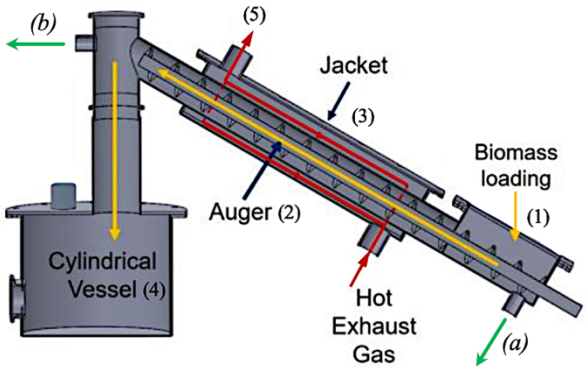

Figure 8-1. Schematic diagram of the pyrolizer with the parts explained. Adapted from [182].

To make the experimental campaign exhaustive, an evaluation of the tars contained in the pyrolysis gases of Test III and Test IV was also performed through a simplified Tar Sampling Protocol methodology [183]: acetone is evaporated under a laboratory hood and by weighing the flask before and after evaporation, the mass of tars in the gases is obtained. This method does not give the absolute mass of tars produced but allows to compare the two tests.

The electrical conductivity (EC) of biochars is measured following the process described in Paragraphs 11.2.3 and 11.2.4.

8.2 Biochar characteristic and EC values

Figure 8-2 shows the biochar after extraction, and Table 11 shows the results of ultimate analysis [184].

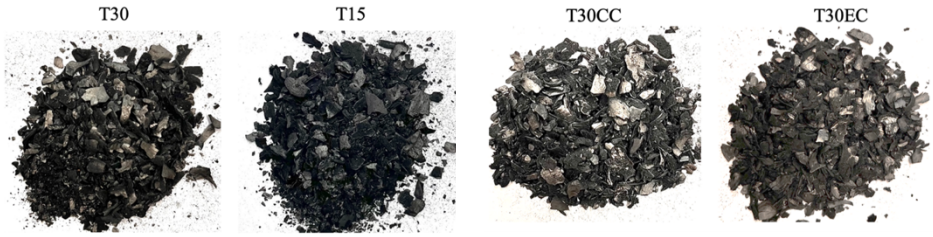

Figure 8-2. Biochar samples from pyrolysis of chestnut (husk and pomace)

Table 11. Elemental composition of biochars and chestnuts biomass.

Samples	C [%]	H [%]	O [%]	N [%]	S [%]	Ash [%]
T30	82.33	1.05	11.41	0.51	-	4.70
T15	82.99	2.14	10.47	0.93	-	3.47
T30CC	86.88	1.86	6.96	0.71	-	3.59
T30EC	80.12	1.78	13.02	0.62	-	4.46
Chestnuts	44.42	5.23	48.68	0.34	-	1.33

Table 12 reports data relative to flow rate, to the volume of gases extracted during Test III and Test IV and to the relative tars content.

Table 12. Comparison of flow rates, volume of extracted gas, and tars between Test III and Test IV.

	Test III - T30CC	**TEST IV - T30EC**
Volume pyrolysis gases extracted [l]	23	48
Test duration	1 h 57 min	1 h 55 min
Flow rate of gases [l h^{-1}]	11.79	25.04
Mass of extracted tars [mg]	250.4	1039.4
Mass of tars normalized on flow rate [mg (l h^{-1})$^{-1}$]	21.23	41.50

Figure 8-3 shows the results of the electric conductivity (EC) measurement campaign on the as-it-is biochar samples (as depicted in Figure 8-2).

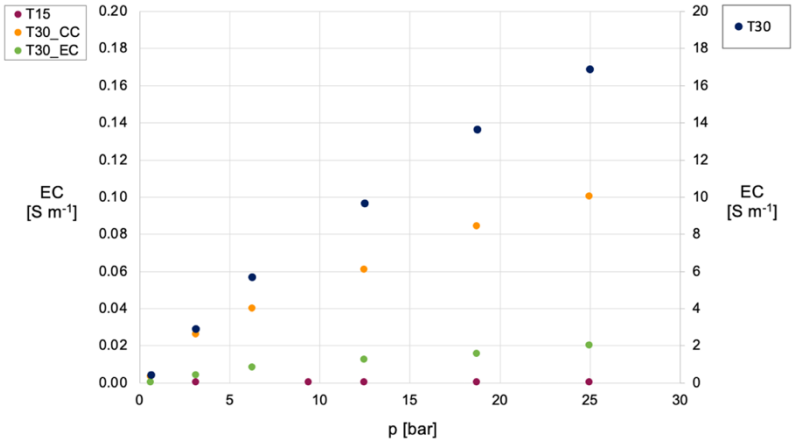

Figure 8-3. Electrical conductivity of T30 sample (right vertical axis) and of T15, T30CC and T30EC samples (left vertical axis)

T30 does not have the highest C content but it is much more conductive than the other samples (EC values are four orders of magnitude higher). This shows that the C content is not sufficient to understand the electrical conductivity of a biochar sample. In this case T30 is strongly influenced by the pyrolysis temperature of 589 °C, about 70 °C higher than T15 and 100 °C higher than T30CC and T30EC, and the residence time of the biomass, 30 minutes.

In T15 the high H_2 content (2.14%) and the lowest ash content (3.47%) can be related to the low residence time of biomass (15 minutes) and thus to the low conversion of biomass into pyrolysis gases and biochar. T15 acts as a dielectric material. The reason probably lies in the reduced conversion of the molecular structure. The biomass was exposed to strong torrefaction more than slow pyrolysis.

T30EC has the lowest C content (80.12%). This result can be related to two factors: a) lower conversion of C contained in the starting biomass since a high amount of pyrolysis gases (volatile hydrocarbon compounds) was extracted and therefore were not further converted, Table 12. In addition, the heat contained in the gases was "lost" and did not cooperate in the pyrolysis process; b) lower conversion of the biomass results in a higher concentration of oxygen (which remains in the biomass) and consequent lower C concentration, on the total of final product.

T30EC exhibits similar EC values as T15.

T30CC, on the other hand, shows slightly higher EC values, probably related to the C content, but still far from the values of T30. This is another experimental confirmation that ~ 600°C identifies the threshold of separation between high temperature biochar and low temperature biochar, at which a reorganization of the molecular structure occurs [109].

8.3 SEM microscopy

The biochar samples images observed by Scanning Electron Microscopy (SEM) are reported in Figure 8-4. SEM permits to qualitatively observe the structure morphology, porosity and the presence of any condensed substances (tars) on the surface of the individual grains.

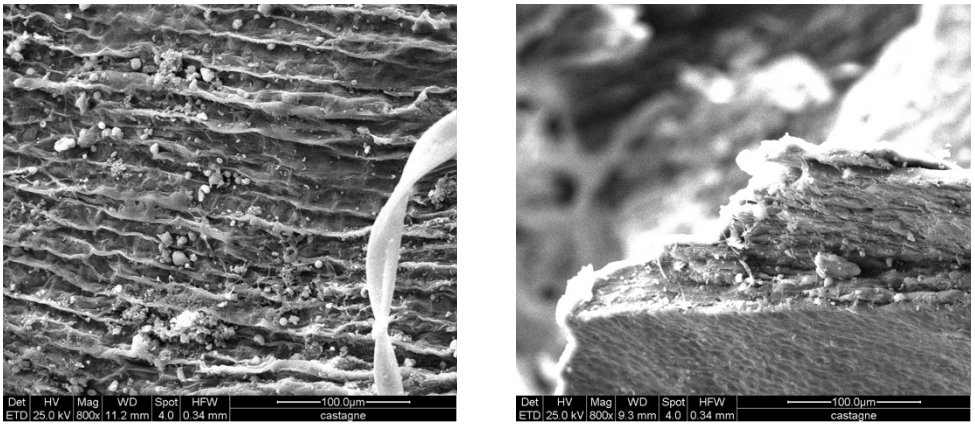

a) chestnut husk before the pyrolysis process.

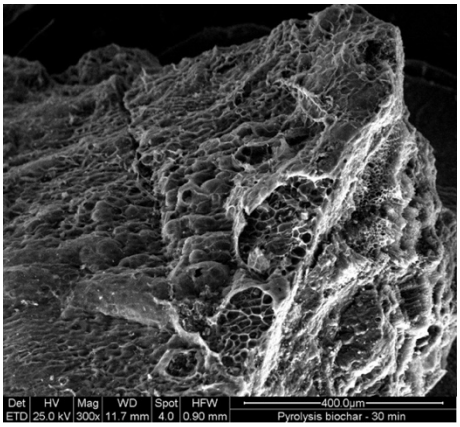

b) T30 sample – 400 μm

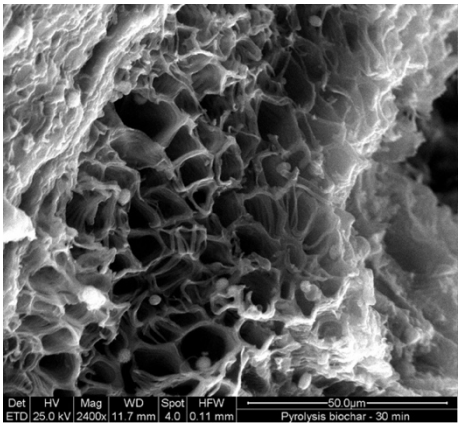

c) T30 sample – 50 μm

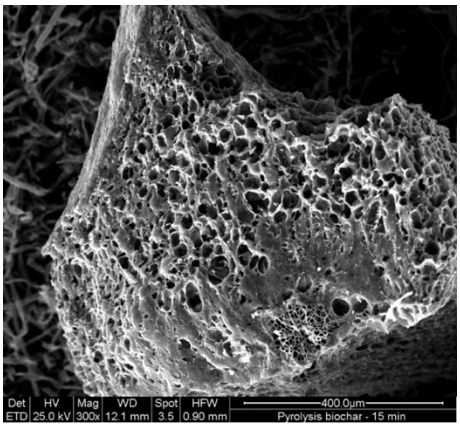

d) T15 sample – 400 μm

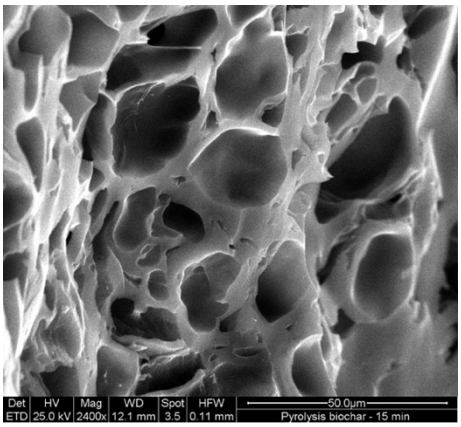

e) T15 sample - 50 μm

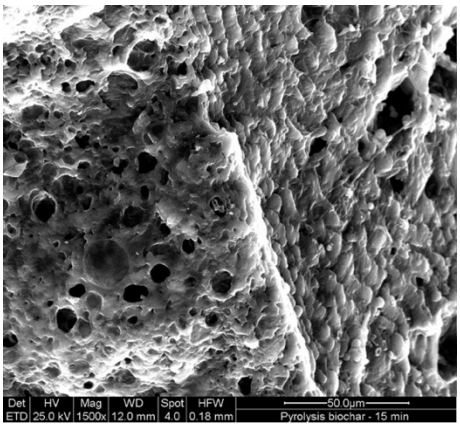

f) T15 sample - 50 μm

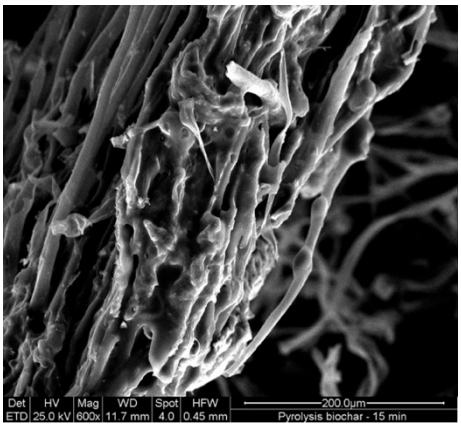

g) T15 sample - 200 μm

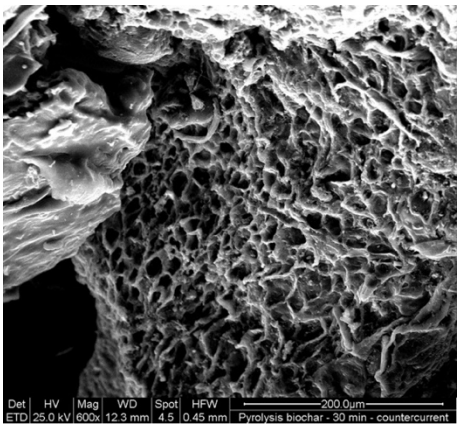

h) T30CC - 50 µm

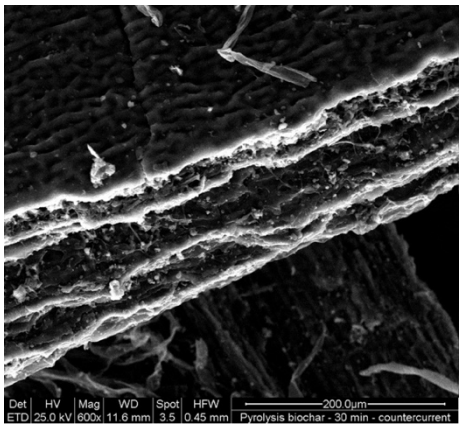

i) T30EC - 200 µm

Figure 8-4. Sem images of biochar samples at different magnifications.

Figure 8-4.a shows the starting biomass that does not exhibit a particularly porous structure.

T30, Figure 8-4.b and Figure 8-4.c, presents instead a high porous structure. In addition to temperatures and residence time, porosity also depends on the type of initial biomass. Spherical agglomerates of a few µm on the surface can be related to tars condensed during cooling phase or to particulate matter particles.

Figure 8-4.d and Figure 8-4.e show the T15 sample (at 2400x magnification) with a structure similar to T30 sample. However, the porosities are not fully formed due to too low residence time. In Figure 8-4.f the biochar surface is "orange-skin-like". This is the result of incomplete thermal conversion and of the tars condensation on the grains. In Figure 8-4.g the filiform structure is typical of the chestnut husk inner part but drops of waxy compounds (tars) are pasted on it.

T30CC sample (Figure 8-4.h) is porous, but probably it is coated with tar compounds. Low porosity is observed in sample T30EC, Figure 8-4.i, even at higher magnifications. This feature also confirms the low EC value of T30EC sample (in the range of 10^{-2} S m $)^{-1}$.

8.4 Conclusion

In conclusion, the experimental campaign revealed significant variations in biochar properties based on pyrolysis conditions. Biochar T30, produced at 589°C with a 30-minute residence time, exhibited exceptional electrical conductivity (EC) due to high pyrolysis temperature and longer residence time. Conversely, T15, with a shorter residence time, demonstrated dielectric behavior.

T30EC, produced with gas extraction, showed lower carbon content and EC values, indicating incomplete conversion. T30CC displayed slightly higher EC values.

The comparison of biochars makes it possible to conclude that the temperature of around 600°C is the threshold for a structural reorganization. Scanning Electron Microscopy images provided visual evidence of varying porosity and structure, confirming the influence of pyrolysis parameters on biochar morphology.

This study underscores that high-temperature biochar, produced via slow pyrolysis and not through gasification, yields high quality and electrically conductive biochar. Challenges persist in achieving high yields and developing sustainable, self-sufficient processes for this type of biochar production.

TECHNICAL FRAMEWORK OF APPLICATION .1

Changes in the thermophysical characteristics of soils by the application of biochar, and possible innovative applications.

9 INVESTIGATION ON THE WATER RITENTION CAPACITY OF BIOCHAR IN INDOOR CULTIVATION.

The following experimental campaign examines the modification of the soil water retention capacity of a substrate after biochar addition. Different biochar types, derived from woodchips and pellets through gasification processes, are employed to assess potential enhancements in water retention.

Understanding the efficacy of biochar in soil moisture management holds critical implications for agricultural productivity, environmental sustainability and innovative application of biochar.
This research aims to provide insights into the optimization of soil properties to alleviate, for example, water stress in agriculture or to be exploited for diverse "industrial" applications.

Keywords: Gasification biochar; water retention capacity; Cannabis Sativa.

A form of this experimental research was presented at European Biomass Conference and Exposition of 2022.

9.1 Overview of the experimental campaign

This small research investigates and confirms the elevate water retention capacity of soil when biochar is buried in it. Biochar structure, in fact, positively influences water retention (and nutrient retention), as deeply seen in Chapter 2, particularly relevant in agricultural soils.

To better investigate the capacity of biochar to increase soil water holding capacity, different types of biochar and a growth substrate for indoor cultivation are used in this test, to standardize the process and, consequently, the measurements [131,185]. Experimental campaign is carried out on Cannabis sativa plants cultivation, which took place in an indoor greenhouse to accelerate the cultivation period and to ensure a controlled grow. The used Cannabis sativa species had low THC and high Cannabidiol (CBD) content, mainly used for therapeutic effect, such as migraine and pain reliever [186]. Indoor cultivation also allows for a limited use of pesticides and ensures a solid production all year long. However, indoor cultivation is significantly more expensive than the open field cultivation since it requires much more energy [187].

9.2 Blends preparation and measurements procedures

To assess the water retention capacity of biochar, biochar was added to a standard substrate in three different concentration and composition. Biochar involved in this study has been produced through gasification using the All Power Labs Power Pallet PP30 gasifier [64]. The starting biomass employed for producing biochars was pine woodchips and pine pellets.

9.2.1 Blends of substrate and biochar

Three different theses, in addition to the control thesis, on Cannabis sativa greenhouse production were tested. Scions were planted in 4-liter pots that have been previously filled with the different blends of substrate. The standard substrate used also as control (CTRL) was composed of coconut fiber "base", for a 70% v/v, and perlites as bulk material, for a 30% v/v. The other 3 blends used were:

- 5% wood-Chips biochar v/v + standard substrate v/v: 5C
- 10% wood-Chips biochar + standard substrate: 10C
- 5% wood-Pellets biochar + standard substrate: 5P

Eights replicates for each treatment are considered, for a total of 32 pots.

In addition, other four pots for each thesis were filled with 4 litres of blend types (the 3 thesis and the control) but without scions planted, for a total of 16 pots. To limit any possible position bias (e.g. influence of heating systems) the placement has been randomized. Table 13 reports all the composition of the

different thesis and Figure 9-1 shows the disposition of the pots into the greenhouse ("e" means "empty", for the pots without plants).

Table 13. Blends composition of the control thesis and of the three tested theses.

CTRL	5P	5C	10C
70% w/w Coconut fibers	70% w/w Coconut fibers	70% w/w Coconut fibers	70% w/w Coconut fibers
30% perlite	25% perlite	25% perlite	20% perlite
	5% wood-Pellets biochar	5% wood-Chips biochar	10% wood-Chips biochar

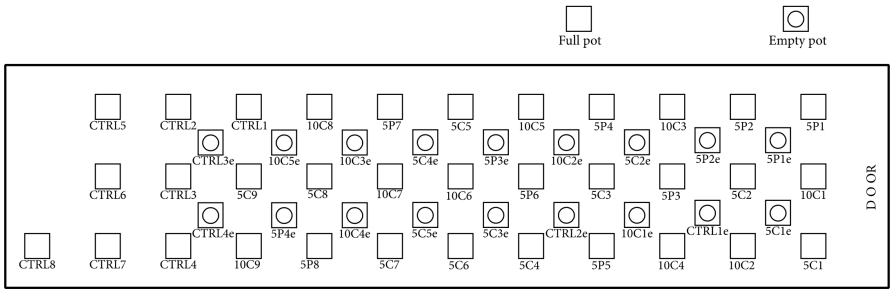

Figure 9-1. Pots disposition at the starting of the experimental campaign. "e" stands for "empty" pots.

All the plants are kept under *fertirrigation regime*: in this way they all received the same amount of water, which gradually increased following the growing stage of the plants. Irrigation system is stopped only before the collection of the flowers at the end of the cultivation period. The greenhouse temperatures were between 22°C and 26°C in function of the growing period and the humidity level is between 60% and 85%. The heating-illumination system worked for 18 hours of light and 6 hours of dark for the vegetative phase (that lasted 6 weeks). After that, 12 hours of light and 12 hours of dark are maintained during the blooming phase (other 6 weeks). Heating-illumination system was composed by 12 panels with LED lights and InfraRed LED for each table. On each table, nine plots were placed. Figure 9-2.a shows the interior of the greenhouse.

Two test on water content was carried out, during two different periods:

- FIRST TEST. During the entire duration of *Cannabis sativa* growth (10 weeks) moisture measurements, into the pots, through a probe was taken: "plants-pots" campaign;
- SECOND TEST. Soil water content (SWC) was measured in the empty pots: *Water field capacity* (saturation level) was achieved artificially

in each pot and the weight was measured periodically to detect the water content: "empty-pots" campaign.

9.2.2 "Plants-pots" tests campaign

The SWC was measured by using an electrical conductivity probe (PCE-SMM1). For each pot, the humidity was measured two times, one in an area close to the plant body and another closer to the pot's walls. Then the mean of these two measures was calculated. The probe was inserted in the substrate for around 10 cm, Figure 9-2.b.

9.2.3 "Empty-pots" tests campaign

To complete the experiment, the water retention capacity of the four different soil mixtures was measured, by weighting the pots containing the substrates without plants (empty-pots test). Specifically, the four additional pots for each thesis were used. They were firstly weighted - to get the dry blends weight - then they were wetted until the achievement of field capacity (saturation level). Water flowed out from the pot thanks to fissures in the walls, Figure 9-2.b. Afterwards, they were weighted at regular interval to assess any potential difference given by the water retention by time.

a) b)

Figure 9-2. a) interior of the greenhouse in which the experimental campaign was carried out; b) humidity probe inserted in a pot.

The difference between dry weight and field capacity weight represents the total water retained for the substrate type mixture. The pots' weight was measured every 12 hours for 8 days in total: the pots were kept in the same room where the plants were grown to assess the water retention capacity in growing condition.

Finally, the difference between the substrate water content at the end of the plant's growth and the substrate water content into empty pots give an estimation (%) of roots water retention among different treatments.

9.3 Results and observation on water retention

9.3.1 "Plants-pots" tests results

The water content values measured into the plants-pots test are reported in Figure 3, where average weekly values are reported. 10C blend seems having the best effect in water retention. The difference with CNTR pots is statistically significant (*p-value*<0.05) in the first weeks of the test and during the last weeks of plants growth. Instead, during the middle weeks (among from the 3rd to the 8th weeks) the difference in SWC measured on control and other theses are not significant. Even if the increase of SWC was not always significant, it is always higher for 10C sample compared with the CTRL.

The final value of SWC are: 33.9 ± 8.8 % for 10C; 25.9 ± 4.8 % for 5P; 26.1 ± 3.5 % for 5C; 22.1 ± 1.8 % for CTRL.

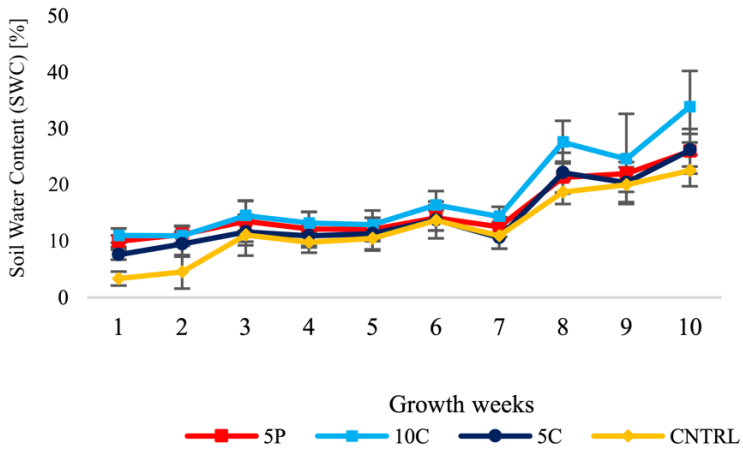

Figure 9-3. SWC during the 10 weeks of "plants-pots" campaign. Values display are the average value measured on the eight different pots of each thesis and the CTRL thesis (also standard deviation is shown).

The water retention increases of theses (5P, 10C, and 5C) compared to the CTRL are showed in Figure 9-4. These results underline how the addition of biochar effectively change the soil physical characteristics. This is due to the peculiar properties of biochar and specifically to its high porosity and low bulk density, as deeply reported in Chapter 2.

The water retaining capacity of all biochar theses is clearly highlighted by the values of water content especially in the first three weeks of the test, when the plants were small, and the roots system could be neglected since its water retention would be very low. However, after the third week a reduction of water retention was detected in 5P and 5C. Only 10C has a substantial increase in water retention compared with the CTRL, about +50%, probably due to the water retained by the roots.

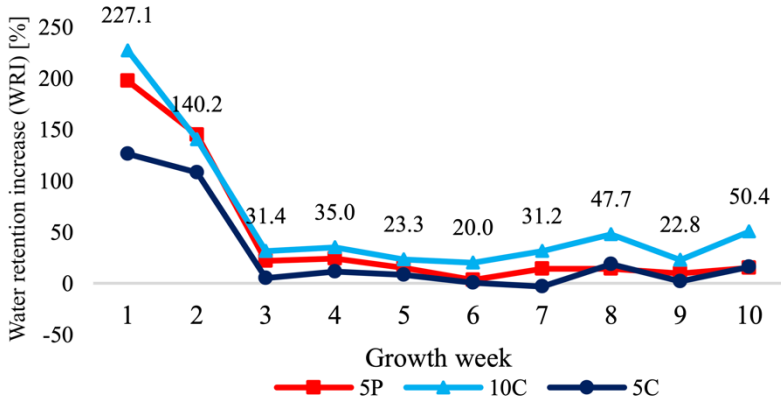

Figure 9-4. Water retention increase (in %) of blends with biochar compared to the CTRL.

The roots of the 10C plants retained much more humidity than expected. This phenomenon occurs only in the late stages of cultivation, when the roots are fully developed, while in the early stages the biochar offers a more effective water retention capability.

9.3.2 "Empty-pots" tests results

Figure 9-5 reports the SWC measured during "empty-pots" campaign. Horizontal axis reports the sampling time (every 12 hours, for 8 days). Results were coherent with the previous one: 10C and 5P have the highest water retention capacity and they are significantly higher than CTRL and 5C (*p-value<0.05*). Without roots, in fact, the effect of biochar on the substrate can be observed more clearly: for this reason, higher WRC values mean greater impact of biochar on the system.

This experimental campaign confirms the high water retention capacity of the soil aided with biochar. Data collected here show that the three different treatments have a good water retaining capacity, but only 10C significantly increase the water retention compared with control.

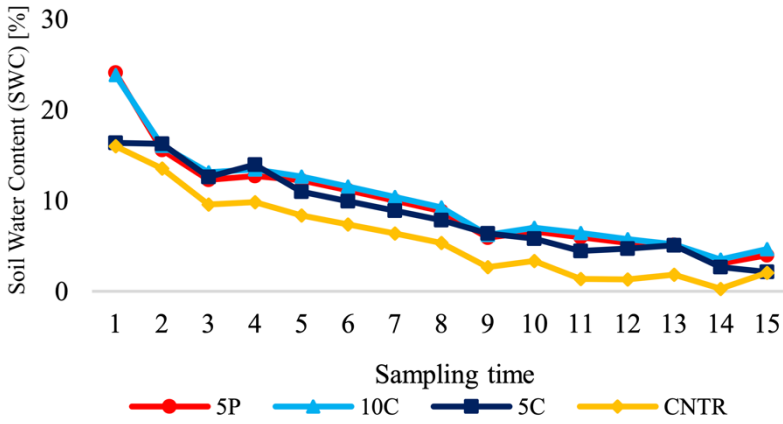

Figure 9-5. Water content of the different thesis after the achievement of field capacity of empty pots.

10 EXPERIMENTAL CAMPAIGNS ON THERMAL AND PHYSICAL PROPERTIES OF BIOCHAR: THERMAL CONDUCTIVITY, SPECIFIC HEAT AND WATER RISING POTENTIAL

The following is a niche topic in the scientific literature. The experimental campaigns concern a) the properties of biochar and soil-biochar mixtures (in dry and wet conditions) with the aim of testing whether there is an improvement in thermal conductivity and specific heat of the soil when biochar is added; and b) the water retention capacity and water capillary rise through an experimental campaign on different soil-biochar matrices to determine the optimal biochar application rate.

In fact, the high water rising potential, the high water retention capacity, the high porosity and the low density make biochar an attractive material to use as filler or as a soil-mixing material which can cover horizontal geothermal ground heat exchangers, improving heat transfer from soil to probes, and consequently improving the efficiency of low-enthalpy geothermal energy systems.

These investigations pave the way for the potential of biochar in optimizing geothermal energy systems and offer insights into its use in sustainable energy applications.

Keywords: Biochar; thermal proprieties; specific heat; water rising potential; geothermal; ground source heat pumps.

These experimental campaigns are part of a larger investigation on the influence of the biochar in soil, focusing on the changes that biochar brings to thermophysical proprieties of the soil. The new enhanced soil proprieties could be interesting in the low enthalpy geothermal sector.

10.1 Background and significance of experimental tests and application scope

The global scientific community and policy institutions are being called upon to change the ways in which people use to produce and consume electricity (Sustainable Development Goal 7 of UN 2030 Agenda [26]). This mission includes reducing and optimizing energy consumption, improving the efficiency of power generation systems, decarbonizing the production of energy, and improving the efficiency of electric and thermal energy user systems. All these previous elements should be combined with the exploration of innovative technologies, use of new materials, and co-existence of the previous goals [26]. A central focus of this effort is to expand the contribution of renewable energy to the global energy landscape by the year 2030. At the same time, the European Union has committed to achieving the net carbon dioxide (CO_2) neutrality by 2050 [188].

In this context, is crucial to move the research on two different fronts:

1. combining carbon storage technologies with renewable energy production
2. integrating waste materials or by-products into the energy production cycle, in a circular perspective.

To date, the scientific community has proposed numerous solutions (none of them is a strong silver bullet), and among these, atmospheric carbon capture and bioenergy carbon capture and storage technologies (BECCS) play a prominent role [189].

One of the most promising strategies in term of carbon storage methodology is the production of biochar through pyrolysis and gasification thermo-conversion of waste biomass. Since biochar has high recalcitrance characteristics, it remains stable for decades in the soil and for this reason it is recognized by the scientific community as a long-term storage method: 100 kg of biochar correspond to about 150 kg of equivalent CO_2 [190,191]. Moreover, the highly porous structure provides to biochar a high capacity to absorb and retain water [127]. Consequently, when incorporated into soil, biochar enhances its moisture level and sustains for an extended duration high level, thereby presumably boosting the soil thermal conductivity.

As anticipated, the aim of decarbonization of energy systems has led to crediting heat pumps (HP) as a promise technology for the electrification of the heating systems in civil or industrial building [192]. HP also contributes to a reduction in the environmental impacts of the heating systems, compared to domestic boilers, in terms of Global Warming Potential (GWP) and emission of both domestic greenhouse gases (GHGs) or other toxic gases such as NOx [193].

The most common HPs are the Air Source Heat Pumps (ASHPs) which use ambient air as free energy source such as air and soil. The problem of

environmentally dangerous refrigerants has been resolved with a new generation of refrigerants that, unlike those used in the past, have low GWP. Although ASHP are cheap, compact and easy to install systems and they don't require special installation work [194], they are penalized by the high variability of air temperature and achieve the best performance when the temperature of the air and the operating fluid are similar [195]. One of the ways to increase the efficiency of HPs is to use the ground as a heat source. Soil temperature remains approximately constant over time due to higher thermal inertia, especially when greater depths are reached. Ground source Heat Pumps (GSHPs) therefore allow more effective heat exchange with the energy source, and for this reason the overall system is more efficient [194]. On the other hand, GSHPs are more expensive, require excavation or drilling in the ground, and often require high yield area for a successful heat exchange [196].

The process of heat exchange with the ground occurs through pipes usually made of high-density polyethylene (HDPE), called geothermal probes (GPs) or Ground Heat Exchangers (GHEs), that extract or release heat to the ground via a working fluid, i.e. water or water-and-antifreeze mix. GPs can be installed vertically or horizontally:

- Vertical probes - borehole heat exchangers (VGPs). They require deep vertical boreholes, installation of casing pipes, use of filler materials or grounting technique application and insertion of probes which can be single U-pipe, double U-pipe and coaxial probes [197]. Therefore, installation is expensive, but heat exchange occurs very efficiently. VGPs require a small surface area field.
- Horizontal probes - shallow ground heat exchangers (HGPs). If compared to the horizontal ones, they require trenches, usually of high volume. High depths are not reached (1.5 to 2.5 meters) but are compensated by high surface areas [198,199]. There are three types of probe distribution: linear distribution, slinky distribution and helical distribution [200]. The cost is lower than VGPs, as well as the heat transfer efficiency is also lower [201].

Since the horizontal shallow GHEs geothermal systems are immersed in the soil at relatively shallow depths, the atmospheric conditions (humidity, temperature, precipitations, ... due to the effects of the weather conditions) can influence the variation of soil temperature and soil moisture content. In addition, the parameters to be evaluated when aiming for the maximum ratio between plant efficiency and cost are several, and they vary depending on the configuration adopted.

This research focuses on improving probe-soil heat transfer effectiveness by targeting not the technological or plant design of the system, but the material used to bury the HGPs, often called backfill material (BM). As also suggested by Hou (2022) [200], future high interest developments in GHEs area include the research for innovative BMs to replace conventional soils to make geothermal

systems more efficient and sustainable. The BMs can often be found among buildings materials (e.g. bentonite, grout or expanded clay aggregates) that, ones mixed with the soil and placed around the GHEs, significantly affect the heat transfer, depending mainly on their thermo-physical properties [202,203]. BMs usually are fractured or porous material, applied as it is or mixed in a solid matrix. The heat transfer in these materials occurs via conduction both in the matrix and water retained in the pores and slightly by convection due to water flowing through the porosities [204,205].

Biochar is very similar to these above-mentioned materials: the novelty of this research lies in the use of biochar as BM.

To date, many studies are unanimous in stating that soil thermal conductivity is a key factor affecting the system efficiency [206]. Moreover, the greatest thermal resistance lays between the HGPs and the soil which significantly impacts the overall system performance. This means that the soil (or other material) around the probes has great influence on the global system efficiency [207].

For this reason, firstly, thermal conductivity and specific heat of *biochar* and/or *soil+biochar* matrices are investigated. In particular, three samples are analyzed: a matrix of soil only (SOIL), a matrix of 80% soil and 20% biochar (SOIL-CHAR), and a matrix of biochar only (CHAR). The goal is to compare standard soil with soil aided with biochar, quantifying improvements and assessing positive or negative contributions of biochar both in dry condition and in wet conditions. The possible contribution of biochar lies in its high water retention capacity, which improves soil thermal conductivity and keeps the soil moist for long periods of time [208].

Additionally, the parameters that most influence thermal conductivity in soil are a) water content, b) microporosities of soil components and c) saturation level of the soil matrix. Bulk density and texture of the soil matrix (above all the sand content), together with the thermal conductivity of the lattice, also play a secondary role on the thermal conductivity of the soil matrix [209]. Since an increase in soil moisture corresponds to a significant increase in the intrinsic thermal conductivity, the addition of biochar (thanks to its porosity and water retention capacity, seen in the previous Section 9) further increases the thermal conductivity of the entire matrix.

Biochar also has high capillarity water uptake power. Using biochar as BM in geothermal fields lapped inferiorly by a water table would result, compared to the case without biochar, increased moisture content at the same soil depth, and less time variability of water content. Geothermal fields located in alluvial plains, where the water table varies seasonally from 4 m to 1.5 m below ground level, Figure 10-1, could be the main sites of this biochar application.

Given the current selling price of biochar (approximately 300 € ton^{-1}) and the relatively undeveloped market, the proposed idea is to add a fraction of biochar into soil or soil-sand mixtures, rather than opting for complete soil

replacement. For this reason, different combinations of soil, biochar and sand are presented to identify the option that allows the best capillary rise of water.

Lastly by mixing biochar with the excavated soil and reusing the obtained mixture using biochar as soil additive for BMs in HGPs, a long-term carbon sink is effectively achieved. This approach offers not only environmental benefits, but also constitutes a strategy for accessing carbon credits and the related trading market. Therefore, using biochar as a BM achieves increased effectiveness of the geothermal system and simultaneously makes an active contribution in the fight against climate change.

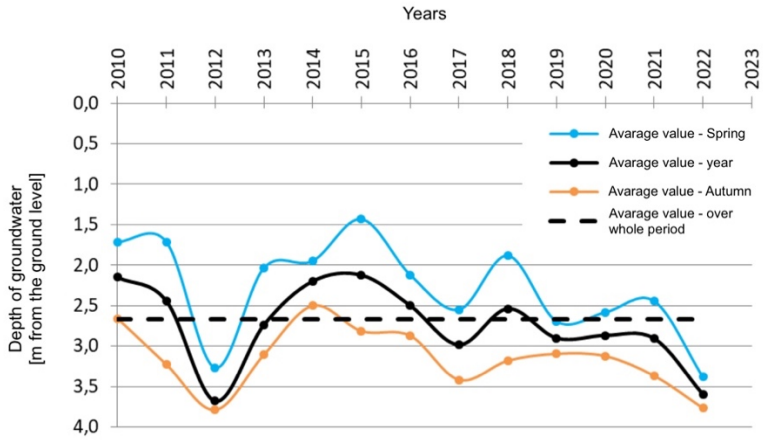

Figure 10-1. . Seasonality variation of the surface water table depth in meters below the ground level. Adapted from [210].

10.2 Experimental campaigns

10.2.1 Biochar and samples composition for thermal properties evaluation

A laboratory analysis campaign was conducted to analyze the thermophysical properties of biochar and its mixtures. Biochar's notable ability to enhance soil water retention and bring it toward saturation conditions, suggests an improvement in soil heat transfer performance. The variability in thermophysical properties due to different starting materials and different biochar production methodologies is high, but it may lead to a better product than already used alternatives like perlite or bentonite [133,211].

Three types of composition are examined: SOIL, SOIL_CHAR mix and CHAR. Then, SOIL and SOIL_CHAR are tested at different moisture level: 0% (DRY), 20% w/w, 30% w/w. CHAR is tested at 0% (DRY) and at 50% w/w. Additionally, SOIL_CHAR and CHAR are tested at higher wet condition: 36% for SOIL_CHAR and 67% for CHAR. The latter is a sample in saturation state to study the thermal

characteristics also in extreme condition. Table 14 provides an overview of all tested sample and their composition and wet level.

Table 14. Tested samples: acronym, composition, humidity level.

Sample	Solid matrix composition	Moisture content [kg_{water} kg_{tot}^{-1}]
SOIL_DRY	100% soil	0%
SOIL_20	100% soil	20%
SOIL_30	100% soil	30%
SOIL_CHAR_DRY	90% soil & 10% biochar	0%
SOIL_CHAR_20	90% soil & 10% biochar	20%
SOIL_CHAR_30	90% soil & 10% biochar	30%
SOIL_CHAR_36	90% soil & 10% biochar	36%
CHAR_DRY	100% biochar	0%
CHAR_50	100% biochar	50%
CHAR_67	100% biochar	67%

Commercial biochar from Bio-Esperia Srl, named BioDea White Onyx, obtained through a 170 kW updraft gasifier, was used. The gasifier has an annual biochar production of capacity of 900 m^3 and utilize high-quality biomass from forest maintenance. The producer claims a biochar yield of 250-300 kg from 1000 kg of dry biomass. The biochar used is certified as a soil improver under Italian regulations and for this reason it can be buried into the soil without further chemical analysis. Table 39 shows the characteristics of BioDea biochar.

To standardize it both to improve direct measurement results and to make it easier to mix with soil, biochar is grinded to obtain a uniform particle size < 1 mm. This biochar is used both for SOIL_CHAR samples and for CHAR samples.

50 kg of soil, initially dried and manually homogenized in grain size, are divided into two equal parts. One part is used for SOIL samples, the other is mixed with 10% of biochar (in mass) to create the SOIL_CHAR samples. The mass of biochar in SOIL_CHAR_DRY is obtained as in E. (10-1):

$$\mathrm{M_{biochar}} = \frac{\mathrm{M_{soil}} \times 10}{100 - 10} \quad [\mathrm{kg}] \qquad (10\text{-}1)$$

Water was added to create the wet samples following Eq. (10-2):

$$\mathrm{M_{water}} = \frac{\mathrm{M_{sample\_dry}} \times \mathrm{y}}{100 - \mathrm{y}} \quad [\mathrm{kg}] \qquad (10\text{-}2)$$

where $\mathrm{M_{sample\_dry}}$ is the mass of the considered sample when it is dry (SOIL_DRY, SOIL-CHAR_DRY and CHAR_DRY); y is the value of humidity level

to be reached: $y = 20$ for 20% w/w wet basis sample and $y = 30$ for 30% w/w wet basis sample, etc.

10.2.1.1 Thermal conductivity measure

The measurement of the thermal conductivity of the sample employed the λ *-Meter EP500e*, a "guarded hot plate" instrument [212]. This device comprises two plates: a bottom fixed plate for specimen placement and an upper motorized plate that, as it closes, adheres to the upper face of the specimen. Utilizing 0.5×0.5 m specimens is recommended for enhanced precision, with a thickness ranging from 0.02 m to 0.2 m. The experimental parameters include the set-point temperature, in this work set at T_{set} = 20°C, a temperature difference between the two plates, in this work set at ΔT = 15 K, and an adjustable specimen compression pressure that ranges from 250 Pa to 2500 Pa, in this work set at 2500 Pa.

This devise can maintain the sample's horizontal center line at the set-point temperature (T_{set} = 20°C), bringing the upper surface and the lower surface to the specified temperature for create the desired difference (ΔT = 15 K). The measurement ends with the determination of a unique lambda value (λ) only when the estimated tentative λ value does not change more than 1% around the estimated value, for a period previously settled as a test parameter (120 minutes). The device also gives the thickness of the sample with relative uncertainty (L ± 0.01 mm) and the error (S in $[W\,(m\,K)^{-1}]$) on the measurement of $\lambda\,[W\,(m\,K)^{-1}]$.

Since the matrices (SOIL, SOIL-CHAR and CHAR) are granular, friable and not compactable, a wooden box was employed to contain the sample and make them as uniform as possible. The box, made of 0.012 m-thick OSB wood, is 0.5×0.5×0.07 m in size and it is waterproofed with epoxy resin. A 0.005 m-thick neoprene tape is placed on the upper perimeter to improve the contact sample-instrument plate and to facilitate compression of the sample.

a) *b)* *c)*

Figure 10-2. Detail of the wooden box with neoprene tape; SOIL_CHAR_DRY matrix placed into the box and leveled; Specimen inserted inside the hot plate instrument and ready to be tested.

All the solid matrices, one by one, (composition and the humidity level in Table 14) are 1) placed in the wooden box, 2) leveled with a metal lath, 3) uniformly compressed with a wooden board and a 50 kg weight, and 4) coated with a transparent film to protect the instrument from humidity. After that, 5) each specimen created as above is placed inside the hot plate instrument for testing. Figure 10-2 show the box, a specimen and the hot plate instrument.

Each specimen, SOIL, SOIL_CHAR, and CHAR with different level of humidity, is tested two time. The second with a 90° rotation compared to the first one. An evaluation of the thermal conductivity of the wooden waterproofed base is also carried out to be able to determine the λ value of the samples inserted in the box. The equation and the variables for calculating the thermal conductivity of the samples are presented in the following section.

Since the tested specimen is composed of two layers of different materials (wood and solid matrix), it is necessary to perform an inverse calculation of series resistances to determine the λ value of the matrix in the specimen. Figure show a simplified stratigraphy of the specimen and Table 15 reports all the variables of the computation.

Table 15. Variables for the computation of the λ values and thermal resistance values. Figure 10-3 shows the specimen's terminology.

Variable	Symbol	Error	Data source
Thickness of the wood base	L_{wood}	1×10^{-5} m	hot plate
Sample thickness (box base + unknown matrix)	L_{sample}	1×10^{-5} m	hot plate
Unknown matrix	L_x [a]	ε_{L_x} [a]	calculation
Wood base thermal conductivity	λ_{wood}	ε_{wood}	hot plate
Sample thermal conductivity (box base + unknown matrix)	λ_{sample}	ε_{sample}	Data from hot plate
Unknown matrix thermal conductivity	λ_x [a]	ε_{l_x} [a]	Data from calculation
Wood base thermal resistance	R_{wood} [b]	ε_{wood}	Data from calculation
Sample thermal resistance. (box base + unknown matrix)	R_{sample} [b]	ε_{sample}	Data from calculation
Unknown matrix thermal resistance	R_x [a]	ε_{R_x} [a]	Data from calculation

[a] Values of the unknown matrix. "x" represents the SOIL, SOIL-CHAR and CHAR matrix.
[b] Thermal resistance is a "specific thermal resistance". Surface area is not considered since it is equal for all the samples.

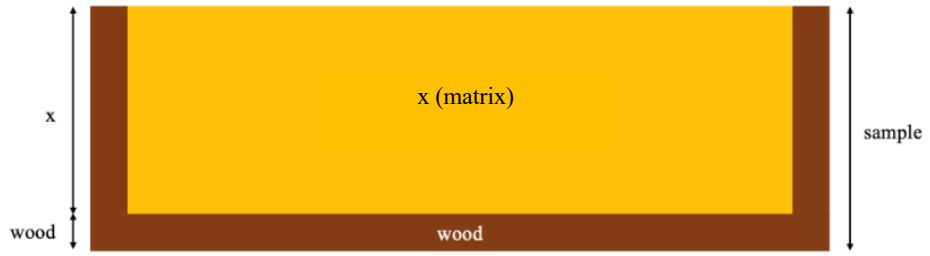

Figure 10-3. Specimen stratigraphy and terminology used in calculations.

Equation (10-3) is used for the calculation of the λ_x value (λ_{SOIL}, λ_{SOIL_CHAR} and λ_{CHAR}):

$$\lambda_x = \frac{(L_{sample} - L_{wood})}{(R_{sample} - R_{wood})} \qquad \left[\frac{W}{m\,K}\right] \qquad (10\text{-}3)$$

where R_{wood} and R_{sample} are obtained through Eqs. (10-4) and (10-5):

$$R_{wood} = \frac{L_{wood}}{\lambda_{wood}} \qquad \left[\frac{m^2K}{W}\right] \qquad (10\text{-}4)$$

$$R_{sample} = \frac{L_{sample}}{\lambda_{sample}} \qquad \left[\frac{m^2K}{W}\right] \qquad (10\text{-}5)$$

The values λ_{wood} and λ_{sample} are the data given by the hot plate, respectively for the wooden base and for each specimen.

The final thermal conductivity value for each solid matrix is calculated as average value of the two tests performed (0° and 90°), Eq. (10-6):

$$\lambda = \frac{\lambda_{x_1} + \lambda_{x_2}}{2} \qquad \left[\frac{W}{m\,K}\right] \qquad (10\text{-}6)$$

The measurement errors are calculated according to the propagation of uncertainties proposed by Kline and McClintock [213], seen in Eq. (11-6).

10.2.1.2 Specific heat measure

From the specific heat point of view, only the SOIL_DRY and the BIOCHAR_DRY are characterized. Combining in different percentages the two components is it possible to calculate the specific heat of the matrices.

The experimental setup used for measuring the specific heat consisted of a 2-liter glass beaker placed in an extruded polystyrene (XPS) box with a minimum wall thickness of 0.10 m. The sealing between the removable lid, also made of XPS, and the box is provided by a neoprene tape placed on the perimeter, Figure 10-3 show the scheme of the experimental setup.

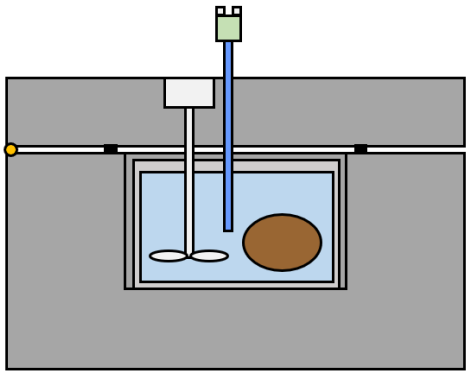

Figure 10-4. Scheme of the apparatus used for the specific heat measure: in grey the XPS walls/lid; in brown the sample; in light-grey and light blue the beaker and water respectively. The stirrer and thermocouple complete the scheme.

Water in the beaker is at room temperature and it is continuously stirred. The water temperature is measured through a K-thermocouple: $T_{H_2O\_start}$. The sample (whose specific heat is to be calculated) is placed in a plastic bag in which a vacuum is made, and it is immersed in a Julabo ME thermostatic bath at 30°C for 3 hours. Subsequently, the sample is transferred into the beaker: the stirrer is still operating to ensure the homogeneity of the water temperature. T_{H_2O} and the air temperature T_{air} are recorded with a Pico-Technology TC08 data logger. The test is considered concluded when the water temperature becomes stabilized between the initial water temperature and the thermostatic bath temperature (30°C).

In addition to the tests with the samples, two *blank tests* are carried out to evaluate the dispersion through the XPS walls.

Equaling the heat transferred from the sample to the water, and subtracting the heat lost through the walls, the unknown specific heat of the sample can be calculated. Heating value computation starts from Eq. (10-7), where $T_{sample\_start} = 30\ °C$ since it is the temperature of the thermostatic bath; at the end of the test, at the equilibrium, $T_{sample\_end} = T_{H_2O\_end}$ (measured through Thermocouple); Cp_{sample} is the unknown value of the sample and therefore of the equation.

$$m_{H_2O} \times Cp_{H_2O} \times (T_{H_2O\_end} - T_{H_2O\_start}) = m_{sample} \times Cp_{sample} \times (T_{sample\_start} - T_{sample\_end}) \quad (10\text{-}7)$$

10.2.2 Biochar and samples composition for water rising potential evaluation

10.2.2.1 Soil mixtures preparation

For water rising potential evaluation, 6 different types of matrixes are tested. Samples are realized using the three main components soil, sand and biochar.

Plain soil: the soil used for creating the samples of this work was analyzed by core drilling up to 108 cm deep. It is characterized by the prevalence of silt and clay from 4 to 105 cm and the appearance of medium sand from 105 to 108 cm, Figure 10-5.a. Given the limited depth of the excavations for the installation of horizontal geothermal probes, it was decided to use the predominantly silt and clay sample. Plain soil is used as control sample and as basis for the other mixtures.

Sand: since sand is present to depth higher than 105 cm and its content is an important factor that influence thermal conductivity, beside water content, porosity and saturation level [209],it was decided to include it among the components of the tested mixtures. Fine standard sand was selected for this work, Figure 10-5.b.

Biochar: the biochar used in this experiment was produced by a Imbert-type reactor of a biomass gasification power plant with nominal power of 150 kW. This is a co-current reactor operating between 800 and 1000°C where the biochar is extracted from the reduction zone. This architecture guarantees a carbonized material that is, on average, higher in micro and nano porosity when compared to pyrolysis chars. This biochar is certified as a soil improver, according to Italian legislation [214], and can therefore be applied as amendment to the soil. Table 16 summarizes the characteristics of the Urbas gasifier biochar used in this research, which is shown in Figure 10-5.c [215].

a) *b)* *c)*

Figure 10-5. Components used for the formation of the mixtures. (a) plain soil, (b) fine sand, and (c) biochar. Each picture represents a 10x10 cm sample.

Table 16. Biochar characteristics declared by the producer.

Parameter	Value
Total Carbon - dry basis	72.4 %
Ash content	20.5 $\%_{m/m\ dry\ basis}$
Fraction of grain size < 0.5 mm	39.2 %
Fraction of grain size 0.5 < φ < 2.0 mm	18.9 %
Fraction of grain size 2.0 < φ < 5.0 mm	25.5 %
Fraction of grain size > 5.0 mm	16.4 %
Density	218 kg m^{-3}

The proportions between the various components of the mixtures were measured in volume (volume/volume) to guarantee simpler measurement, both during the tests and in any future field applications. The soil was mixed both with biochar (in different proportions) and sand to create a map of different mixtures to be tested with the open-tube method. The compositions of the samples are shown in the Table 17. All the mixtures were previously air-dried and the starting moisture contents are reported in Figure 10-6.

Table 17. Description of the composition of the different samples.

Name	Soil [% v/v]	Biochar [% v/v]	Sand [% v/v]
100T	100 %	-	-
80T-20C	80 %	20 %	-
65T-35C	65 %	35 %	-
50T-50C	50 %	50 %	-
100M	70 %	-	30 %
65M-35C	45.5 %	35 %	19.5 %

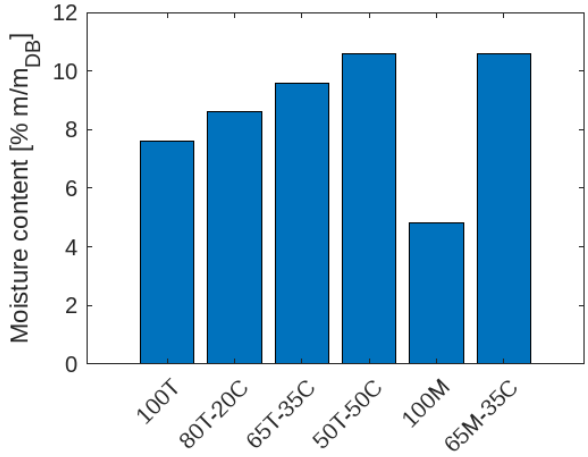

Figure 10-6. Moisture content of the different samples at the beginning of the experiment.

10.2.2.2 Water capillary rise measure

The utilized test methodology follows the studies conducted by Lane and Washburn [216] who proposed a simplified method for evaluating the permeability of soils to rising water. Although the method dates back almost a century, it is still used today as a reference in the development of empirical or analytical models for calculating capillarity rise [217,218].

The original method consists of repeated measurements of the height and rate of capillary rise in carefully controlled columns of air-dried soil placed into transparent tubes with a diameter of 2" or 4" for direct visualization of the wetted front and consequent measurement of the height of the water rising. The lower part of the tube is closed with a perforated copper plate and the soil is compacted with a mallet to obtain a compact medium reproducing the real case of undisturbed soil. The columns are then immersed vertically in a pan of tap water. The measurements of the height of the waterfront are performed hourly (or daily) until no variation in the front are observed. The trend of the water capillary rise is recorded with respect to time.

The method adopted in this work employs the use of opaque PVC tubes with an internal diameter of 10 cm (approx. 4”) and a height of 100 cm. The bottom of each tube was capped using a nylon net to allow the flow of water from the pan into the soil and its upward rise. The tubes were filled with the sample to be tested, subjected to a pressure of 2 kPa and placed vertically on a pan containing 3 cm of gravel and 4 cm of water. The net water head was set to 1 cm, and it was kept constant throughout the duration of the experiment with continuous refills. Differently from Lane and Washburn suggested method, to compensate the adoption of opaque tubes, instead of visualizing the waterfront, the moisture content of the samples was measured using a proper

sensor. The moisture measurements were carried out through a ECH2O EC-5 Soil humidity probe [219] inserted periodically into specific slots made in the cylindrical wall of the tube and spaced 5 cm one from the other. This allowed the quantitative evaluation, not only qualitative, of the performance of each sample. It must be pointed out that each slit was sealed with duct tape after the humidity measurement to avoid any contact between samples and air.

Figure 10-7.a shows a photo of the experimental apparatus while Figure 10-7.b shows the insertion of the humidity probe in the tube through the slot.

a) b)

Figure 10-7. a) Whole experimental setup and b) detail of the humidity probe inserted in a slot.

10.2.3 Carbon storage calculation

When buried into soil, biochar has a good stability, up to hundreds of times the starting feedstock. This happens as a portion of organic carbon remains stable in the soil for centuries. VERRA proposes a strict methodology for quantifying both the emission reductions and the storage of carbon examining a) the biomass handling before biochar production, b) process used for the biochar production, and c) the final application of biochar (in soil or other application) [46]. Using VERRA method, a simple computation of carbon stored in a typical shallow geothermal field, with biochar as BM, was carried out. The computation followed some assumptions: short distances biomass transport, pro-duction of biochar through gasification, neglection of biochar transport, exploitation of renewable sources energy for auxiliary operations of the gasifier, no greenhouse gas emission during production process.

10.3 Results of the tests and observations

10.3.1 Thermal conductivity and specific heat results

Table 18 reports all the results of the two experimental campaigns: thermal conductivity and specific heat.

Table 18. Samples thickness, thermal conductivity (with the respective uncertainty) and specific heat.

	Sample thickness L [mm]	**Thickness uncertainty** [mm]	**Thermal conductivity** λ_x [W (m K)$^{-1}$]	**Thermal conductivity uncertainty** ε_{λ_x} [W (m K)$^{-1}$]	**Specific heat** Cp [J (kg K)$^{-1}$]
WOOD	11.37	0.01	102.54×10^{-3}	1×10^{-3}	-
SOIL_DRY	40.00	0.01	228.50×10^{-3}	0.05×10^{-3}	930
SOIL_20	84.16	0.01	380.66×10^{-3}	0.22×10^{-3}	-
SOIL_30	84.36	0.01	1200.00×10^{-3}	1.11×10^{-3}	-
SOIL_CHAR_DRY	83.89	0.01	221.86×10^{-3}	0.06×10^{-3}	-
SOIL_CHAR_20	84.98	0.01	376.24×10^{-3}	0.12×10^{-3}	-
SOIL_CHAR_30	86.83	0.01	1132.24×10^{-3}	0.90×10^{-3}	-
SOIL_CHAR_36	32.28	0.01	1867.93×10^{-3}	0.1×10^{-3}	-
CHAR_DRY	19.40	0.01	70.00×10^{-3}	0.02×10^{-3}	1310
CHAR_50	22.2	0.01	500.00×10^{-3}	0.02×10^{-3}	-
CHAR_67	21.7	0.01	2480.20×10^{-3}	0.03×10^{-3}	-

Literature indicates that the thermal conductivity of biochar ranges from 0.10 to 0.13 W $m^{-1}K^{-1}$: it is strictly influenced by the production temperature that subsequently affects porosity, molecular structure and physicochemical properties [211]. Therefore, when it is dry biochar shows lower thermal conductivity compared to standard soil, as also confirmed by data collected in this work.

Incorporating biochar into soil, generally, does not notably modify its thermal conductivity under dry conditions. However, humidity plays a predominant role. This affirmation is supported by the SOIL_CHAR_36 sample that shows the highest thermal conductivity among SOIL and SOIL_CHAR matrices. Moreover, CHAR_50 and CHAR_67 underline the significant impact of water content on thermal conductivity: a small increment in humidity content,

about 17%, leading to a substantial rise in the thermal conductivity value of the matrices, about 400 %.

Concerning the specific heat, the SOIL_CHAR specific heat is calculated as a weighted average of the specific heats of its components (SOIL and CHAR). The specific heat of SOIL sample is in line with values found in literature: 1.17 to 2.25 kJ kg^{-1} $°C^{-1}$ for clay-soils, 0.83 to 1.67 kJ kg^{-1} $°C^{-1}$ for sandy-soils, with 20/25% moisture content and 1300 kg m^{-3} of density [220]. The specific heat of dry biochar is slightly higher than that dry soil. Moreover, the addition of biochar may further rise the specific heat of the mixture due to its water retention potential, increasing the maximum soil moisture level and water persistency in soil/matrix. Following this logic, for high moisture levels, it can be assumed that the specific heat of water becomes prevalent, while the contribution of biochar to the specific heat of soil is negligible.

10.3.2 Water rising potential results

The capillarity rise tests took place over 11 days and the moisture content measurements of the different substrates were recorded every 12 hours with a spatial resolution of 5 cm along the cylindrical test column. The environmental conditions during the test were the same for each tube with average temperatures and relative humidity of 19.2°C and 62 %RH.

Figure 10-8 reports all the results obtained in the test: x-axis shows the hours since the start of the test and the y-axis shows the height of the column. The color bar indicates the humidity level recorded over time at intervals of 5 cm up the column, while the black lines identify the maximum humidity gradient between one height and the next, aiming at reproducing the position over time of the wet front that would be observed following the Lane and Washburn methodology using transparent tubes. The images show how plain soil (100T) and soil mixed with sand (100M) lead to almost similar maximum (over a 11-day period) capillary rise and water content, see Figure 10-9.a and Figure 10-9.b.

It is observed that the addition of biochar significantly increases both the capillary rise and the water content of the mixture, and this behavior intensifies by increasing the volume percentage of the biochar used. By adding 20% v/v of biochar (80T-20C sample) a doubling of the average column humidity and the maximum capillary rise is observed. These values rise to over 2.5 times if 50%v/v biochar (50T-50C sample) is added. 50T-50C do not show a significantly greater rise in the level of the wet front than the 65T-35C sample, only the moisture level seems to be more homogeneous along the column at each instant of measurement. This is an important finding as it allows to identify the optimal amount of biochar to be mixed and the balance between improves and economic costs.

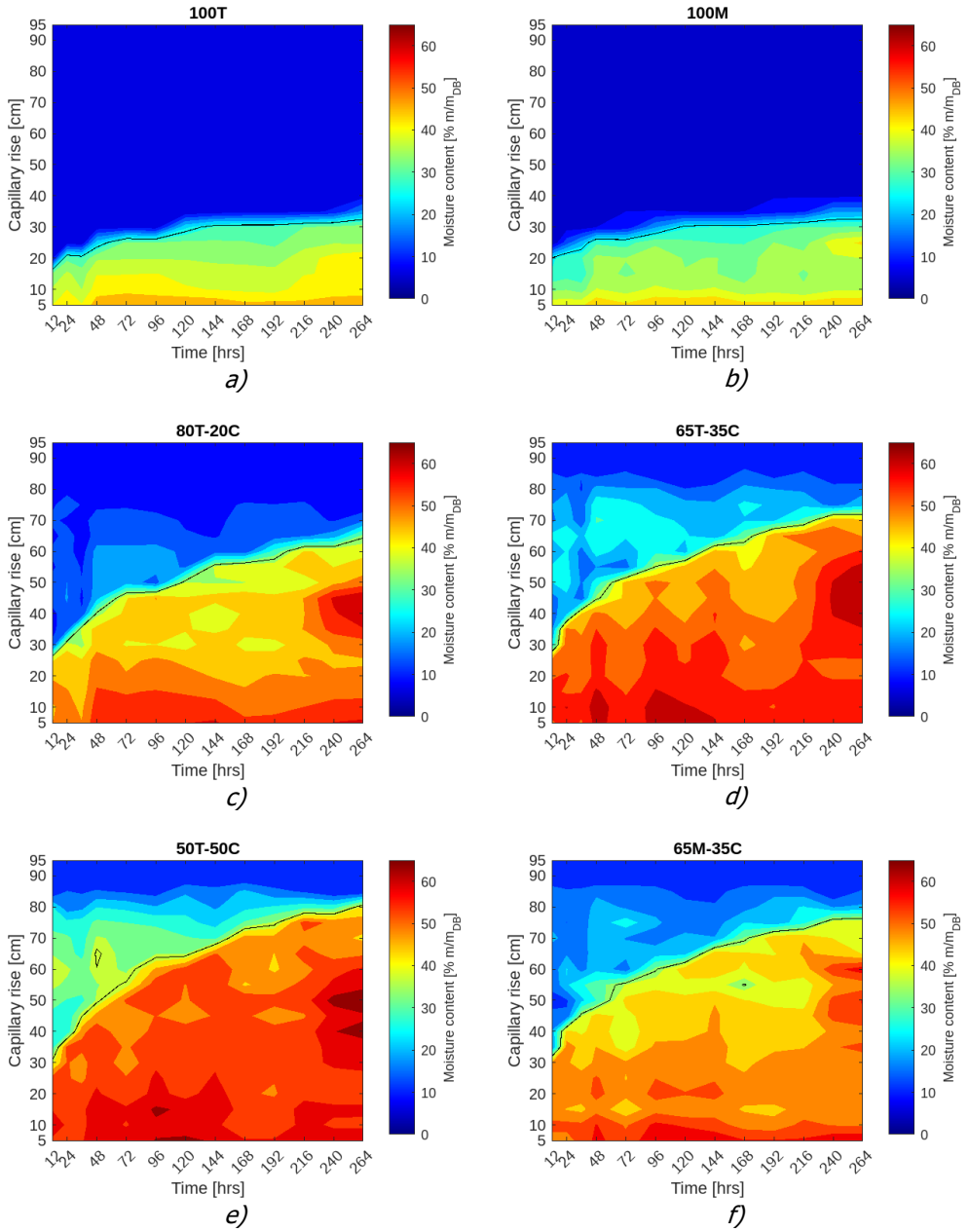

Figure 10-8. Capillary water rise over time for each tested sample and moisture content at the different heights along the columns: a) 100T sample; b) 100M sample; c) 80T-20C sample; d) 65T-35C sample; e) 50T-50C sample; f 65M-35C sample.

Figure 10-9.a shows the maximum levels reached by the water referred to the free water surface in the pan, during the test period. The best result was achieved by sample 50T-50C: 81.3 cm and a 154% improvement over the control. Similar results were obtained by the 65M-35C sample (sand-soil-biochar

mixture) which reached 77.3 cm, a 141% in-crease over both the control, 100T and 100M control, that reached the same level. The sand-less analogue sample 65T-35C reached a level of 72.3 cm, equivalent to a 125% increase. Finally, with a 100% increment, sample 80T-20C was the least performing. These results show that the use of biochar in small quantities gives limited benefits, while shares greater than 35% give excellent results in terms of capillarity rise.

Slight improvements in soil moisture have been shown by going from 35% to 50% biochar use in the mix. This suggests that percentages of biochar close to 50% could be the maximum conveniently applicable for this type of use. Instead, to increase the performance of the 35% biochar mix, a fraction of sand (19.5% over the total) can be added to allow a slightly greater water uptake.

Although sand improves capillarity, it reduces the water retention of the mixture, as observed in Figure 10-9.b. The best in terms of average moisture at the end of the period is 50T-50C sample followed by 65T-35C, respectively 50.1% and 46.4%. The 65M-35C sample exhibits a good water retention of 43.6%, but it is lower compared to the sand-less analog sample. This trend is also confirmed by the two control samples, 100T and 100M: the sample with sand shows a lower moisture content than the soil. Finally, the 80T-20C sample has a moisture content of 38%, an effect of the low amount of biochar used.

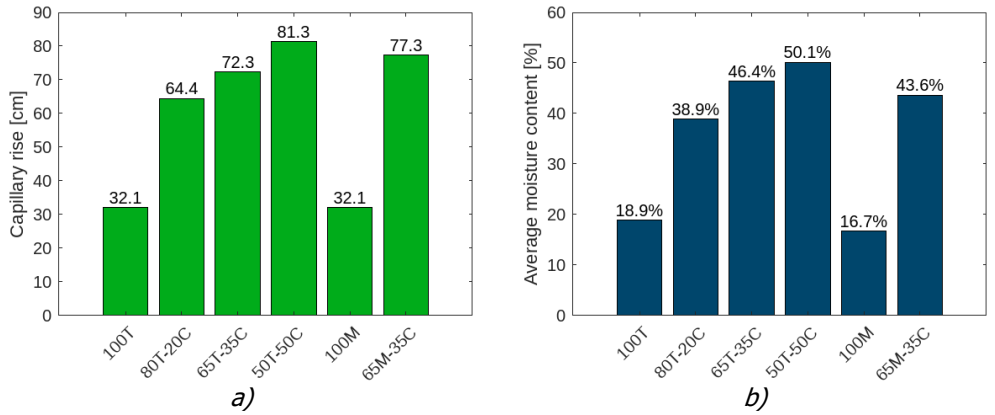

Figure 10-9. Comparison between the maximum capillary rise (height of the wetted front) (a) and the average column moisture (b) at the end of the sampling period of 11 days.

As summary, Figure 10-10 shows the comparison between the different capillary rise trends in the substrates indicating the wet front line.

The most promising samples are those with a biochar content greater than 35% confirming that sand contributes to the capillarity phenomena. The 65M-35C curve, in fact, lies almost equidistant between the 65T-35C curve (which remains below) and the 50T-50C curve (which remains above).

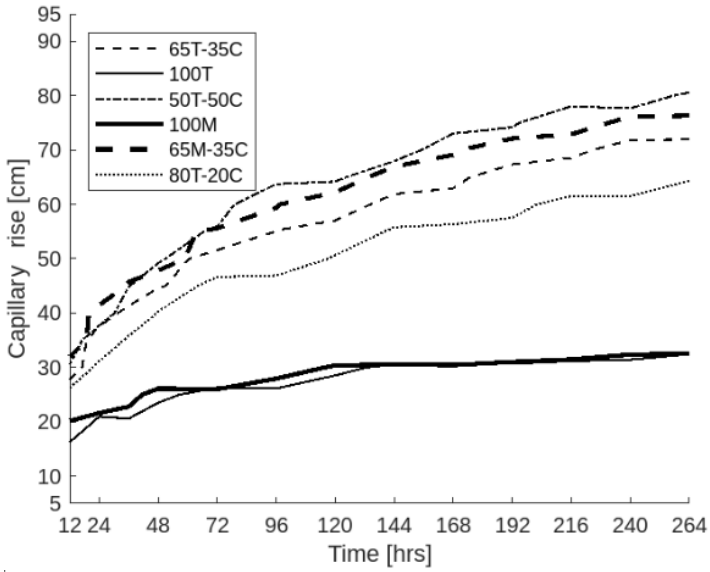

Figure 10-10. Comparison of waterfront's trends of the different sample, over the 11 days sampling period .

10.3.3 Carbon storage capability results

Following the methodology proposed by *VERRA*, carbon storage is quantified. Starting from data in Table 16, the carbon storage potentials in terms of equivalent carbon dioxide (CO_2eq), are obtained and shown in Table 19. As the amount of applied biochar increases, the amount of carbon potentially stored also increases. Furthermore, carbon credits can be sold in the carbon trading market: one carbon credit corresponds to 1 ton of CO_2eq stored for a value of € 80 [221]. This means that carbon credits can be an economic profit for the owner of the geothermal plant. To date, in an underdeveloped market framework, the cost of biochar is € 300 ton^{-1}, while € 190 is gained from the sale of the corresponding carbon credits. It is pointed out that for an excavation of a geothermal field of 100 m^2 and 3 m deep, in the case of 50T-50C mixture, 32.7 tons of dry biochar are needed, for a cost of € 9800. Considering the conversion into carbon credits, a carbon storage of 77.2 tons of CO_2eq is realized and corresponds to an income of 6170 €, equal to 63% of the initial investment. This *payback mechanism* is not available for any other BMs.

To give context to this application, let's consider a house with a surface area of 100 m^2 in the Middle Europe, with a 111 kWh m^{-2} average space heating consumption per year [222] equipped with a 4kW heat pump that operates for 3000 hours per year. Coupling the heating system with a geothermal field and estimating in 25 m^2 kW^{-1} its surface area extension [223], a geothermal field of 100 m^2 is considered for this analysis. European statistics estimate the average carbon footprint of households in Europe in 7 kg CO_2eq m^{-2} y^{-1} [224]. Therefore,

the impact for the space heating of the case considered is equal to 0.7 ton CO_2eq y^{-1}. According to the carbon storage results calculated before, if 50% of biochar is used as BM mixed with soil, a household with the explained characteristics has a carbon-neutral heating operation until approximately the 100th year from construction. In fact, the carbon stored in the biochar balances the carbon dioxide emitted during the operation of the heating system.

Table 19. Carbon storage potential of the different mixtures, per cubic meter.

Name	Biochar content [% v/v]	Biochar per each cubic meter [kg]	Carbon stored [kg of CO_2eq]
100T	-	-	-
80T-20C	20 %	43.6	103
65T-35C	35 %	76.3	180.3
50T-50C	50 %	109	257.5
100M	-	-	-
65M-35C	35 %	43.6	180.3

10.4 Conclusions and future perspectives

While biochar addition doesn't significantly alter soil thermal conductivity in dry conditions, the water retention capacity of biochar increase the wet level of soil and, consequently, the thermal conductivity of the substrate. These findings are crucial for confirming that the novel application of biochar is a suitable BM for low enthalpy geothermal fields since it brings improvement, combining the improvement of the energy efficiency of geothermal systems and the topic of the carbon storage.

These experimental campaigns demonstrates that the utilization of biochar significantly enhances:

a) thermal conductivity: in CHAR_50 and CHAR_67 an increment of 17% in humidity content rises thermal conductivity of about 400 %
b) water uptake: an impressive 150% improvement is observed when biochar constitutes 50% of the solid matrix.

Biochar has proved to be an effective method of maintaining high moisture levels of the soil. In contrast to sand, which diminishes water retention due to the lack of microporosity, the different pore sizes of biochar are a key feature that make it an excellent fluid retainer.

These findings offer valuable insights for determining the optimal biochar application rate. Striking a balance between biochar cost and benefits is essential during the selection of the composition for the most suitable mixture: the compromise is a biochar application rate between 35% and 50%.

Future investigations could include measuring thermal conductivity and specific heat varying biochar shares as BM.

Using biochar as BM may not have a disruptive impact on the global carbon removal capabilities, given the limited diffusion of geothermal systems. However, the impact for unit area is relevant (if a 35%-50% rate of biochar is used), as high quantities of biochar can be employed in a single geothermal application if compared to cultivated fields.

11 EXPERIMENTAL INVESTIGATION ON METHODS FOR THE BIOCHAR ELECTRICAL CONDUCTIVITY MEASUREMENTS.

What is the real electrical conductivity of biochar?
As emphasized in Chapter 2, high-temperature biochar exhibits an atomic-level structure like graphite. Many studies and regulations or standard about biochar chemical analysis, suggest the measure of electrical conductivity through aqueous solutions method. The following study challenges these methods by first identifying an appropriate "dry-methodology" (starting from existing literature) and then testing several biochar samples to identify the more accurate electrical conductivity "dry" measured.

Although this research falls into a niche, this topic contributes to a broader investigation on the value of electrical conductivity perceived by soil microorganisms when they are in in contact with biochar grains, for better understanding how biochar participates in electron transfer among all soil species.

Keywords: Electrical conductivity; Biochar; Gasification; Grain size; Morphology; Physical-chemical parameters.

A form of this work is also published in "Measurement - Journal of the International Measurement Confederation". Available online from 10 October 2023.

11.1 Biochar characteristics and the prime role of electrical conductivity

Biochar needs to meet specific requirements reported in the European Biochar Certificate or the International Biochar Initiative [79,225]. The intrinsic properties of biochar depend mainly on the chosen feedstock and on the thermochemical parameters of the biomass-to-biochar conversion process (temperature, residence time, type of thermochemical process) [38,226,227]. Other extrinsic properties of biochar depend on the dimensions of the grains (biochar particle size). In fact, inside most gasification reactors the fuel (i.e. wood chip or wood pellet) geometry remains almost unchanged, producing only a reduction in size, especially at temperatures above 700/800 °C) [228]. However, the extraction of biochar from the reactor often takes place through augers and conveyor belts. For this reason, biochar undergoes crushing and size reduction processes. The result is a biochar with a wide particle size distribution.

Biochar is globally recognized as one of the most promising materials for carbon sequestration since it falls into the carbon negative concept [229,230]. This carbon storage effect is not limited to the biochar carbon content, but it is multiplied by the facilitating role that biochar plays in the development of soil microflora and microfauna. The increase in microbial activity contributes to the reduction of atmospheric CO_2 through an effective stabilization of carbon within the soil [231,232].

Literature studies highlight how the *electron transfer mechanism* is fundamental for soil geochemical and biochemical transformations [112,233]. Biochar, as a highly conductive material, triggers the processes that improve the "carbon negative priming" mechanisms through a profound interaction with the soil biome: thanks to the carbon structure of the biochar as well as its porous morphology, soil organisms can exploit the biochar's higher electrical conductivity (EC) for mutual microbial interactions, resulting in more stable carbon being mineralized in soil [112,171,234]. Lehmann and Joseph (2015) [228] properly described the advantages of electrical conductivity shifting the biomass conversion towards graphite-like structures.

The EC has always been considered an important parameter in the study of carbonaceous materials and it is obtained by measuring the electrical resistance R [Ω] of a specific volume of material [235,236]. The methods used for EC measurement, developed in literature for various applications, have been recently applied to biochar to estimate the consequent soil improvement effects that lead to the creation of soil geo-conductor phenomena [111,112]. In fact, the latest developments suggest that [135]:

1. the soil EC is considered an indicator of agricultural soil fertility and quality;

2. the electron transfer dominates the exchange processes between biome and nutrients in the soil;
3. the biochar significantly improves the interaction described in bullet 2.

It therefore becomes crucial to know the electrical conductivity EC [S m^{-1}] of the biochar before applying it to the soil.

Parl et al. (2021) [237] demonstrated that biochar can be used as a low-cost, eco-friendly, and electrically conductive material for Terahertz applications. Its terahertz conductivity was measured through time-domain spectroscopy, using a sapphire femtosecond laser and a photoconductive antenna for the terahertz pulse generation. The results showed an increase from few S m^{-1} for the biochar obtained at 600 °C to 10^2 S m^{-1} for the biochar obtained at 800°C.

Two main aspects influence the EC of biochar: the chemical composition of the feedstock and the thermochemical process used for biochar production. Starting from 400°C, the biomass carbon is converted first into amorphous portions of aromatic carbon and then into an ordered structure in crystalline planes until it assumes graphitic-like structures when it is processed at temperatures above 1000°C [94,238,239]. This metamorphosis converts the dielectric biomass into electrically conductive biochar: the higher the process temperature, the more the biochar crystallizes and increases in EC [110,240]. The measurement of the EC enables the evaluation of the biochar's quality in terms of quantity of graphitic-like fraction present [110,228].

The chosen thermo-chemical conversion process can also affect the final chemical composition of the biochar by modifying its carbon/ash shares [241,242]. These two elements also depend on the composition of the starting biomass, and they are considered among the main causes of the biochar's final EC. Several studies state that ash has a dielectric-like behavior and the higher its amount, the lower the biochar EC [243–246]. Conversely, the behavior relating to the carbon content directly affects the quality of the internal crystalline structure and its increase corresponds to an increase in the EC [247].

What really affects the EC, however, is the biochar microscopic structure of the C atoms.

11.1.1 Electrical conductivity measurement methods. A review

To identify a proper method to measure biochar EC, a literature review is carried out. Two main methods are currently used, neither of which can consider all the parameters that are responsible for the biochar conductivity in its soil application:

1. the International Biochar Initiative (IBI) suggests using the procedure indicated by the US Composting Council and adapting it to biochar. This

method involves dispersing the biochar in a solution of distilled water. This procedure is affected by the number of ions that are dissolved and is not able to take into consideration the biochar particle size and atomic structure [79,130];

2. the alternative method used in several works, including those by Hoffmann et al. (2019) and Kane et al. (2021) [247,248], applies the standards for carbon powders proposed by Celzard et al. (2002) [236]. It requires a reduction of the biochar sample into a small particle size or powder. It is then placed in an electrically insulated cylinder and compressed at variable pressure. By measuring the resistance offered by the biochar under those specific conditions, and knowing the volume changes, the electrical conductivity is calculated. The method, therefore, recognizes that particle size affects EC. To allow a comparison between samples, this method bypasses the problem by homogenizing the samples and grinding them to fine sizes.

A consistent niche of works in literature have adopted the latter method to biochar samples: Gabhi et al. (2017) [249] tested a commercial biochar, applying pressure up to 100 bar to a monolithic grain, and found EC values that ranged between $5*10^{-5}$ S m^{-1} and 400 S m^{-1}. Kennedy et al. (2005) [250] started from rice husk to produce biochar in a pyrolysis reactor at 400°C. The obtained ECs were in the order of 10^{-4} -10^{-3} S m^{-1} at pressures that ranged from 0.76 to 5.78 bar. Bartoli et al. (2022) [75] measured the EC of several biochars produced at 700°C from waste biomasses, testing them from 0 to 1500 bar, with results between 10^{-2} S m^{-1} and 1 S m^{-1}. Antal and Gronli (2003) [115]report the tests performed on two packed samples of the same biochar: resistivity of 1.24 Ω cm at 196 bar and 0.27 Ω cm at 980 bar were measured. In Quosai et al. (2018) [251] the measured EC had values from 1.81 mS m^{-1} to 119 mS m^{-1} for three different biomasses pyrolyzed at 900°C and tested at only 1.27 bar. All the above-mentioned works put little or no stress on the effects that biochar particle size or biochar morphology have on the test results. Celzard t al. (2002) [236] is the first study that recognizes the complexity of the phenomena beyond the EC measurement, showing how different morphologies of the very same starting carbonaceous powders lead to different EC results. Other authors have identified, for uncompressed monolithic biochar EC = 0.02 S m^{-1} and for biochar produced by hydrothermal carbonization of vineyard pruning tested at 6.45 bar, EC ranging from 52 S m^{-1} - 100 S m^{-1}. Other works in literature attempted to isolate the variables involved during the EC measurement by producing *ad hoc* biochar or measuring its "monolithic properties" (starting from the work of Duba (1997) [252]) but the results still show high variability of the EC: 0.2 S m^{-1} - 185 S m^{-1} as reviewed in Kane et al. (2021) [248]. Nan (2016) [253] applied the EC measurement under compression to biochar particles obtained from different biomasses at various temperatures. This demonstrates that EC is noticeably

influenced by the applied pressure, temperature and feedstock. A peak value of about 1700 S m^{-1} at 300 bar was obtained for red oak pyrolyzed at 1000°C [253]. A complete summary of this literature review is reported in Table 20.

Table 20. Summary of main biochar EC values from literature review.

Feedstock	Wood biomass	Pressure range	EC range	Reference
Gabhi et al., 2017	Sugar maple, oak, and hickory	0.4 - 100 bar	$5*10^{-5}$ - 400 S m^{-1}	[249]
Kennedy et al., 2005	Rice husk	0.76 - 5.78 bar	$328*10^{-4}$ - $202*10^{-3}$ S m^{-1}	[250]
Bartoli et al., 2022	walnut shells, lignin rich residue from bio-ethanol production and sewage sludge	0 – 1500 bar	10^{-2} - 1 S m^{-1}	[75]
Kane et al., 2021	Ball-milled lignin feedstock, wheat stem and cellulose feedstocks	Based on sample deformation	0.2 S m^{-1} - 185 S m^{-1}	[248]
Antal et al., 2003	Babacu nut	196 and 980 bar	1.24 Ω cm and 0.27 Ω cm	[115]
Quosai et al., 2018	Dark roast coffee chaff light roast coffee chaff and soy hulls	1.27 bar	$1.81*10^{-3}$ $3.50*10^{-3}$ and 119 $*10^{-3}$ S m^{-1}	[251]
Jiang et al., 2013	Red cedar wood	No compression	0.02 S m^{-1}	[254]
Hoffmann et al., 2019	Vineyard pruning	6.45 bar	52 S m^{-1} - 100 S m^{-1}	[247]
Debevc et al., 2022	Mixture of almond shells and hulls (only 300 mg of sample	Up to 9 kg cm^{-2} (1.25 bar – 11.24 bar)	0.005 S m^{-1} - 0.278 S m^{-1}	[255]
Duba et al., 1977	Pyrolyzed coal from Roland Seam of the Wyodak Mine (Wyoming)	No compression. Surfaces coated with conductive silver paint.	10^{-3} S m^{-1} - 10^{2} S m^{-1}	[252]
Nan, 2016	Red oak	300 bar	1700 S m^{-1}	[155]
Nan, 2016	Yellow-poplar	680 bar	750 S m^{-1}	[253]
Nan, 2016	Willow	170 bar	275 S m^{-1}	[253]

The criticism of the high variability of EC values measured on biochar samples is also highlighted by Kane et al. (2021) [256]. This study testifies to

the fact that further investigation is needed. As a reference point, it is important to outline that this variability issue is reported in literature also for more refined samples such as activated carbons and graphite materials [132,257]. Biochar is often composed of a mixture of packed powders or grains: new parameters arise among the known parameters, morphology and composition, which influence the measurement of the EC:

a. the granulometric distribution of the sample
b. the arrangement and orientation of the grains within the measured specimen.

In fact, the measurement of electrical resistance depends on both the grain-grain and grain-electrode plates contacts. A greater number of grains in the specimen implies a greater number of contact resistances affecting the measurement, and the larger the size of the individual grain, the more relevantly its initial orientation affects the test [138,249].

11.1.2 Experimental campaign to discuss the electrical conductivity values

This work is aimed at presenting an extended testing campaign on a single batch of biochar and to use the results obtained to discuss the limits of the proposed piston-based methodology ([236]) or measuring the EC when it is applied to biochar samples. The work seeks to help the scientific community to better discuss the approach to EC measurements and the meaning of the results obtained through this methodology.

The results of the testing campaign showed how a single batch of biochar can lead to a wide range of EC values. Outlining this behavior may help to raise awareness of major flaws in the proposed method: the final EC value is strongly dependent on biochar sampling and testing conditions. Different testing regimes lead to different EC and there is no evidence that the obtained values reflect how the EC is truly perceived by the microorganisms of the soil where the biochar will be applied. The research described in this paper starts from the chemical-physical characterization of different particle sizes of a single batch of a commercial biochar obtained from the sieving of a single starting sample. The EC trends obtained have been re-arranged as a function of carbon content and ash content then compared with literature data as a validation of the proposed method.

The experimental campaign consists of fifteen measurements of EC at variable pressure from four samples of the same biochar, each with different grain cut-off diameters. To isolate the size effects, half of the sieved samples were ground before repeating the EC measurement.

11.2 Biochar samples and electrical conductivity measurement apparatus

In this work, biochar obtained through a thermochemical gasification process was investigated. The reactor used for the biochar production consisted of a single throat downdraft "Imbert" gasifier working with air as the gasification agent. The temperatures of Imbert reactors peaked at the combustion zone, corresponding to the throat (close to 1000 °C). The charred biomass that passes through the combustion zone then reaches the final zone below the throat where the temperature drops to approximately 550–600 °C. The extraction of the biochar is usually located here, where the temperature is higher than the most common dew points of tar compounds. High-temperature extraction and long persistence in the reduction environment leads to an "high quality characteristics" biochar [38,58,215,258].

11.2.1 Biochar samples

The biochar was selected among the biochar listed in the Italian national database as certified soil improvers. The purchased biochar was produced in a gasification plant of the above-described type with a nominal power of 200 kW (electrical) using fir wood chips. The specific architecture of this system allows the biochar to be quenched in a water bath before being extracted from the reactor base pan. This extraction method results in a soaking wet biochar. For this reason, all the samples were completely dried at 105°C for 6 hours to prevent the EC measurement to be affected by any water content. After, 3 different samples were created through sieving the as-received material with a model AS200 RETSCH vibrating sieve equipped with sieves with mesh sizes of 3 mm and 5 mm. Three samples with different grain cut-off diameters (Ø) were thus obtained: Ø < 3 mm - *BC_F* (Fine BioChar); 3 < Ø < 5 mm - *BC_3*; Ø > 5 mm – *BC_5*. A sample from the as-received biochar was added, named *BC_AR.* All the characteristics of all biochar are reported in Table 4.

A part of the *BC_AR, BC_F, BC_3* and *BC_5* samples were then ground with an electric mixer obtaining the relative fine and homogeneous samples and subsequently labeled: *BCG_AR, BCG_F, BCG_3* and *BCG_5*. The samples and the relative abbreviations are listed in Table 21. All non-ground biochar samples are labeled with the acronym *BC_x*, the sample created from the same material, while ground will be labelled with *BCG_x*, where the suffix *"G"* indicates the grinding passage.

Table 21. Biochar used in the tests and relative particle size.

Sample code	Description	Sieving range
Non-ground samples (BC_x)		
BC_AR	Biochar as received	-
BC_F	Sieved under 3 mm	Ø<3 mm
BC_3	Sieved between 3 and 5 mm	3<Ø<5 mm
BC_5	Sieved over 5 mm	Ø>5 mm
Ground samples (BCG_x)		
BCG_AR[1]	Ground from BC_AR	-
BCG_F[1]	Ground from BC_F	-
BCG_3[1]	Ground from BC_3	-
BCG_5[1]	Ground from BC_5	-

[1] BCG = biochar after grinding. Particle size of ground samples are 0<Ø<75 μm = 64.1%; 75<Ø<150 μm = 14.7%; 150<Ø<250 μm = 4.3%; 250 μm<Ø<1 mm = 16.9%.

11.2.2 Chemical-physical analyses

All the eight samples from Table 21 were analyzed using a Micromeritics Instrument Corp instrument to obtain the Brunauer–Emmett–Teller (BET) specific surface area [120].

The true density of the biochar samples was measured using a Micromeritics AccuPyc II 1340 helium pycnometer.

The ash content was measured gravimetrically by leaving the sample at 600°C for 6 hours in a Lenton AWF 12/5 muffle and by measuring the initial and final mass of the sample accordingly to the ASTM E1755-01 [184].

The ultimate analysis was carried out using a Thermo Scientific™ FLASH 2000 CHNS Analyzer (Thermo Fischer Scientific Inc., Milan, Italy) which allows for the evaluation of finely ground samples only. For this reason, the ultimate analysis was carried out on *BCG_x* samples, extending the validity of the results to non-ground samples (*BC_x*).

The qualitative pH values of the samples were measured through a litmus paper in a biochar-distilled water solution with a 1:10 w/w dilution ratio.

EDS Analysis was realized through a ESEM Quanta-200, Fei Company - Oxford Instruments.

11.2.3 Experimental apparatus for the electrical conductivity measurement

The electrical conductivity of the biochar was measured through the experimental apparatus depicted in Figure 11-1.a.

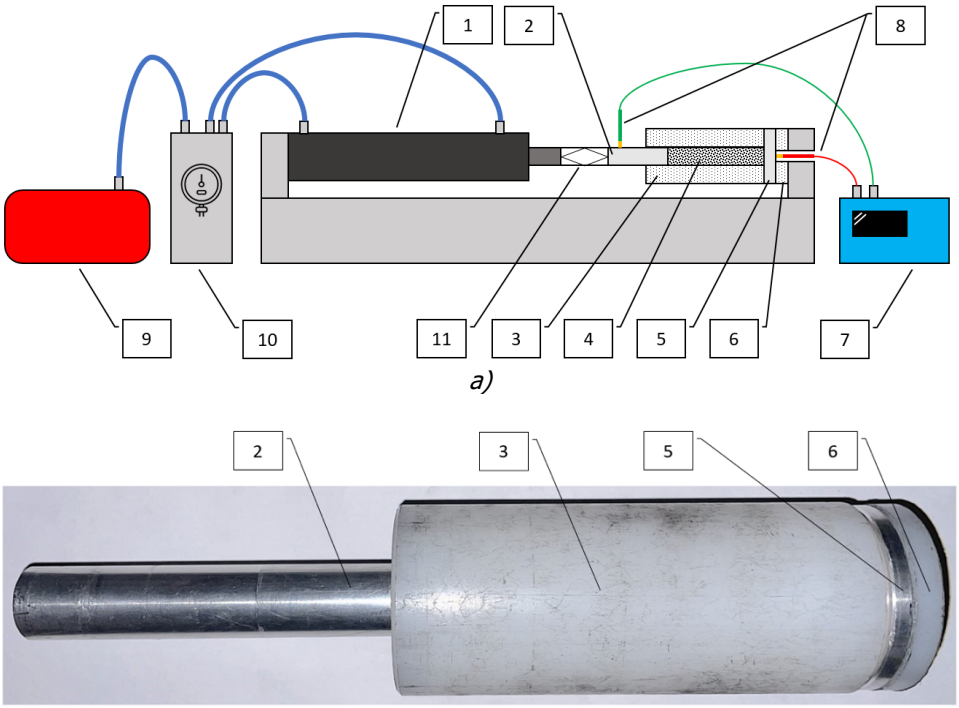

Figure 11-1. Experimental device for the measurement of the electrical conductivity of char (a) and detail of the aluminum plunger and PTFE cylinder (b).

The system consists of a pneumatic cylinder (1) whose rod is rigidly connected to an aluminum plunger (2). The aluminum plunger is tightly fitted into a PTFE cylinder (3) where it compresses the sample material whose electrical conductivity is to be measured (4). The sample is kept confined inside the PTFE cylinder by an aluminum plate (5) which defines the other extremity of the measurement volume. A PTFE disc (6) electrically isolates the measurement volume from the instrument support structure. The electrical resistance value is measured through a Metrix MTX3292 ohmmeter (7) equipped with two electrical clips (8) connected respectively to the aluminum piston and to the aluminum plate. The pneumatic cylinder is operated using the compressed air stored in the air vessel (9) that is constantly maintained at a pressure of 10 bar. A 12 VDC pressure switch (10) controls the movement of the pneumatic cylinder by setting the operating pressure to a target value in the range from 2 to 10 bar through a pressure-reduction valve. The reduction of the cross-sectional area between the aluminum and the pneumatic pistons acts as a pressure multiplier; therefore, the pressure effectively transmitted on the char sample varies from 0.62 to 24.98 bar. This pressure value was recorded through a load cell (11). The length of the char sample was measured using an analogic caliper inserted between (2) and (4). The instruments used are listed in Table 22 together with the respective sensitivity and measurement uncertainty.

Table 22. Description of the instruments used in the experimental campaign.

Instrument	Range	Sensitivity	Accuracy
Load cell – DHS300	0-300 kg	0.1 kg	± 0.45 kg (0.15 % fs)
Ohmmeter – Metrix MTX3292	0-1000 Ω	0.01 Ω	± 0.1 % mv
Analogic caliper	0-150 mm	0.1 mm	± 0.2 mm
Digital scale – KERN PLE3100-2N	0-3100 g	0.01 g	± 0.02 g

* fs = full scale; mv = measured value.

11.2.4 Procedure for the electrical conductivity measurement

Before each measurement the samples were dried at 105°C for 6 hours. For each test, a graduated cylinder (sensitivity ± 1 ml) was used to sample 20 cm^3 of dried biochar, then weighed with the KERN PLE3100-2N laboratory balance and finally poured in the PTFE cylinder (3 in Figure 11-1). The char-filled PTFE cylinder was then placed in the PTFE cylinder. To standardize the preparation of the different samples, the filled cylinder was manually shaken for a fixed, short period of time before closing it with the aluminum plugger. This procedure was followed for all samples and consisted in a simplified version of the ASTM density measurement standard. The aluminum plunger (2) was then manually inserted into the PTFE cylinder until it reached the biochar. The measurement procedure was started following a sequence of steps: 1) regulation of the target pressure to be applied to the pneumatic cylinder through the pressure switch; 2) activation of the pressure switch and consequent compression of the biochar by the aluminum plunger; 3) reading of the force and the electrical resistance respectively through the load cell and the ohmmeter; 4) measurement of the sample length variation using the caliper (from the total length of the PTFE cylinder and the length of the aluminum plunger it was possible to back-calculate the compressive strain and the bulk density of the biochar at variable pressure values); 5) deactivation of the pressure switch. Subsequently, the next pressure value was set on the pressure-reduction valve and the steps described above were repeated. This sequence was repeated for each of the 14 pressures investigated within the range 0.6 - 25.0 bar. Appendix B reports a flow chart with the procedure step-by-step.

11.2.5 Calculation of the electrical conductivity values and other parameters

The PTFE cylinder containing the biochar has an inner diameter $ID_{PTFE} = 20^{\frac{+0.2}{+0.1}}\,mm$ and length $L_{PTFE} = 100\,mm$ while the aluminum plunger has an outer diameter of $OD_{Al} = 20^{\frac{-0.1}{-0.2}}\,mm$ and total length of $L_{Al} = 120\,mm$.
For each pressure step, the length of the outer cylinder $L_{Al,out}$ was measured and through Eq. (11-1) the effective volume occupied by the biochar was calculated.

$$V_{biochar} = \left(L_{Al} - L_{Al,out}\right) \cdot \pi \cdot \frac{ID_{PTFE}^2}{4} \qquad [m^3] \qquad (11\text{-}1)$$

Knowing the mass of the inserted sample $M_{biochar}$, the bulk density of the material is calculated through Eq. (11-2):

$$\gamma_{biochar} = \frac{M_{biochar}}{V_{biochar}} \qquad \left[\frac{kg}{m^3}\right] \qquad (11\text{-}2)$$

The biochar EC was calculated through the electric resistance of the sample $R_{biochar}$ measured through the multimeter. The sample length $L_{biochar}$ was calculated according to Eq. (11-3) and the sample surface area $A_{biochar}$, constant for each sample and approximated to the aluminum plunger circular surface area.

$$L_{biochar} = L_{PTFE}\left(L_{Al} - L_{Al,out}\right) \qquad [m] \qquad (11\text{-}3)$$

The electrical conductivity value was then calculated through Eq. (11-3) and Eq. (11-4), as proposed by [232]:

$$EC_{biochar} = \frac{L_{biochar}}{A_{biochar} \cdot R_{biochar}} \qquad [S \cdot m^{-1}] \qquad (11\text{-}4)$$

The resistivity of the biochar could then be calculated according to Eq. (11-5):

$$\rho_{biochar} = \frac{1}{EC_{biochar}} \qquad [\Omega \cdot m] \qquad (11\text{-}5)$$

11.2.6 Uncertainty computation

Uncertainty analysis was carried out to estimate the expected accuracy of the experimental data measurement. The methodology implemented was demonstrated by Kline and McClintock (1953) [213]; it describes the uncertainty

evaluation of a single-sample experiment through the second-power equation reported in Equation (11-6).

$$\omega_R = \left[\left(\frac{\partial R}{\partial v_1}\omega_1\right)^2 + \left(\frac{\partial R}{\partial v_2}\omega_2\right)^2 + \cdots + \left(\frac{\partial R}{\partial v_n}\omega_n\right)^2\right]^{0.5} \qquad [-] \qquad (11\text{-}6)$$

where: *R* is the result under uncertainty investigation and it is a function of n independent variables v_i (as reported in Equation (11-7)) while ω_i is the known uncertainty correlated to the independent variable v_i and ω_R is the result uncertainty interval [259].

$$R = R(v_1, v_2, \ldots v_n) \qquad [-] \qquad (11\text{-}7)$$

The accuracies of the instruments used are shown in Table 22. For visual clarity, the resulting graphs do not report the error bars. Uncertainty value results are listed in Table 23 and continue in Appendix A.

11.3 Biochar analysis, EC values and discussion on correlation relationships

11.3.1 Chemical-physical analyses of the biochar samples

The results of the final analysis and the ash content, expressed in $\%_{w/w}$, of the investigated biochar are reported in Table 23. It is possible to see how the carbon content increased as the particle size increased. *BCG_F* is approximately 25% lower than *BCG_3* and *BCG_5* which instead contained respectively 76.3% and 75.0% of total carbon. This behavior is confirmed by Kalina et al. (2022) [260] and is mainly caused by the fact that larger grains are subjected to less intense gasification processes that tend to preserve a greater fraction of carbon. In essence, the longer a particle lies in the reactor environment, the more its carbon is converted, which ultimately reduces the particle size.

The ash content is measured as residual solids after treatment in a muffle at 600°C for 6h, except for the *BC_AR* which contains the entire range of particle sizes of the as-received biochar and settles its ash content to an intermediate value of 36.8%. This result has been obtained through a set of three different measurements that showed a variability of ± 10% from the mean value (40.07 %w/w, 38.31 %w/w and 32.06 %w/w). Data show that for samples *BC_F, BC_3* and *BC_5* the ash content decreased from 41.7% to 9.2% as the granulometry increases. The results for the *BCG_x* and *BC_x* samples had approximately the same ash content, demonstrating that the grinding process did not affect the composition of the samples. The ash content increase in the finest biochar samples was due to the concentration of the fine fractions of inorganic material that concentrated in the smaller fractions of biochar due to the sieving process.

Table 23. Ash content, ultimate analysis, true density, and EDS analysis.

	Ash[1] [%w/w]	N[2] [%w/w]	C[2] [%w/w]	H[2] [%w/w]	O [%w/w]	True density ± Std.Dev. [g cm^{-3}]	pH
BC_AR*	36.8	0.24	55.22	0.77	11.77	2.2313 ± 0.0040	10
BCG_AR	33.6	0.24	55.22	0.77	10.17	2.1854 ± 0.0032	10
BC_F	41.7	0.21	51.11	0.56	6.42	2.2606 ± 0.0042	10
BCG_F	41.8	0.21	51.11	0.56	6.32	2.2437 ± 0.0060	10
BC_3	12.3	0.33	76.28	0.61	10.48	2.0592 ± 0.0080	10
BCG_3	14.0	0.33	76.28	0.61	8.78	2.0547 ± 0.0012	10
BC_5	9.2	0.31	74.96	0.50	15.03	2.0496 ± 0.0045	9
BCG_5	10.4	0.31	74.96	0.50	13.83	2.0496 ± 0.0024	9

EDS[3]	C	O	Na	Mg	Si	P	S	Cl	K	Ca
BC_AR	90.0	4.99	-	0.54	0.19	0.87	-	-	0.78	2.62

[1]*± 0.1%;* [2]*±* 0.01%; [3]All elements in *[%w/w]*, no error is available. *Mean value of three ultimate analyses.

Furthermore, the above-mentioned trend for the ash content confirms what has already been described in literature and supports the validation of the method used [73]. Finally, data show that as the ash increased the carbon content decreased linearly ($R^2 = 0.98$), as expected, Figure 11-2.a.

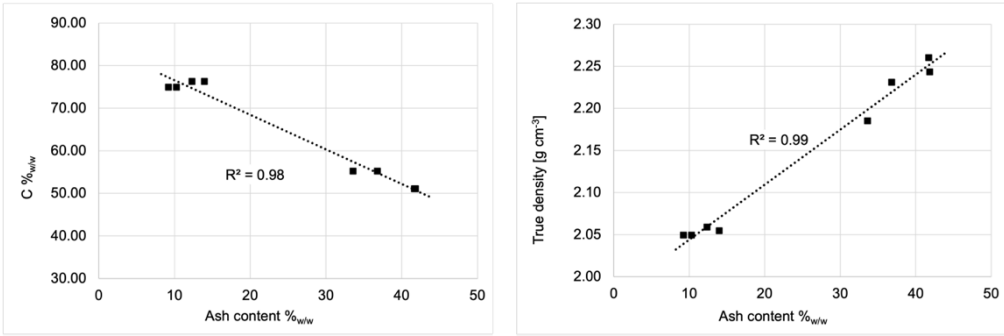

a) *b)*

Figure 11-2. Carbon content a) and true density b) vs ash content of the BC_x and BCG_x biochar samples. Error bars are not graphically reported since they are small: ± 0.01% (see Table 23).

As for the true density, the data follow the same trend: *BC_AR* sample settled at an intermediate value of 2.2313 g cm^{-3} while for other samples, the density increased when the grain size decreased, from 2.0496 g cm^{-3} for BC_5 to 2.2606 g cm^{-3} for *BC_F*. This trend confirms for the findings on bulk density by [261] and is explained by the fact that ashes have higher density than the carbonaceous fraction. Figure 11-2.b. shows the linear behavior just described.

Concerning particle size distribution, the *BC_AR* samples and the ground samples were characterized after grinding in the knife mixer. The results are reported in Table 23.

Table 24. Particle size distribution of BC_AR samples and samples after grinding with the knife mixer.

Sample	***Range of particle size***	***Fraction***
BC_AR	Ø > 5 mm	5.0 %
	5 > Ø > 3 mm	18.0 %
	Ø < 3 mm	77.0 %
BCG_AR; BCG_F; BCG_3; BCG_5	0 < Ø < 75 µm	64.1 %
	75 < Ø < 150 µm	14.7 %
	150 < Ø < 250 µm	4.3 %
	250 µm < Ø < 1 mm	16.9 %

The particle size distribution conducted on the BC_AR sample shows a clear shift towards finer fractions which justifies the similar results obtained in the chemical analysis (Table 23) and influences the EC trend as described in the following paragraph.

11.3.2 Electrical conductivity of the biochar samples

The measurements of the electrical conductivity are carried out on *BC_x* and *BCG_x* samples. The graphs of Figure 11-3.a and Figure 11-3.b represent the EC results as a function of the pressure applied to the specimen. The complete data are reported in Table A.1 and Table A.2, Appendix A. For better visual clarity, error bars are not reported on the graphs. Refer to Appendix A (Figure A1) for the graphs containing error bars. As expected, the EC of the samples increased when the pressure increases with a positive pressure dependence, as also reported also by Sánchez-González et al. (2005) [262]. The increase in conductivity due to compression was not always linear, likely a consequence of the non-isotropic biochar microstructure and of the shape of the grains [132]. This rising trend of conductivity with compression is related to several factors such as the increasing number; the broadening of contacts between biochar particles; and the collapsing of the porosity resulting in the reduction of the internal void fraction of the structure [249]. In general, it can

be stated that better contact between grains and/or particles allows for better conductivity, but the quality of particle packing also plays a fundamental role. To confirm this, findings show that as the sample grain size increased, samples also show an increase in EC at the test pressure of 25 bar ($EC_{@25bar}$). *BC_5* had 97 S m^{-1} while *BC_F* had 43 S m^{-1}, the maximum and the minimum values found. *BC_AR* stopped at the intermediate value 64 S m-1. Regarding the grinding samples, contrary to the prevision, the maximum EC value obtained was *BCG_3* (82 S m^{-1}) and not *BCG_5* (68 S m^{-1}) for the non-ground sample. Sample *BCG_F* had the lowest value, equal to 44 S m^{-1}. The *BCG_AR* had a value of 69 S m^{-1}, the intermediate value between the two final values, the same as in the non-ground case. The *BC_AR* and *BCG_AR* values were very close. The difference between the two *BC_x* final values was 54 S m^{-1} while the BCG_x was a notably smaller 38 S m^{-1}. The complete data are reported in Table A.1 and Table A.2, Appendix A.

In general, with exception for the as-received samples *BC_AR*, there was a high variability of the EC value measured, even when samples with the same composition, ash, and carbon content, *(BC_x and BCG_x)* or particle size fraction *(BC_5, BC_3, BC_F)* were compared. The composition and particle size were not the sole factors that affect the EC value of the samples. Therefore, these results testify that morphology of the biochar grains is as important a factor as the ones listed before in terms of affecting the EC measurements. Referring to Figure 11-3.a and Figure 11-3.b, it is presumed that EC values increased similarly for both ground and non-ground samples at low pressure (below 5 bar) because the increased carbon content and decreased density affected the EC more than the packing factor. At high pressures (above 5 bar), differences between EC values increased because packing factors, aggregation, porosity and voids are more relevant than the biochar composition.

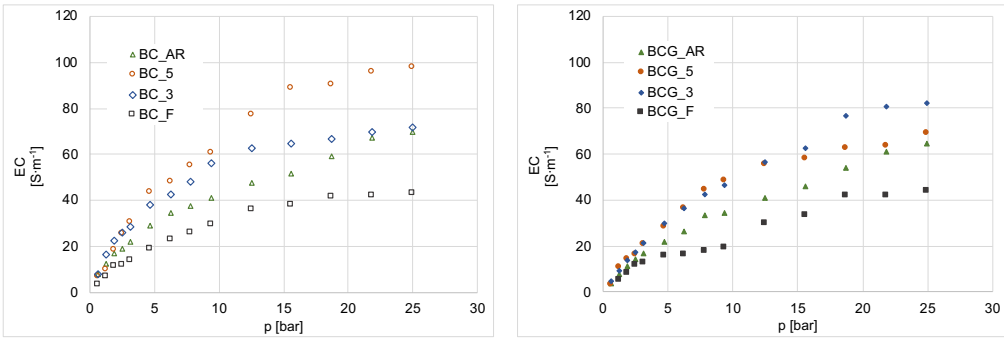

Figure 11-3. Electrical conductivity vs pressure applied to non-ground (a) and ground (b) char samples.

To obtain additional information on the morphological influence on the piston-cylinder method, the compressive strain (ε) was evaluated as a function

of the applied pressure for each sample. Figure 11-4 shows the graphs for the non-ground (Figure 11-4.a) and ground (Figure 11-4.b) char samples. The complete data are reported in Table A.3 and Table A.4 in Appendix A. Error bars are not reported on the graphs for better visual clarity. Refer to Figure A.2 for the graphs containing error bars.

It was observed that the *BC_5* and *BC_3* samples had much more elongated curves than samples *BC_AR* and *BC_F*. These trends were justified by the lower number of contacts between char particles which, therefore. generated higher contact pressures on each individual grain. Where the pressure concentrated, the forces could locally exceed the material resistance, resulting in fractures that produced a rearrangement of the particles leading to a greater displacement of the piston compared to the samples with finer particle size *(BC_F)*. The as-received char sample *(BC_AR)* had similar results to the fine fraction *(BC_F)*; the result was justified by the abundant presence of fine particles (<3 mm) in the as-received material which tended to saturate the spaces between the larger grains, thus reducing the contact pressure between them; the result was additionally justified by the enhanced ash content that allow BC-AR and BC-F samples to withstand high pressures.

The ground biochar samples (Figure 11-4.b) offered higher compressive resistance than the non-ground samples, settling on maximum compressive strain values between 25% and 30%. In this case, no appreciable differences between the different samples tested were noted. When ground, the packing factor changed due to different size distribution and particle reorganization. Furthermore, ash content was non-influent and did not lead to differences between the ground samples.

For low pressures (below 5 bar) only minor differences were found between compression strain values both for non-ground and ground samples.

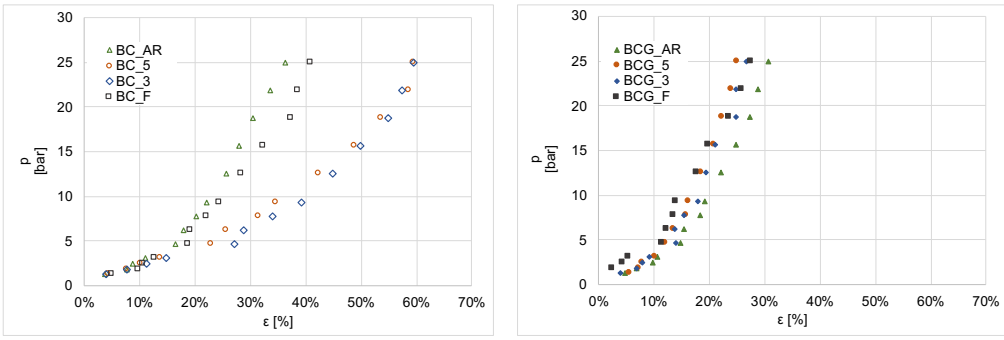

a) *b)*

Figure 11-4. Pressure vs compression strain for non-ground a) and ground b) char samples.

Table A.3 and Table A.4 show the values of p, EC and ε with the respective instrumental uncertainties calculated according to the method described in paragraph 11.2.5. Referring to the relative uncertainties, not shown in the table

in the interest of brevity, a maximum value of 3.1% was recorded in the calculation of the maximum EC and of 3.6% in the calculation of the maximum ε.

11.3.3 Role of ashes and carbon content on electrical conductivity

Many results in literature report a direct correlation between the increase in ash content and the increase in EC when the EC is measured by dispersing the biochar in water [263,264]. In their works Hoffmann et al. (2019) and Barroso-Bogeat (2014) [247,265], instead, identify a decrease of the EC as the ash content increases when tested in a compressed insulating cylinder.

The results of this research confirmed the latter research mentioned above, showing a reduction of the EC with the increase of the ash content ($\%_{w/w}$) since ashes are insulators. Only comparisons on the $EC_{@25bar}$ are hereby presented. The *BC_5* sample had the lowest ash content equal to 9.2%$_{w/w}$ and resulted in a value of $EC_{@25bar}$ equal to 97.8 S m^{-1} while the *BC_F* sample with the highest ash content (41.7 %$_{w/w}$) had $EC_{@25bar}$ = 43.0 S m^{-1}, for a reduction by more than half. The *BCG_X* sample with lowest ash content was *BCG_5* (10.28 %$_{w/w}$), with $EC_{@25bar}$ = 69.1 S m^{-1} while the *BCG_F* sample had ash equal to 41.7 %$_{w/w}$ and $EC_{@25bar}$ = 44.0 S m^{-1} that decreased by about 30%. While in the *BC_x* case there was a linear reduction, in the ground samples the *BCG_3* had $EC_{@25bar}$ = 82.1 S m^{-1}, about 13 S m^{-1} more than the *BCG_5*, and an increase in ash of about 4%. However, the general trend showed a continuous decrease in the EC as the ash content in the biochar increased. In Figure 11-5.a and Figure 11-5.b the reduction described is shown for the samples *BC_X* and *BCG_X* respectively. Error bars are not reported on the graph for better visual clarity. Refer to Appendix A (Figure A.1) for the graph containing error bars. The reduction of EC as the ash content increased was justified by the dielectric nature of the ashes. This was confirmed by the evaluation of the EC carried out on a sample of pure ash whose experimental results are reported in Figure 11-5.c. In fact, it can be observed that the EC followed the same trend as the *BC_x* and *BCG_x* samples, settling, however, at values four orders of magnitude lower.

Conversely, an increase in the carbon content led to an increase in the EC, in agreement with what was also reported by Usevičiūtė and Baltrėnaitė-Gedienė (2021) [245]. In the case of the *BC_x* samples, the EC value was doubled in correspondence with a 25% increase in the carbon content (Figure 11-5.d). In the same range of increase in carbon content, the EC value of *BCG_x* samples increased by 30% (Figure 11-5.e). *BC_x* samples showed a high variation of EC with respect to both ash content increase and carbon content increase, compared to *BCG_x* samples which had a small difference between the final EC values. Therefore, assuming as a first approximation that the ash content was not prevalent in the char and, therefore, has little or no fertilizing value, the results obtained on all the samples analyzed in this work demonstrate that

biochar characterized by low ash and high carbon contents have a higher EC and are more suitable both for uses in agriculture and carbon storage, as well as potential substitute material for carbon powders and carbon black [266–268].

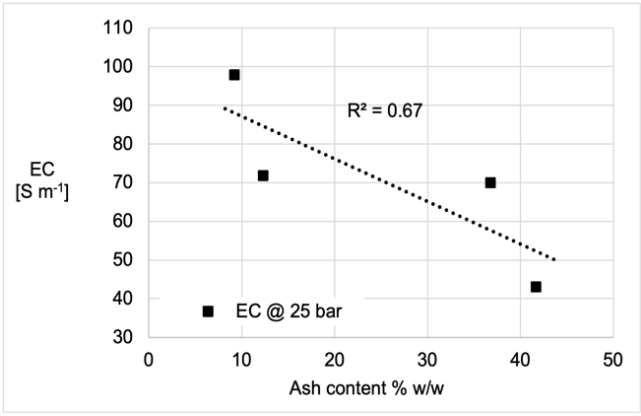

a)

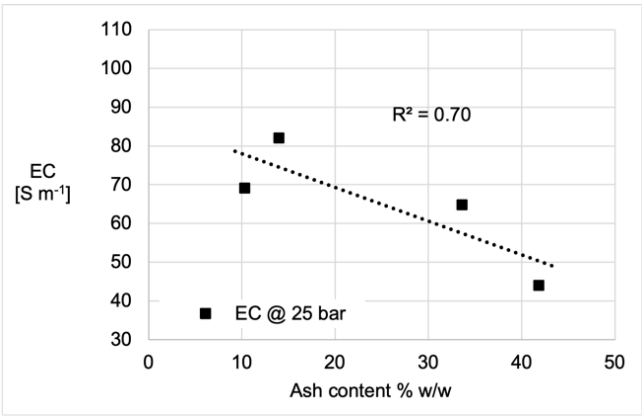

b)

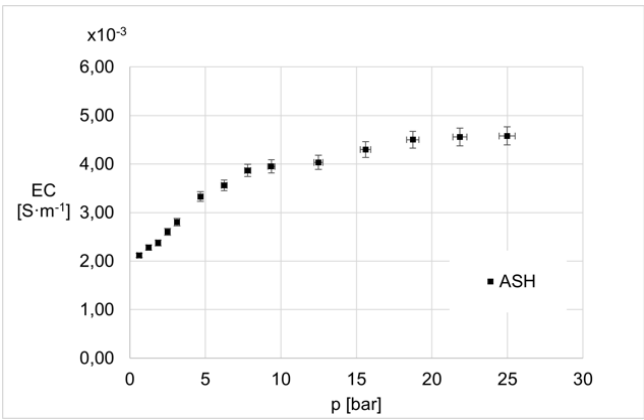

c)

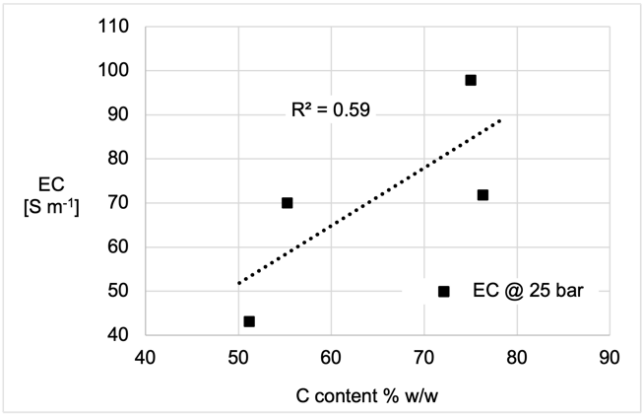

d)

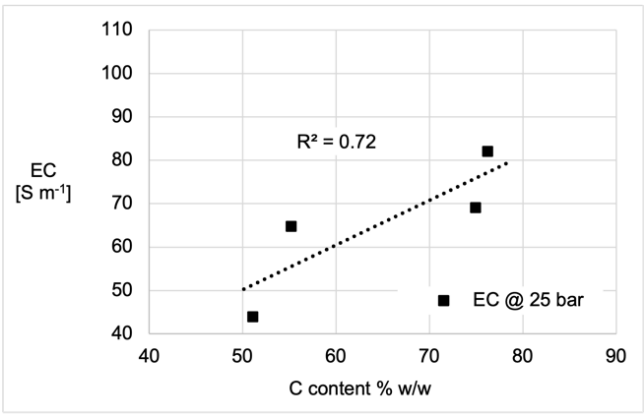

e)

Figure 11-5. EC and the ash content trend of the BC_x a) and BCG_x b) char samples; EC vs pressure applied to a sample of pure ash c); EC and the carbon content trend of the BC_x d) and BCG_x e) char samples.

11.3.4 Role of morphology in electric conductivity measurement

From the EC values obtained by analyzing the samples of different grain sizes, a trend emerged indicating that the EC increase as the size of the grains increases, as suggested by the contact resistance theory. The number of grains present in the volume of biochar tested (20 cm^3) depended on the bulk density of the sample considered; a greater number of grains (of smaller average diameter) corresponded to a greater number of contacts in the unit of volume and, consequently, to a greater total resistance of the sample, following Holm's theory [269]:

$$R_{contact} = \frac{(\rho_{item1} + \rho_{item2})}{4 \cdot a_{contact}} \quad (11\text{-}8)$$

where $R_{contact}$ is the value of the final contact resistance; ρ_{item1} and ρ_{item2} are the two specific resistivities of the two materials; $a_{contact}$ is the radius of the contact area between the two items.

The *BC_x* samples showed a higher EC (equivalent to lower resistance) than the *BCG_x* samples whose behavior was comparable to that of the so-called carbonaceous powder (e.g., carbon black, graphite powder, etc.). In fact, several studies in literature report similar behaviors: Euler (1978) [270] affirms that for the same applied pressure there is a direct proportionality between EC and grain size; Celzard et al. (2002) [236] reports that the major contribution to the total EC of the investigated specimen comes from the contact resistances which are known to be greater than the resistance of the specimen structure. The results validate that biochar follows the carbon powder theory and show high data variability during the measures. This again confirms the importance of providing all the physical and chemical characteristics of the biochar and the boundary condition of the test.

The grains of dusty samples, when subjected to increasing pressures during EC measurement, become compact and reorganize. The number of contacts and contextually the contact surfaces between the grains increase with the consequent reduction of the overall resistivity, i.e., an increase in the EC [271]. This study confirms that biochar follows the same behavior: with the same grain size, the EC increases with increasing compression. The *BC_x* samples reach higher compression strain than the *BCG_x* samples which are already tightly packed at the beginning of the test. The $EC_{@25bar}$ reached by each *BC_x* is always higher than its respective *BCG_x:* this effect can be ascribed to the number of contacts between grains that are created during the test due to the rupture of the larger particles. The fractures created in the *BC_5* and *BC_3* samples lead to a reduction of the particle size which, however, never reaches the granulometry of the ground samples *BCG_5* and *BCG_3*. In Figure 11-6 the difference between the before-test and after-test samples is reported along with a comparison to the *BC_F* sample before and after the test.

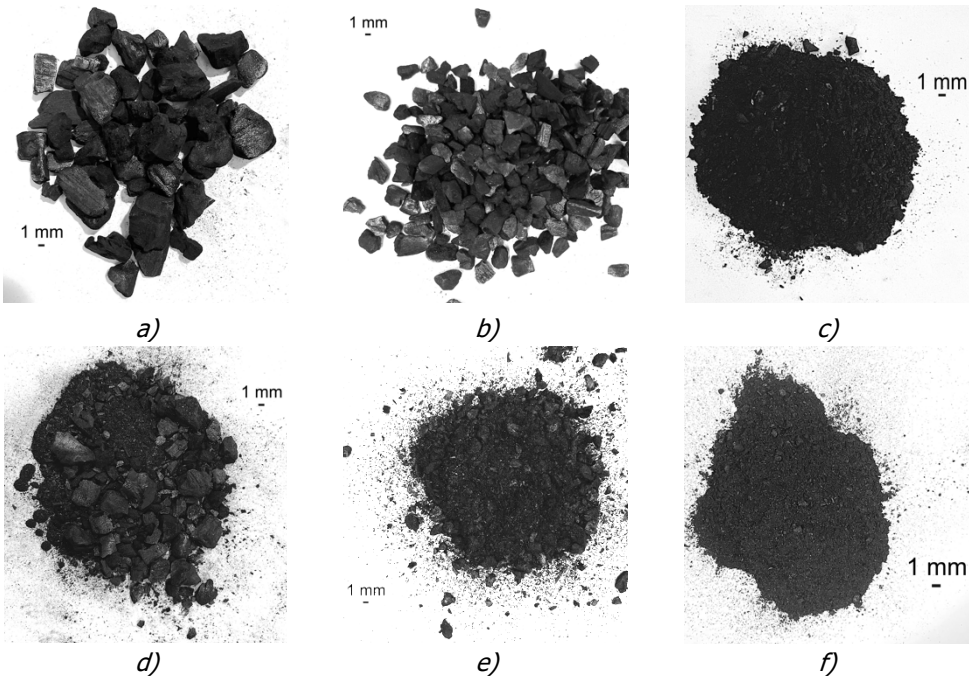

Figure 11-6. BC_5 sample before a) and after d) compression inside the PTFE cylinder; BC_3 sample before b) and after e) compression; BC_F before c) and after f) compression.

In Appendix C, Figure C.1 reports SEM microscope images performed on some biochar samples.

Comparing samples with the same composition and similar particle size (BC_F and BCG_F), a small difference between the EC curves was observed (Figure 11-4.a and Figure 11-4.b). Given the same elemental composition this behavior is attributable to an almost identical packing of the samples during the compression phase. This result supports what was previously stated.

On the other hand, comparing samples with similar granulometry but different elemental composition (BCG_x), different trends of the EC were noted as the pressure increased, different final EC values ($EC_{@25bar}$) were reached (Table 23). This result confirms the importance that carbon, and ash contents have in determining the EC value and it calls to attention the method used by Celzard et al., Sánchez-González et al., and Janerka et al. [236,262,272] which was broadly adopted for carbonaceous powder: the necessity of using powdered samples, the cornerstone of this method, is not sufficient to guarantee the achievement of a unique value of the biochar's EC. Even at high pressures, it is hard to state that the identified EC value is associated with the microcrystalline structure of the biochar's internal structure rather than with the macroscopic arrangement characteristics of the different grains.

Focusing only on the electrical characteristics, the fact that the same biochar performed differently in reaching separate final EC values opens the discussion

about which of the obtained results is the true EC of a specific biochar. This work, in fact, also wants to stimulate the debate on whether the EC measured in piston compression tests could be considered the same EC perceived by soil biota. In biological applications, the biochar improves the electron transfer mechanisms at a microscopical level where local interactions between microorganisms and the internal microcrystalline biochar structure take place. These kinds of interactions are far from being affected by morphology and particle size factors that strongly affect the pressure-based EC measurements. It is possible to speculate that the microorganisms perceive the "bulk" EC of the skeletal biochar structure, which may be very different from the EC measured with the piston method. In fact, as a final reference point, the EC values obtained in this as well as in many cited works are far from the graphite EC (in the order of 10^6 S m^{-1}, [273]) implying that, possibly the piston methodology is far from recording the EC values that truly characterize the biochar behavior in biological applications.

11.4 Insights to recall and recommendations toward the scientific community

- Different testing conditions strongly affected the conductivity measured. Actions, such as samples grinding or sifting, varied the electrical conductivity up to 41% and 85% respectively, showing how morphology is a *dominant and essential factor* affecting the final EC value.
- Biochar composition affects the EC: the shares of the tested biochar with higher ashes content showed lower electrical conductivity values.
- The fact that different particle sizes derived from the same biochar may have different compositions, resulting in different ECs, lead to the recommendation to properly describe the sampling methods when testing biochars.
- EC increases with pressure; EC increases with biochar carbon content (reaching 97.79 S m^{-1} @25 bar); biochar ashes are dielectric (4.58 S m^{-1} @25 bar) (collected data confirm the established literature knowledge).
- Important findings are demonstrated: reduces the grain size of biochar causes lowering the EC-pressure trend; therefore, EC measured in compression-methods is strongly affected by the biochar granulometry (43.04÷97.79 S m^{-1} @25 bar). The method for EC compression in carbonaceous powders, therefore, has limitations when applied to biochar, and the results should always be contextualized by applied pressure, morphology and composition.
- Experimental results open the discussion to further investigations aimed at higher goal of defining a testing a methodology that will provide an electrical conductivity value that reflects what is perceived by the microorganisms interacting with the char particles in soil, co-composting and anaerobic digestion applications.

- Microorganisms' interactions with biochar surface are not affected by the particle size, sample packing or applied pressure, pushing the scientific community to *rethink how this parameter should be measured*.

TECHNICAL FRAMEWORK OF APPLICATION .2

Biochar in organic waste composting facilities.

12 GASIFICATION BIOCHAR IN ORGANIC FRACTION OF MUNICIPAL SOLID WASTE COMPOSTING PROCESS. ENHANCEMENTS OF THERMAL ENERGY AND REDUCTION OF GREENHOUSE GASES EMISSION

The addition of biochar to composting is an innovative procedure for enhanced the decomposition process. This following research presents an experimental campaign in which the same gasification biochar, with two different particle sizes, is added to an Organic Fraction of Municipal Solid Waste (OFMSW) composting process in very small quantities (3% by mass) to study:

- how the application of high temperature biochar contributes to elevating temperatures in aerobic composting processes. This elevation, in turn, reduces the risk of pathogen proliferation, shortens composting time, yields a high-class final product compared to standard compost;
- the energy released during degradation process. A thermodynamic model was developed that, starting from measured temperature, outline the energy generated by the composting processes;
- what is the most effective biochar among the examined ones;
- the reduction of GHGs (methane, nitrous oxide) and ammonia emissions from composting processes with the specific goal of mitigating gases emissions from this type of anthropogenic activity .

Keywords: OFMSW; compost; gasification biochar; COMBI, biochar granulometry, temperature; thermal model; GHGs emission, ammonia emission.

A form of this research is also published in "Science of the Total Environment" and "Journal of Environmental Management", respectively available online from 11 January 2022 and from 10 January 2023

12.1 Composting process of organic waste and biochar addition

The uncontrolled decomposition of organic waste is significantly responsible for GHGs emissions [274]. Waste generated at municipality level by homeowners and businesses are defined as municipal solid wastes (MSW) [275]. According to the EU Directive 2018/851 [276], in Europe the organic fraction of MSW (OFMSW) is composed of biodegradable garden and park waste, food and kitchen waste from households, offices, restaurants, wholesale, canteens, caterers and retail premises as well as comparable waste from food processing plants. The Organic Fraction of Municipal Solid Waste (OFMSW) accounts for a large part of all the organic waste produced globally. To date, the average annual OFMSW production in the EU represents approximately 50% of the total MSW produced, resulting in an average of 130 tons per capita per year [277]. In the present day OFMSW is mostly processed through anaerobic digestion or composting as reported by Di Maria et al. [278]. These processes are often combined to maximize the yield in terms of biogas and organic recycled material.

Composting is an *aerobic process* that enables an environmental and economic return from the disposal of the OFMSW [279]. Recent years have seen an increasing interest in the optimization of composting processes, especially with the addition of new so-called *bulking agents and composting amendments* such as biochar [156,164].

12.1.1 Biochar in composting process

Although mainly used as a soil amendment in agriculture [156], in recent years several innovative uses of biochar have been investigated, such as: conditioner for improving biogas production [280] innovative material in degradation processes [281] and in the production of new nanomaterials [282]. In recent years, biochar is increasingly studied and considered to be one of the most promising amendments for composting organic waste [164].

Biochar seems capable of reducing the composting process GHGs emissions, as reported by Sánchez-García et al. (2015) [162], while improving the quality of the final product [85,170]. Additional validation from recent studies shows that biochar improves the microbiological environment for the composting bacteria, providing physical support for microbial growth and chemical mineralization, resulting in improved organic matter (OM) degradation and consequent humification [283,284]. Furthermore, thanks to its unique properties, biochar can increase the temperature of the thermophilic phase as it accelerates microbial activity [285,286]. Finally, the COMBI final product also improves crop productivity and reduces the compactness of the soil [156,181].

The technique of addition biochar to composting process is known under the name of co-composted biochar (COMBI). For producing COMBI a specified amount of biochar is added at the beginning of the composting process. In the last two decades, the benefit of the direct application of biochar in soil has been well consolidated, but in the last years the attention of the scientific community has shifted to more complex biochar applications such as water filtering, microbial remediation of contaminated soil, sludge treatments, and last-but-not-least, as additive in co-composting processes [179,180,287–290].

12.1.2 Biochar as composting improver

In literature there is a lack of information about *how the biochar used in composting experiments is produced*. This leads to uncertainties about what is the best biochar to be used as an amendment for composting processes. Almost all published experiments, as reported also in Antonangelo et al. (2021) [156], use biochars produced at relatively low temperature (between 400 and 650 °C), typical of pyrolysis processes. Sánchez-Monedero et al. (2018) [283] reports a list of different "low temperature" biochar utilized in the last six years in this research field.

Most of the studies agree in an effective biochar rate application of 3-10% w/w (dry basis); lower quantities are not sufficient for noticing any valuable effect [283]. It should also be pointed out that very few studies consider biochar granulometry as a governing parameter for the improvement of the composting processes [291].

In recent years, several research studied *co-composted biochar* from both an agronomic and production process point of view. Over the last five years, several field tests have been performed to understand the advantages of co-composted biochar when applied to soil, in particular its impact on soil fertility, soil health and crops productivity. Pandit et al. (2020) [292] has applied co-composted biochar to a corn field and find an increase of the amount of available potassium, calcium and magnesium in the soil and the corn yield by 243%. Sánchez-Monedero et al. (2019) [154], who tested tomato and grape production, confirmed that co-composted biochar improved soil nutrient and organic carbon soil contents and sustained the biological activity. Finally, Teodoro et al. [293] argues that co-composted biochar is an excellent soil conditioner that maximizes its potential in the absorption of heavy metals. Other research follows methods for testing new organic material or mixtures of organic material to obtain a value-added final product. Co-composting of biochar with food waste and poultry manure [294], grain waste [291] and green waste, bean dregs and tea residues [295] provides opportunities for waste recovering to produce nutrient-and-organic-rich compost.

12.1.3 Biochar effect on the composting thermal behavior

Biochar used in this experimental campaign is produced at high temperatures through an Imbert type woodchip gasifier. The chosen downdraft gasifier works at a peak temperature between 800 °C and 1000 °C and biochar is extracted after the high temperature reduction zone [38]. Following Haug (1993) [296] and Arrigoni (2018) [297], the composting temperature has been used as key variable for the evaluation of the quality of the process in terms of composting stability and pathogen control.

A first aim of this work is to define the impact on aerated OFMSW composting process of two different granulometries of the same biochar produced at high temperatures in a downdraft gasifier, when it is used as a composting amendment at minimum application rate. The choice of using two granulometries of biochar, fine char (FB) and coarse char (CB), is made to better understand the differences between the governing characteristics of the biochar's effects: intrinsic biochar properties versus bulking agent properties.

In addition, a thermal power balance model was set up to quantify the increase in microbiological activity related to FB and CB use. From an engineering point of view, thermal behavior is governed by the thermal power generated by the microbiological activity, consequently the temperature as the only directly measurable parameter. The created model *quantifies the thermal energy produced* and decouples the evaluation of the decomposition process from the variation of the temperature due to external factors, such as mass shape, thermal dispersion and ambient temperature. Working with the model, the specific thermal energy generated per mass of initial compostable material was quantified for each thesis.

Two different biochar granulometries are considered whereas in the current literature there are no studies aimed at identifying which is the best biochar granulometry in order to make OFMSW composting processes more efficient. He et al. (2019) and Yin et al. (2021) [164,298] apply different particle sizes of biochar in animal manure aerobic composting to analyze GHGs emissions, but no results are presented about process temperatures or thermal energy production.

12.1.4 Biochar effect on the composting emission

Since in composting facilities it is necessary to assess the environmental impact of the gas emissions generated by the decomposition process, beside the thermal behaviour study, a long experimental campaign is carried out to understand the reduction, if any, of biochar on the composting emission. To achieve the goal of reducing GHGs, as recommended by the Sustainable Development Goals 2030, it is necessary to develop and adopt innovative waste

management processes [26]. One of the most promising processes, in the context of biodegradable waste, is co-composted biochar (COMBI) [299].

Alongside water vapor, other important GHGs emitted during composting processes are CO_2, CH_4 and N_2O. NH_3 is also emitted during composting, and it is usually monitored because it is an important precursor of atmospheric particulate matter [179].

Literature findings prove that the addition of biochar at the beginning of the composting process causes the reduction of CH_4, and N_2O, but it is still difficult to properly quantify this impact. However, all the literature results agree in some measure on the reduction of these GHGs. Yin et al. (2021) [164] reported a CH_4 reduction from 12.5% to 95.3% compared to the control; Vandecasteele et al. (2016) and Awasthi et al. (2017) [161,300] measured N_2O reductions of 14% and 97.2%, respectively.

Literature studies on CO_2 emissions from co-composting processes give conflicting results. Some researcher has identified a decrease in CO_2 emission compared to the control thesis: Wang et al. (2018) identified a 26% reduction [301], while Vandecasteele et al. (2016) a 51% [161]. On the contrary, Czekała et al. (2016) found an increase in CO_2 emitted [302], while Sánchez-García et al. found no variation between thesis and control [162]. The scientific literature also provides conflicting data for NH_3: both emission reductions and increases have been found [303,304].

The reduction of gaseous emissions in composting certainly occurs thanks to biochar working as *bulking material* (high porosity and low density), but increasingly more researchers have started to agree that the main reason may lie in the *interaction between biochar and organic material* as also seen in Chapter 2 [305]. Two variables influence this interaction: the biochar electrical conductivity and the contact surface between the biochar grain and the organic matter [298,306]. This research is focused mainly on the latter. For this reason, to vary the contact surface between the biochar and the surrounding composting material, different biochar grain sizes have been tested. The reduction in the grain dimensions should decrease the bulking effect while increasing the total available external surface are of biochar. The greater the contact surface, the greater the potential interaction with organic matter, and thus, the exchange of chemical species and/or electron between the actors of the biodegradation biota [156]. However, further studies are necessary to confirm the correlation between the particle size of biochar and the generation of decomposition gases, including GHGs [164].

Therefore, another important goal of this research is to quantify the GHGs emission reduction compared to the emission in a standard process. CH_4, N_2O and CO_2 are measured, as GHGs. At the same time, NH_3 is also monitored as it

is useful in the mass balances of the compost nitrogen mineralization and is considered a precursor gas in the formation of atmospheric particulate matter.

Monitoring the emissions over two months provides a way to see the emission evolution and to identify differences between theses and control and between the forced active (or aeration phase) and static (or maturation) phases of the composting process (details in following paragraphs).

12.2 Experimental campaign and materials

12.2.1 Setup of the experimental campaign

For this research, nine compost bins of 1 m^3 were used. Each thesis consists of three replicas. The first thesis is the "control" bin (CTRL) in which a OFMSW mixture is used. The second thesis (CB) adds coarse biochar to the standard mixture. The third thesis (FB) adds grinded fine biochar to the OFMSW mixture. Both CB and FB theses use the same mass of biochar. The nine bins were independently aerated by an air blower with the air inflation rate managed by a control-logic acting on temperature sensors and automatic valves. The experiment was divided into two phases: an active phase (or aeration phase) of 31 days characterized by active aeration, and a static phase (or maturation phase) of 32 days, with no mechanical aeration provided, for a total period of 63 days, according to the standard compost residence time [307]. After filling the bins, the material was never mixed or stirred to better simulate the aerated static pile behavior (ASP) [308].

12.2.2 OFMSW raw material

10 tons of OFMSW were collected for the composting tests. The tests were carried out in a municipal composting plant owned by AIMAG S.p.a. After a visual selection to remove plastic, glass and aluminum from incoming material, an amount of green and brown waste was added as bulking agent. Eventually, a fraction of material, here referred to as "under-sieve" was also added, according to the standard production process adopted by the company in which the test was performed. Under-sieve material comes from previous composting cycles within the production plant and is mainly composed of wood pieces that have not passed through the sifting stage. Under-sieve is commonly used as a starter material, acting as an inoculum of the microbiological species for the compostable material [309]. At the end of the process, it is recovered for reuse in the next cycle. To obtain the final mix (FM), 10000 kg of OFMSW were mixed with 2980 kg of wood and 4700 kg of under-sieve fraction. To complete the preprocessing phase, the FM was passed through a bio-shredder (Doppstadt - DW 3060 model) to reduce and homogenize the granulometry. The final mix was then ready to fill the compost bins.

12.2.3 Biochar

The biochar used in this experiment was produced by a gasification power plant based on an Imbert type, single-throat downdraft reactor (nominal power of 150 kW). In these architectures the temperatures of the heart of the reactor ranges between 800 °C and 1000 °C when fully operational [38]. One of the peculiarities of downdraft reactors consists in having the char extracted from the reduction zone [133]. Here hot gases react with the carbon structure, resulting in a carbonized material that is, on average, lower in condensable content and higher in micro and nano porosity when compared to pyrolysis chars. The biochar produced in the plant used in this work was certified for use as a soil conditioner in agriculture, according to the Italian law (MIIPAF) [214]. The chosen gasifier reactor uses a liquid seal drum in the char extraction line at the end of the gasification process. The particle size distribution is reported in Table 25, from the producer data sheet.

Table 25. Size particles of the biochar as obtained from the gasification facility.

Larger diameter of particle	Value
ø > 5 mm	16 %
2 < ø < 5 mm	26 %
0.5 < ø < 2 mm	19 %
ø < 0.9 mm	39 %

Different biochar granulometries might come from different parts of the power plant itself, even though they are collected all together, e.g., fine char particles are also collected from the filtration stage [258]. Consequently, they might have different properties and different compositions. To ensure this variability was avoided to guarantee the exact same composition of both the coarse and fine biochar; only the coarser fraction (ø > 5 mm) was used, and part of it was ground. Consequently, 0.3 m^3 of biochar with a diameter higher than 5 mm was obtained by wet sifting. This quantity was then divided into two equal parts of 0.15 m^3 each, equivalent to a volume/volume share of 5% (0.05 m^3 per bin):

- 0.15 m^3 had no further treatment. This fraction will be referred to as "coarse biochar" (CB) henceforth; ϕ > 5 mm;
- 0.15 m^3 were ground through a screw grinder and produced a fine char slurry. This fraction will be referred to as "fine biochar" (FB) henceforth.

The granulometries of the biochar both pre and post pre-treatment are reported in Figure 12-1.

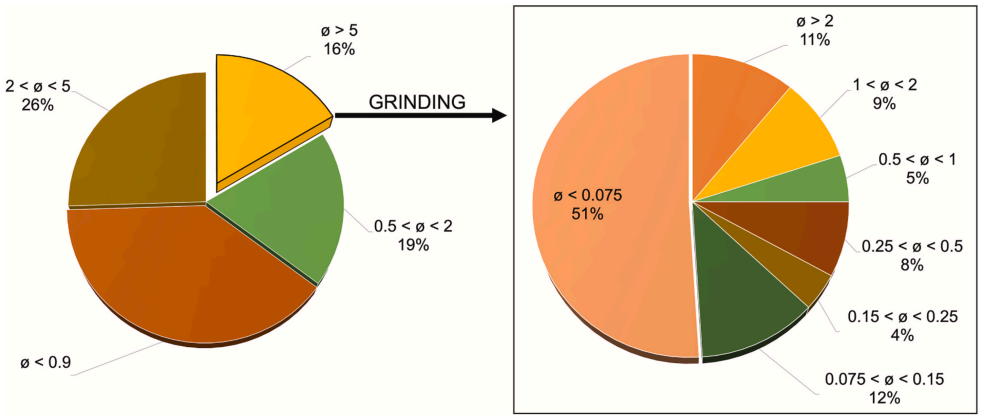

Figure 12-1. Biochar particles-size distribution: as received, before the sifting and after the grinding step. All values are in mm.

The Brunauer–Emmett–Teller (BET) surface area of both granulometries was also measured to include this parameter in the results discussion [120]. BET surface area was measured by a Micromeritics Instrument Corp tool.

It is important to point out that due to the natural decrease of the biochar volume after the grinding step, while the masses of FB and CB used were equal, the volume/volume fractions of char-composting material mixture were different, leading to a 5% v/v for the CB mixture and 3% v/v for the FB mixture. The preliminary biochar characterization in terms of composition and physical parameters is shown in Table 26.

Table 26. Datasheet of the biochar characteristics according to the producer and measured moisture content of CB and FB.

Parameters (from char datasheet)	**Value**	**Units**
Moisture content	71	%
pH	9.12	pH Unit
Ash content	20.5	% *
Density	620	kg m^{-3}
Total carbon	72.4	% *
Water retention	50.60	g
Polycyclic aromatic hydrocarbons (PAH)	< 0.005	mg kg^{-1}
Parameters (measured)	**Value**	**Units**
Moisture content – CB	85	%
Moisture content – Fb	83	%

* (dry matter)

12.2.4 Compost bins design and construction

The compost bins used during the experiment had a net volume of 1 m^3. The volume of the experimental reactors found in literature varies between 0.004 m^3 and 2 m^3 [308,310]. As in this research the idea was to replicate at pilot-scale what happens at facility scale, lab scale dimensions were not suitable for this approach. Considering the initial compostable mix to be coarse and heterogeneous, it was necessary to use sufficiently large volume bins to better simulate the full-scale municipal composting process. However, having to effectively manage the bins, especially during the filling and emptying phase of the composting material, a volume of 1 m^3 was opted for. The bins were made with thermal insulation panels of extruded polystyrene foam (XPS) with a thickness of 6 cm and a thermal conductivity equal to 0.038 W $m^{-1}K^{-1}$. The bins had internal dimensions of 1 m (length) x 1.15 m (width) x 1.20 m (height) and could be easily transported with the help of wood pallets positioned under each bin. As reported in Figure 12-2, the air distribution system was placed at the bottom of each bin. The air distribution system consisted of a metallic grid on which an air sparger was fixed. Each air distribution was composed of a main common-rail PVC tube and five PVC distribution tubes placed perpendicularly to the main one. All tubes had a diameter of 0.02 m. Each tube had 10 holes of 0.003 m in diameter, distributed along the entire length of the pipes at 0.08 m from each other. The holes are directed downwards, thus reducing the risk of fouling and clogging due to leachate or debris felling from the composting pile.

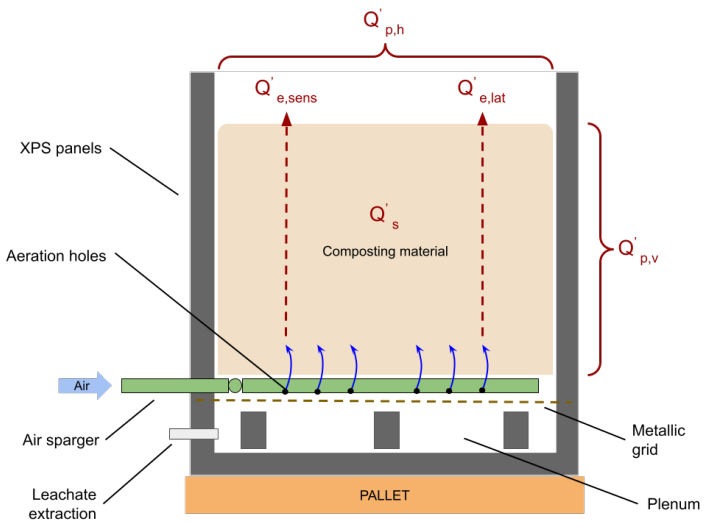

Figure 12-2. Explanatory scheme of the compost bins used during the experimental campaign. The factors affecting the thermal balance are shown in red.

The leachate produced by the material was collected under the grid (placed at 10 cm from the bottom) and did not remain in contact with the compostable

material. The extraction of the leachate was possible by means of a valve positioned on a side wall of the bin, 3 cm from the bottom.

12.2.5 Bins filling and chemical-physical analysis of organic matter

The final mix (FM) was divided into three piles of 3 m^3 meters each. One pile was designated for the CTRL thesis and did not undergo further treatment. A second FM pile was mixed with CB and, similarly, the FB was applied to the third pile. The nine bins were loaded using a mechanical shovel and then positioned at random to eliminate any effects of the surrounding environment on the test performance. After, 30 kg of finished compost were added on top of the compostable material in each individual bin to create a 6 cm thick permeable layer for thermal insulation. Each bin was weighed before and after loading the material.

In this way, each bin was filled with 1 m^3 of material. To thermally insulate the surface a 30 kg layer, 6 mature compost 60 mm thick was added then accurately removed at the end of the process. At both the beginning and the end of the whole experimental test, each bin was weighed to calculate the weight reduction for mass balances purposes. The headspace height over the compost surface was measured each time that the GHGs emission measurements were performed to monitor the trend of volume reduction. The masses of organic material with the respective labels are shown in Table 27.

Table 27. Weights, volumes and density of the material that has been placed inside each bin during the filling phase.

Thesis	Volume of material [m^3]	Mix net weight [kg]	Mix density [kg/m^3]	Average density [kg/m^3]
CTRL1	0.88	495	562	568 ± 20.7
CTRL2	0.90	495	551	
CTRL3	0.83	490	591	
CB1	0.87	500	540	531 ± 10.8
CB2	0.85	485	534	
CB3	0.90	500	519	
FB1	0.81	445	519	531 ± 13.9
FB2	0.80	465	546	
FB3	0.83	465	527	

During the filling of each bin, ten samples of the FM were performed: while the mix was slowly loaded, ten samples of approximately 1 kg were picked up using a palette. Sampling was done approximately every 100 liters/50 kg, which corresponds to 10 cm of mix heigh added inside the bin. The ten samples were

merged to create a single representative sample of 10 kg for each bin. Total solid (TS), pH, ammonium nitrogen (NH_4^+-N) and electrical conductivity (EC) were determined on the nine fresh samples [311,312]. The nine 10 kg samples were subsequently dried and ground for further analysis: volatile solid or organic matter (VS) [311]; total Kjeldahl nitrogen (TKN); total organic carbon (TOC) [214]; total phosphorus (Ptot) using the standard EPA 3051A and SM 4500-P-C [313]; extractable organic carbon (TEC), humic and fulvic acids (HA+FA), humification degree (DH) [314] and heavy metals contents: Nickel (Ni), copper (Cu), Zinc (Zn), Chrome (Cr), Cadmium (Cd), Mercury (Hg), Lead (Pb) and Potassium (K) using the standard EPA 3051A and SM 3111-B [313].

The same sampling and analysis operation was repeated at the end of the maturation phase.

12.2.6 Aeration system

The aeration system was composed of a blower (power = 2.2 kWe), an open- source Arduino®-based control panel and a circuit of tubes and motorized valves. The blower could supply up to 50 $m^3 h^{-1}$ of air. To regulate the flow, two valves for each bin were placed downstream of the blower. The first valve, common for all the nine air ducts, consisted of a fast-opening solenoid valve which interrupted the air flow. After that, a manifold distributed the air to the nine branches, one for each composter. A slow electro valve was installed on each branch. The valve opened when air was blown into the respective bin. The aeration system was completed by a gas totalizer mounted just after the blower. It allowed for the measurement of the flow rate and the total blown air volume. The combination of slow and fast valves was used to prevent any overlap between the aeration of different composters. Aeration is at the base of two important processes:

- mass oxygenation: the bacteria contained in the material need oxygen to carry out the aerobic degradation processes. Anaerobic conditions must be avoided [296];
- temperature control: the temperature cannot rise above 70 °C to avoid the depletion of the microbial population [296,315]. The optimal conditions are between 55 and 60 °C in thermophilic conditions [316].

The aeration method is described in Appendix D. Aeration methodology and algorithm.

During the starting phase of the composting process, aeration starts after temperatures passes 45 °C. In the case presented, this happened at the end of day two. Days three and four were used to control whether the baseline value of 35 seconds for 25 minutes for the aeration control was suitable for the case-specific boundary condition (composting material and weather). The continuity of the temperature rising confirmed the chosen value. Afterwards, two different insufflation periods were used to adapt the air flow to the decomposition

temperature trend, keeping the chosen value as the central point. The flow rate of the air blower was 18 m^3 h^{-1}.

12.3 Measurement methodologies and devices

12.3.1 Temperature measurements

The temperatures of the decomposing mass were measured with "Type T" thermocouples and TC-08 thermocouple data loggers from Pico Technology®. In each bin two thermocouples were positioned in the central section of the compost bin. These two thermocouples were inserted through the side wall of the bin and placed at a height of 80 cm ($T_{c,up}$) and 20 cm ($T_{c,down}$) from the bottom, so that the temperatures of the different composting layers could be read. Nine extra "Type K" thermocouples used for aeration management, one for each bin, controlled by Arduino® were also utilized. These thermocouples were inserted into the core of each bin 50 cm from the bottom. From MAX6675 modules produced by Maxim Integrated®, the temperatures were read from the Arduino® board and recorded. A calibration was performed to make the data read from Pico Technology® loggers and Arduino® Board comparable.

12.3.2 Thermal energy balance of the composters

As the heat produced during the composting process results directly from aerobic microbial degradation of organic matter, the amount of thermal energy produced during the entire process must be examined. A thermal balance based on heat transfer theory was applied in order to assess and quantify the thermal energy production rate over time (thermal power). All equations assumed that the composting material had a constant atmospheric pressure and constant specific heat capacity. The natural mass decrease over time was considered linear during the entire experimental period. The ambient and inlet air temperatures were measured over the entire process by means of "Type T" thermocouples. The composting process (i.e. the microbiological activity) guarantees sufficient thermal power to cope with heat dispersions of different natures while increasing the temperature of the composting material itself [317].

Microbiological thermal power generation is herein defined as:

- $\dot{Q}_c$: thermal power from microbiological processes.

Thermal power dispersions are herein defined as:

- $\dot{Q}_{p,v}$: convective heat transfer losses from the vertical wall of the bins.
- $\dot{Q}_{p,h}$: convective heat transfer from the top horizontal layer of the bins.
- $\dot{Q}_{e,sens}$: sensible heat power losses due to mechanical aeration (considering the difference between the temperature of inlet and outlet air).

- $\dot{Q}_{e,lat}$: latent heat power losses due to water vaporization in both natural convection and forced aeration.

Process thermal power:

- $\dot{Q}_s$: thermal power necessary to change the temperature of the composting mass from one time-step to the other. To be considered negative while the mass cools down.

The heat loss for radiation is considered negligible for the working temperatures, according to Shaw and Stentiford [318]. Heat transfer through the bottom of the bin is negligible and can be considered adiabatic due to the insulation and the absence of convective phenomena on the surface. The thermal balance is reported in (12-1) and (12-2) and in Figure 12-2, and can be summarized as: the power generated through the microbial activity is either used to raise the compost temperature or dispersed.

$$\dot{Q}_c = dispersions + process\ thermal\ power \qquad [m] \qquad (12\text{-}1)$$

$$\dot{Q}_c = \dot{Q}_{p,v} + \dot{Q}_{p,h} + \dot{Q}_{e,sens} + \dot{Q}_{e,lat} + \dot{Q}_s \qquad [m] \qquad (12\text{-}2)$$

In the interest of simplicity, the calculation process is better described in Appendix E. Thermal model and iterative procedure. All the following calculations were made twice for each bin considering respectively $T_{c,up}$ and $T_{c,down}$. In particular, the assumption of thermally homogeneous material was taken into account, i.e. the material for each composter was first considered to have a temperature equal to $T_{c,up}$ and then to $T_{c,down}$. The results were derived by taking the average of the two calculations made considering the different temperatures. The complete description of the equations that rule each of the thermal power contributions that are previously listed is provided in Appendix E. Thermal model and iterative procedure.

12.3.3 Emission measurements

Multiple emission measurements were periodically performed throughout the composting period using the LumaSense Photoacoustic Gas Monitor INNOVA 1412, a photoacoustic multi-gas analyser [319].

The gas sampling campaign included eight emission measurements during the active phase (two measurements per week) and four measurements during the maturation phase (one measurement per week). Because the aeration was intermittent, the emission measurements were performed both with active aeration (ON) and paused aeration (OFF).

For consistency, when talking about emissions, "Static" and not "Maturation" will be used, since it is easier to associate "Static" with the second phase in which blower is off.

A static measurement chamber was used. The chamber, measuring L 1040 mm x W 1200 mm x H 500 mm, was placed above the bin to capture the gases emitted by the decomposing mass. The chamber, made of polycarbonate, had an outlet chimney equipped with a shut-off valve. A small fan placed inside the chamber acted as a gas stirrer to prevent gas stratification. Before each measurement, the bins were carefully sealed together with the chamber. The analyser had a limit of detection in the order of ppb and simultaneously measured CO_2, N_2O, NH_3, CH_4 and H_2O with a frequency of a measurement every two minutes. After taking measurements, the instrument returned a) data without cross-gas interference, b) data without water vapor cross interference and c) standardized data at 20 °C and 101325 Pa [319].

During the aeration ON periods, the outgoing flow from the bin was fully captured through the chamber with an open shut-off valve. By placing the analyser sampling probe on the chamber chimney, the concentrations of NH_3, CH_4, N_2O and CO_2 in the outgoing gas stream were detected. The emissive flow E_{ON} $[mg_{gas}\ ton^{-1}\ min^{-1}]$ during the periods of active aeration was quantified through (12-3), modified from Pedersen et al. (2010) [320].

$$E_{ON} = = \frac{(C_{gas_{AirOut}} - C_{gas_{AirIn}}) \cdot \dot{Q}_{ForcedAeration}}{M_{SM}} \quad [mg_{gas}\ ton^{-1}\ min^{-1}] \qquad (12\text{-}3)$$

where: $C_{gas_{AirOut}}$: concentration of the gas measured in the offtake hood flow [mg m^{-3}], $C_{gas_{AirIn}}$: concentration of the same gas in the external air [mg m^{-3}], $\dot{Q}_{ForcedAeration}$: flow rate of the forced aeration system [m^3 min^{-1}] e M_{SM}: mass of SM in the bin [ton].

During the aeration OFF periods, there was no conveyed emission flow, and the Static Chamber Methodology (SCM) was used. The SCM allowed for the detection of biomass emissions in the absence of a continuous gas flow [320–323]. This technique used the previous static measurement chamber, with a closed shut-off valve, to create a closed and sealed headspace above the surface of the biomass, where the gases diffused and concentrated. The concentration of the gas in the headspace increases progressively and linearly during an initial period until it reaches a plateau. When there is no longer linearity in the gas concentration increase over time, the saturation of the headspace is reached, and the measurement is stopped. The angular coefficient of the regression line

calculated over the linear section of the saturation curve represents the emission potential of the biomass.

The emissive flow E_{OFF_A} $[mg_{gas}\, m^{-2}\, min^{-1}]$ generated during the aeration OFF periods, per emissive area and per unit of time, is calculated using Eq. (12-4):

$$E_{OFF_A} = \frac{\Delta c}{\Delta t}\frac{V_{cha}}{A_{bin}} \qquad [mg_{gas}\, m^{-2}\, min^{-1}] \qquad (12\text{-}4)$$

where: $\Delta c/\Delta t$ [mg m^{-3} min^{-1}]: concentration gradient over time of the linear part of the emission curve (in correspondence to the angular coefficient of the interpolating line), V_{cha}: volume of the headspace [m^3] where the gases concentrate above the emitting surface A_{bin} [m^2].

The emissions calculated during the aeration OFF periods per surface unit, E_{OFF_A}, must be rearranged according to the emitting surface of the bin and to the mass with Eq. (12-5), obtaining E_{OFF} $\left[mg_{gas}\, ton^{-1}\, min^{-1}\right]$.

$$E_{OFF} = \frac{E_{OFF_{Area}} \cdot A_{bin}}{M_{SM}} \qquad \left[mg_{gas}\, ton^{-1}\, min^{-1}\right] \qquad (12\text{-}5)$$

where the A_{bin}: emissive surface of the bin [m^2] and M_{SM}: mass of SM inserted in the bin [ton].

The hourly emissions during the active phase E_{ACT} $\left[mg_{gas}\, ton^{-1}\, h^{-1}\right]$, measured for each monitoring session, are calculated using Eq. (12-6):

$$E_{ACT} = E_{ON} \cdot \Delta t_{ON} + E_{OFF} \cdot (60 - \Delta t_{ON}) \qquad \left[mg_{gas}\, ton^{-1}\, h^{-1}\right] \qquad (12\text{-}6)$$

where Δt_{ON}: minutes of aeration per bin per hour.

The cumulative emissions of each individual bin $E_{ACT_{tot}}$ $\left[g_{gas}\, ton^{-1}\right]$ are calculated using a discrete integral over time of the eight measurements related to the active phase, Eq. (12-7):

$$E_{ACT_{tot}} = \sum_{i=1}^{8} \frac{E_{ACT_i} + E_{ACT_{i+1}}}{2} \cdot \frac{(t_{i+1} - t_i)}{1000} \qquad \left[g_{gas}\, ton^{-1}\right] \qquad (12\text{-}7)$$

where t_i: instant of each measurement and $t_{i+1} - t_i$: interval time between two consecutive measurements in hours.

During the static composting phase, four emission measurements were performed using Static Chamber Methodology. The emissive flow relating to the static phase E_{STAT_A} $[mg_{gas}\, m^{-2}\, h^{-1}]$ is calculated through Eq. (12-8):

$$E_{STAT_A} = \frac{\Delta c}{\Delta t}\frac{V_{cha}}{A_{bin}} \qquad [mg_{gas}\, m^{-2}\, h^{-1}] \qquad (12\text{-}8)$$

where: $\Delta c/\Delta t$ [mg m^{-3} min^{-1}]: concentration gradient over time of the linear part of the emission curve (in correspondence to the angular coefficient of the interpolating line), V_{cha}: volume of the headspace [m^3] where the gases concentrate above the emitting surface A_{bin} [m^2]. Eq. (12-9) is used to correlate the emissions to the SM mass in the bin E_{STAT} $[mg_{gas}\, ton^{-1}\, h^{-1}]$:

$$E_{STAT} = \frac{E \cdot A_{bin}}{M_{SM}} \qquad [mg_{gas}\, ton^{-1}\, h^{-1}] \qquad (12\text{-}9)$$

where A_{bin}: the emissive surface of the bin [m^2], M_{SM} is the mass of SM inserted in the bin [ton].

The cumulative emissions of each bin $E_{STAT_{tot}}$ $[g_{gas}\, ton^{-1}]$ are calculated using a discrete integral over time of the four measurements related to the static phase, Eq. (12-10):

$$E_{STAT_{tot}} = \sum_{i=1}^{4} \frac{E_{STAT_i} + E_{STAT_{i+1}}}{2} \cdot \frac{(t_{i+1} - t_i)}{1000} \qquad [g_{gas}\, ton^{-1}] \qquad (12\text{-}10)$$

where t_i: instant of each measurement and $t_{i+1} - t_i$: time interval between two consecutive measurements, in hours.

The emissions of the entire composting process are the sum of the emissions of the active phase $E_{ACT_{tot}}$ and the static phase $E_{STAT_{tot}}$ $[g_{gas}\, ton^{-1}]$, Eq. (12-11):

$$E_{TOT} = E_{ACT_{tot}} + E_{STAT_{tot}} \qquad [g_{gas}\, ton^{-1}] \qquad (12\text{-}11)$$

12.3.4 SEM images and statistical analyses

The analysis of variance (ANOVA) for repeated testing with Tuckey's test (a common post hoc test) was conducted. This test enabled the comparison of the average value of overall cumulative emissions of each thesis (CTRL, FB, and CB)

in pairs and, therefore, made it possible to identify significant differences between the three theses investigated.

Scanning electron microscope (SEM) images of the pre- and post-composting biochar were performed. A Quanta-200, Fei Company - Oxford Instrument was used. A sample of non-composted and composted biochar grains were abraded through a lapping machine to expose both a section of the internal volume and the external surface of the grain. At the same time, energy dispersive X-ray spectroscopy (X-EDS) microanalysis of the exposed surfaces were performed using the Oxford INCA-350 microanalysis system coupled to the microscope.

12.4 Results on thermal power, emission and final co-composted product

12.4.1 Process temperatures

Process temperatures were collected as described in Paragraph 12.3.1. The thermal behavior of the different theses was described using a temperature dependent indicator. The average temperature of each individual thesis was calculated starting from the data collected by the two thermocouples (read by PICO system®) inserted in each bin, for a total of 6 thermocouple for each thesis. Data computation was divided into "active composting phase" and "maturation composting phase" due to the nature of the two processes being extremely different, as reported in Paragraph 12.2.1.
The average temperatures obtained were:

- CB thesis: during active phase 61.96±0.56 °C and during maturation phase 56.05±0.24 °C;
- FB thesis: during active phase, 61.84±0.35 °C and during maturation phase 55.18±1.86 °C;
- CTRL thesis: during active phase 57.53±0.43 °C and during maturation phase 49.83±1.38 °C.

It was confirmed that the average temperatures of the char-additivated theses were higher than those of the control, as the error bar did not overlap. However, no significant differences were noted between the two particle size fractions (CB and FB).

From the trend in Figure 12-3, which shows both the active and the maturation phases, it is possible to notice that the temperatures of FB and CB always remained higher than those of the CTRL. Of note, after a sudden rise in the FB curve during the first half of the active phase, the CB always remained at higher temperatures. Therefore, in the CB and FB theses, biochar led to a sudden increase in temperature during the starting phase. During maturation, it

maintained higher temperatures compared to the CTRL thesis that cooled faster. The minimum temperature difference between the biochar theses and the CTRL was registered during the central composting phase. The maximum temperature reached by each single bin was used to calculate the average maximum temperature of each thesis. The average temperature of the biochar theses, 71.12±1.38 °C for CB and 70.12±0.47 °C for FB, were higher than the mean maximum temperature of the control thesis, 64.10±0.72 °C. The error bars did not overlap. It was therefore confirmed that the biochar allowed the mass to reach higher temperatures than the temperatures reached using the standard composting process.

Notably, the temperatures dropped between days 35 and 39. It was the only period where the FB and CB temperatures reached lower values compared to the CTRL. The most probable reason is that the sharp drop in temperatures of that period was due to the temperature peak that happened in the days before. In turn, that temperature peak was due to the cut-off of forced aeration. Forced aeration kept the temperature below a level which might be significantly harmful for the biome. During that peak, the FB and CB theses reached significantly higher temperatures than the CTRL temperature. Consequently, the biome of the biochar theses were severely affected by the temperature peaks whereas the biome of the CTRL suffered less, as its peak temperatures were still in the range of appropriate temperatures suitable for the biome to survive. Because of the microbial activity being slowed down for the high temperatures of the previous days, the biochar theses took more days to recover than the CTRL.

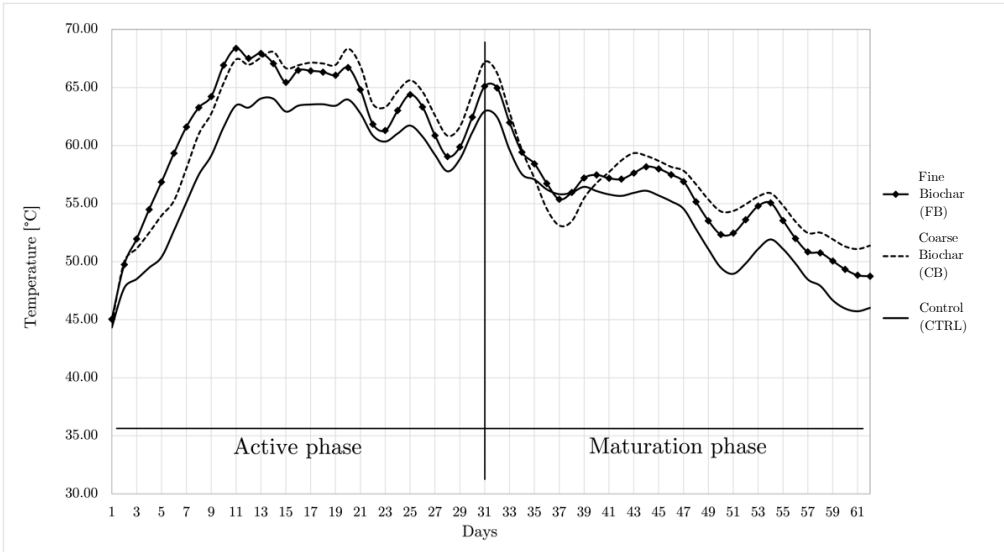

Figure 12-3. Temperature trend during the active phase and the maturation phase. The graph is built on the daily average temperature of the entire process.

12.4.2 Biochar effect on thermal power generated by the composting process

The trend of the power produced over time per kg of initial compostable mass for the three theses is shown in Figure 12-4. As can be seen, it is evident that biochar (both CB and FB) led to a significant increase in the production of thermal energy due to the enhanced microbiological reactions of the composting process. This behavior is in line with the results presented by Zhang et al. (2021) and Wei et al. (2014) [285,286].

Wu et al. (2017) [306] reports that the interaction between biochar and organic matter changes the surface of biochar due to the biotic (co-metabolic decay of carbon and organic matter or degradation of available carbon on the biochar surface) and abiotic oxidation (facilitated by the high temperature during composting). Another interaction mechanism is the adsorption of heavy metal and other organic matter, that led to an increase of the functional group on the external layer of the biochar. These phenomena, combined with the high-water retention capacity of the biochar, the high electrical conductivity and the high cation exchange potential, are to be considered the reason why the proliferation of decomposition microorganisms is greater during co-composting process. Finally, since temperature is the key variable used to study the performance of composting, it is possible to consider a direct correlation between higher temperatures and greater microbiological activity.

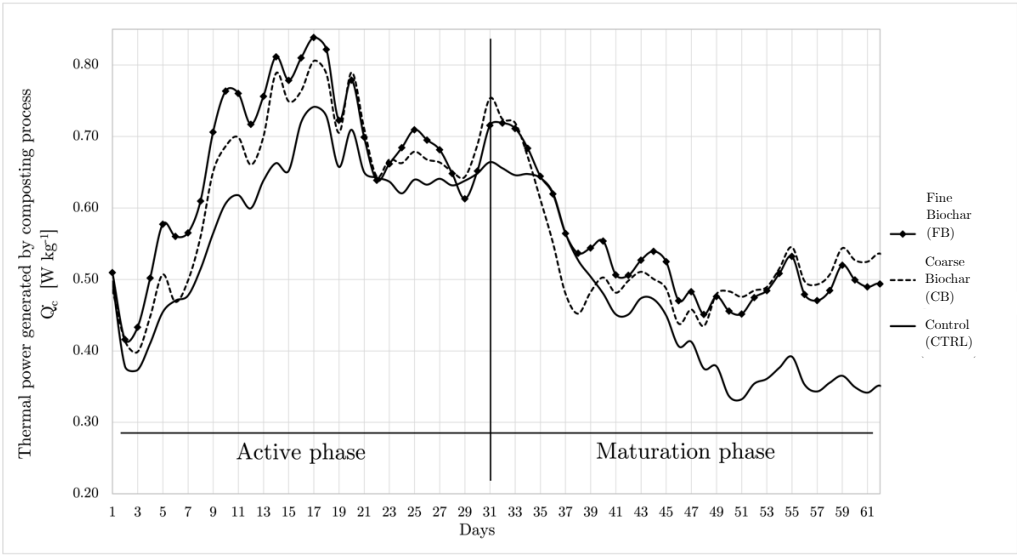

Figure 12-4. Composting thermal power trend over the active and the maturation phase, as a result of thermal balance calculation.

Results reveal that fine biochar (FB) was more effective during the first 15 days of composting and then settled on values similar to those of the coarse

biochar. The compost with fine biochar generated an average of 0.70 W per kg of initial composting mass, whereas the compost with coarse biochar generated an average of 0.68 W per kg. The control compost had an average value of 0.63 W per kg.

In Figure 12-5, the percentage distribution of thermal power losses is shown. The distribution of the dispersed powers, according to the balance presented in Appendix E. Thermal model and iterative procedure, was almost the same for both fractions of biochar.

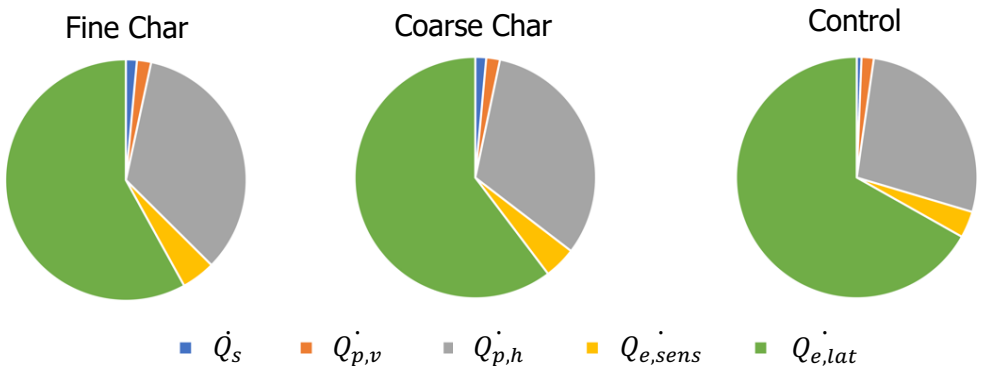

Figure 12-5. Percentual distribution of thermal power loss. The energy is expressed as MJ produced over kg of organic material.

The losses due to latent heat of evaporation amounted to about 60% of the total losses. Losses due to natural convection of the upper face of the material amounted to about 30% of the total losses. In the CTRL case, the losses of latent heat of evaporation amount to about 70% of the total losses. This may derive from two factors: lower temperature differences with the environment resulted in lower thermal losses, and the absence of biochar reduced the water retention capacity of the material, thus increasing the evaporation rate. However, it is not possible to notice significant differences between the two biochar granulometries. Overall, considering CB, FB, and CTRL theses, the distribution of the losses is in line with the results obtained by [324] where the heat losses due to the latent heat of evaporation represents the first cause of heat loss. In Table 28, the thermal energy produced during the active and maturation composting phase is shown. The energy is expressed as MJ produced over kg of initial compostable mass. The results are consistent and in line with the literature [325,326].

Table 28. Thermal energy produced by the composting process over kg of initial compostable mass. Thermal energy is expressed in [MJ kg^{-1}].

Composting phase	Thermal energy - FB	Thermal energy - CB	Thermal energy - CTRL
Active	2.0	1.9	1.7
Maturation	1.0	1.0	0.8
Active + maturation	3.0	2.9	2.5

Overall, the biochar showed a significant capacity for thermal power improvement (i.e. organic matter degradation due to microbiological reactions) both during the active and maturation phase. The fine biochar seemed to have a slightly stronger thermal power improvement effect during the first half of the active phase. When the peak temperatures were reached, the two granulometries started to behave in the same manner. It was not easy to find a valid reason for this trend. It was concluded that a partial reason could be that the fine biochar had less effect as a bulking material and consequently the mass has less porosity. The mass being more compact and less susceptible to air convection through the pores, this trend could be attributed to lower losses of sensible and latent heat which depend on air flow convection.

Furthermore, FB was characterized by a higher surface that could interact with the composting material. When the entire composting process was considered, there was a less significant difference between the two biochar granulometries. The average thermal power generated with fine biochar was 0.62 W per kg of initial compostable mass. The thermal power generated by coarse biochar was 0.62 W per kg of initial compostable mass. The control thesis generated an average thermal power of 0.54 W per kg of initial compostable mass.

12.4.3 Emissions reduction

The emission trends obtained from the twelve measurements, per emissive surface, are shown in Figure 12-6.a to Figure 12-6.d. The trends are built on the average value of the single emission data measured from the three bins of each thesis.

The first six days of composting were characterized by an increase in CO_2 emissions. This increase followed the same trend as the bin temperature. This phenomenon indicates the aerobic degradation of the organic substance. From day seven, emissions stabilized and began to decrease in the final part of the active phase (from day 28): the more easily biodegradable organic substance started to reduce and became a limiting factor in the activity of the bacteria. During the static phase, the absence of aeration and the lower availability of the

labile organic carbon that had already been degraded led to a decrease in microbial activity and, consequently, a reduction in CO_2 emissions (days 28-63).

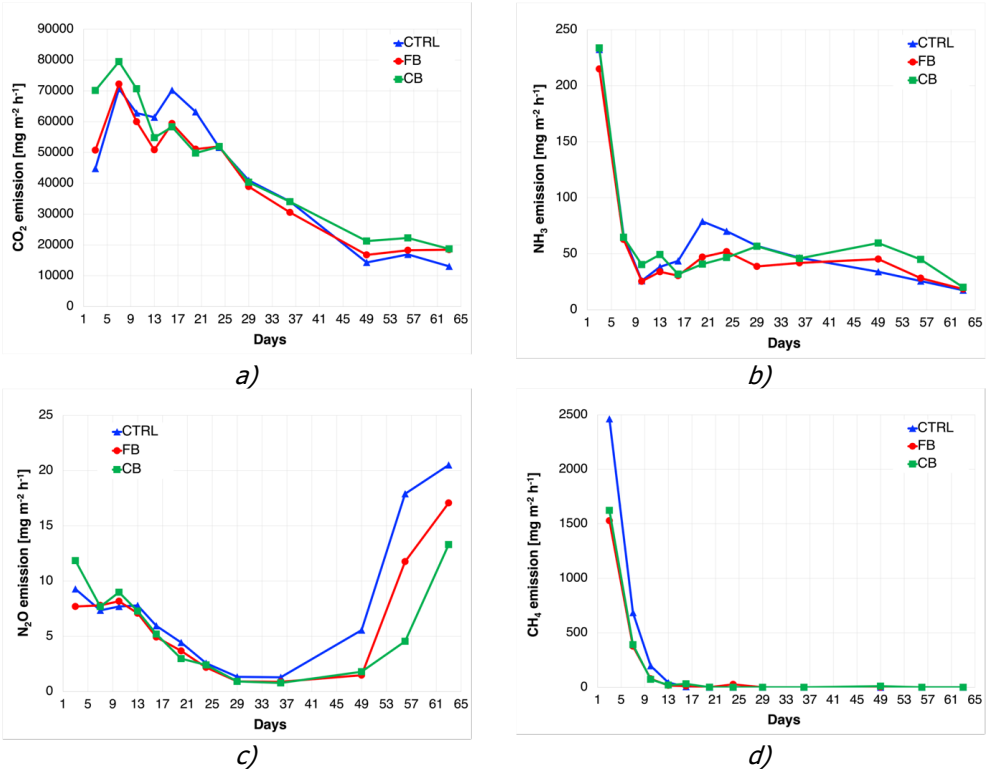

Figure 12-6. a) to d) emissions trend detected during the twelve monitoring sessions of the four monitored gases.

The hourly NH_3 emissions per unit area decreased in the first 10 days from values above 200 mg m^{-2} h^{-1} to values around 40 mg m^{-2} h^{-1}. The emissions then stabilized at values between 40 and 60 mg m^{-2} h^{-1} until the fiftieth day of composting. In the last monitoring period, a further and significant reduction in emissions was recorded for all three theses. The biochar theses showed lower oscillations of the NH_3 emissions, which resulted in a more homogeneous and more constant composting process than the CTRL thesis. The decrease in emissions may be due to several factors: 1) biochar absorbed the ammonium ions (NH_4+) on its surface, preventing the passage of these ions from the liquid phase to the gaseous phase, effectively blocking NH_3 production, [327]; 2) in the static phase, there was a reduced stripping effect by the aeration and water evaporation [328,329]; 3) the natural convection inducted aeration during the static phase together with the absence of large amounts of degradable material slowed down the microbial activities and reduce NH_3 emissions [330,331].

CH_4 emissions showed a similar trend to those of NH_3, as outlined in Figure 12-6.b and Figure 12-6.d. The CH_4 emissions started from high initial values, dropped in the first eight days, zeroed at day 13 and then remained null. This trend indicates high microbial respiration activity and good organic substance aerobic stabilization. In fact, because of biochar, the mass density is reduced, allowing better aeration, and facilitating the proliferation of methanotrophs bacteria instead of methanogens bacteria [158]. Moreover, Liu et al. (2017) suggests that biochar binds and retains NH_4+, making these ions less available as elements for CH_4 production [332]. The difference in maximum values of CH_4 between biochar theses and those of the CTRL was approximately 1500 mg m^{-2} h^{-1} for the CB and FB theses and 2500 mg m^{-2} h^{-1} for the CTRL.

N_2O emissions decreased continuously throughout the active composting phase. Several aspects were involved in the N_2O reduction: the NH_4+ and NO_3- ions retention by the biochar slowed the denitrifying bacteria activity; the greater organic matrix-biochar interaction promoted the bind to the biochar surface of stable functional groups (carboxylic, carbonyl, …) which do not react in N_2O formation reactions; the reduced mix density allowed for better aeration pathways [298,333]. Data collected during the active phase confirms that good aeration prevents anaerobic and nitrification-denitrification processes. These processes were primarily responsible for the N_2O generation as intermediary gas; therefore, low emissions were measured. The measures campaign identified an N_2O emissions increase during the static phase. Despite this, the emissions detected in the biochar thesis were lower than in the CTRL. The CB thesis emitted less N_2O than the FB thesis.

From Eq. (12-3) to (12-11), the cumulative emission of the composting process was calculated and the results are reported in Table 29.

Table 29. Cumulative emission per mass unit during the composting process

Thesis		**kg CO_2 ton^{-1}**	**g N_2O ton^{-1}**	**g NH_3 ton^{-1}**	**g CH_4 ton^{-1}**
CTRL	Average value	116.7 (8.7)	20.8 (0.8)	167.0 (11.9)	536.1 (32.0)
FB	Average value	120.4 (9.7)	16.2 (2.0)	160.0 (13.2)	312.9 (53.3)
	FB vs CTRL	3%	- 22%	- 4%	- 42%
CB	Average value	123.3 (4.4)	12.7 (0.6)	173.4 (14.6)	283.2 (58.3)
	CB vs CTRL	6%	- 39%	4%	- 47%
	CB vs FB	2%	- 22%	8%	- 10%

(in brackets the standard deviation value).

The CB thesis emitted 2% more CO_2 than the FB thesis which, in turn, emitted 3% more CO_2 than the CTRL, though the statistics are not significant since the p-values of the Tuckey test are respectively p = 0.536 and p = 0.791. The addition of biochar facilitated the aerobic degradation processes of the organic substance, causing an increase of CO_2 production and limiting the anaerobic processes that generate CH_4. For this reason, the CB and FB theses showed significantly lower CH_4 emissions than the control, respectively -47% (p = 0.019) and -42% (p =0.023). The same trend occurred for N_2O that showed a 39% reduction (p = 0.001) for the CB theses and 22% (p = 0.1) for the FB theses when compared to the CTRL. The CB thesis emitted +4% (p = 0.751) NH_3 and the FB thesis emitted -4% NH_3 (p = 0.714) compared to the CTRL, but the differences were not statistically significant.

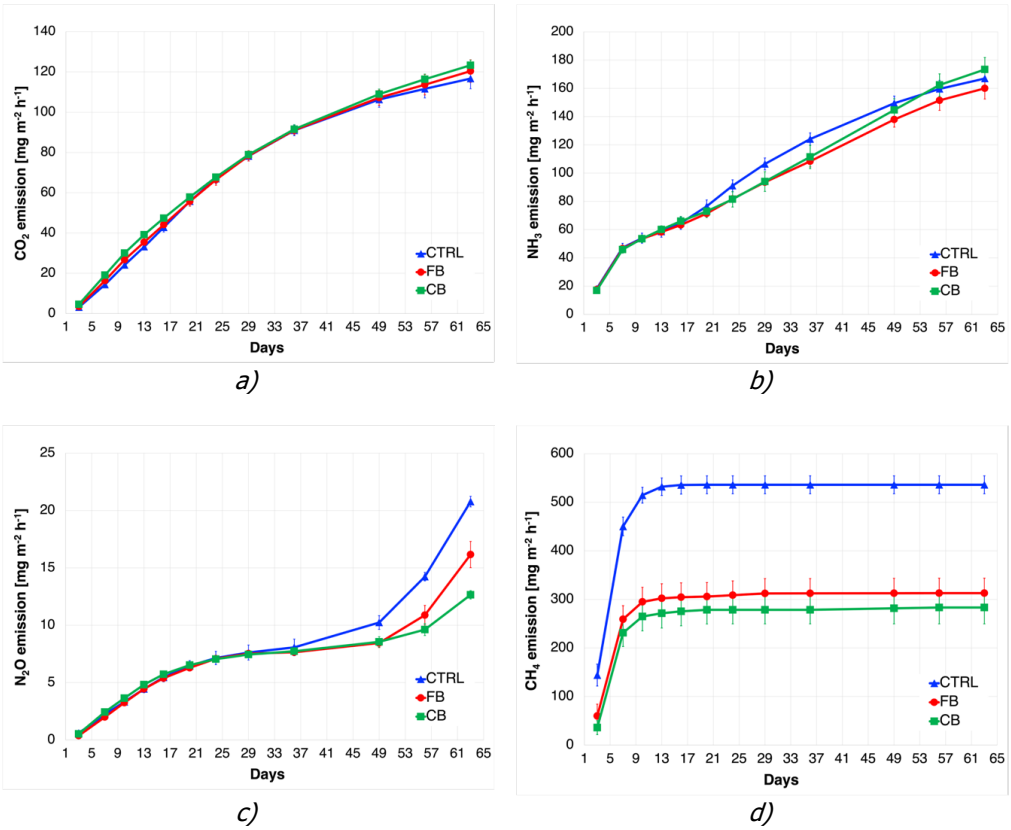

Figure 12-7. Cumulative emission temporal trends per ton of initial organic material and for the four gases that were investigated during the experimental campaign.

The use of coarse biochar proved more efficient compared to fine biochar: coarse biochar reduced N_2O by 22% and CH_4 emissions by 10%. On the contrary, the FB thesis showed a reduction effect of NH_3 emissions, even if statistically not significant, compared to both the CTRL and the CB theses. This

behavior could be explained by the adsorption of NH_4+ to the largest available surface of fine biochar. Figure 12-7 illustrates the cumulative emissions temporal trends per ton of organic material.

As shown from the graphs in Figure 12-6.b to Figure 12-6.e and Figure 12-7, the contribution to the cumulative emissions of NH_3 and CO_2 during the active phase (0-28 days) and during the static phase (29-63 days) was similar. For CO_2, the active phase was responsible for 65% of the total cumulative emissions. For the NH_3 emissions, the active phase contributed to 59% of the total cumulative emissions. Conversely, CH_4 emissions during the active phase contributed to 99% of the total cumulative emissions, Figure 12-8. 95% of CH_4 was produced in the first week of composting. This data led to the deduction that, by creating the conditions for establishing a rapid aerobic degradation in the first days of the decomposition process, CH_4 emissions can be significantly reduced. The biochar included in the CB and FB theses made it possible to obtain an organic mix characterized by low density and high porosity, facilitating the uniform diffusion of oxygen, and creating an optimal microenvironment for aerobic bacteria. This was also confirmed by the sudden initial increase in the temperature of the organic mass (Figure 12-3) and by the higher process temperatures of biochar-aided thesis related to the CTRL thesis.

Regarding N_2O emissions, significant differences between the three theses emerged only during the last days of the static phase. No differences in emissions were found during the active phase, which was responsible for 47% of total cumulative emissions. Other studies in literature have also found an increase in nitrification processes in the final stages of composting [334]. The intensification of the nitrification-denitrification process in the final phase leads to the production and emission of N_2O. In addition, the biochar also enhances nitrification and denitrification during the final static phase since it improves passive aeration conditions and creates a good environment for the nitrifying bacteria [162,335].

Figure 12-8.c shows the cumulative emissions of monitored GHGs in CO_2eq. The conversion is based on the GWP factors for N_2O and CH_4 [336]. The quantification of CO_2eq allows for evaluation of the effectiveness of biochar in emissions reduction. Following the procedure suggested by Sayara and Sánchez (2021) the CO_2 produced during the process had biogenic origins and, therefore, was not considered in the computation [337]. The FB and CB theses had a GWP of 13.0 ± 1.5 kg CO_2eq ton^{-1} and 11.3 ± 1.4 kg CO_2eq ton^{-1}, while the CTRL thesis had a GWP of 20.5 ± 0.9 kg CO_2eq ton^{-1}.

The FB and CB theses had a lower impact of 36.4% and 45%, respectively, compared to the CTRL thesis. The addition of biochar to the SM, at 3% by weight, was effective and sufficient in significantly reducing GHGs emissions. In the CRTL thesis, N_2O gas contributed to 27% of the overall GWP, while CH_4 contributed 73%. For the FB and CB theses, N_2O contributes 33% and 30%, respectively, while CH_4 contributed 67% and 70%, respectively.

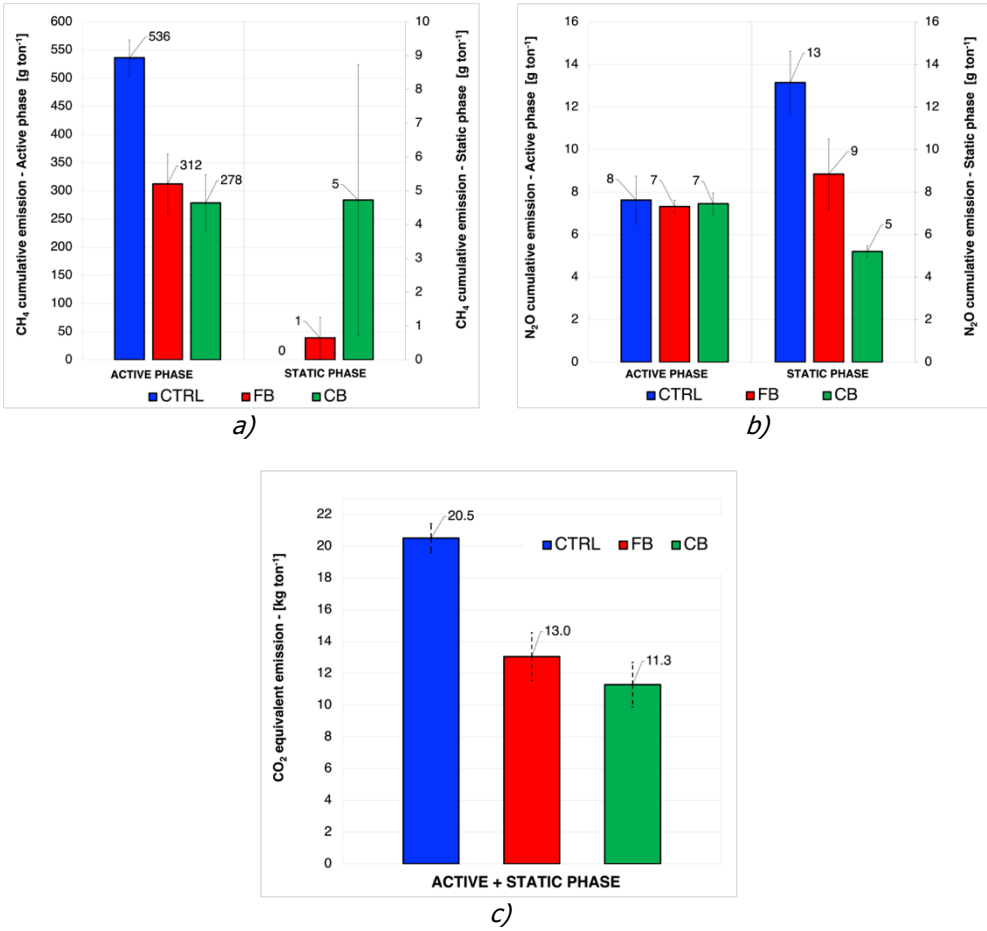

Figure 12-8. Contribution of the active and static phases of the composting process to the totalized emissions of CH_4, a), and N_2O b). c) calculation of the greenhouse effect on CO_2eq of the different theses during the composting process. (Static and Maturation are equivalent terms).

A greater GHGs reduction effect was found in the CB thesis compared to the FB thesis. Because the coarse biochar had a BET surface area of 639.8431 m^2/g and the fine biochar 494.0930 m^2/g, the different reduction effect is likely due to a) the greater adsorption capacity of the coarse biochar, b) the bulking material effect of the biochar and c) the greater BET surface area compared to fine biochar. In the fine biochar, the grinding process may have destroyed some of the microstructures of the original biochar. It is possible to advance two hypotheses to explain why the fine biochar did not reduce GHGs emissions better than the coarse biochar despite the greater contact surface between the biochar and the organic matter. A first reason is that the biochar was applied wet during the creation of the organic mixes. The tendency to agglomerate could have caused an inhomogeneity in the mixing, reducing the correct diffusion and the

total biochar-OFMSW contact surface. A second reason lies in the fact that the higher temperature of the CB thesis had a greater effect on the reduction of GHGs production than the reduction effect given by the interaction between fine biochar and microorganisms [338,339].

The results, however, indicate that although the bulking effect is low, fine biochar reduces GHGs emission due to the interaction properties between organic material and biochar. Furthermore, results demonstrates that the fine fraction of biochar can be used without risk of establishing anaerobic degradation processes, management difficulties (e.g., biochar agglomerates or organic material clusters) and excessive compaction of the organic mix.

12.4.4 Physical-chemical analysis of biochar aided compost

The initial material inserted into the nine bins and the final composted mix extracted from the bin have been sampled as described in paragraph 2.5. The chemical characterizations of the initial and final composed SM are reported in Table 30.

The analyses on the final product have shown, for the parameters under investigation, that all theses investigated comply with the European legislation on fertilizers. The composted material can be included both in CMCs and Product Functional Categories (PFCs), [340]. This shows that the biochar, mixed with OFMSW at 5% v/v (3% w/w) in two different grain sizes, does not compromise the conformity of the composted product in chemical-physical terms.

Despite the alkaline characteristics of the biochar, the analyses showed that the final composted products of the three theses had a similar pH: 7.6 for the CB and FB theses and 7.9 for the CTRL, starting from initial pH values of 5.6 for CB and FB and 5.5 for the CTRL.

In the three bins of the CTRL thesis, an average of 493 ± 3 kg of SM with a density of 568 ± 21 kg m^{-3} was loaded. For the CB thesis, 495 ± 9 kg of mix with a density of 532 ± 11 kg m^{-3} was used, and for the FB thesis 458 ± 12 kg of mix with a density of 530 ± 14 kg m^{-3} was used. The addition of biochar resulted in a 7% lower density for both the biochar-aided theses compared to CTRL. This variability may derive from the further shovel mixing operations that followed the biochar addition to the mix. The average final net composted mass was 287 ± 10 kg for the three CTRL bins, 308 ± 3 kg for the three CB bins and 285 ± 17 kg for three FB bins. The weight losses during the process were 42% for CTRL and 38% for both CB and FB theses.

Concerning the moisture content, the biochar aided theses maintained a higher water content than the CTRL: 29% for CB and FB compared to 21% for the CTRL. Similar results are found in soils where biochar is applied as it is: biochar, in fact, is already used to contrast water stresses (Haider et al., 2020). Greater water retention by the decomposing mass results in a more favourable

environment for microbial metabolism. The addition of biochar can regulate moisture changes in composting piles and increase the water retention capacity of the mixture [341,342].

The CTRL thesis lost 22.5 kg of total solids (TS) and 22.1 kg of volatile solids (VS) during composting. The CB thesis lost 23.6 kg of TS and 25.3 kg of VS, while the FB thesis lost 24.0 kg of TS and 25.4 kg of VS. Compared to the CTRL, the biochar-aided theses lost 15% more of VS (i.e., organic matter). This result is supported both by the higher process temperatures reached by the CB and FB theses and by the higher CO_2 production compared to CTRL (Table 29) which testify the greater aerobic and exothermic microbial activity. Several authors have confirmed the proliferation of microorganisms in the composting matrix with biochar and the increasing in metabolic activity with consecutive higher respiration [343–345]. This result was also confirmed in this study where the biochar shares used are below the values suggested by literature.

Despite the high inhomogeneity of the organic mix, not conducting the experiment at laboratory scale and the difficulty in the samplings collection, the difference between the mass balances of the ashes of the three theses were modest and, therefore, the samples are representative of the organic mass. The TS reduction is in line with that measured for VS. The composting process did not bring significant changes to the content of TOC, TEC, and HA + FA in all three theses.

The Total Kjeldahl Nitrogen value (TKN) was reduced by 2% during composting for the CTRL thesis, while it was reduced by 3% and 4% for FB and CB, respectively. The nitrogen emitted into the atmosphere in terms of ammonia (NH_3-N) and nitrous oxide (N_2O-N) emissions was equal to 74.3 g for the CRTL thesis, 65.1 g for FB and 74.7 g for CB (Table 30).

In the CTRL thesis, the amount of NH_4^+-N shares on Total Kjeldahl Nitrogen decreases from 14.1% to 9.1%. In the FB thesis it remained constant, from 12.8% to 12.4% and in the CB thesis it increased from 13.9% to 16.4%. All values are expressed as ratio on TKN. It is possible to deduce that in the biochar theses there was a greater mineralization of organic nitrogen with an increase in ammoniacal nitrogen. This was found both as a value calculated on total nitrogen [% TKN] and on fresh organic matter [mg/kg FM], reported in Table 30. Given the higher concentration of NH_4^+-N and the higher process temperatures, a higher NH_3 emission was expected in the biochar theses; despite this, no statistically significant increases or variations in NH_3 emissions were found in the CB and FB theses.

Concerning the heavy metals, magnesium (K) and potassium (P), no significant changes in concentration were detected between the biochar aided and CRTL theses (Table 30).

Table 30. Chemical characterization and mass balance of initial mix and final composted mix: average value and standard deviation value.

		CTRL initial	kg (*)	CTRL final	kg (*)	FB initial	kg (*)	FB final	kg (*)	CB initial	kg (*)	CB final	kg (*)
Mass of FM	*[kg]*	493		287		458		285		495		308	
Moisture	*[%FM]*	49.4		20.9		50.41		*28.43*		*50.71*		*28.75*	
pH	*[-]*	5.5 ± 0.1		7.9 ± 0.3		5.6 ± 0.1		7.6 ± 0.5		5.6 ± 0.1		7.6 ± 0.3	
TS	*[g/kg FM]*	506 ± 10	*249*	790 ± 50	*227*	495 ± 5	*228*	715 ± 60	*204*	492 ± 12	*244*	715 ± 9	*220*
VS	*[g/kg FM]*	351 ± 2	*174*	528 ± 56	*151*	346 ± 7	*159*	467 ± 42	*133*	346 ± 20	*172*	474.± 22	*146*
	[%TS]	69.5 ± 1.8		66.7 ± 3.1		69.9 ± 2.2		65.4 ± 3.1		70.3 ± 3.0		66.4 ± 4.0	
TKN	*[mg/kg FM]*	9322 ± 589	*4.6*	14270 ± 1123	*4.1*	9092 ± 332	*4.2*	12755 ± 1804	*3.6*	8809 ± 287	*4.4*	12220 ± 94	*3.8*
	[%TS]	1.8 ± 0.2		1.8 ± 0.1		1.8 ± 0.1		1.8 ± 0.1		1.8 ± 0		1.7 ± 0	
NH_4^+-N	*[mg/kg FM]*	1322 ± 193	*0.65*	1276 ± 461	*0.37*	1160 ± 58	*0.53*	1525 ± 361	*0.45*	1225 ± 57	*0.61*	2008 ± 347	*0.62*
	[%TKN]	14.1 ± 1.2		9.1 ± 3.6		12.8 ± 1		12.4 ± 4.3		13.9 ± 0.5		16.4 ± 2.9	
EC	*[mS/cm]*	3.8 ± 0.5		5.1 ± 0.3		3.8 ± 0.2		4.8 ± 0.1		3.9 ± 0.2		4.5 ± 0.6	
TOC	*[%TS]*	37.1 ± 3	*92.6*	37.7 ± 2.3	*85.6*	36.7 ± 3.4	*83*	38 ± 1.6	*77.5*	38.9 ± 2.3	*95.0*	38.7 ± 5	*85.3*
	C/N	20.2 ± 2.3		20.9 ± 0.8		20 ± 2		21.4 ± 0.6		21.8 ± 1.3		22.4 ± 2.3	
K	*[mg/kg FM]*	5899 ± 617	*2.9*	9314 ± 674	*2.7*	6346 ± 472	*2.9*	9487 ± 784	*2.7*	5735 ± 351	*2.8*	7940 ± 499	*2.4*
	[%TS]	1.2 ± 0.1		1.2 ± 0		1.3 ± 0.1		1.3 ± 0		1.2 ± 0.1		1.1 ± 0.1	
Ptot	*[mg/kg FM]*	2923 ± 136	*1.4*	4569 ± 213	*1.3*	2965 ± 293	*1.4*	4366 ± 756	*1.2*	2852 ± 101	*1.4*	4151 ± 19	*1.3*
	[%TS]	0.6 ± 0		0.6 ± 0		0.6 ± 0.1		0.6 ± 0.1		0.6 ± 0		0.6 ± 0	
NO_3-N	*[mg/kg FM]*	0.454 ± 0.36	*0.22*	2.977 ± 0.99	*0.85*	1.532 ± 2.03	*0.70*	0.696 ± 0.58	*0.20*	9.38 ± 9.18	*4.64*	1.16 ± 0.11	*0.36*
TEC	*[%TS]*	17 ± 1.3	*42.3*	14.9 ± 1.4	*33.8*	16.3 ± 0.4	*37.1*	14.1 ± 0.6	*28.8*	17.1 ± 0.6	*41.8*	14.8 ± 0.9	32.7
HA+FA	*[%TS]*	9.7 ± 1.1	*24.3*	8.5 ± 1.3	*19.3*	9.6 ± 1	*21.9*	8.1 ± 0.5	*16.6*	9.7 ± 1	*23.5*	8.1 ± 0.6	*17.9*
Ni	*[mg/kg DM]*	11.4 ± 0.9	*2.84*	11.5 ± 1.2	*2.61*	18.2 ± 1.4	*4.14*	14.9 ± 0.4	*3.0*	10 ± 0.2	*2.4*	14 ± 0.2	*3.1*
Cu	*[mg/kg DM]*	37.5 ± 8.6	*9.34*	28.9 ± 2.3	*6.56*	29.7 ± 4.2	*6.74*	38.4 ± 3.4	*7.8*	31.9 ± 6.8	*7.8*	34.7 ± 3	*7.6*
Zn	*[mg/kg DM]*	170 ± 10	*42.5*	160 ± 12	*36.4*	214 ± 9	*48.8*	175 ± 18	*35.8*	186.± 14	*45.6*	193 ± 7	*42.7*
Cr	*[mg/kg DM]*	33.7 ± 7.1	*8.41*	24.5 ± 6.4	*5.56*	25.5 ± 7.1	*5.78*	19.1 ± 0.9	*3.9*	15 ± 1	*3.7*	20.9 ± 3.5	*4.6*
Cd	*[mg/kg DM]*	0.2 ± 0	*0.05*	0.2 ± 0	*0.04*	0.3 ± 0	*0.06*	0.2 ± 0	*0.04*	0.2 ± 0	*0.04*	0.2 ± 0	*0.04*
Hg	*[mg/kg DM]*	0.2 ± 0.1	*0.05*	0.2 ± 0.1	*0.04*	0.2 ± 0.1	*0.04*	0.1 ± 0	*0.02*	0.2 ± 0	*0.04*	0.2 ± 0.2	*0.04*
Pb	*[mg/kg DM]*	7.3 ± 0.4	*1.81*	11.2 ± 2.7	*2.55*	10.3 ± 0.6	*2.4*	12.7 ± 1.4	*2.6*	8 ± 1.2	*2.0*	11.5 ± 0.8	*2.5*

12.4.5 Biochar coating

Figure 12-9 shows the biologically activated biochar, co-composted for 63 days. Table 31 displays the analysis through X-EDS of the pre-composting biochar and of the co-composted biochar. The co-composted biochar presented on the surface, even if in trace amounts, sodium, chlorine and sulphur, presumably in the form of salts. These elements, initially contained in the biodegradable organic substance, became available for use by soil microorganisms. In addition, oxygen almost doubled, an indication of the presence of carboxylic and carbonyl groups.

As shown in Figure 12-9.a, the external surface of the biochar was covered with a nutrient-rich organic coating composed of organic material, mineral salts and nutrients. This indicates the interaction between biochar and the organic mass. The aging process took place quickly, also facilitated by the high temperatures reached during degradation as well as the high quantity of organic matter available. The nutrient-rich organic coating that covers biochar makes the biochar not only a porous matrix capable of adsorbing nutrients and minerals but also acts as an active hotspot for the utilization of these nutrients [346].

Figure 12-9.b shows the internal section of a co-composted biochar grain. It is noted that the biofilm phenomenon occurred on the surface, while it did not affect the internal portion. Since there is no fracturing of the biochar grains, it can be assumed that, during the composting period, there was no degradation of the labile carbon. Therefore, this research has shown that in just eight weeks of composting at high temperatures and in an environment where organic matter is available, the biochar has undergone a surface aging process as evidenced by the coating on the biochar grains.

The formation of the nutrient-rich organic coating combined with the intrinsic characteristics of biochar (EC, CEC, WR), further increases the advantages that biochar in its co-composted form brings to the soil when applied as a soil improver in agriculture.

Table 31. X-EDS spectroscopic analysis of the elements presents on the surface of the biochar before and after composting. Some elements, not initially present on the biochar, are present in the coating of the biochar after composting.

Elements*	C	O	Na	Mg	Si	P	S	Cl	K	Ca	Total
Not composted Biochar	90.0	4.99	-	0.54	0.19	0.87	-	-	0.78	2.62	100
Co-composted biochar	85.9	9.64	0.32	0.32	0.36	0.36	0.31	0.57	0.91	1.31	100

*All results in % weight/weigh.

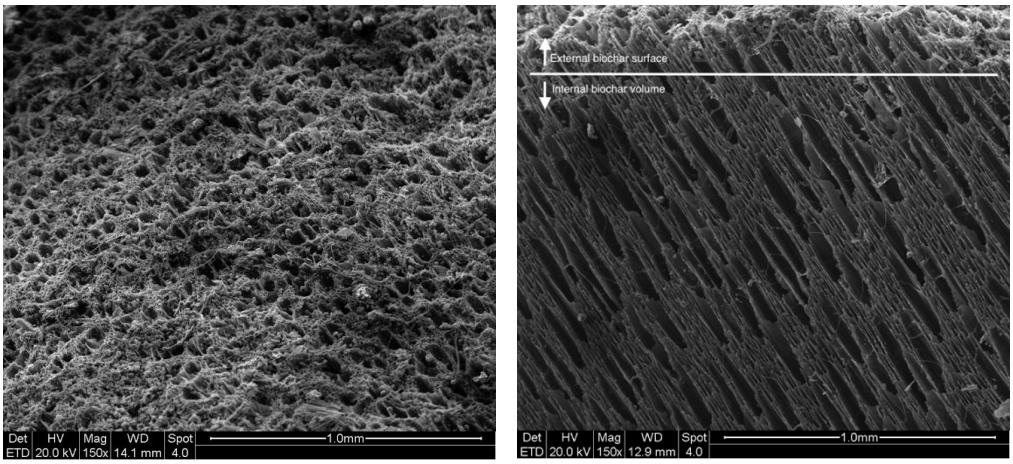

a) *b)*

Figure 12-9. SEM investigation. a) External surface of co-composted coarse biochar with external surface layer of biological origin called biofilm. b) Internal section of the co-composted coarse biochar. No biofilm was observed within the biochar.

12.4.6 Further and overall considerations

Considering the results presented in the previous paragraphs, it is hard to find a significant difference between the two biochar granulometric fractions investigated (FB, CB). However, the increase in thermal power generated during the composting phase is evident indicating that there is a significant improvement and acceleration of the microbiological processes of composting. These results are in line with Liu et al. (2018) [347]. They found out that biochar can improve the stability of the process while increasing the temperatures of the composting material. Notably, the FB and CB theses dissipated more thermal power than the CTRL thesis. The average temperatures are 4 °C higher and peak temperatures reach more than 6 °C higher than the control for the two biochar theses. The similar behavior of fine and coarse biochar on the temperatures and thermal power trends prove that the bulking action is not the most important effect given by the biochar.

The FB appears to have a slightly stronger effect than the CB during the first 15 days of the process. As it stands, it is difficult to attribute a meaning to this trend. The FB is assumed to have acted more distributed within the material, as expected. Furthermore, the results highlight how the bulking agent property of biochar in general is secondary to the intrinsic properties of the material (distribution of porosity, electrical conductivity, water retention capacity, cation exchange capacity). As proof of this, coarse biochar performs worse than fine biochar during the first 15 days of the active phase. If the most important feature

of biochar would have been its bulking agent properties, the opposite behavior should have been observed. Also, the thermal energy generated during the active phase is slightly higher in the case of fine biochar. Unfortunately, given all the assumptions made in the thermal model, it cannot be said with scientific certainty that fine biochar has given significant improvements to the composting process compared to coarse biochar.

In terms of water retention capacity moisture content analysis at the end of the composting process shows that the thesis without biochar presents a water content ratio of 20% w/w and the thesis with biochar (FB and CB) presents a water content ratio of 30% w/w.

The positive impacts of biochar were observed in terms of process temperatures reached by the decomposing organic material and, consequently, in thermal energy production. Results shows that the impact of fine biochar on the thermal power of organic waste composting is slightly higher than the impact of coarse biochar. In particular, FB increased the thermal energy production of 20% over CTRL, CB increased the thermal energy production of 16.0 % over CTRL. This shows that in FB thesis there is a greater microbial ecology as the composting material-biochar interaction is improved thanks to a wider contact surface area between the two parts. In CB thesis there is an increase in thermal energy but lower than FB: probably due to the granular nature of coarse biochar the contact surface area is restricted and therefore the microbial activity is lower.

The emission monitoring campaign detected a 22% and 39% decrease in N_2O using fine and coarse biochar, respectively, while CH_4 was reduced by 42% and 47%, respectively, compared to the control. In CO_2 equivalent terms, the use of 3% coarse biochar w/w alone can reduce emissions by 45% compared to the control. Biochar aided theses showed increased temperatures as well as increased CO_2 emissions. Both factors affirm the increased aerobic microbial activity.

The bulking effect is not the sole emission reduction mechanism that takes place in the co-composting process. After it was proven by this research that biochar size is not the key factor that affects the emission trends, it is possible to speculate on future industrial applications where the biochar obtained through gasification is sieved. Coarse biochar can be used for noble purposes such as agriculture, filtration systems or innovation in materials industry, while fine biochar, which has a lower quality and cost, can find a valuable niche of application in organic waste composting.

Finally, the investigation on the application of minimal amounts of biochar for the composting process will help for understanding the sustainability of organic waste management facilities. These results are fundamental for practical considerations about the future integration of biochar in composting plants.

13 FEASABILITY OF HIGH TEMPERATURE BIOCHAR APPLICATION IN COMPOSTING FACILITES. A TECHNO-ECONOMIC AND ENVIRONMENTAL INVESTIGATION.

The feasibility study of biochar applied in composting facilities is explored in this research, from an economic, technical and environmental point of views. The integration of biochar in this category of specialized and with well-established processes plants, requires careful consideration.

The analysis examines different sources of biochar, including internal production via gasifiers of different size. Two different application rates are considered, while the economic analysis is based on the payback period concept, considering the sale of the energy produced. The environmental evaluation is based on credit carbon quantification.

The research addresses an increasingly relevant question: whether innovative solutions such as biochar are not only theoretically sustainable but also technically-economically viable. It also aims to promote the adoption of environmentally friendly practices even in established plants, thereby contributing to create more sustainable industries.

Keywords: Biochar; Gasification; Co-Composting; Carbon dioxide emission; Technical feasibility, Economic evaluation, Payback time; Carbon credits

A form of this research is also published in "Sustainable Energy and Assessment", available online from February 2024.

13.1 Motivation of the feasibility study

Municipal waste management is an increasingly crucial issue, with constant efforts to make the involved process more circular, moving away from landfill in favor of recycling. In Italy during the 2020, waste destined for landfill amounted to 6 million tons, more than 5 million tons were incinerated and almost 8 million tons underwent biological treatment, half of which was composted. A 23% of the Organic Fraction of Municipal Solid Waste (OFMSW) produced is processed using biological treatments: composting, integrated anaerobic treatment and anaerobic digestion. Composting itself represents about 13% [348] of this framework. Biological treatment is therefore one of the main waste management strategies in Italy, with further scope for expansion through increased recycling. However, composting is the predominant method among biological treatments, but it has a considerable environmental impact due to high greenhouse gas emissions (GHGs). The future challenge is undoubtedly to increase the fraction of waste composted to reduce the other unsustainable practices (e.g.: landfills and waste-to-energy plants) [274,349]. At the same time, since composting processes are not exempted from GHGs emissions - in particular carbon dioxide, methane and nitrous oxide - it is essential to refine processes and technologies used for reducing the environmental impact and GHGs emission, and for improving the quality of the final product [337].

The composting process was defined by Italian agency ANPA as the *solid-phase biological stabilization of organic waste under aerobic conditions*. It is based on exothermic chemical reactions initiated by microorganisms in organic matter [350]. Henceforth, it is imperative to acknowledge that this process transcends mere volumetric reduction. Instead, it signifies a metamorphosis of organic waste into a reusable compost of considerably higher quality than the initial material. A transformation attributed mainly to the well-controlled industrial processes. The process is governed by several critical parameters: the carbon-to-nitrogen ratio, maintained at approximately 30:1; the moisture content, preserved in the range 53%-67%, the oxygen concentration to avoid anaerobic conditions, over the 10% v/v; the control of the waste size through shredding operation, ranging from 10 to 50 mm; the temperature regulation: good conditions between 55-60 °C and lower than 70°C to preserve the microbial population; the maintenance of pH levels within specific boundaries, that is in the pH range of 6-8 for OFMSW composting. Nutrients, such as carbon and nitrogen, act as an energy source for microorganisms, while moisture and oxygen are essential to perform the chemical reactions behind the complex bio-transformation processes [296]. The accelerated and controlled industrial composting process results in a humus-like product that is useful for increasing the biological fertility of soil [351], as well as for preventing soil erosion [352] or restoring contaminated sites where new soil is needed [353,354].

In the context of OFMSW composting, three types of facilities can be identified: a) open-field aerated heaps: these involve the creation of windrows, periodically turned to ensure oxygenation; b) static heaps with forced or passive aeration: they utilize perforated tubes on the pavement to provide air and promote aerobic decomposition; c) closed bioreactors, also known as biocells: these employ forced aeration initially, followed by maturation in open windrows. Other types of bioreactors are rotating cylinders, silos, biocells equipped with constant mixing mechanisms [315]. All these configurations aim to oxygenate the organic mix to minimize the emissions of GHGs and unpleasant odors.

Against the backdrop of the constant search for solutions to efficiently treat OFMSW and reduce GHGs emissions, one viable answer is the innovative approach of co-composted biochar [299,355,356].

To date, the main gaps found in literature in the field of co-composting concern:

a) the lack of research exploring the same type of waste (green waste, OFMSW, food waste, etc.) and the same type of biochar (pyrolysis temperatures, granule sizes, etc.) to evaluate the effective impacts on the decomposition;
b) the economic feasibility and practical application of biochar in composting processes [357]. This research aims to start filling this gap, also highlighted by Nguyen et al. (2022) [358].

Finally, co-composted biochar also offers access to carbon credits. Due to its high content of stable carbon, biochar is considered one of the most promising solutions for long-term carbon sequestration (hundred-year time horizon) [16,41]. Therefore, its application in composting processes offers a twofold advantage: on the one hand, biochar is already mixed with compost ensuring its effective burial when the compost is used in agriculture or for other applications, and on the other hand, once certified, co-composted biochar allows access to the carbon credit market leading to economic gains [46].

This research presents the exploration of the technological and economic feasibility of using biochar as additive in composting processes. First, facilities that opt to use biochar necessitate a reliable and continuous supply chain to maintain seamless operations. Second, due to the emerging market of biochar, establishing a long-term supply proves to be a hurdle. Additionally, a comprehensive economic evaluation is imperative to predict the cost-effectiveness of incorporating biochar into the composting process. To ensure the supply of biochar and to abate costs, this study proposes an innovative way of hybridizing composting facility and gasification power plant, resulting in a pioneering study where a gasifier is installed and integrated in a OFMSW treatment facility. Moreover, an analysis of the environmental benefits resulting

both from the reduction of composting process GHGs emission and carbon storage is considered.

Gasification is preferred to other biochar production processes despite the lower yield of biochar [76] (pyrolysis, torrefaction, hydrothermal carbonization) because it can combine several benefits:

- gasification produces both thermal and electrical energy from renewable source, which can be sold on the energy market, allowing a fast repay of the economic investment;
- gasification is often an autothermal process, unlike pyrolysis or torrefaction. No-external energy sources are required;
- higher temperatures are reached during gasification than other processes. High temperature biochar has larger surface area [118] that affects the behavior of the organic matter biota [102], with the consequence of an enhanced microbial activity and a higher GHGs reduction;
- standards for the quantification of the credits assigns to the biochar produced through "high technology systems" a higher number of carbon credits as this biochar type is mainly composed of stable carbon [94,102]. "High technology systems" recover and reuse the pyrolytic gases, exploit at least 70% of the generated thermal energy, abate the emission of atmospheric pollutants, and control the production temperature [359].

A real case-study of a OFMSW composting facility in Italy is studied. To carry out a real-case feasibility study, evaluating both technical and technological issues as well as economic aspects, different scenarios were investigated. Besides the current situation of the composting facility, used as a baseline to identify improvements in the other scenarios, five different scenarios are studied. The first scenario involves purchasing biochar from an external producer and applying it to the whole OFMSW organic mix currently treated in the composting plant. All other studied scenarios propose the installation of gasification plants of different power capacity (500 kW, 1 MW and 1.7 MW) in the composting facility, to produce the biochar on-site. Therefore, in the scenarios with reduced gasifier capacities, an additional amount of biochar was assumed to be purchased to nevertheless co-compost the entire organic mix. To have a larger number of scenarios to work on, and to better evaluate which solution is most feasible, in one scenario the purchase of the additional biochar was not considered. All scenarios are detailed in 13.2. Since they are often located in remote areas and owned by publicly owned multi-utilities, waste treatments or composting facilities are suitable for hosting even high-power gasifiers.

About gasification, a manufacturer with long field experience in designing and building gasification systems is considered. SynCraft GmbH produces durable and reliable fixed-bed gasifiers capable of receiving even unfavorable biomass feedstocks, distinguishing them from other gasifier manufacturers. To ensure the robustness of the gasifier and its full functionality even in non-optimal conditions, the company has identified specific fixed electrical capacities to optimize the plant architectures. The available capacities are in the range of 200 kW to 1000 kW. These systems are modular, allowing for the expansion of electric capacity even beyond the maximum power available module. This versatility contributes to addressing the challenge of highly variable flows of available biomass, both from seasonal and annual point of view. During periods of pruning or riverbanks maintenance, there is sufficient biomass available for accumulation and use during times of scarcity. The choice of gasifier capacity has been made by considering seasonal variability, annual availability and storage capacity to mitigate shortages. SynCraft, by marketing the same plant in various sizes, provides greater flexibility for the evaluation of the optimal capacity to be installed in this specific case study. For these reasons, this work considers the different gasifier sizes proposed by SynCraft GmbH, with a detailed assessment of their techno-economic feasibility conducted for the different scenarios.

Though this seasonal fluctuation presents new challenges in biomass management, gasification technology ensures a constant energy output, in contrast to others renewable sources (e.g.: photovoltaics). Furthermore, also biochar is continuously produced, allowing for material accumulation and its utilization at later stages of the processing. Figure 13-1 compares actual pathways and the novel proposed alternative pathways for biomass exploitation. In the studied scenarios, different sizes of gasifier are considered with different implication on the biomass management but also import advantages in terms of production of biochar (with environmental benefits), and high-efficiency production of thermal and electric energy (with economic gain) [360].

Finally, to estimate the environmental benefits introduced by the application of biochar in the composting process chain, are considered both the demonstrated capacity of reducing GHGs during the composting process thanks to the interaction between biochar and soil biota, and the carbon storage capability, both aspects scientifically recognized [102,164].

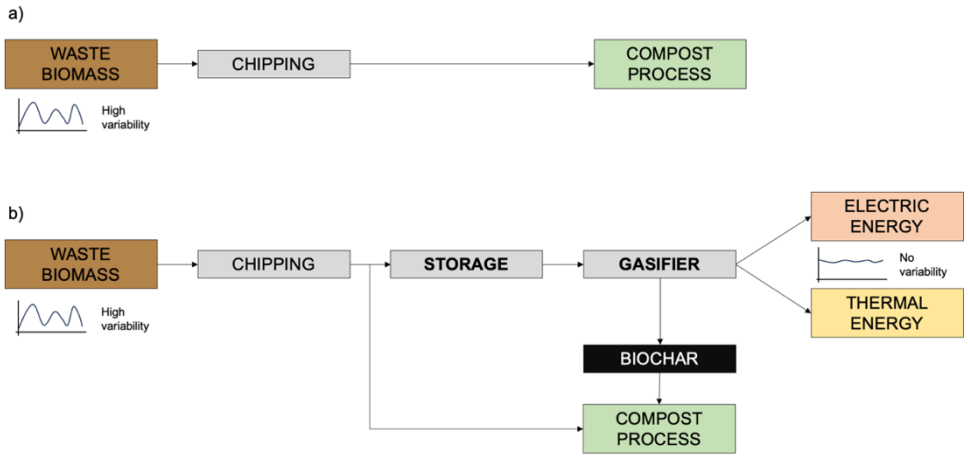

Figure 13-1. a) Actual pathway of biomass in compost plant; b) the new possible pathway in compost plants for full exploitation of waste biomass

13.2 Feasibility study approach and analyzed scenarios

The composting facility considered in this work is in Italy, and the OFMSW used comes from several provinces. In addition, the facility also collects large amounts of residual woody biomass resulting from maintenance and mowing operations: waste biomass, public green pruning, hydrogeological restoration work, etc. The amount of woody biomass accepted is less than the demand for disposal since the facility does not require high amounts of wood for the composting operations.

Since this research aims to investigate the economic, technological, and environmental aspects of the facility, data used are either public or provided directly by the facility manager to make the feasibility study as close as possible to reality. Beside the analysis of the current situation, three different and more sustainable ways were evaluated to determine the most advantageous ways of biochar application in composting operation.

From an economic perspective, the analysis focuses on annual cash inflows and outflows, excluding revenues from waste disposal services that the multi-utility receives from the provincial administrations involved. These revenues, linked to the "Italian tax on waste disposal", are neglected in the work since they are the result of private contracting and are, therefore, highly variable both geographically and on the amount of waste disposed. Since the effects of these revenues are the same for all scenarios, they do not affect the overall comparison.

The technological analysis is based primarily on experimental data or technical reports provided by the facility manager and literature data where necessary. The technological analysis focuses primarily on the installation of a

gasification plant. Regarding the composting process, standard facility operations already in use are taken as a reference. The aim is to evaluate the costs associated with the initial installation, maintenance, and operation of the gasification plant and to investigate whether the biochar management operations are feasible.

The environmental impact analysis is based on direct measurements conducted in an emission monitoring campaign at the facility. The goal is the quantification of emissions as equivalent carbon dioxide (CO_2eq). In parallel, the amount of carbon stored due to the biochar incorporated into the co-composted final product was investigated in terms of Carbon credits (CAC).

The next paragraphs present the facility current situation (CS), used as baseline, and the five scenarios analyzed in this work:

1. **Scenario 1 (S1)**: all the biochar needed for the co-composting process of whole Organic mix is purchased. In S1, biochar is applied to the entire organic mix.
2. **Scenario 2 (S2)**: installation of a 500 kWe gasification co-generator power plant. Production of a portion of the total biochar demand and purchase of the remaining part. In S2, biochar is applied to the entire organic mix.
3. **Scenario 3 (S3)**: installation of a 1000 kWe gasification co-generator power plant. Production of a portion of the total biochar demand and purchase of the remaining part. In S3, biochar is applied to the entire organic mix.
4. **Scenario 4 (S4)**: installation of a 1000 kWe gasification co-generator power plant. Production of a portion of the total biochar demand and no other biochar amount is purchased. In S4, two processes occur: standard composting and co-composting.
5. **FULL**: installation of a 1700 kWe gasification co-generator power plant. Production of the total biochar demand. In FULL, biochar is applied to the entire organic mix.

Synoptic diagram is reported in Figure 13-2 for describing the scenarios. Furthermore, paragraphs 13.2.2, 13.2.3, 13.2.4, 13.2.5, 13.2.6 are reserved respectively for S1, S2, S3, S4 and FULL Scenario, to provide all the necessary information and to describe in detail the input data, the desired output values and the method applied for the economic, technological, and environmental assessments.

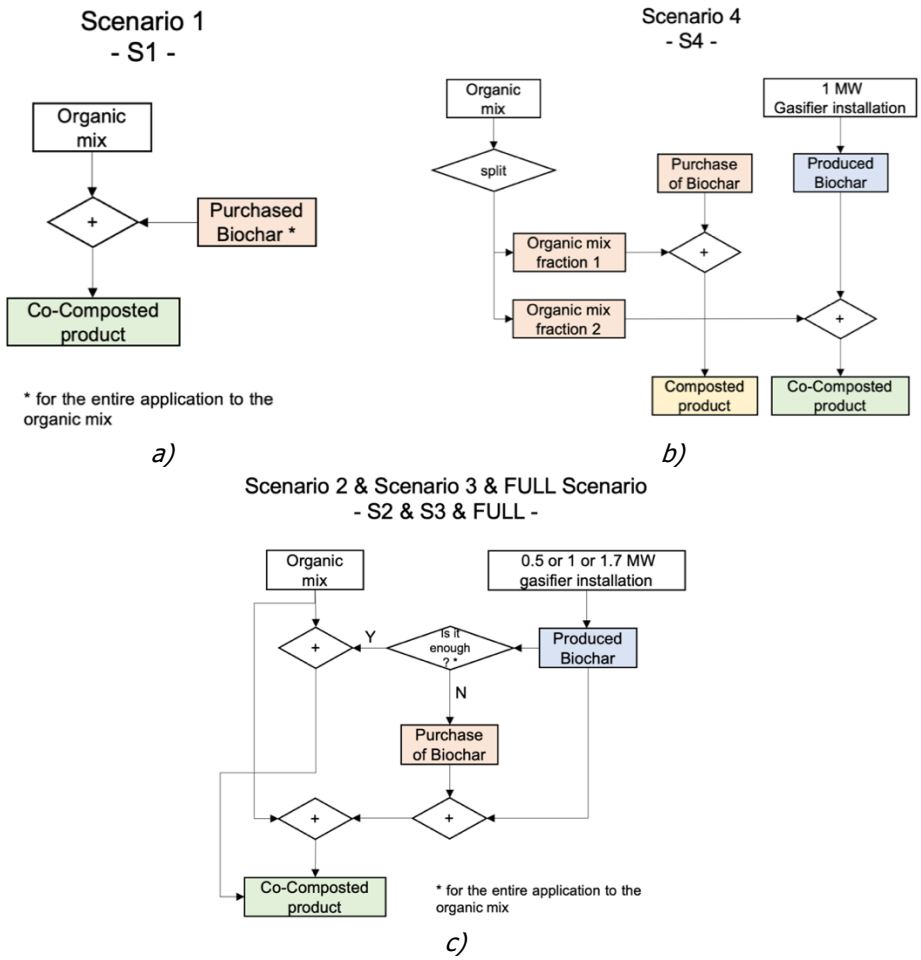

Figure 13-2. Synoptic diagram of the five scenarios: a) S1; b) S4 and b) S2, S3 and FULL Scenario.

13.2.1 Facility overview and Current Situation (CS)

The composting facility considered has a treatment capacity of 4300 tons of organic mix simultaneously. The organic mix is composed of 50% w/w of OFMSW, 20% w/w of degradable "new-wood" and 30% of "bulk-wood" (wood with a size of 10-20 cm is used for reducing the density of the OFMSW), Figure 13-3. A final sieving allows separation of a) non-degraded wood that will be re-put at the beginning of the process and b) plastic pieces and other inert materials (~7%) that will be destined to landfill. The facility has eighteen biocells, equipped with forced floor-aeration, that are filled with about 350 m^3 (230-240 tons) of organic mix each one. The composting cycle lasts eighteen days: each day a different cell is emptied and refilled. The organic mix is reduced by 75% in volume at the end of the cycle. The second stabilization phase takes place in some aerated trenches constantly mechanical turned.

Figure 13-3. OFMSW and "bulk-wood" before mixing in the composting facility.

Table 32 collects the data used for the study. The reference year is 2019 since it represents the last year whose data are reliable and historically significant. The years up to 2021 contain anomalies due to the impact of the COVID-19 pandemic, while the 2022 and 2023 data are not published at the time of the study. To date, the final compost is sold at the nominal price of $C_{compost} = 1 \text{ €} \, \text{tons}^{-1}$, since the real economic returns are from private contracting for waste disposal services.

Table 32. Facility overview.

Symbol	Description	Value	Measurement unit	Notes
M_{OFMSW}	OFMSW: Agronomic + residential origin	25564	tons y^{-1}	1,2
$M_{biomass}$	Waste biomass: biomass granted to the facility	11113	tons y^{-1}	1,2
$M_{organic\_mix}$ $V_{organic\_mix}$	Organic mix: initial mix processed	51128 90013	tons y^{-1} m^3 y^{-1}	3
$M_{compost}$	Compost: outgoing compost from the process	19904	tons y^{-1}	1,2
$Y_{compost}$	Compost yield	39%	w/w	
ED	Electricity demand: energy consumption of the entire facility	4169	MWhe y^{-1}	1,2
$R_{compost}$	Income from compost sales	19904	€ y^{-1}	-

[1] Facility technical reports (year 2019) provided by the facility manager. [2] "AIMAG Sustainability report 2019".
[3] 50% w/w OFMSW, 20% w/w "new-wood", 30% w/w of "bulk-wood".

The OFMSW is mainly composed of food and kitchen waste from the residential houses (e.g. leftover food or rotten food, vegetable and fruit scraps, coffee grounds, pure cellulose paper, ...) or waste from the agricultural sector

(e.g. rotten fruit and vegetables, bad products not marketable or damaged by adverse weather events, processing waste, ...).

13.2.2 Scenario 1: biochar purchase

S1 includes the application of biochar to the whole organic mix in Table 32. The biochar is mixed with the Organic mix at 3% w/w wet basis. This amount is shown to be adequate to improve the biodegradation process, reduce GHGs, and improve the final product. This low application rate has an effect in terms of economic benefits since less biochar must be purchased. In S1 the amount of biochar to apply to the whole Organic mix, $M_{biochar\_OM}$, Eq. (13-1), is totally purchased.

$$M_{biochar\_OM} = M_{organic\_mix} * 3\% \qquad [kg] \qquad (13\text{-}1)$$

The biochar selected for S1 is sold by the Italian company BioDea. BioDea biochar is produced at temperatures close to 1000 °C starting from conifer woodchips obtained through forest maintenance. The physical-chemical characteristics of this biochar are: Total Nitrogen N < 0.5% w/w; Carbon from carbonates < 0.1% w/w; Maximum water retention = 115%; Salinity = 110 mS m^{-1}; pH = 9.85; Ash content (dry basis) = 4.6%; H/C (mole fraction) = 0.2; Total Carbon (dry basis) = 72% and density = 500 kg m^{-3} (Table 39).

13.2.2.1 Expenditures

Considering a retail purchase price of $€_{biochar\_unit} = 0.3\ € \ kg^{-1}$, the biochar-related expenses in S1 are calculated via Eq. (13-2). This higher price is a precautionary measure. Specific contractual conditions may apply if a large amount of biochar is purchased, which could result in a lower price.

$$C_{biochar} = €_{biochar\_unit} * M_{biochar\_OM} \qquad [€] \qquad (13\text{-}2)$$

13.2.2.2 Revenues

The selling price of the final biochar-aided compost is kept the same as the standard compost of CS, $€_{co-comp\_unit} = 1\ € \ tons^{-1}$. This choice is prudent. In fact, biochar makes the final product an enriched soil conditioner with high carbon-content, which could justify a higher selling price. A deep evaluation is needed to determine whether the improved characteristics of the soil conditioner support a higher price, considering possible customer demand. This evaluation is beyond the aims of this research. Eq. (13-3) shows the computation of revenues from the sale of co-composted material.

$$R_{co-compost} = €_{co-comp\_unit} * M_{co-compost} \qquad [€] \qquad (13\text{-}3)$$

where $M_{co-compost} = M_{compost} + M_{biochar\_OM}$ [tons].

13.2.3 Scenario 2 – S2: 500 kWe gasifier for biochar production and biochar purchase

S2 involves the installation at the facility of a gasification power plant with the purpose of producing biochar. In this scenario the whole organic mix is co-composted. In S2, it is assumed that the facility will be able to process more biomass than the CS, resulting in a greater amount of wood conferred to the facility. Considering the availability of storage and handling space and the fact that biomass processing is already being performed on-site, the increase in biomass amount is not considered a limitation for the development of this model. This applies to all other scenarios.

The SYNCRAFT CW1800-500 power plant has been selected for installation in the facility [173]. The choice of this gasifier is due to a) it is fully equipped (gas cleaning, biochar and ash discharge, electric power generation, thermal energy recovery, ...), b) it is ready-to-install by the manufacture, c) waste biomass can be easily employed thanks to the floating bed reactor technology, e.g., offcuts and sawmill by-products. Wood chips from waste biomass have been also tested in less-flexible gasifiers (e.g. downdraft/Imbert reactor) demonstrating excellent results [361,362]. SYNCRAFT CW1800-500 has a nominal electrical power of 500 kWe. The affordable initial investment and the limited management operation for small-scale systems are possible reasons for installing this model. The characteristics of the SYNCRAFT CW1800-500 are given in Table 33.

Table 33. Combined heat and power plant SYNCRAFT CW1800-500 and SYNCRAFT CW1800x2-1000.

Symbol	Definition	SYNCRAFT CW1800-500	SYNCRAFT CW1800x2-1000		
		Value	Value	Meas. Unit	Note
E_{e_gasif}	Electrical power	500	1000	kWe	2
E_{t_gasif}	Thermal power	740	1404	kWt	2
T_{ope}	Operating time	8000	8000	h y^{-1}	2
ε_{gasif}	Fuel consumption/ Efficiency of gasifier	0.72	0.71	kg $kWhe^{-1}$	2
$Y_{biochar}$	Biochar yield	16.6	16.6	% $M_{biochar}\, M_{wood}^{-1}$	2
$\rho_{biochar}$	Biochar density	230 - 250	230 - 250	kg m^{-3}	3

[1] This value fit in the ranges reported in literature, e.g. 5-10% [363] and 14-25% [364]. [2] Manufacturer's data [173]. [3] [365]

In all SynCraft power plants, wood chips are loaded through a bottom-push charge system in a first pyrolysis reactor in which the biomass reaches 500 °C and it is transported via auger. The pyrolyzed wood is then pushed into the second stage of the system: the floating bed gasification reactor that reaches 850 °C. The produced syngas passes through a filter that separates biochar and retains a fraction of the tars content. Through a cooler and a scrubber (to complete the gas cleaning), the syngas is brought from 700 °C to 25 °C and sent to an internal combustion engine for electrical energy production. Thermal energy both from the engine and from the cooler are recovered and exploited. Approximately 10% of the electricity from gasifier is self-consumed. The system is scaled according to the desired electric capacity.

13.2.3.1 Expenditures for the gasifier installation

For the gasification plant economic evaluation, the study conducted by Wei et al. is used [58]. Prices are updated considering the inflation rate (IR) from the fourth quarter of 2008 (Q4-2008) to the second quarter of 2023 (Q2-2023) equal to $\mathrm{IR} = 45.53\ \%$ (index: USCPI31011913), and the dollar-to-euro exchange rate (ER) at the end of Q4-2008 equal to $\mathrm{ER} = 1.3917\ \$\ €^{-1}$ (Banca d'Italia). All variables' computations and equations used for this paragraph are included in Appendix F.7. Cash flow and payback time.

The expenditures related to the biomass sourcing is null since the purpose of the study is to exploit residual biomass already delivered at the facility where the gasifier is installed. The cost of drying is assumed to be negligible, given the gasifier's self-consumption. All data are reported in Table 34.

13.2.3.2 Other expenditure voices: biochar and diesel fuel

Given the biochar yield of $\mathrm{Y_{biochar}}$, the gasifier cannot provide the required biochar amount to achieve the $3\%\ \mathrm{M^{3}_{biochar}}\ \mathrm{M^{-3}_{organic\ mix}}$ application. Therefore, it is necessary to purchase an amount of biochar $\mathrm{M_{biochar\_buy}}$, see Eq. F. 6 and following equations reported in Appendix F.2. Other expenditure voices: biochar and diesel fuel.

Additionally, diesel fuel consumption for biomass shredding is also estimated. Contrary, no additional cost for biochar mixing procedures is considered since these operations are already currently performed during the preparation of Organic mix also in CS. See Eq. F. 10.

13.2.3.3 Revenues

The evaluation of revenues from the sale of electricity and thermal energy was calculated through Eq. F. 11. All data are reported in Table 34.

The revenue for thermal energy was calculated through Eq. F. 12. In this equation, the $€_{\mathrm{E_t}}$ value is halved compared to the rate declared by the leading energy provider in Emilia Romagna region, as a precaution. Given the still-developing nature of district heating in Italy, offering cost-effective rates to

nearby residents may be necessary, thus justifying the hypothesis of a lower selling price in this model. All data are reported in Table 34.

Regarding the compost sale, the price of the final biochar-aided product is the same of the standard compost of CS, calculated through (13-3).

Revenues related to the sale of carbon credits, which can be calculated based on the biochar contained in the final product, will be discussed in paragraph 13.4.

13.2.3.4 New biomass to be sourced

The requirement to operate the gasifier for $8000\ \mathrm{h\ y^{-1}}$ implies that a greater amount of waste biomass, than currently collected, will be supplied to the facility. The missing quantity can be calculated based on the data in Table 32 and Table 33, as shown in Eq. F. 13.

13.2.4 Scenario 3 – S3: 1000 kWe gasifier for biochar production + biochar purchase

S3, similarly to S2, involves the installation at the facility of a 1000 kWe gasification power plant with the purpose of producing biochar. Also, in this scenario the biochar is applied to the whole Organic mix. The assumptions are the same for S2 case. A SYNCRAFT CW1800x2-1000 is selected for S3.

Since the nominal output of the gasifier is higher than S2, the biomass required $\mathrm{M_{wood\_gasif}}$ and the biochar produced $\mathrm{M_{biochar\_buy}}$ increase, as well as the new biomass $\mathrm{M_{biomass\_new}}$ to be found. The equations used to calculate the quantities involved are Eqs. F. 6 - F. 8, Eq. F. 13 and Eq. F. 14. Expenditures and costs are computed following Eqs. F. 1 - F. 5 and Eqs. F. 9 - F. 12. All data are reported in Table 34.

13.2.5 Scenario 4 – S4: 1000 kWe gasifier for biochar production

S4 involves the installation of a 1000 kWe gasifier. In this scenario, to assess whether sustainability is greater, there is no additional purchase of biochar. Only biochar produced by the installed gasifier is utilized in the composting process. Only a share of Organic mix is aided with biochar and is co-composted: the remaining share is treated via standard composting process.

Biochar production in S4 is the limiting factor. The amount of Organic mix to which the biochar, produced through the gasifier, can be applied is given by Eq. F. 15

13.2.5.1 Expenditures

S4 expenditures can be calculated through Eqs. F. 1 - F. 5 and Eq. F. 10. The cost for the biochar is null since no biochar is purchased, $\mathrm{C_{biochar_{S4}}} = 0\ €$.

13.2.5.2 Revenues

The evaluation of revenue from the sale of electricity and thermal energy is calculated through Eq. F. 11 and Eq. F. 12. As in S2 and S3, it is necessary to source the missing biomass to ensure operations.

The co-compost selling price does not change, $€_{\mathrm{co-comp\_unit}} = 1\ € \ \mathrm{tons}^{-1}$, and the related revenue is calculated as in Eq. (13-3). Revenues from the sale of standard compost are calculated with Eq. F. 17. All data are reported in Table 34.

13.2.6 Scenario 5 – FULL: 1700 kWe gasifier for biochar production

In this scenario, it is planned to install a gasifier plant capable of producing the amount of biochar sufficient for total application to the organic mix. Considering the electric capacity of the models proposed by SYNCRAFT company and the yield of biochar production, the gasifier should have a capacity of at least 1700 kWe. For simulate the FULL scenario $\mathrm{E_{e\_gasif}} = 1700\ \mathrm{kWe}$, $\mathrm{E_{t\_gasif}} = 2468\ \mathrm{kWt}$, $\varepsilon_{\mathrm{gasif}} = 0.72\ \mathrm{kg\ kWhe^{-1}}$, $\mathrm{Y_{biochar}} = 16\ \%$ are used in according to manufacturer's stated data. The equations used to calculate the quantities involved are Eqs. F. 6 - F. 8, Eq. F. 13 and Eq. F. 14.

In FULL scenario the biomass amounts for the gasifier operation and produced biochar amounts are clearly higher. The scenario assumptions remain the same as in S3 and S4.

Expenditures for the purchase of biochar is null and revenues from the sale of any surplus of biochar are neglected. Expenditures and costs are computed following Eqs. F. 1 - F. 5 and Eqs. F. 9 - F. 12.

All data are reported in Table 34.

13.3 Cash flow and payback time

To assess economic feasibility, the cash flows of the different scenarios are studied and compared. In the cash flow calculation, actual maintenance expenditures of the facility are neglected: routine and extraordinary maintenance, expenses incurred for electrical consumption and fuel cost for standard operations.

Annual income and annual expenditures are calculated as the total of the individual items of the different scenarios. The Net Present Value (NPV), on the other hand, is calculated according to Eq. F. 18 and different Weighted Average Capital Costs (WACC) were applied: 1%, 3%, 5% and 10%.

Table 34. Input data and parameters for the economic model.

Symbol	Definition	Value	Meas. Unit	Source
General parameter				
ECC	Equipment capital cost	2800	$\$\ kWe^{-1}$	[366]
$F_{building}$	Factor related to infrastructure construction costs	0.25	%	[366]
$F_{installation}$	Factor related to gasifier installation costs	0.20	%	[366]
$F_{overhead}$	Factor relating to " not predictable" costs	0.25	%	[366]
$F_{auxiliary}$	Factor related to the costs of auxiliary equipment	0.20	%	[366]
GAI	Gross Annual Income - Worker salary	30 000	$€\ y^{-1}$	[1]
$\%_{tax}$	Italian tax on energy sale	0.52	%	[1]
$\%_{social\ insurance\ contributions}$	Taxes related to the social welfare	31	%	[1]
$\%_{termination\ pay}$	Salary deduction returned at the end of the contract	13.5	%	[1]
$FC_{shredder}$	Diesel fuel consumption of the shredder	0.56	$l\ m_{biomass}^{-3}$	[367]
ρ_{wood}	Density of pruning and other wood from agriculture/public maintenance	500	$kg\ m^{-3}$	[368]
Outcome				
$€_{biochar\_unit}$	Biochar unitary cost	300	$€\ ton^{-1}$	
$€_{diesel\_unit}$	Diesel fuel	1.677	$€\ l^{-1}$	[369]
Income				
$€_{co-comp\_unit}$	Compost unitary selling price	1	$€\ ton^{-1}$	
$€_{E_e}$	Price for the electrical energy sale in Italy. Mean value of 2023 first six months	123.81	$€\ MWe\ h^{-1}$	[370]
$€_{T_e}$	Price for the thermal energy sale via district heating, in North of Italy.	0.0907	$€\ MWt\ h^{-1}$	[371][2]

[1] Data released by various government agencies: Italian National Institute of Statistics, Ministry of Labor, Emilia-Romagna Region. [2] the value is halved compared to data declared by the most important Emilia Romagna region energy provider, to remain prudent.

13.4 Carbon footprint and carbon credit

The computation of carbon credits related to the use of biochar was performed through the VERRA Standard. VERRA has designed and published a simplified methodology by which it is possible to identify the amount of carbon stored in biochar once it is buried or applied to soil as an agricultural soil conditioner. The methodology divides the calculation flow into three different stages: 1) sourcing stage - stage of purchasing and collection of waste biomass; 2) production stage - stage of biomass pretreatment and thermochemical conversion to biochar; 3) application stage - stage of application of biochar in a permanent end use, in soil or other eligible off-soil applications. The methodology considers CH_4, N_2O and CO_2 emissions from production processes, and quantifies them in terms of CO_2eq during the monitoring period. In this study, the calculation of carbon credit was performed imposing the following assumptions: a) the recommended input is utilized for prudence, whether the method suggests zero or maximum values; b) only waste biomass within a 200 km transport radius is taken into account and zero emissions attributed to degradation are considered, thanks to the fast utilization; c) emissions from field spreading operations are excluded, as they are performed by farmers; d) renewable energy is used for auxiliary equipment and gasifier start&stop, except for the wood shredding system fueled by diesel. *Appendix F.8. Carbon footprint and carbon credit revenue (VERRA standard)* reports some of the equations proposed by the VERRA methodology for calculating carbon credits.

The GHGs reduction estimation was based on data collected at the facility during a co-composted biochar testing campaign (see the work explained in GASIFICATION BIOCHAR IN ORGANIC FRACTION OF MUNICIPAL SOLID WASTE COMPOSTING PROCESS. ENHANCEMENTS OF THERMAL ENERGY AND REDUCTION OF GREENHOUSE GASES EMISSION). The results showed reductions up to 45% of CO_2eq. In this study only CH_4 is considered, as it is the only GHG continuously monitored in the facility. The CH_4 emission factor of the facility is $\mathrm{EF}_{\mathrm{CH}_4} = 2.23 \cdot 10^{-3}$ [$\mathrm{ton\ CH}_4\ \mathrm{ton\ mix}^{-1}$]. Therefore, the emissions from the composting process are calculated through Eq. F. 24

13.5 Technological result

Results reported in Table 35 confirm the technical feasibility of applying biochar to composting plants, both in total (S1, S2, S3, FULL) and partial application (S4). Biochar blending is feasible during the preparation of organic mix, simultaneously with OFMSW and the others wood fractions.

In S1, approximately 1534 tons of biochar per year must be purchased and it is mandatory to identify a reliable supply chain that guarantees the demand for biochar over the long term. In S2 the installation of a medium-sized plant is

considered, as outlined in paragraph 13.2.3. This avoids purchasing a share of the total biochar required for co-composting the 51128 tons of organic mix. To date, the biomass collected by the facility and not used in composting process (Unused virgin wood, Table 35) is not enough to reach the required 2880 tons of woody biomass for the $8000\ \mathrm{h\ y^{-1}}$ gasifier operation (Required biomass for gasifier operation, Table 35) despite the relatively low electric capacity installed. An annual purchase of 1992 tons of new biomass fuel is necessary (New biomass to be found, Table 35). Moreover, the biochar self-production does not cover the total biochar requirement of 1534 tons: approximately 1056 tons per year are still to be purchased from external sources. The costs for this yearly biochar procurement are added to the annual expenses of the gasifier. The plant construction area is small, about 175 m^2, achieved by repurposing existing warehouses or designating new locations. These facilities typically are situated in rural areas with available land for new infrastructure.

S3 sees a doubling of installed power. To ensure the gasifier operation, 4793 tons per year of new woody biomass must be purchased, more than five times the amount currently available at the facility, for a total of 5680 tons. Nevertheless, the biochar produced annually doubles to 943 tons, leaving only 591 tons to be purchased every year. The costs for this yearly biochar procurement are added to the annual expenses of the gasifier. From a management perspective, given the large amount of biomass required, it is necessary to schedule wood delivery to reduce total storage volume. For biochar, daily usage eliminates the need for large storage volumes. The plant construction area is small, about 205 m^2.

S4 aspires to use only self-produced biochar. To be able to compare S4 with another scenario and to keep the initial investment low, the installation of a 1000 kWe gasifier, as for S3, is chosen. The purchase of additional biochar is excluded. Like S3, it is necessary to provide a total of 5680 tons of woody biomass and the gasifier ensures a production of 943 tons per year of biochar. These 943 tons of biochar are applied to 31429 tons of organic mix. The remaining part is treated via standard composting process. In the FULL scenario, the gasifier electric capacity is determined to ensure that the biochar produced will meet the requirements for application to whole organic mix. The plant's annual biomass demand is 9792 tons, with 8905 tons to be newly sourced, representing a tenfold increase over the current facility's available wood. Consequently, in the FULL scenario the supply and storage issues are key factors during the design phase. However, the biochar production of 1567 tons per year adequately meets the application demand of 3% w/w for co-composting the whole of the Organic mix. The plant construction area is estimated to be at a maximum of 400 m^2.

Two technological challenges have been identified: the resource of new biomass and the installation and operation of a gasifier in a waste treatment facility. About the first issue, thanks to the increasing focus on waste recovery, maintenance of public green areas and control of riverbanks biomass, more and

more residual biomasses are suitable. To date, composting facilities have not expressed interest in receiving waste woody biomass given the internal low utilization. However, logistically, and contractually, the collection of biomasses will be like the OFMSW management. This approach also offers a solution to the challenges commonly associated with biomass power plants: new equipment, wood availability, road congestion and emissions, as reported by Duc Bui et al. (2023) [372]. The integration of gasification plants into pre-existing biomass collection facilities avoids the introduction of additional complexities.

Also, the installation of the gasifier is not an obstacle. A biogas production system is already installed at the facility object of this study. In fact, the distance from the central areas of near cities (where these facilities are often built) facilitates the authorization process, the feasibility of building new infrastructure or renovation old hangars and the ease of handling large quantities of materials (biochar, biomass, OFMSW, ...) make these sites suitable for the construction of energy production plants. In addition, new job opportunities are generated.

In Italian regulations, biomass cogeneration plants up to 1000 kWe can be authorized through a *Simplified Permit Procedure* (PAS), which is a more streamlined process than the complex procedure required for higher-electric capacity power plants [370]. The authorization aspect, therefore, should also be considered during decisions phase, regarding the evaluation of the S2, S3, S4 or, conversely, the FULL scenario.

Since from a technical point of view the gasifier installation is feasible, to evaluate the best scenario an economic analysis is realized.

Table 35. OFMSW, biomass and biochar results. Gasifier energy production.

	List	***CS***	***S1***	***S2***	***S3***	***S4***	***FULL***	***Meas. Unit***
COMPOST PROCESS	**OFMSW**	25564	25564	25564	25564	25564	25564	tons y^{-1}
	Bulk wood	10226	10226	10226	10226	10226	10226	tons y^{-1}
	Virgin wood collected	11113	11113	11113	11113	11113	11113	tons y^{-1}
	Unused virgin wood	887	887	887	887	887	887	tons y^{-1}
COMPOST RESULTS	**Organic mix before composting**	51128	51128	51128	51128	51128	51128	tons y^{-1}
	Required biochar	-	1534	1534	1534	943	1534	tons y^{-1}
	Co-composted final product (with biochar)	-	21438	21438	21438	13200	21438	tons y^{-1}

	Standard final product (without biochar)	19904	-	-	-	7647	-	tons y^{-1}
ENERGY PRODUCTION	**Nominal gasifier electric capacity**	-	-	500	1000	1000	1700	kWe
	Electrical energy produced - $E_{e\_produced}$	-	-	4000	8000	8000	13600	MWhe y^{-1}
	Thermal energy produced - $E_{t\_produced}$		-	5920	11232	8000	19744	MWht y^{-1}
BIOMASS AND BIOCHAR	**Required biomass for gasifier operation**	-	-	2880	5680	5680	9792	tons y^{-1}
	New biomass to be found (no purchase)	-	-	1993	4793	4793	8905	tons y^{-1}
	Produced biochar	-	-	478	943	943	1567	tons y^{-1}
	Biochar to purchase	-	1534	1056	591	0	-	tons y^{-1}

13.6 Economic result

13.6.1 Cost for gasifier installation

Table 36 shows the economic results of the model used for estimates the gasifier costs. The plant electric capacity changes for S2, S3, S4 and FULL. The model includes the estimation of unexpected costs, $C_{contingency}$, as a share of maintenance costs $C_{maintenance}$, to provide more robustness to the cost estimation. However, this precautionary approach may be disadvantageous if the model is applied to large power plants. In fact, typically as the installed capacity increases, maintenance costs per kWh should decrease [373]. The high annual maintenance cost for all scenarios, $C_{operating}$, highlighted the need to maximize the plant's utilization for all the operating hours specified by the plant manufacturer.

The cost of the trained employee, on the other hand, C_{labor}, affects the annual cost by a small share, about 15%. This suggests that a hypothetical increase in man-hours would have little impact on the overall cost estimation of this study.

Table 36. Economic results of the gasifier installation.

	Cost list	S2	S3	S4	FULL	Meas. Unit
CAPITAL EXPENDITURE	**Cost of the gasifier equipment -** $C_{equipment}$	1 005 964	2 011 928	2 011 928	3 420 277	€ *
	Cost of the gasifier installation - $C_{construction}$	469 840	939 680	939 680	1 597 457	€ *
ANNUAL OPERATING COST	**Total cost of the gasifier operation -** $C_{operating}$	237 464	474 928	474 928	807 378	€ y^{-1}
	Cost of maintenance - $C_{maintenance}$	56 948	113 895	113 895	193 622	€ y^{-1}
	Cost for general voices - $C_{general}$	90 258	180 516	180 516	306 878	€ y^{-1}
	Unexpected costs - $C_{contingency}$	90 258	180 516	180 516	306 878	€ y^{-1}
	Cost of the employee - C_{labor}	43 350	43 350	43 350	43 350	€ y^{-1}

* Initial cost. $C_{operating} = C_{maintenance} + C_{general} + C_{contingency}$

13.6.2 Cash flows and payback time

Table 37 shows all the expenditures, revenues and cash flow of the CS and different scenarios. In S1, purchasing the total amount of biochar required is not economically viable. Despite the sale of carbon credits on the European EU ETS market, the purchase of the biochar is not affordable and leads to an annual loss of about € 110 800. Therefore, it can be concluded that S1 is not feasible.

With the installation of the gasifier, instead, the application of biochar to the composting process becomes profitable. The cash flow is positive and increases with the increase in the electric capacity of the plant, as shown in the last row

of Table 37. Contextually, the initial investment increases: from about 2 147 738 € of S2, with an electric capacity of 500 kWe, to about 7 302 308 €, with an installed capacity of 1700 kWe, of FULL scenario. In S2 the expense of purchasing biochar (316 724 €) must be counted since self-production is not sufficient, which is the case in the FULL scenario.

The initial investment for S3 and S4 is the same, equal to 4 295 475 €. The most important difference is the purchase of biochar for application to the Organic mix: in S3 it amounts to 177 284 € annually, while in S4 is null. The different amount of biochar aided to the organic mix, 1534 tons per year for S3 and 943 tons per year for S4 (Table 35), results in different amounts of carbon stored and consequently different numbers of carbon credits: the revenue from Carbon credits in S3 is 326 392 € and in S4 are 200 039 €. Also, for S2 and S3 the revenues from carbon credit are considered and reported in Table 37.

From the cash flow in Table 37it is evident that FULL scenario offers a clear economic advantage over S2, with a gain twice that of S3 and S4, but with a significant initial investment. Therefore, the FULL scenario is feasible but requires a careful evaluation.

Between scenarios S3 and S4, which differ only in the absence of biochar purchase in the latter, S4 proves to be the more advantageous option. However, this advantage occurs at the expense of reduced environmental benefits, particularly in terms of GHGs emissions during the composting process and the storage of carbon in the final compost. Paragraph 13.7 will discuss environmental benefits.

Table 37. Detailed economic results of the CS and of the different scenarios considering the update of prices to Q2-2023: cost, revenues, and cash flow.

	List	CS	S1	S2	S3	S4	FULL	M. U.
COST	Initial cost of the gasifier - C_{tot}	-	-	2 147 738	4 295 475	4 295 475	7 302 308	€
	Cost of biochar purchasing - $C_{biochar}$	-	460 148	316 724	177 284	0	0	€ y^{-1}
	Cost for annual operation of the gasifier * - $C_{operating} + C_{labor}$	-	-	280 814	518 278	518 278	850 728	€ y^{-1}
	Cost of diesel fuel - C_{diesel}	-	-	5 411	10 671	10 671	18 397	€ y^{-1}
	Additional handling cost (for biomass)	-	-	812	1 601	1 601	2 759	€ y^{-1}

REVENUE	Revenue from selling standard compost - $R_{compost}$	19 904	-	-	-	7 647	-	€ y^{-1}
	Revenue from selling biochar-aided compost - $R_{co-compost}$	-	21 438	21 438	21 438	13 200	21 438	€ y^{-1}
	Revenue from selling the electrical energy - $R_{electrical}$	-	-	237 721	475 441	475 441	808 250	€ y^{-1}
	Revenue from selling the thermal energy - $R_{thermal}$	-	-	257 653	488 845	488 845	859 308	€ y^{-1}
	Revenue from selling Carbon Credits - $R_{Carbon\ credit}$	-	327 954	327 162	326 392	200 039	332 294	€ y^{-1}
TOTAL	Annual outflows	0	460 148	603 761	707 835	530 550	871 884	€ y^{-1}
	Annual inflows	19 904	349 392	843 974	1 312 116	1 185 172	2 021 291	€ y^{-1}
	Cash flow	19 904	-110 757	240 213	604 282	654 622	1 149 407	€ y^{-1}

* Includes the cost of running the annual gasifier and the cost of the trained employee.

Figure 13-4 shows the payback times for S2, S3, S4 and FULL scenarios. Different values of WACC are imposed and a period of 25 years, considered the lifetime of the gasifier plant without extraordinary maintenance, is used. The results show that in the best case for S2 there is a payback time of nine years, while with WACC at 10% the payback time increases to 25 years. S2 should be excluded due to the high payback time if the capital cost from investors is high. For S3, the payback time starts from eight years with WACC at 1% to fourteen years in the case of WACC 10%. S4 sees a payback time from seven years (WACC = 1%) up to twelve years (WACC = 10%), while FULL scenario has an investment payback of seven years and eleven years (respectively, WACC = 1% and WACC = 10%), despite the high initial investment and under the assumption of thermal energy exploitation and electric energy dispatch.

The payback period of S3, S4 and FULL scenarios underscores that the initial capital investment for the gasifier system is repaid through the revenue from energy and Carbon credits sales: all these scenarios offer substantial benefits in terms of economic incomes.

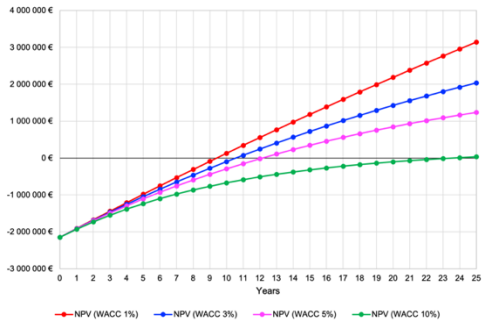
4 000 000 €
3 000 000 €
2 000 000 €
1 000 000 €
0 €
-1 000 000 €
-2 000 000 €
-3 000 000 €
0 1 2 3 4 5 6 7 8 9 10 11 12 13 14 15 16 17 18 19 20 21 22 23 24 25
Years
NPV (WACC 1%)
NPV (WACC 3%)
NPV (WACC 5%)
NPV (WACC 10%)

a)

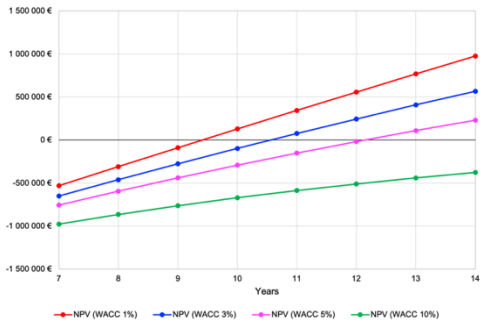
1 500 000 €
1 000 000 €
500 000 €
0 €
-500 000 €
-1 000 000 €
-1 500 000 €
7 8 9 10 11 12 13 14
Years
NPV (WACC 1%)
NPV (WACC 3%)
NPV (WACC 5%)
NPV (WACC 10%)

b)

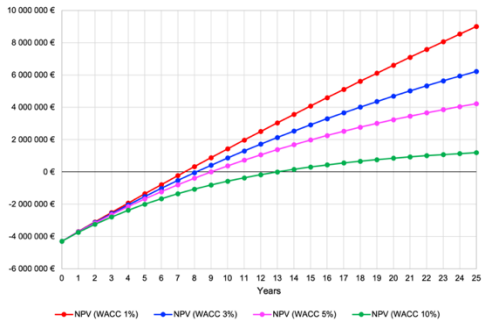
10 000 000 €
8 000 000 €
6 000 000 €
4 000 000 €
2 000 000 €
0 €
-2 000 000 €
-4 000 000 €
-6 000 000 €
0 1 2 3 4 5 6 7 8 9 10 11 12 13 14 15 16 17 18 19 20 21 22 23 24 25
Years
NPV (WACC 1%)
NPV (WACC 3%)
NPV (WACC 5%)
NPV (WACC 10%)

c)

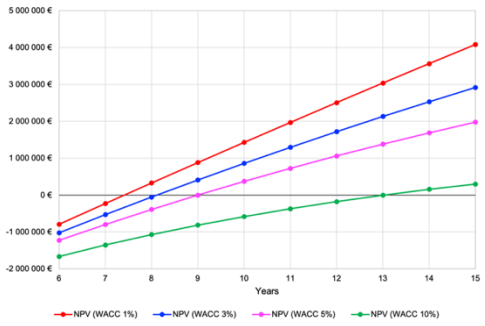
5 000 000 €
4 000 000 €
3 000 000 €
2 000 000 €
1 000 000 €
0 €
-1 000 000 €
-2 000 000 €
6 7 8 9 10 11 12 13 14 15
Years
NPV (WACC 1%)
NPV (WACC 3%)
NPV (WACC 5%)
NPV (WACC 10%)

d)

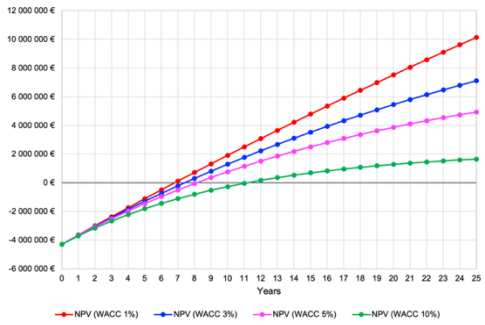
12 000 000 €
10 000 000 €
8 000 000 €
6 000 000 €
4 000 000 €
2 000 000 €
0 €
-2 000 000 €
-4 000 000 €
-6 000 000 €
0 1 2 3 4 5 6 7 8 9 10 11 12 13 14 15 16 17 18 19 20 21 22 23 24 25
Years
NPV (WACC 1%)
NPV (WACC 3%)
NPV (WACC 5%)
NPV (WACC 10%)

e)

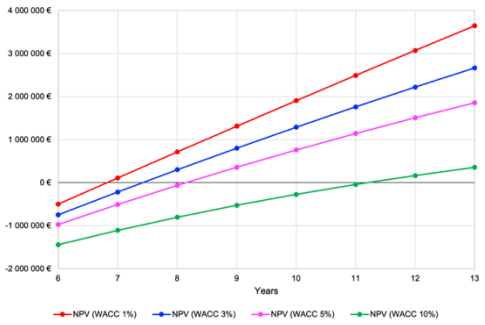
4 000 000 €
3 000 000 €
2 000 000 €
1 000 000 €
0 €
-1 000 000 €
-2 000 000 €
6 7 8 9 10 11 12 13
Years
NPV (WACC 1%)
NPV (WACC 3%)
NPV (WACC 5%)
NPV (WACC 10%)

f)

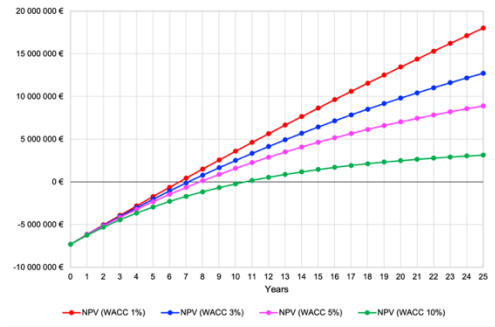

g)

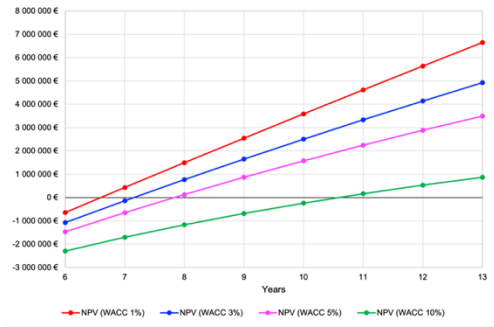

h)

Figure 13-4. Payback time of a) S2, c) S3, e) S4 and g) FULL scenario; with a focus on the break-even point range of years of the same Scenarios, respectively b), d), f) and h).

13.7 Environmental results

Figure 13-5.a illustrates the CO_2eq stored in biochar-aided compost (convertible in Carbon credit) according to VERRA methodology. The conspicuous disparity observed between S4 and the other scenarios is due to the reduced quantity of biochar incorporated at the beginning of the composting process. The Carbon Credit allocations for S1, S2, S3, FULL scenarios are almost equal; 3604, 3595, 3587 and 3652 $\mathrm{tonn\,CO2eq\,y^{-1}}$. The differences are attributed to different CO_2eq emissions from the diesel fuel utilization for biomass pretreatment. Despite the lower carbon storage, 2198 $\mathrm{tonn\,CO2eq\,y^{-1}}$, S4 enables the facility to achieve self-sufficiency in biochar production with relatively low electric capacity gasifier plant. The GHGs reduction related to the addition of biochar in the composting process is not included in Carbon Credits computation.

This study also estimated the reduction of CH_4 emissions. Only CH_4 is considered since the facility exclusively monitors and measures CH_4. Figure 13-5.b shows the results: the significant reduction compared to CS is evident in the case of total application of biochar to the Organic mix (S1, S2, S3 and FULL) while with a partial application of biochar (S4) the environmental benefit derived from GHGs reduction is very small.

In summary, while S4 exhibits advantages in economic and biochar independence terms, it falls short in its potential for emission reduction and carbon storage from an environmental perspective, thus abandoning an important added value of co-compost.

Comparing Figure 13 5.a and Figure 13 5.b reveals that in scenarios S1, S2, S3 and FULL the co-composting process is carbon-negative, with assumption of considering solely methane emission. Whereas S4 maintains a carbon-positive status.

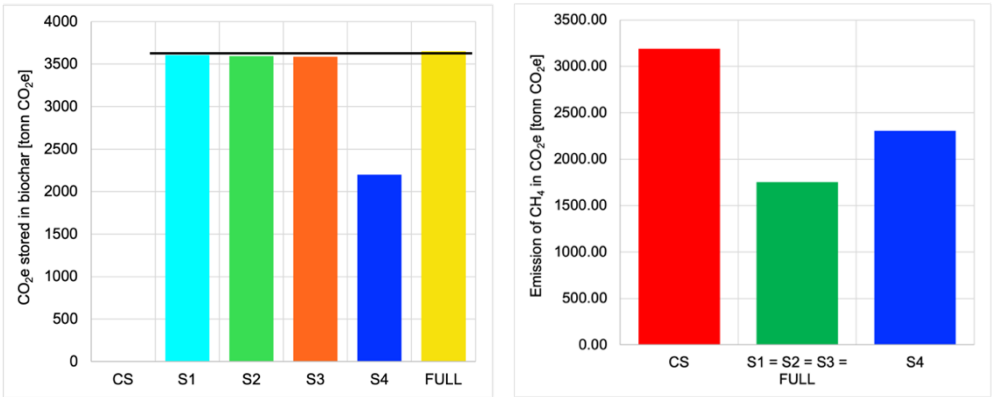

a) *b)*

Figure 13-5. a) Carbon credits calculated and estimated using the VERRA standard and b) emission of CH4 in the four scenarios.

13.8 Higher biochar application rate

To extend the study and assess the feasibility of a higher application rate of biochar into composting process, some calculations were performed at 10% w/w a frequently studied fraction [283]. In this study, 3% w/w biochar was utilized as one of the lowest fractions identified in the literature that yielded important advantages to the composting process and maintained a trade-off between benefits and economic-technical aspects [358]. An emission measurements campaign was conducted on the considered facility, with biochar at 3% w/w, providing the experimental data utilized in this work. Contrary, for biochar at 10% w/w, the reduction factors for CH_4 applied in this paragraph are from literature: values range from an abatement of 10.8% [358], to 55.5% [332] and up to 81.5 percent [161]. The average value used here is 49.3%. Scenarios S1, S2, S3, and S4 are based on the assumptions seen in previous paragraph.

In FULL scenario a 5.5 MW gasifier power plant was installed to totally cover the production of the required biochar.

For the economic results, S1 is not considered since it is already unviable in the 3% application. At 10% biochar, also S2 is economically unfeasible as the biochar produced through the gasifier is significantly lower than the biochar required and consequently the fraction to be purchased is excessively high. In S3, the investment only repays for WACC=1% and 3%, with payback time of 16 and 19 years respectively. In the case of a higher WACC (5% and 10%), S3 will not be repaid. S4 exhibits low payback times of 7, 8, 9, and 11 years for WACC values of 1%, 3%, 5%, and 10%, respectively. However, it comes with reduced environmental benefits. Specifically, carbon storage is approximately six times lower than other scenarios, that generates about 12000 Carbon Credits. Additionally, emissions reduction is only 9%, compared to S2, S3, S4, and FULL

scenario, where a 49% reduction is observed, Figure 13-6. Finally, FULL is the most promising scenario from the perspective of balancing environmental benefits and economic payback, despite a high investment of 23M€. Payback times are 14, 18 and 23 years (WACC of 1%, 3% and 5%) while in the case of WACC=10% there is no investment repayment. However, the 10% application rate shows little more benefits than 3%: the emission reduction goes from 45% to only 49% and the payback time increases. The initial step in achieving environmental and economic sustainability in co-composting involves employing a low biochar application rate. This rate could potentially be increased in the future, leveraging the expected growth of the biochar market and Carbon Credit trading.

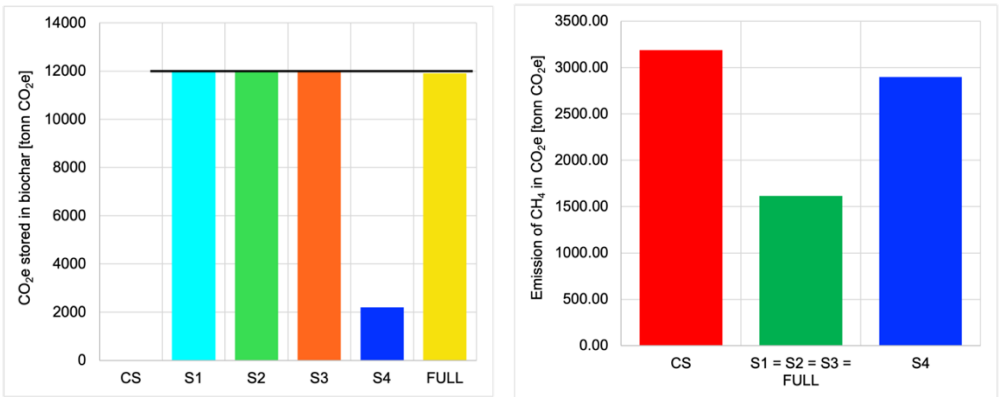

Figure 13-6. Environmental results of 10% w/w biochar application: a) carbon credits generated by the integration of biochar in the co-composting process; b) CH4 emission reduction compared to CS.

13.9 Final consideration on results

The co-composted biochar novel approach represents a significant contribution in addressing challenges related to waste treatment, high-quality compost production, and climate change mitigation. Biochar integration into composting processes is practical, feasible and economically viable and combines industrial sustainability, processes efficiency and circular economy goals.

From a technological point of view, mixing biochar at the OFMSW mix is feasible as well as the installation of gasification systems in the composting facility. However, this work has identified a few management-related issues. In S2, S3, S4, and FULL scenario it is imperative to ensure additional biomass sourcing and integrate expertise for the gasification plant management. For S1, S2, S3, and S4, there is a need to seek a long-term biochar supply.

S1 is economically unviable. In S2 the purchase of a high amount of biochar leads the payback time, in the worst case, to 25 years. S2 is feasible if the initial investment cost is sustainable without external financing or with low capital cost. S4 compared to the twin-scenario S3, presents a shorter payback time, anyway both recoup the investment in maximum 14 years (WACC = 10%). From environmental point of view, in S4 less aided biochar means higher GHGs emission during composting. FULL scenario is the most cost-effective, but it involves a high initial investment. When applying biochar at 10% w/w, the advantages diminish, resulting in longer payback periods (in some cases the investment does not return) and in a lower emissions reduction. For all scenarios, the mains incomes are from the sale of electrical energy, thermal energy, and Carbon credits. The estimated plant lifespan is 25 years.

Finally, the production of renewable energy through gasification systems achieves carbon storage targets and allows access to the Carbon Credit trading system. The addition of biochar to the composting process ensures soil application and biochar burial since compost is used as an agricultural soil conditioner. S1 leads to substantial carbon storage and reductions in GHGs emissions but imposes the purchase of biochar. Equivalent advantages are reached in S2, S3, and FULL scenario with additional benefits of partial or complete biochar self-production and new incomes from energy sales. S4 is the least promising scenario in terms of Carbon credits and GHGs reduction.

The realization of these assumed scenarios undeniably represents a challenging endeavor that demands commitment and interest. Enhancing the recovery of waste biomass, harnessing it for energy purposes, adopting district heating, exploring biochar's second life, and quantifying associated carbon credits all remain areas where we continue to learn and strive to seamlessly integrate into our daily lives. These efforts are integral to climate change adaptation and resilience, and we must persist in the face of initial obstacles.

TECHNICAL FRAMEWORK OF APPLICATION .3

Biochar application in agro-industrial facilities.

14 APPLYING BIOCHAR TO SWINE FARM FOR GREENHOUSE GASES AND AMMONIA EMISSIONS REDUCTION.

This study introduces a novel approach utilizing biochar to mitigate emissions from pig farm slurry. It explores diverse application methods to optimize biochar's interaction with swine slurry. By investigating biochar's efficacy in emission reduction, the study aims to promote sustainable agricultural practices and environmental management. Moreover, it seeks to enhance soil fertility through biochar incorporation, mitigating environmental impacts linked to intensive farming.

The findings offer promise for addressing swine management challenges in livestock farming while improving soil health and reducing the GHGs emissions and highlight the importance of innovative solutions in developing sustainable agricultural alternatives.

Keywords: Swine slurry; Emission; Gasification biochar; GHGs abatement; Ammonia abatement.

A form of this research was presented to the 31st European Biomass Conference and Exposition

14.1 Biochar for emission reduction in the farming context

European environmental policies, in recent years, have given more and more space to sustainable development, environmental protection and recovery of materials and waste to increasingly promote circular economy processes [340,374,375]. In the field of agriculture, the increasingly stringent regulations on the treatment of animal waste, application of fertilizers or manures in field and farm emissions opened the challenge about the design of new technological solutions to comply with the regulation limits.

The livestock sector is responsible for 22% of GHGs emissions, near to the 24% of the emissions from the industrial sector [24]. For this reason, since 2018, the European regulation known as the "Effort sharing Regulation 2021-2030" has imposed new limits on greenhouse gas emissions also in the agricultural and livestock sectors [376]. In Italy the agriculture is responsible for 7% of greenhouse gas emissions and of these the 79% is due to livestock activity. Agriculture and livestock are respectively responsible for 94% and for 84% of ammonia emissions [377]. Considering the close link between agriculture and ammonia emissions, the National Emission Ceilings (NEC) directive has set the European targets for the reduction of NH_3 in 2020 by –5% and in 2030 by –16% compared to the emissions of 2005 [378].

This work fits into the European and national context in a circular economy perspective and aims to study innovative ways to reduce the environmental impact of pigs' farms. The innovation in particular lies in the use of biochar from gasification to reduce greenhouse gases (GHGs) and ammonia (NH_3) emissions released by slurry storage. In pig farms, "lagoons" are still very common as a type of storage. There are coverage techniques for containing emissions, but they are often technically unfeasible and economically unsustainable. In these cases, new solutions for reducing emissions (especially NH_3) could provide important support to the agricultural world in complying with regulation limits.

Biochar, to date, is usable as soil improver in agriculture following the European regulation. For these reasons, in some works in scientific literature, biochar is already applied or added to biological processes to reduce emissions.

In this research, three different methods of applying biochar to pig slurry storages were investigated to identify the best treatment for GHGs and NH_3 reduction [299,379]. The tested methods, *MatChar*, *FiltChar* and *AeroChar*, will be analyzed in following paragraph. Research also investigates the possibility to use the exhausted biochar (the biochar used to reduce emissions from the slurry storage) as nitrogen-rich soil amendment to improve soil productivity. Based on the concept of circular economy, the treated mix slurry-biochar or the exhausted biochar can be re-used, reducing the amount of chemical fertilizer. In this context, if the farm produces enough residual biomass from cultivations, the production of biochar can take place internally to the farm (through small-sized

gasifiers), otherwise the biomass can be conveyed to a dedicated power plant and biochar can be purchased at a reduced price.

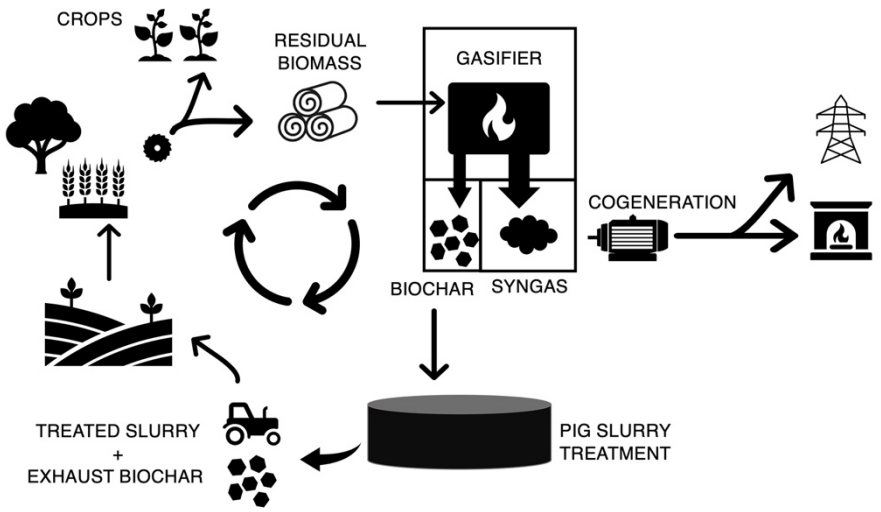

Figure 14-1. Circular economy concept of this work.

A preliminary economic analysis was carried out to evaluate the economic feasibility of the most promising treatment (MatChar, AeroChar or FiltChar) selected on the emissions abatement potential. Finally, biochar is considered a highly recalcitrant material. The European Biochar Certificate (EBC) reports that 74% of the total carbon originally contained in biochar remains in the soil after one hundred years [359]. The IPCC in the report "Climate Change 2022: Mitigation of Climate Change" claims that biochar could have the potential of removing 2.6 billion tons of CO_2 equivalent (CO_2eq) from the atmosphere every year [7]. Biochar is considered a Carbon Sink: 100 kg of biochar contain about 150 kg of CO_2 equivalent [190]. For these reasons, biochar, after a Life Cycle Assessment procedure, would allow the farmer to access carbon credits and derive economic benefits from them.

14.2 Experimental system and biochar treatments of swine slurry

To study the emissions from the storage of pig farms and to study the possible reduction of GHGs and NH_3 gases thanks to the application of biochar, a long experimental campaign lasting nine months was designed. The experimental system, consisting of twelve tanks of 1 m^3 each, was hosted by a pig livestock in Emilia Romagna - Italy. The twelve tanks were used as temporary storage in which the pig slurry to be differently treated was inserted. The different treatments have been designed based on different physical, chemical, or biological principles of interaction between biochar and pig slurry. Therefore,

three types of treatments were created: MatChar, FiltChar and AeroChar. For each type, three prototypes were built and mounted on three different slurry storage pilot tanks. In this way, three replicates were obtained for each treatment, for a total of nine thesis tanks. The remaining three tanks were used as a control, to be able to make comparisons with the gases emitted. Table 38 describes each treatment.

Table 38. Description of the treatments tested.

Type of treatment	Description	Emission reduction mechanism
MatChar	**Floating mats to cover the storage.** Thanks to a physical containment action, the mats prevent the diffusion of gases and odors from the slurry liquid matrix to the air. The mats have a surface area of 50x50 cm^2 and a thickness of 5 cm. A 2 cm thick extruded polystyrene frame allows floating while a plastic net with 3 mm x 3 mm mesh contains the biochar. The floating mats can be easily placed on the surface of the slurry and follow the rise or fall of the storage level. It can be removed when needed.	A cover (for example a thick plastic sheet) reduces both the emissive surface area and increases the resistance of the surface to gas volatilization [380]. MatChar treatment was used to investigate whether biochar, thanks to absorption and adsorption mechanisms, further reduces emissions compared to the coverage effect alone [381].
FiltChar	**Adsorbent hermetic filter crossed by the slurry.** Thanks to a pump, the slurry is taken from the tanks and is pushed through a hermetic filter that is composed of an external case and an internal steel cylinder, with walls made of metal grid, inside which biochar is placed. The slurry is forced to flow through the biochar which acts as adsorbent material of the NH_3 and other elements, and it is subsequently reinserted into the tank.	Filtering with biochar, used as activated carbon, allows the reduction of emissions by different mechanisms: electrostatic attraction, ion exchange, cation exchange, adsorption, absorption, formation of active biofilms on the surface. The governing parameters (residence time in the filter, contact surface, ...) can significantly influence the system [381,382].

	By reducing the ammonia content in the treated slurry, a reduction of NH_3, N_2O and odor emissions from final storage is assumed.	
AeroChar	***Biochar is used as a substrate for the growth of nitrifying-denitrifying bacteria.*** The system includes an open-top reactor and a pumping system. The reactor contains biochar inoculated with nitrifying and denitrifying bacteria. The principle of biological nitrogen removal is exploited: aerobic (nitrifying) stages are alternated with anoxic (denitrifying) stages by means of timed filling-emptying phases of the reactor, in a similar way of biological treatment of wastewater. Since the biochar is characterized by a strongly basic pH value, before inoculation it was previously washed with pig manure so that the optimal conditions for bacterial proliferation were immediately created.	Abatement of emissions in nitrifying-denitrifying systems occurs via multiple pathways. Biochar is already tested as a good substrate by some studies. Biochar improves the environment for the proliferation of bacteria and facilitates their interaction with the precursors of GHGs and NH_3, thanks to the high cation exchange and adsorption capacity of the biochar (e.g.: ammonium ions NH_4+-N and nitrate NO_3-) [383–385].

Figure 14-2 shows the render and the final realization of the experimental systems. FiltChar and AeroChar prototypes were managed by an electrical panel which regulated the loading and emptying of the filters and reactors according to the desired reaction times.

The biochar used in this work is a commercial biochar called BioDea White Onyx purchased from the Italian company Bio-Esperia Srl and produced through an updraft type gasifier with a power of 170 kW. The characteristics declared by the manufacturer are contained in Table 39.

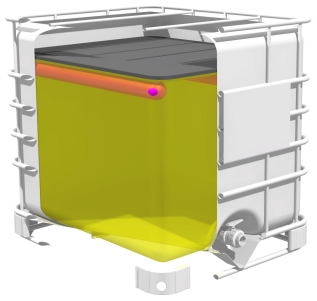

a) complete system on the left, mats in the tank on the right. The floating external frame and the plastic net that allows biochar-slurry contact are clearly recognizable

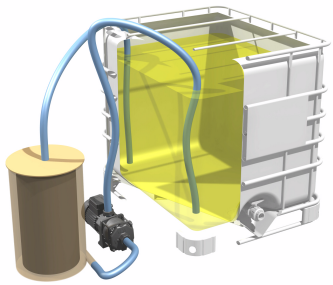

b) complete system on the left, detail of the filter filled with biochar on the right. The cut on the side has been created to facilitate the passage of the slurry into the filter.

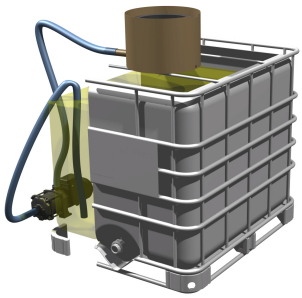

c) complete system on the left, reactor full of slurry on the right. The slots for the overflow discharge can be seen near the upper limit.

d) General view of the experimental system composed of tanks and prototypes for a total of three repeated for the three treatments, in addition to the three control tanks.

Figure 14-2. Rendering and details of the experimental systems. a) MatChar; b) FiltChar; c) AeroChar; d) General view.

Table 39. Characteristics of the BioDea White Onyx biochar declared by the producer.

Parameter	Value
Total nitrogen (N)	< 0.5%
Carbon from carbonates (c)	< 0.1%
Maximum water retention	115%
Total biological Carbon (dry basis)	72%
Salinity	110 mS m^{-1}
pH	9.85
Ash content	4.6 % d.w.
Molar H/C ratio	0.2
Fraction of grain size < 0.5 mm	1 %
Fraction of grain size < 2.0 mm	1 %
Fraction of grain size < 5.0 mm	60 %

14.3 Emissions measurement campaign and methodology

Three experimental campaigns lasting 60 days each representing the different seasonal conditions were carried out: winter campaign, spring campaign and summer campaign. The emissions were monitored every ten days to identify the temporal evolution. To simulate the process that takes place in real farms, a "dynamic storage" was adopted: 7 liters of fresh manure were added every day to simulate the filling of real storages (in doses and timing). The real storages, in fact, are filled daily as they are essential for the correct pig slurry management in the stables.

The monitoring of emissions from tanks followed the "Static Chamber" experimental measurement methodology proposed by Pedersen et al. (2001) [320,322]. This method used a static chamber positioned on the tanks to create a sealed headspace above the surface of the slurry, where the gases concentrated. The gases concentration in the headspace increases linearly until it reaches a plateau. When this condition occurs, the headspace is in saturation condition, and the measurement is stopped. The angular coefficient of the regression equation (calculated during the linear increase) is the emission potential of the slurry. The gas concentration in the chamber was measured with the IR photoacoustic gas analyzer INNOVA Lumasense 1412 [319]. The emissions of each gas are calculated through Eq. (14-1).

$$E_{Area} = \frac{\Delta C}{\Delta t} * \frac{V_{static\ chamber}}{A_{emissive\ area\ of\ tank}} \qquad \left[mg_{gas} m^{-2} h^{-1}\right] \qquad (14\text{-}1)$$

Through Eq. 2. the data was calculated on the volume of slurry contained in the tank.

$$E_{Volume} = E * \frac{A_{emissive\ area\ of\ tank}}{V_{total\ slurry\ in\ the\ tank}} \qquad [mg_{gas} m^{-3} h^{-1}] \qquad (14\text{-}2)$$

The cumulative emissions of each tank, over 60 days, are calculated through the discrete integral in Eq. (14-3):

$$E_{cum} = \sum_{i}^{6} \frac{E_i + E_{i+1}}{2} * (t_{i+1} - t_i) \qquad [mg_{gas}\, m^{-3}] \qquad (14\text{-}3)$$

The gases monitored during the experimental campaign were a) nitrous oxide N_2O, b) methane CH_4 and c) ammonia NH_3. In addition to these, olfactometric analyzes were performed by "Dynamic Olfactometric test" carried out with the Olfasense GmBh T08 olfactometer in according to EN 13725:22 measuring the odor concentration in Odor Unit per cubic meter of air [ouE/m^3] [386].

The total cumulative emissions, useful for evaluating which treatment has reduced emissions the most, were calculated as the sum of the cumulative emissions of the winter and summer experimental campaigns and twice the cumulative emissions of the spring campaign, Eq. (14-4). The autumn campaign, in fact, was considered equal to the spring campaign, assuming similarity of ambient temperature and atmospheric conditions.

$$E_{tot} = E_{cum_{winter}} + E_{cum_{summer}} + 2E_{cum_{spring}} \qquad [mg_{gas} m^{-3}] \qquad (14\text{-}4)$$

14.4 Other analysis

14.4.1 Biochar analysis

The biochar was analyzed both before the treatments and at the end of the experimental campaign, keeping the samples from the different treatments. The parameters analyzed and the respective methods used were the following: Total solid (TS), pH and ammonium nitrogen (NH+4-N) were determined with Environment Department Piedmont Region and ISPRA documents [312,377]; volatile solid (VS) following ISPRA, 1985 regulation [311]; total Kjeldahl nitrogen (TKN) and total organic carbon (TOC) through the MIIPAF regulation [214]; total phosphorus (Ptot) using the standard EPA 3051 A and SM 4500-P-C [313]; Copper (Cu) and Zinc (Zn) using the standard EPA 3051 A and SM 3111-B [313].

14.4.2 Preliminary economic analysis

The economic analysis concerns AeroChar, as the most promising treatment from the enriched nutrient content (NP) point of view. Therefore, only data relating to this treatment are here shown. The initial cost of the system has not been considered. The analysis intends to study the economic sustainability of the treatment investigating the possible replacement of chemical nitrogenous fertilizers with the nitrogen-enriched biochar from the AeroChar system and the relative economic aspect. The regulatory context of the Emilia Romagna region and the market of Italian agronomic fertilizers and biochar were considered.

14.5 Experimental results

14.5.1 GHGs and ammonia emission results

The results demonstrated a great variability of the emissions from the tanks during the different seasonal phases. This behavior was expected. During the design of the experiment, in fact, three measurement campaigns were planned in different periods of the year to compensate the variability. The autumn season was considered similar to the spring one and therefore the campaign of measures in autumn was not foreseen. CH_4 and N_2O emissions showed the greatest variability. Figure 14-3 shows the CH_4 cumulative emissions for each seasonal measurement campaign. The highest emission occurred during the warmer months than in the months with colder climates, at equal temporal evolution and equal slurry volume.

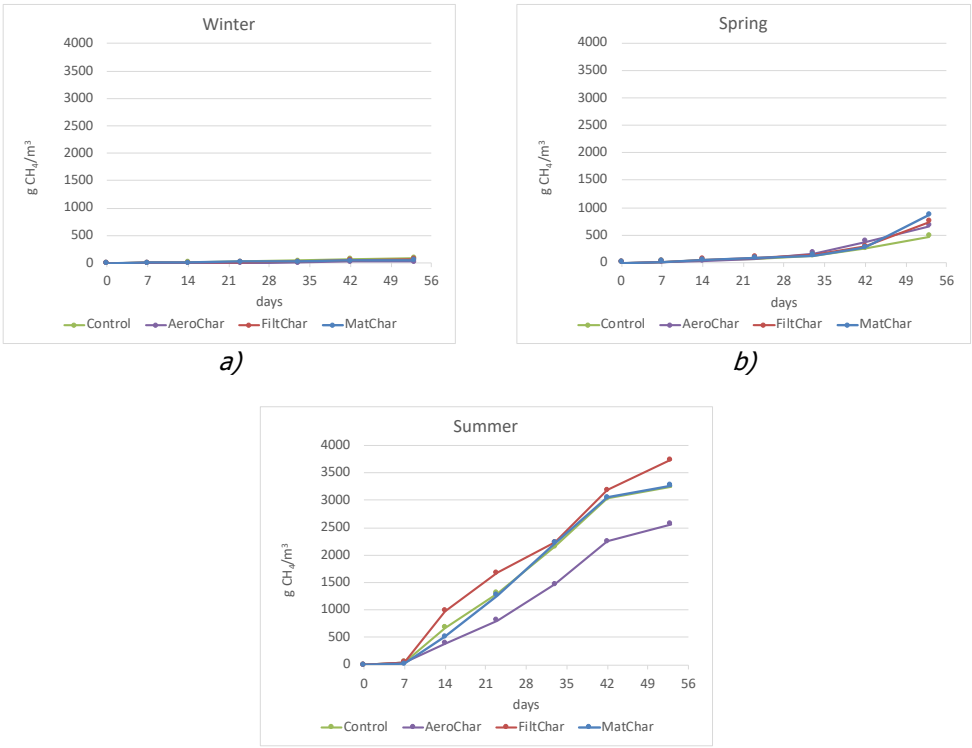

Figure 14-3. Temporal evolution of the cumulative emissions E_{cum} of CH_4 of the three campaigns: a) winter; b) spring/autumn; c) summer. The vertical scale is the same for all three graphs to compare the results.

Also, the trend of N_2O emissions follows the expectations. There is an increase in emissions during the summer months, but the quantity emitted by the tanks is three orders of magnitude lower than CH_4. Figure 14-4 shows the data relating to the experimental campaigns. Spring emissions reach a maximum value that is about half of summer emissions, while winter emissions remain below $1\ g_{N_2O}\ m^{-3}$.

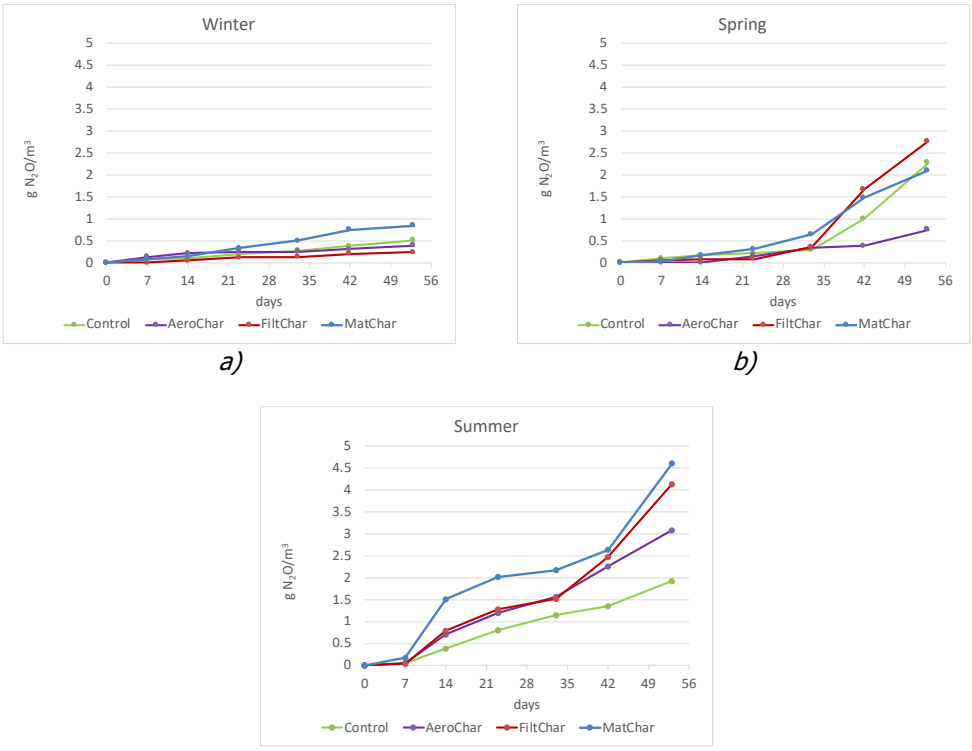

Figure 14-4. Temporal evolution of the cumulative emissions E_{cum} of N_2O of the three campaigns: a) winter; b) spring/autumn; c) summer. The vertical scale is the same for all three graphs to compare the results.

Comparing graphs in Figure 14-3 and Figure 14-4, it can be seen clearly the lower quantity of N_2O emitted compared to CH_4. The measurement of N_2O is however essential to evaluate the environmental impact since N_2O, in the Global Warming Potential (GWP) calculation, has a conversion coefficient into CO_2eq of 265 [7]. Figure 14-5 shows the temporal evolution of NH_3 emissions.

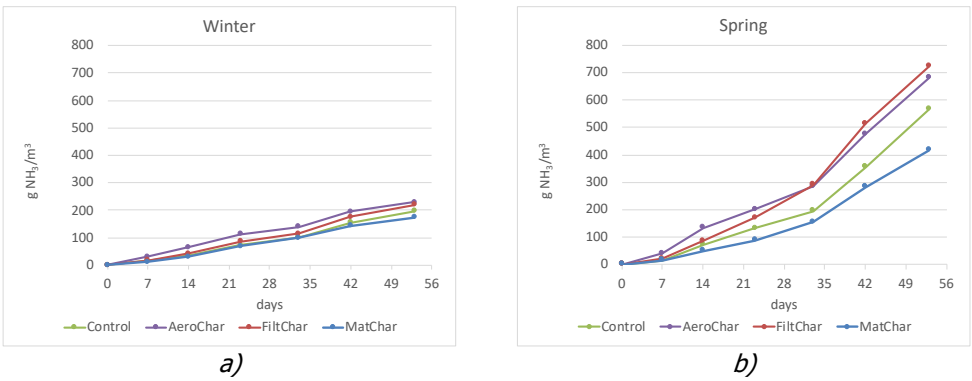

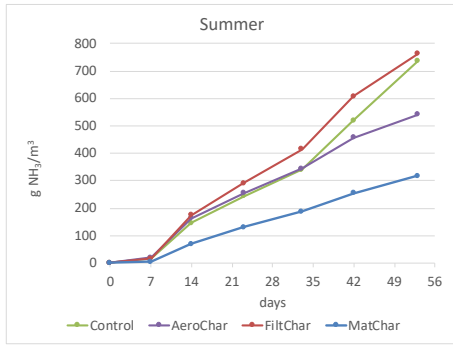

c)

Figure 14-5. Temporal evolution of the cumulative emissions E_{cum} of NH_3 of the three measures campaigns: a) winter; b) spring/autumn; c) summer. The vertical scale is the same for all three graphs to compare the results.

Regarding the total cumulative emissions, primary parameter for evaluating the best treatment, the results have highlighted interesting aspects, Figure 14-6.

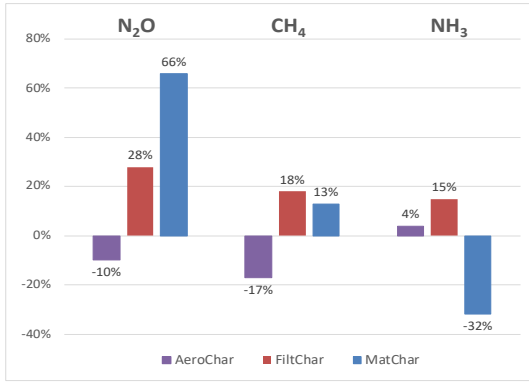

Figure 14-6. Changes in total cumulative emissions E_{tot} of N_2O, CH_4 ed NH_3. Figure reports the variation (reduction or increase) compared to the control.

The most promising treatment in reducing ammonia emissions is MatChar. NH_3 emissions were reduced by an average of 32% compared to the control, with a minimum reduction of 11% in the winter period and a maximum of 56% in the summer period. This is mainly due to covering the slurry with mats. However, MatChar increases N_2O emissions by 66%. This increase is explained by the fact that the biochar acts as a solid crust and facilitates the formation of a slurry crust on the surface of the tanks. Incomplete nitrifying-denitrifying processes take place within these solid formations, due to the alternation of aerobic and anaerobic phases, which lead to the formation and emission of N_2O. It is important to underline that N_2O emissions expressed as N-N_2O were only 2% respect NH_3 emissions as N-NH_3. FiltChar treatment was found to be the least effective, probably for two reasons: a) the effectiveness of the biochar in

capturing the ammonia is quickly exhausted b) slurry pumping and mixing favor emissions which are higher compared to a stationary storage. AeroChar treatment was effective in reducing CH_4 and N_2O emissions, respectively -17% and -10% compared to the control, mainly thanks to the oxygenation of the slurry. It caused a little increase in NH_3 emissions. In AeroChar, biochar is used as a substrate for microorganisms which, thanks to the establishment of aerobic-anaerobic reactions due to the alternation of oxygen and anoxic environments (nitrifying-denitrifying biological slurry treatment), reduce the production of CH_4 and N_2O.

The AeroChar and MatChar treatments were found to be able to mitigate the olfactory impact of the pig slurry storage, by 63% and 40% respectively compared to the control. In particular, the oxygenation of the slurry in the AeroChar treatment reduces odors as well as CH_4 emissions. FiltChar did not demonstrate significant odor reduction. Figure 14-7 shows the data relating to odorous emissions.

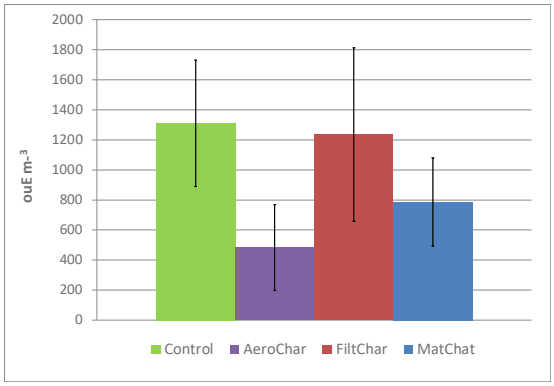

Figure 14-7. Odorous emissions of the different treatments and the control.

14.5.2 Discussion on the biochar characteristic

Biochar through the contact with the slurry during the storage/treatment phase incorporates micro and macro nutrients improving its nutrient characteristics. If it is used in soil application as fertilizer, it can release nutrients into the soil.

The characteristics of the final biochar compared to the "Original biochar", shown in Table 40, testify to the enrichment process following the contact with the slurry in the different theses. FiltChar biochar and AeroChar biochar record the greatest increase in nitrogen (TKN) and phosphorus (Ptot) content, with an average C:N ratio in the two theses of about 30, compared to the initial one of 93. It should be remembered that the ideal C:N ratio of an amendment is around 10, equivalent to the ratio of the already humified organic matter. Although

MatChar biochar provides a more efficient reduction in NH_3 emissions, it is less enriched in nutrients than AeroChar and FiltChar biochar, due to less interaction between slurry and biochar (MatChar remains on the surface as floating material). The C:N ratio of MatChar biochar thesis is 46. It should also be noted a) the decrease in pH of the biochar, that is typically basic and b) the absorption of water witnessed in the reduction of dry matter (TS) content after the treatment.

Table 40. Chemical-physical Biochar characterization before and after his application in the three different treatments to reduce emissions from pig slurry storage.

Name	pH [-]	TS [g kg_tq^{-1}]	VS % ST	TKN [mg kg_tq^{-1}]	P_{tot} [mg kg_tq^{-1}]	Zn [mg kg_tq^{-1}]	Cu [mg kg_tq^{-1}]	TOC [g kg_tq^{-1}]	TOC C/N
"Original biochar" * (before treatments)	10.4	978	88	6209	1111	295	20	576	93
FiltChar biochar	8.2	356	77	9217	1690	77	20	250	34
Variation between MatChar and Original biochar	-20%	-64%	-12%	+48%	+52%	-74%	--	-57%	-63%
AeroChar biochar	8.5	301	79	9345	2942	56	18	199	28
Variation between AeroChar and Original biochar	-20%	-69%	-10%	+51%	+165%	-81%	-11%	-65%	-70%
MatChar biochar	8.5	392	89	6664	1255	101	16	277	46
Variation between MatChar and Original biochar	-18%	-60%	+1%	+7%	+13%	-66%	-22%	-52%	-50%

14.6 Economic feasibility of AeroChar: a real case simulation

The data used during the economic analysis are collected in Table 41. Wheat crop and 46%-Urea fertilizer were taken as references in the calculations.

A medium-sized pig livestock with a slurry production of $\sim 4000\, m^3$ is considered (1200 pigs with an average weight of 110 kg each one). For this amount of slurry, about $9373\, kg\, y^{-1}$ of biochar are necessary for AeroChar treatment. The total expense for the biochar is $\sim 2800\, €\, y^{-1}$. The emissions reduction of 10% for N_2O and 17% for CH_4 justify this additional annual cost for the farmer. The application of biochar, compared to the covering system with plastic sheets, has the added value of obtaining a soil conditioner rich in nitrogen which can be used in the field. Starting from the nitrogen content in the sewage

(Table 41), it is calculated that through the slurry spreading the nitrogen efficient supplied to the field is equal to $93.5\ [kg_N\ ha^{-1}]$. Consequently, the nitrogen to be supplied with nitrogen fertilizers (Urea) is equal to $96.5\ [kg_N\ ha^{-1}]$. Based on the previous results, the cost for Urea is $110\ €$. If the Urea is replaced with biochar, it will be necessary $10\ 326\ kg\ ha^{-1}$ of AeroChar biochar, since the nitrogen content is only $0.009\ [\mathrm{kg_N}\ /\ kg_{biochar}]$ (Table 40), corresponding to a purchase cost of $760\ €\ ha^{-1}$ of "Original biochar". Therefore, for this type of crop, the use of biochar as a nitrogen amendment is not convenient compared to commercial fertilizers.

However, a new soil improver with greater agronomic proprieties - well-known characteristics of biochar + high nitrogen content - and greater economic value than normal biochar emerges from this study. Biochar "activated by slurry" can be resold on the market as fertilizer for use in non-extensive crops, for example horticulture, at a higher price than biochar and thus become a new source of income for farmers.

Table 41. Input data for the calculation of AeroChar economic feasibility.

Data	Value	Measurement Units	Source
Soil amendment			
Amount of N fertilizer for wheat	190	$kg_N\ ha^{-1}$	[387]
Nitrogen efficiency of pig slurry spreading	55%		[388]
Maximum slurry spreading (regulation limit)	170.0	$kg_N\ ha^{-1}$	[387]
Urea cost	530	$€\ tonn^{-1}$	[389]
AeroChar treatment			
Treated slurry	9.0	m^3	data project
"Original biochar" amount used (before)	21.09	kg	data project
AeroChar biochar amount extracted (after)	85.98	kg	data project
Biochar application rate	2.3	$\frac{kg\_biochar}{m^3\_slurry}$	data project
Weigh ratio biochar	4.08	$\frac{kg\_biochar\_after}{kg\_biochar\_before}$	data project
Biochar cost	300	$€\ tonn^{-1}$	data project
Pig Farm			
Amount of slurry per year	4000	m^3	data project

15 GASIFICATION PYROWEEDING AND ITS RESULTING BIOCHAR: A PIONEERING SUSTAINABLE SOLUTIONS FOR AGRICULTURE

In this research, a new weed control technique is proposed and explored, especially in agricultural crops, but applicable also in urban context.

The research focuses on the weeding operation in agriculture. A *biomass-powered flame-weeding gasification-based* machine for pyroweeding has been developed, for an environmentally sustainable weed control practice. The machine and a brief qualitative study on its efficacy on crops (pomegranate field and vineyards) are presented.

Also, a comparison between this system and the more standard chemical and mechanical techniques is carried out. Results reveals that pyroweeding not only brings cost reduction but is also the only potentially carbon-neutral or, even, carbon negative technology among the studied alternatives.

Keywords: Weed control; Pyroweeding; Gasification; Biochar; Carbon negative

This research is part of a larger work on pyroweeding, sustainable agriculture and environmental impact analysis.

15.1 Weed control and pyroweeding

Weed control is a management practice used for maintaining municipal green spaces and in agricultural crops. In agriculture, weeds steal water and nutrients to the crops, create shade, and stagnant water ponds, which can lead to the proliferation of fungal and bacteria diseases. Moreover, they obstruct essential cultivation activities like suckering, pruning, and applying protective treatments.

In vineyards farming, there is a growing interest in organic methods, particularly in managing the space between rows. Italy has seen a rise in the total area of organic vineyards, surpassing 100,000 hectares. Even among non-organic winemakers, there is a trend towards adopting more sustainable agricultural practices due to consumer awareness of environmental issues.

However, widespread acceptance of sustainable weed control practices remains a challenge. A survey conducted in 2022 among 110 Italian winemakers reveals that the 55% still rely on herbicides, while the rest employ mechanical methods. Chemical methods are favored for their cost-effectiveness, rapid application speed (5-6 km/h), and few annual treatments (up to 2 or 3) which maintain costs per hectare very low. On the other hand, mechanical weeding is criticized for its slow speed (2-4 km/h), the need for more frequent treatments (4-6 per year), and its inability to fully eradicate weeds around stumps and poles. These lacks significantly impact the overall cost of the operation [390,391].

Recent efforts have focused on promoting *thermal weeding* as a viable alternative to chemical and mechanical methods, particularly due to its alignment with organic agricultural practices. Moreover, thermal weeding shares advantages with chemical treatments in terms of speed and effectiveness.

Among thermal weeding techniques, open flame technology stands out, utilizing LPG-fueled burners to elevate weed temperatures, leading to rapid withering and drying within days. However, the notable risk of fire remains a concern, prompting exploration of alternative thermal methods like hot water, steam, or foams [392].

The primary barrier to widespread adoption of thermal weeding alternatives are the high operational costs, caused by fossil fuel usage [393]. In urban areas, weeding occurs 2-3 times annually to prevent weed-induced floor damage, reducing hazards on pedestrian and cycle paths and mitigating cars accidents. Due to the chemical risks posed to urban populations, herbicide usage is often restricted. Several studies validate the effectiveness of LPG-fueled flame weeders in urban settings, although the cost of LPG restricts its viability from economic and environmental perspectives.

This background is important foundation for researching and developing *biomass-powered flame-weeding gasification-based machines*, aimed at

reducing operating expenses by exploiting the pruning from vineyard maintenance, agriculture, and urban green waste. For example, vineyard prunings are often disposed of through open burning or shredding on-site, with high emission of harmful substances (CO, PM10, VOC, HC) and especially GHGs gases, (CH_4, N_2O). Only small fraction of pruning is sent to thermoelectric plants for energy exploitation since they are often far away.

To date, other sectors (foundries, food processing, ... [394,395]) have already experienced significant benefits from transitioning from LPG to gasification-based technologies. The agro-industrial sector has yet to make progress in this field, despite the large quantities of biomass at its disposal. The utilization of biomass gasification for flame weeding emerges not only as a powerful solution for the exploitation of this residual biomass, for reducing costs of weed-control operations and for bringing greater sustainability in agriculture, but it is a potent opportunity for achieving carbon negativity and enhancing carbon storage. In fact, compared with other thermal systems, *gasification-based weeding systems* have the potential to produce biochar, turning pyroweeding into a *carbon-negative practices*. The biochar produced during the weeding operation can be re-used in agriculture field or in cities since it acts, respectively, as soil improver and as a buffer against extreme weather events in urban environments.

In few points the reasons why pyroweeding is an appropriate solution are summarized here:

- strong reduction of GHGs emissions and operational costs compared to LPG systems;
- no need for a gas conditioning system or engine block. This solution eliminates many components responsible for costly maintenance of traditional gasification power plants;
- pyroweeding gasification-based generates biochar, driving the entire process towards carbon negativity.

15.2 Pyroweeding apparatus prototype

The prototype developed to investigate the operation of gasification-based pyroweeding is explained below. The chosen basis for the prototype is a Power Pallet model 30 (PP30) by All Power Labs [64]. The PP30 includes various components for gas conditioning, crucial for fueling the internal combustion engine. Studies by Milne et al. [396] indicate that no pollutant limits are imposed on direct syngas combustion in furnaces or in flares for heat generation. Consequently, in the prototype, the syngas is directly burned in a movable flame that can be directed toward the undesired weeds. The engine and the gas conditioning stage are removed, and new stages and components are fabricated. In Figure 15-1.a the functioning scheme and in Figure 15-1.b the final prototype are shown. Gas making unit components, unchanged from the PP30, include a

hopper, feeding system, single-throat reactor, and cyclone. The cyclone traps carbon particulate matter (>200µm) produced in the reactor, preventing pipe blockages. Biochar is collected at the bottom of the reactor since the architecture of PP30 rector remains unchanged. The reactor's flow system shifted to positive pressure: a 230 V-AC blower pumping fresh air inside the gasifier. This set-up prevents premature blower damages due to tars and syngas pollutants, reducing system costs and enhancing feasibility. The syngas flare used for the flame weeder was constructed using the original PP30 flare directly connected to the cyclone with a stainless steel pipe. A small 12 V-DC blower is added to for air tangential insertion: activation of the blower enables premixed combustion that brings the flame inside the flare; deactivation of the blower shifts to diffusive flame out of the flare. The electric generator in the prototype is necessary for powering the AC and DC blowers.

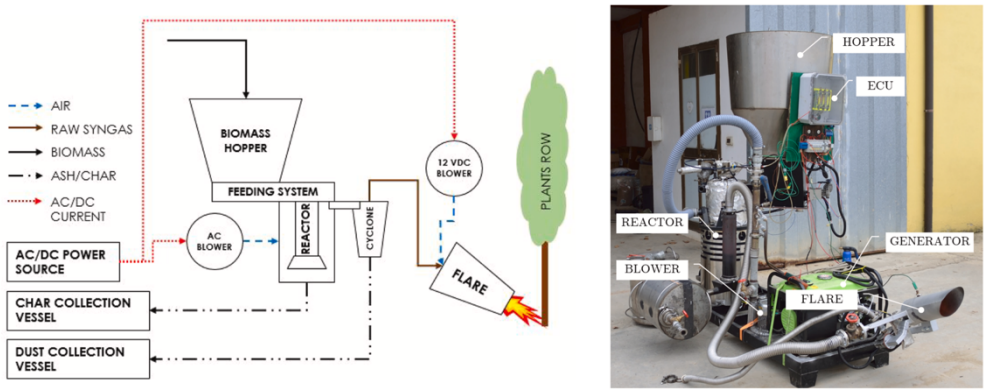

a) *b)*

Figure 15-1. a) functioning scheme of the pyroweeding prototype built starting from a PP30 gasifier; b) finished prototype.

15.2.1 Testing the pyroweeding apparatus

An initial test was carried out both to test the apparatus and to study the efficacy of pyroweeding on inter-row weed. The prototype was tested in a pomegranate field and a vineyard, utilizing intra-row cross flaming where the flame moves perpendicular to the direction of travel, affecting weeds and crops. To prevent crop damage, the flamer's speed was set at 3.5 km/h, following literature recommendations. The burner height and tilt are two parameters that affects the treatment. In both tests the burner was positioned about 0.15 meters above the soil, with an angle of 45° to avoid terrain collisions.

The air flowrate (blown inside the reactor) was 16.9 kg/h for pomegranates and 18.1 kg/h for vineyards, that means a syngas flowrate (based on an LHV of 6.00 MJ Nm^{-3} and a syngas composition of 12.6% of CO_2; 23.7% of CO; 43.5%

of N_2; 3.3% of CH_4; 16.9% of H_2) of 34.3 kg h^{-1} and 36.9 kg h^{-1} respectively. This resulted in thermal power outputs of 50.9 kW and 54.9 kW at the flare. The qualitative results, one day after the test, of the weed control are illustrated in Figure 15-2These tests confirmed the effectiveness of pyroweeding with minimal crop damage and optimized energy output.

a) vineyards – 1 day after the treatment

b) pomegranate fields – 1 day after the treatment

Figure 15-2. Qualitative results of the pyroweeding treatments. These were an initial tests and a quantitative analysis, for example, on the variation in weed color during the weeks after treatments would give numerical results.

15.3 Comparison between pyroweeding and other weeding treatments

Since pyroweeding falls in a carbon-negative concept, a brief comparison between this innovation and other weeding technology are realized for deeply studying the environmental benefit/impact. The considered technology are the chemical weeding system (CWS), the mechanical weeding system (MWS) and the gasification-based thermal weeding system (TWS).

A single-row herbicide sprayer is considered as CWS that use Glyphosate as herbicide, with an application rate of 3.24 kg ha^{-1} $year^{-1}$, adhering to production regulations. Operational speeds ranges between 4.5 and 5.8 km h^{-1}.

MWS involves physically removing weeds using tillers, cutting and turning weed roots. It's an alternative to chemical methods for organic vineyards but suffers from low speed, poor effectiveness, and incomplete weed removal near obstacles. Operational speeds is set at 3 km h^{-1} with 5 treatments per year.

For TWS the previous presented prototype is considered. Fueled by ENplus A2 pellets, gasification-based thermal weeding's effectiveness relies on heat transfer and temperature control: the applied average effective energy dose is

390 kJ m^{-2}. In this treatment, the novelty is the biochar that is produced during weeding operations as a "by-product" of gasifier that, able to store carbon and when applied to the soil (as a soil improver) offers long-term carbon sequestration. For this reason, gasification-based TWS holds promise for revolutionizing weed management in agriculture.

For all the three technologies a tractor-mounted equipment, powered through the Power Take Off (PTO) of the tractor, is considered.

In the emissions analysis, in terms of CO_2eq values, are considered according to the Ecoinvent database for LCA, through *OpenLCA* software [397]. For the CWS emissions related to glyphosate production and usage, along with diesel consumption for the tractor, are evaluated. In the MWS only emissions associated with diesel used for the tractor are taken into account. For the TWS are considered: the emissions for pellet production, the syngas combustion, the diesel usage for the tractor and the biochar production through a gasifier power plant.

15.3.1 Environmental comparison between the three techniques

The environmental analysis focuses on CO_2 emissions, presented as CO_2e. Table 42 summarizes model outputs for various methods. This research is part of a wider work on pyroweeding techniques [398].

Chemical weeding exhibits the highest CO_2eq emissions, with a fraction of 75% attributed to Glyphosate production and usage.

Mechanical weeding emits CO_2eq only due to the tractor diesel consumption: values are comparable to thermal weeding (see below). However, often MWS necessitates more than the five annual treatments considered in the model, caused by the lower weeding effectiveness.

Thermal weeding (for which three treatments every year are considered, similarly to CWS) shows emissions four times lower than CWS. Moreover, in this simulation, biochar is capable of offsetting other emissions by about 23.5%. This means that, if a significant amount of biochar is produced during weeding operation, the pyroweeding could be a carbon-neutral or even a carbon negative technology.

Finally, using TWS instead of herbicides, cuts the impacts on environments by over the half. Compared to mechanical methods, the TWS reduces emissions by 39%. Gasification-based pyroweeding, to date, is the only potentially carbon-neutral technology for weeding. This assessment sheds light on the environmental impacts of different weeding methods, helping to make "scientific" decisions toward sustainable agricultural practices.

Table 42. Emission in CO_2eq from the three treatments analyzed.

Techniques	Emission typology	Amount [$kgCO_2eq\ ha^{-1}\ y^{-1}$]
MWS	Diesel consumption	118.1
	Total emission	118.1
CWS	Glyphosate production	101.5
	Glyphosate usage	139.3
	Diesel consumption	42.5
	Total emission	282.3
TWS	Wood pellet production + transportation	36.2
	Direct syngas combustion (null since it is biogenic)	0
	Pollutants emissions during syngas combustion	13.4
	Diesel consumption	44.3
	Carbon storage of biochar	-22.0
	Total emission	71.9

15.3.2 Details on the gasification-based TWS

Increasing biochar co-production by approximately 20% could achieve carbon neutrality in weeding treatments. 20% is a value often reached by non-portable gasifiers or large pyrolizers. An innovative option might be to use the gasification reactor not only for pyroweeding operations, but also coupled with a gas cleaning system and an endothermic engine for thermal and electrical power production. The system could be "modular": parts for power production remain permanently installed in a dedicated hangar and only the reactor can be removed and mounted on the tractor during the pyroweeding operation. In this way, by exploiting the residual biomass available in the farm, it is possible to enhance biochar production volumes and generate electricity for commercialization.

16 OVERALL CONCLUSIONS

This thesis investigates several aspects related both to the biochar characteristics and to the biochar uses in different applications, examines the properties of biochar produced through both pyrolysis and gasification processes, and propose innovative areas of application. The findings from this research provide important contributions to the field of sustainable development, waste management and renewable energy systems.

First of all, attention was given to the properties of biochar produced under different pyrolysis conditions. Biochar produced with the same process but at different temperature revealed significant variations in physical and chemical characteristics. In particular, biochar produced at higher temperatures shows high electrical conductivity values, suggesting that the condition of the production process, primarily the temperature, directly affects the "conversion" of biochar. For this reason, a long measurement campaign on different biochar samples is carried out to correlate the temperature of the process with the grade of thermo-conversion of the woody biomass from insulating material to electrically conductive carbon-matrix. Results has revealed that the electrical conductivity is a good parameter on which biochar can be classified in terms of "quality": the higher the temperature production, the more organized the internal structure of the biochar, the higher the electrical conductivity.

However, it was found that the electrical conductivity value is strongly influenced by the test conditions. It was observed that variations are closely related both to its composition and to the biochar particle size, underscoring the importance of accurately describing methods used during biochar testing. This finding highlights the need to define a standard methods to measure the electrical conductivity of biochars and for classifying biochar on its electrical conductivity themself.

As is already known, biochar - mainly thanks to its porosity - leads to soil improvements: it increases the soil moisture, it increases the retention of nutrients, and it increases the crop productivity. For completeness, an investigation on these characteristics using an "high temperature biochar" (i.e. "high electrical conductivity biochar") were carried out and the above-described results was confirmed.

Furthermore, a study on the addition of biochar to a soil matrix has shown a significant impact both on soil water retention capacity over time and on the water capillary rise potential. The ability of biochar to increase the soil moisture, contributes to keeping the soil more wet for a longer time, modifying the thermal conductivity of the matrix. This phenomenon is particularly relevant for geothermal sector (e.g., low-enthalpy geothermal fields) since wetter soil tends to reduce the soil thermal resistance, potentially facilitating heat transfer

between probes and soil. The enhancement of the efficiency of geothermal systems through the simple application of biochar is a promising subject worthy of further study. In fact, increasing the thermal conductivity of the soil using biochar may improve the overall performance of geothermal heat pump systems, enabling more efficient extraction of thermal energy from the subsurface. Moreover, the application of biochar in geothermal fields can also have significant environmental benefits, contributing to soil carbon storage and climate change mitigation, making the household heating systems "carbon neutral" for many years. Lastly, biochar provide access to the carbon credit market, creating a possible source of revenue.

If in geothermal sector the most important biochar characteristic is porosity, the electrical conductivity characteristic is the key factor for the soil biome proliferation - since organisms use electron transfer for their activities – and it is a trigger for boosting carbon storage in soils.

To test the actual increase in biologic activities, a long experimental campaign involved one of the most well-known and industrially exploited biological environments: composting processes. Research conducted on composting has shown that the addition of biochar to degradable organic material leads to a significant increase in thermal energy production during the composting process. This phenomenon can be mainly attributed to an improved microbiological activity within the composted material. The introduction of biochar into the composting process, in fact, provides both a porous surface that acts as good substrate for the colonization and proliferation of microorganisms, and as electrically conductive medium that facilitates electron transfer between species, effectively improving microbiological activity. Heat is a by-product of the enhanced microbiological activity that leads to a higher velocity of decomposition and to a better stabilized final product.

In addition, optimized microbial activity reduces the greenhouse gases emissions. A more complete and rapid decomposition of organic matter decreases the amount of volatile organic material available for transformation into gases. This is also facilitated by biochar's behavior as adsorbent material: by capturing and adsorbing gaseous substances (thanks to the high porosity) or the greenhouse gases (e.g., methane and nitrous oxide) biochar increases the residence time of the substances in the organic mass, allowing their transformation into other stable and/or solid compounds. A more stable and mature compost, already during the initial moments of the decomposition, emits fewer greenhouse gases into the atmosphere.

A techno-economic analysis on a typical composting facility has shown that the integration of biochar into organic waste treatment processes is industrially feasible and cost-effective. In addition, since biochar consists mainly of recalcitrant (long-term stable) carbon, most of it remains stored in the soil, thus contributing to carbon removal from the atmosphere and to climate change

mitigation. Moreover, the use of biochar can generate economic benefits through carbon credits thanks to both the carbon content and the greenhouse gases emissions reduction during the composting processes. Biochar is the only waste additive among those that can be used (e.g., expanded clay aggregate, zeolite, ...) to fall within a carbon negative framework.

Furthermore, the studied have included the innovative applications of biochar in the agricultural and environmental sector. Pyro-weeding process represents a promising solution to reduce the reliance on chemical herbicides and/or liquid propane gas for weeding operations, particularly in organic farming. This technique involves the use of flames to burn weeds via gasification-based machines, which promote sustainability by utilizing wood-fueled systems, making the treatment carbon-negative and allowing the carbon storage thanks to biochar which plays a key role in this technology.

A second innovative application of biochar is in pig farming sector. Using biochar to treat swine slurry, when it is stored in the lagoons, can reduce unpleasant odors and the emission of greenhouse gases (such as nitrous oxide or methane) and other pollutant gases (as ammonia). Biochar not only absorbs gases generated by the swine slurry during the storage, but also facilitates the conversion of gases or compounds into non-volatile substances, preventing their emission into atmosphere. The exhausted biochar exhibits different characteristics depending on the specific application – such as filtration, substrate for biological abatement or material for surface cover – and it can be applied as a soil improver.

These innovative applications of biochar offer new opportunities to improve sustainability in agricultural and farming practices, going towards the European environmental policies and the necessary reduction of anthropic greenhouse gas emissions.

In summary, biochar represents a promising solution for addressing challenges related to waste management, sustainable production of high-quality by-products (e.g. compost), climate change mitigation, and innovation in agricultural and livestock practices. The in-depth explorations presented in this thesis, along with the obtained results, provide valuable insights for developing more sustainable and resilient practices.

The experimental nature of this thesis has highlighted some challenges and gaps both in terms of applications and related to biochar itself. It is important to underline that some difficulties were encountered. The main one was the variability in the behavior of the biological systems, and consequently in the results collected, as well as in the chemical composition and physical characteristics of the biochar. These variabilities underscore the need to conduct further experiments and investigations to reach ultimate conclusions. Further difficulty addressed was the large-scale availability of biochar with specific

characteristics and grain size. Large-scale production and the creation of a dedicated market are definitely the two industrial challenges that need to be approached in the near future, to enable the diffusion and the effective use of biochar.

Despite this the strong results of this thesis, that add up to a robust scientific literature, allow us to state that biochar and the production processes (gasification and high-temperature pyrolysis) are promising and feasible technologies, and offer concrete and achievable pathways towards a future where environmental sustainability aligns with and contributes to economic growth.

Appendix A.

Table A.1. Electrical conductivity results on biochar samples

w [kg]	*P [bar]*	*EC [S m^{-1}]*			
		BC_AR	***BC_5***	***BC_3***	***BC_F***
2.0	- -	7.81 ± 0.10	6.72 ± 0.07	7.91 ± 0.10	3.38 ± 0.06
4.0	1.25 ± 0.14	12.22 ± 0.17	9.87 ± 0.11	16.21 ± 0.21	6.77 ± 0.13
6.0	1.87 ± 0.15	16.96 ± 0.24	18.60 ± 0.22	22.63 ± 0.31	11.40 ± 0.23
8.0	2.50 ± 0.15	19.17 ± 0.27	25.24 ± 0.31	26.00 ± 0.37	11.92 ± 0.24
10.0	3.12 ± 0.15	21.90 ± 0.32	30.35 ± 0.38	28.70 ± 0.43	14.00 ± 0.29
15.0	4.68 ± 0.17	29.01 ± 0.44	43.41 ± 0.62	37.90 ± 0.62	18.77 ± 0.40
20.0	6.25 ± 0.19	34.50 ± 0.55	47.88 ± 0.70	42.60 ± 0.76	22.73 ± 0.50
25.0	7.81 ± 0.21	37.40 ± 0.61	55.21 ± 0.88	48.21 ± 0.92	26.14 ± 0.60
30.0	9.37 ± 0.23	41.12 ± 0.69	60.63 ± 1.01	55.96 ± 1.16	29.40 ± 0.69
40.0	12.49 ± 0.29	47.69 ± 0.84	77.38 ± 1.47	62.76 ± 1.44	35.85 ± 0.89
50.0	15.61 ± 0.34	51.54 ± 0.93	88.66 ± 1.89	64.68 ± 1.63	37.97 ± 1.00
60.0	18.74 ± 0.40	59.09 ± 1.11	90.45 ± 2.12	66.94 ± 1.87	41.60 ± 1.19
70.0	21.86 ± 0.46	67.29 ± 1.32	95.81 ± 2.52	69.87 ± 2.07	42.08 ± 1.22
80.0	24.98 ± 0.52	69.92 ± 1.43	97.79 ± 2.63	71.76 ± 2.23	43.04 ± 1.30

Table A.2. Electrical conductivity results on ground biochar samples

w [kg]	*p [bar]*	*EC [S m^{-1}]*			
		BCG_AR	***BCG_5***	***BCG_3***	***BCG_F***
2.0	- -	3.80 ± 0.07	3.05 ± 0.05	4.76 ± 0.09	- -
4.0	1.25 ± 0.14	7.97 ± 0.16	10.73 ± 0.19	9.17 ± 0.19	5.41 ± 0.15
6.0	1.87 ± 0.15	11.40 ± 0.24	14.11 ± 0.25	13.64 ± 0.29	8.30 ± 0.16
8.0	2.50 ± 0.15	14.46 ± 0.31	16.56 ± 0.29	17.37 ± 0.37	11.62 ± 0.33
10.0	3.12 ± 0.15	16.94 ± 0.37	20.66 ± 0.38	21.24 ± 0.46	13.05 ± 0.38
15.0	4.68 ± 0.17	21.75 ± 0.49	28.52 ± 0.53	29.74 ± 0.67	15.68 ± 0.48
20.0	6.25 ± 0.19	26.59 ± 0.62	36.38 ± 0.69	36.38 ± 0.83	16.36 ± 0.51
25.0	7.81 ± 0.21	33.33 ± 0.80	44.61 ± 0.87	42.56 ± 0.99	17.65 ± 0.56
30.0	9.37 ± 0.23	34.55 ± 0.84	48.52 ± 0.95	46.77 ± 1.12	19.27 ± 0.61
40.0	12.49 ± 0.29	40.82 ± 1.03	55.46 ± 1.11	56.61 ± 1.38	29.97 ± 0.99
50.0	15.61 ± 0.34	45.88 ± 1.20	58.26 ± 1.20	62.50 ± 1.55	33.69 ± 1.14
60.0	18.74 ± 0.40	54.02 ± 1.46	62.51 ± 1.31	76.95 ± 2.01	41.88 ± 1.49
70.0	21.86 ± 0.46	60.94 ± 1.68	63.49 ± 1.36	80.76 ± 2.11	41.80 ± 1.53
80.0	24.98 ± 0.52	64.81 ± 1.83	69.12 ± 1.51	82.05 ± 2.20	44.03 ± 1.65

Table A.3. Compressive strain at variable pressure on biochar samples

***w* [kg]**	***p* [bar]**	***ε* [m m^{-1}]**			
		BC_AR	***BC_5***	***BC_3***	***BC_F***
2.0	- -	- -	- -	- -	- -
4.0	1.25 ± 0.14	0.0375 ± 0.0033	0.0436 ± 0.0027	0.0395 ± 0.0032	0.0491 ± 0.0045
6.0	1.87 ± 0.15	0.0765 ± 0.0033	0.0763 ± 0.0027	0.0758 ± 0.0032	0.0982 ± 0.0045
8.0	2.50 ± 0.15	0.0879 ± 0.0033	0.1022 ± 0.0027	0.1122 ± 0.0032	0.1049 ± 0.0045
10.0	3.12 ± 0.15	0.1091 ± 0.0033	0.1362 ± 0.0027	0.1469 ± 0.0032	0.1272 ± 0.0045
15.0	4.68 ± 0.17	0.1645 ± 0.0033	0.2650 ± 0.0028	0.2704 ± 0.0032	0.1867 ± 0.0045
20.0	6.25 ± 0.19	0.1792 ± 0.0033	0.2561 ± 0.0028	0.2875 ± 0.0033	0.1920 ± 0.0045
25.0	7.81 ± 0.21	0.2020 ± 0.0033	0.3147 ± 0.0029	0.3397 ± 0.0033	0.2210 ± 0.0046
30.0	9.37 ± 0.23	0.2215 ± 0.0033	0.3460 ± 0.0029	0.3918 ± 0.0034	0.2433 ± 0.0046
40.0	12.49 ± 0.29	0.2557 ± 0.0034	0.4237 ± 0.0030	0.4487 ± 0.0035	0.2835 ± 0.0046
50.0	15.61 ± 0.34	0.2801 ± 0.0034	0.4877 ± 0.0030	0.4992 ± 0.0035	0.3237 ± 0.0047
60.0	18.74 ± 0.40	0.3046 ± 0.0034	0.5354 ± 0.0031	0.5482 ± 0.0036	0.3728 ± 0.0048
70.0	21.86 ± 0.46	0.3355 ± 0.0034	0.5858 ± 0.0032	0.5735 ± 0.0036	0.3862 ± 0.0048
80.0	24.98 ± 0.52	0.3632 ± 0.0035	0.5940 ± 0.0032	0.5940 ± 0.0037	0.4085 ± 0.0048

Table A.4**:** Compressive strain at variable pressure on ground biochar samples.

***w* [kg]**	***p* [bar]**	***ε* [m m^{-1}]**			
		BCG_AR	***BCG_5***	***BCG_3***	***BCG_F***
2.0	- -	- -	- -	- -	- -
4.0	1.25 ± 0.14	0.0466 ± 0.0049	0.0551 ± 0.0041	0.0392 ± 0.0049	- -
6.0	1.87 ± 0.15	0.0686 ± 0.0049	0.0735 ± 0.0041	0.0686 ± 0.0049	0.0238 ± 0.0068
8.0	2.50 ± 0.15	0.0980 ± 0.0049	0.0796 ± 0.0041	0.0784 ± 0.0049	0.0442 ± 0.0068
10.0	3.12 ± 0.15	0.1054 ± 0.0049	0.1020 ± 0.0041	0.0907 ± 0.0049	0.0544 ± 0.0068
15.0	4.68 ± 0.17	0.1479 ± 0.0049	0.1341 ± 0.0041	0.1402 ± 0.0049	0.1151 ± 0.0068
20.0	6.25 ± 0.19	0.1544 ± 0.0050	0.1347 ± 0.0041	0.1373 ± 0.0049	0.1224 ± 0.0069
25.0	7.81 ± 0.21	0.1838 ± 0.0050	0.1592 ± 0.0041	0.1544 ± 0.0050	0.1361 ± 0.0069
30.0	9.37 ± 0.23	0.1912 ± 0.0050	0.1633 ± 0.0041	0.1789 ± 0.0050	0.1395 ± 0.0069
40.0	12.49 ± 0.29	0.2206 ± 0.0050	0.1857 ± 0.0042	0.1936 ± 0.0050	0.1769 ± 0.0069
50.0	15.61 ± 0.34	0.2475 ± 0.0050	0.2082 ± 0.0042	0.2108 ± 0.0050	0.1973 ± 0.0069
60.0	18.74 ± 0.40	0.2721 ± 0.0051	0.2224 ± 0.0042	0.2475 ± 0.0050	0.2347 ± 0.0070
70.0	21.86 ± 0.46	0.2868 ± 0.0051	0.2388 ± 0.0042	0.2475 ± 0.0050	0.2585 ± 0.0070
80.0	24.98 ± 0.52	0.3064 ± 0.0051	0.2510 ± 0.0042	0.2672 ± 0.0051	0.2755 ± 0.0071

Figure A1. Electrical conductivity vs pressure applied to non-ground a) and ground b) char samples, with error bars.

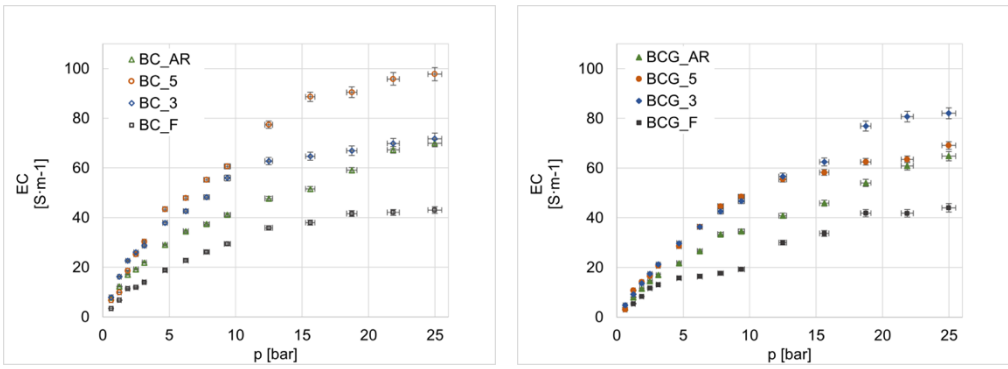

a) b)

Figure A2. Pressure vs compression strain for non-ground a) and ground b) char samples, with error bars.

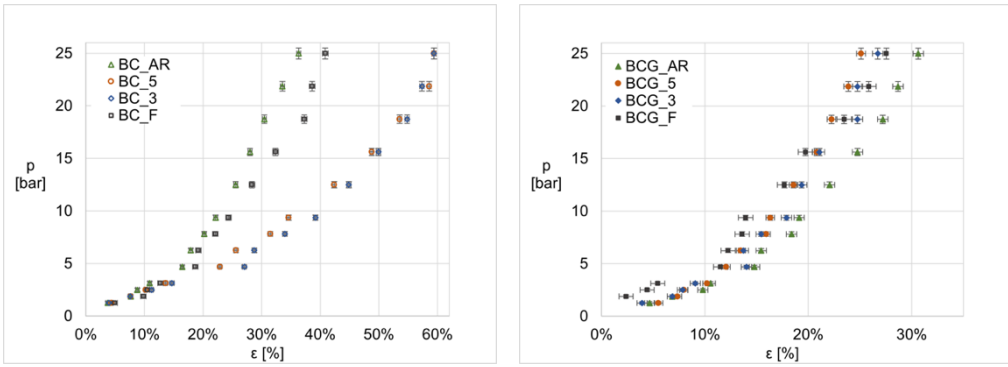

a) b)

Appendix B.

Figure B.1. Flow chart of the preparation of each biochar sample and measurement procedure.

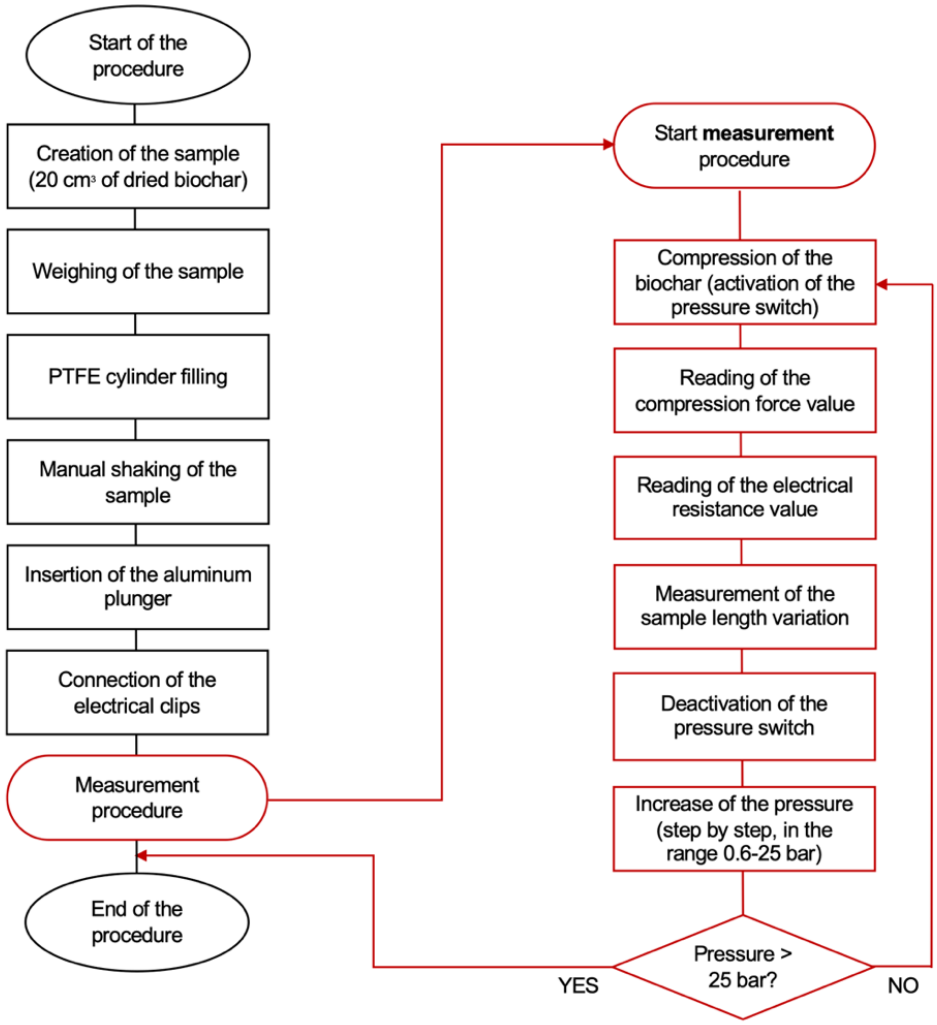

Appendix C.

Figure C.1. SEM images of a) the BC_AR sample where the heterogeneous nature of the biochar is visible (a vast range of grain sizes) and b) of the BC_3 where the grain shows a reduced amount of fines compared to a).

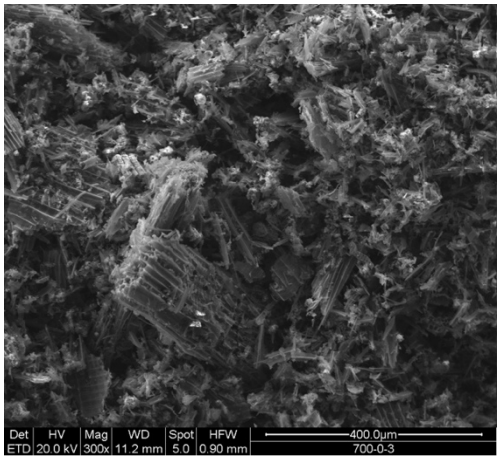

a)

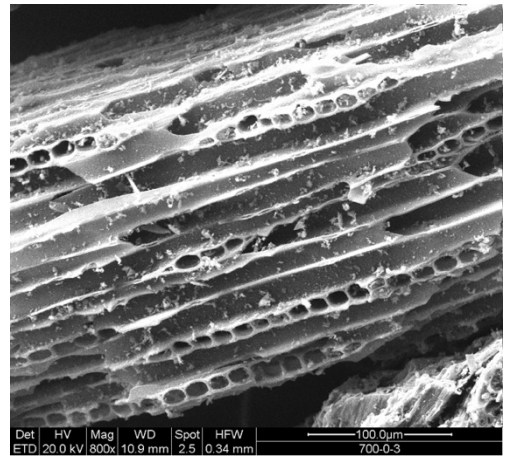

b)

Appendix D. Aeration methodology and algorithm

There are two alternative modes to aerate the compost bin: intermittent and continuous. In the first mode the air is insufflated at regular intervals, usually at higher flow rates than in the continuous operation mode. The risk in the intermittent mode is the occurrence of anaerobic areas inside the mass. The temperatures, however, are more uniform within all the bins than in the continuous case, which has low temperatures near the air sparger and higher temperatures in the layers above [399]. Furthermore, if not properly managed, continuous aeration presents a higher risk of over-cooling and over-drying the material. In this experiment, intermittent aeration was applied.

The management of insufflation periods of the bins was based on the mass temperature, measured through a Type K thermocouple placed in the central point (core) of each bin. To provide proportional control of the aeration, three temperature ranges were defined and associated to three insufflation periods.

The core of the control unit is Arduino®-based and managed the opening and closing of the solenoid valve and electro valves according to the algorithm shown after. The duration of a full cycle was set to 25 minutes. The algorithm was set up to allow the temperature of organic material mass to be raised to values in the range of 55-60 °C and, subsequently, to keep them in this range, as reported in

Table 43. An air meter (totalizer) was placed downstream of the blower to monitor the air usage.

Figure D.1 shows the diagram of the aeration system.

The duration of the blowing periods for each single bin is recorded in an Arduino® internal log. These data combined with the total cubic meters totalized by the air meter enable the calculation of the air amount delivered to each bin (in m^3) through a simple proportion of the total air cubic meters and the aeration time of each single bin. Quantifying the air supplied for each bin is essential to compute the NH_3 and GHGs emissions during the active composting phase.

Table 43. Duration of the aeration periods during the active phase of the composting process. The durations changed in real-time based on temperature feedback.

Day of experiment	Temperature range	Aeration period
1st to 4th day	T < 55°C	35 s every 25 minutes
	55 < T < 60°C	35 s every 25 minutes
	T > 60 °C	35 s every 25 minutes
5th to 8th day	T < 55°C	20 s every 25 minutes
	55 < T < 60°C	35 s every 25 minutes
	T > 60 °C	120 s every 25 minutes
9th to 31st day	T < 55°C	20 s every 25 minutes
	55 < T < 60°C	35 s every 25 minutes
	T > 60 °C	60 s every 25 minutes

Figure D.1. Schematic of the aeration system

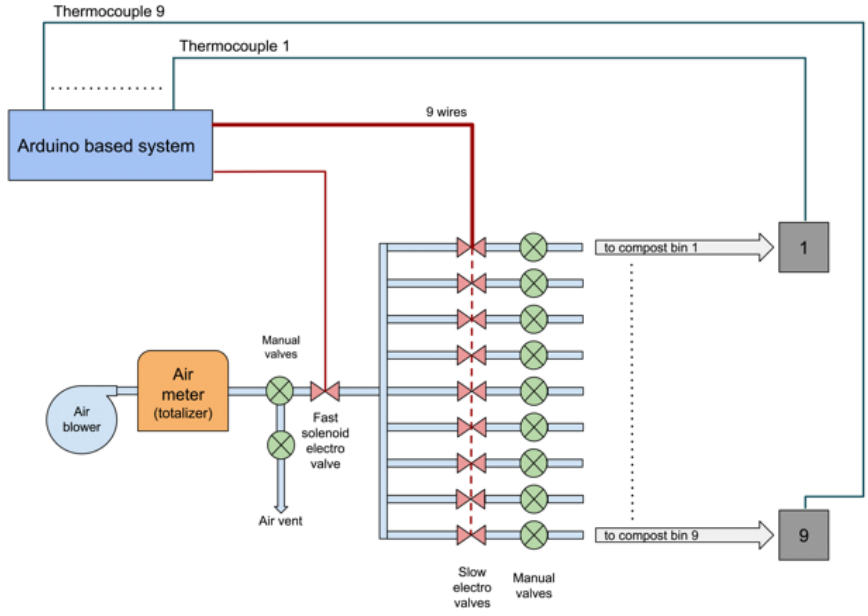

Following standard operation, the first temperature raise was performed without aeration in order to properly start the composting pile. The flow chart of the algorithm implemented in Arduino® for managing the aeration of the bins is shown in Figure D.*2*.

Figure D.2. Arduino algorithm for the automatic valves control.

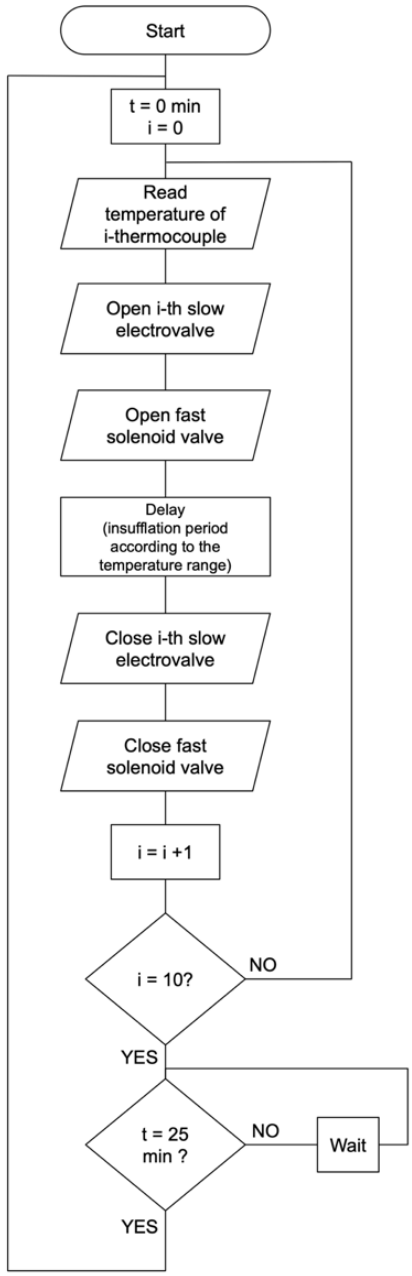

Appendix E. Thermal model and iterative procedure

Appendix E.1 Natural convection equations

Convection is mathematically described using the Nusselt number (Nu). As the value of Nu increases, the phenomenon of convection is increasingly developed. The Nusselt number is expressed as (Equation E.1):

$$\frac{\dot{Q}_{conv}}{\dot{Q}_{cond}} = \frac{h\,\Delta T}{\lambda\,\Delta T/L_c} = \frac{hL_c}{\Delta T} = Nu \qquad E.1$$

where h is the convection coefficient (W $m^{-2}K^{-1}$), L_c is the characteristic length (m), and λ_a is the fluid thermal conductivity (W $m^{-2}K^{-1}$). For the natural convection there are different analytical solutions obtained for simple geometries under certain simplifying hypotheses. In this model the simplified vertical and horizontal flat plate models were applied [400]. In using these correlations, all the properties of the fluid must be evaluated at the film temperature, which is defined as Equation E.2:

$$T_f = \frac{(T_{sp,e} - T_\infty)}{2} \qquad [°C] \qquad E.2$$

where $T_{sp,e}$ (°C) is the surface temperature and T_∞ (°C) is the temperature of the fluid at a sufficient distance from the surface. In the present discussion, T_∞ is always considered equal to the measured ambient temperature T_{amb} (°C). When the average Nusselt number and, consequently, also the average convective coefficient is known, the thermal power transmitted by natural convection from a solid surface at $T_{sp,e}$ to the surrounding fluid is expressed by Newton's law for cooling as (Equation E.3)

$$\dot{Q}_{conv} = h\,A_{sp}(T_{sp,e} - T_\infty) \qquad [kW] \qquad E.3$$

where A_{sp} is the heat exchange surface area and h is calculated from B.1 at the film temperature, T_f. During experimental campaign it was not possible to measure the surface temperature $T_{sp,e}$ with certainty. Therefore, an iterative method was implemented.

Appendix E.2 Iterative procedure for $T_{sp,e}$ approximation

The iterative process is based on the equivalence between the thermal power provided by the compost by conduction towards the external surface and the thermal power dissipated by the surface through convection. The algorithm for the iteration process is shown in

Figure E. 1. Iteration algorithm for convective superficial temperature - $T_{sp,e}$.

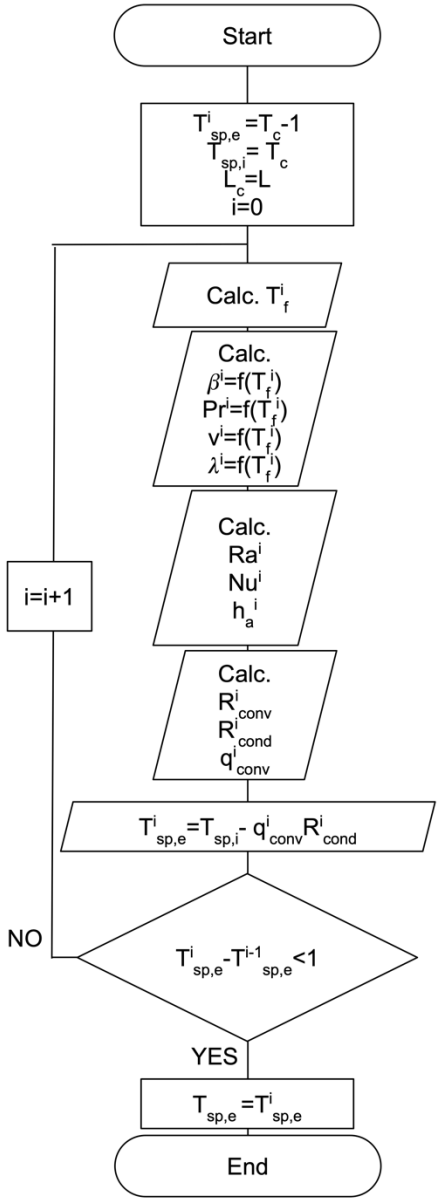

Conduction thermal power is calculated as shown in Equation E.4 while the convection one follows Equation E.5.

$$\dot{Q}_{cond} = \frac{T_{sp,i} - T_{sp,e}}{R_{cond}} \quad [kW] \quad E.4$$

$$\dot{Q}_{conv} = \frac{T_{sp,e} - T_{\infty}}{R_{conv}} \quad [kW] \quad E.5$$

where R_{cond} and R_{conv} are expressed as shown in Equation E.6 and E.7:

$$R_{cond} = \frac{s}{\lambda A_{sp}} \quad E.6$$

$$R_{conv} = \frac{1}{hA_{sp}} \quad E.7$$

where s [m], is the thickness of the resistant layer. λ (W $m^{-2}K^{-1}$) is the thermal conductivity of the material of which the layer is made. By equating Equation E.4 with Equation E.5, Equation E.8 is obtained, which is then used to iteratively calculate a sufficient approximation of the convective superficial temperature $T_{sp,e}$.

$$T^{i}_{sp,e} = T_{sp,i} - \dot{Q}^{i-1}_{conv}\, \dot{R}^{i-1}_{cond} \quad [°C] \quad E.8$$

Fluid parameters were calculated as a function of the film temperature. The internal surface temperature $T_{sp,i}$ is considered equal to the temperature of the compost T_c. To run the iteration process, it is necessary to set an initial hypothetical value for the external surface temperature (T^0) that allows for the completion of the first iterative calculation. The process stops when the difference between the calculated value of T^i and the previous value T^{i-1} is less than or equal to 1 °C. A final approximation of the external surface temperature makes it possible to estimate the thermal dispersions by convection occurring on the surface of the insulating walls of the bins as well as the top side of the composting mass, in following paragraphs.

Appendix E.3 Power dissipated for convection from vertical plate: $\dot{Q}_{p,v}$

The model herein implemented is the "vertical plate" model for natural convection, presented by Cengel [400]. The internal surface temperature $T_{sp,i}$ was considered equal to the temperature of the compost T_c as the compost mass was considered thermally homogeneous. The characteristic length L_c *was* equal to the height of the dissipating surface that was 0.7 m. The external part of the

insulation wall was considered thermally homogeneous as well. The value of the Nusselt number (Nu), in the case of a vertical wall, was calculated according to Equation E.9, which was valid for the entire range of value of the Rayleigh number (Ra_L).

$$Nu = \left\{ 0.825 + \frac{0.387\, Ra^{1/6}}{[1 + (0.492/Pr)^{9/16}]^{8/27}} \right\}^2 \qquad E.9$$

Appendix E.4 Power dissipated for convection from upper face of the composting material: $\dot{Q}_{p,h}$

The model herein implemented is the "horizontal plate" model for natural convection, presented by Cengel (1998) [400]. The upper side of the compost is considered as a hot surface in a colder environment. The net force acts upward, forcing the fluid to rise. The heated fluid rises freely, inducing considerable convective motions and therefore an effective heat exchange.

The upper part of the composting material was covered with a layer of non-active compost that also acted as a thermal insulator. Its thermal conductivity was assumed equal to 0.48 W $m^{-1}K^{-1}$, according to Ahn et al. (2009) [401]. The internal surface temperature $T_{sp,i}$ was considered equal to the temperature of the compost T_c and the surface was considered thermally homogeneous. The characteristic length L_c *was* calculated according to Equation E.10.

$$L_c = A_{sp}/p \qquad [m] \qquad E.10$$

where A_{sp} (m^2) is the area of the convective horizontal surface and p (m) is the perimeter of the convective surface. The horizontal convective surface was considered thermally homogeneous and the value of the Nusselt number (Nu) was calculated according to Equation E.11 and E.12.

$$Nu = 0.54\, Ra^{1/4} \quad when\ Ra = 10^4 \div 10^7 \qquad E.11$$

$$Nu = 0.15\, Ra^{1/3} \quad when\ Ra = 10^7 \div 10^{11} \qquad E.12$$

Appendix E.5 Power dissipated for sensible heat loss due to forced dry air: $\dot{Q}_{e,sens}$

The sensible heat loss due to the forced blowing of air was calculated considering the temperature difference between the incoming and outgoing air, taking into account the specific heat of the dry air. Regarding the incoming air, the temperature ($T_{a,in}$) was measured downstream of the blower to consider the internal energy increase given by the mechanical work of the blower itself. Regarding the temperature of the outgoing air ($T_{a,out}$), it was considered equal

to the average temperature of the compost. As a consequence, by applying Equation E.13, it was possible to calculate the power dissipated per hour due to sensible heat dispersion based on the forced blowing volumetric flow.

$$\dot{Q}_{e,sens} = \dot{V}\ \rho_a\ c_{p,a}\left(T_{a,out} - T_{a,in}\right) \qquad [kW] \qquad E.13$$

where $\dot{V}$ (m^3h^{-1}) is the volumetric air flow, ρ_a is the density of air at atmospheric pressure at 20°C which has a value of 1.204 kg m^{-3} and $c_{p,a}$ is the specific heat of dry air at atmospheric pressure and at a temperature of 27 °C, with a value of 1.005 kJ $kg^{-1}K^{-1}$.

Appendix E.6 Power dissipated for latent heat of vaporization of water: $\dot{Q}_{v,lat}$

The total power dissipated due to the vaporization of the water contained in the material was calculated by addressing the problem under two aspects. First, the pre and post composting mass water content was taken into account, bearing in mind that in composting processes this parameter significantly decreases over time. This made it possible to quantify, with good approximation, the total thermal energy spent per bin to evaporate a known amount of water. For simplicity, only the enthalpy of water vaporization was considered for calculating the aforementioned power, according to the Equation E.14.

$$\dot{Q}_{e,lat} = \dot{V}\ \rho_a\ h_{vap} \qquad [kW] \qquad E.14$$

where h_{vap} is the vaporization enthalpy of water at atmospheric pressure and 0 °C which has a value of 2501.3 kJ kg^{-1}.

The second aspect to consider is the variation of vapour emission over time to be able to give an estimate of the trend of the dispersed power throughout the duration of the composting process. To do this, a static chamber was used in combination with a photo-acoustic gas analyzer (INNOVA 1412i), with which the water vapor content of the inlet and outlet humid air was measured twice a week. However, it to point out that this measurement system is subject to significant errors when it comes to water vapor due to condensation phenomena within the measuring chamber. It was therefore decided to use the data provided by the analysis carried out with the static chamber to evaluate only the trend of evaporation over time. The amount of water evaporated per hour was calculated by parameterizing the trends measured with the static chamber to the amount of total evaporated water calculated, considering the pre and post composting water content. A corrective coefficient was obtained for each composter that took into account the underestimation given by the static chamber method. This coefficient was calculated for each bin by dividing the total quantity of evaporated water, considering the degree of humidity of the compost before

and after composting, by the total quantity of evaporated water calculated as the sum of the measurements of the static chamber during the entire composting process.

Appendix E.6 Thermal power expressed for temperature increase of the composting mass: $\dot{Q}_s$

In addition to the thermal power dispersion as described in the previous paragraphs, part of the thermal power generated by the microbiological degradation was used as sensible heat for the temperature increase of the composting mass and was referred to as "process heat". The process heat of the composting mass was calculated following Equation E.15:

$$\dot{Q}_s = m\, c_{p,c} \frac{\Delta T_c}{\Delta t} \qquad [kW] \qquad E.15$$

where m (kg) is the mass of the composting material in kg, $c_{p,c}$ is the specific heat capacity of the compost with a value of 1.21 (kJ $kg^{-1}K^{-1}$) according to Bach et al. (1987) [324], considered constant during the entire process ΔT_c (°C) is the difference between two subsequent temperature measurements of composting material over time and Δt (h) is the time between two subsequent temperature measurements.

Appendix F. Variables computation and adopted equations

Appendix F.1. Expenditures for the gasifier installation

The cost of the entire gasification system is obtained through Eq. F. 1

$$C_{tot} = C_{equipment} + C_{construction} \quad [€] \quad \text{F. 1}$$

where $C_{construction}$ is the cost of installing and setting up the gasification system while $C_{equipment}$ is the cost for the gasifier purchase and it is determined through Eq. F. 2:

$$C_{equipment} = \frac{ECC}{ER} \quad [€\ kWe^{-1}] \quad \text{F. 2}$$

where ECC is the Equipment Capital Cost, average estimated valor on different micro-gasifier models, calculated on units of power [kW], Table 34.

$C_{construction}$ is evaluated as a percentage of $C_{equipment}$ through the application of some factors to consider different aspects of gasifier installation, Eq. F. 3:

$$C_{construction} = C_{equipment} * (F_{building} + F_{installation} + F_{overhead} + F_{auxiliary}) \quad [€\ kWe^{-1}] \quad \text{F. 3}$$

The gasifier operational expenses are calculated according to Eq. F. 4:

$$C_{operating} = C_{maintenance} + C_{general} + C_{contingency} \quad [€\ year^{-1}] \quad \text{F. 4}$$

where $C_{maintenance}$ is the cost relating to maintenance, $C_{general}$ covers all overhead expenses necessary for the operation of the facility and $C_{contingency}$ concerns all expenses that cannot be predicted, and it is set equal to $C_{general}$. These costs, $C_{maintenance}$, $C_{general}$ and $C_{contingency}$, are evaluated starting from the unit cost per installed kWe [€ kW^{-1}] per year, provided for each individual cost by Wei et al. (2009) [366].

C_{labor} is the labor cost of a trained employee for running the gasifier. It is estimated through the Gross Annual Income (GAI) for Italy in July 2023, as shown in Eq. F. 5

$$C_{labor} = GAI * (1 + \%_{social\ insurance\ contributions} + \%_{termination\ pay}) \quad [€\ year^{-1}] \quad \text{F. 5}$$

Appendix F.2. Other expenditure voices: biochar and diesel fuel

$M_{biochar\_buy}$ is estimable via Eqs. F. 6, F. 7 and F. 8.

$$M_{wood\_gasif} = E_{e\_gasif} * T_{ope} * \varepsilon_{gasif} \quad [kg] \quad \text{F. 6}$$

$$M_{biochar\_gasif} = M_{wood\_gasif} * Y_{biochar} \quad [kg] \quad \text{F. 7}$$

$$M_{biochar\_buy} = M_{biochar\_OM} - M_{biochar\_gasif} \quad [kg] \quad \text{F. 8}$$

where M_{wood_gasif} is the gasified biomass, $M_{biochar\_gasif}$ is the amount of biochar self-produced with the gasifier, $M_{biochar\_buy}$ is the amount of biochar to be purchased to meet the requirement for co-composting the entire Organic mix $M_{biochar\_OM}$, which remains the same for S1. The cost of biochar in S2 is solely attributed to the missing fraction, Eq. F. 9.

$$C_{biochar\_buy} = M_{biochar\_buy} * €_{biochar\_unit} \quad [€] \quad \text{F. 9}$$

Eq. F. 10 shows the procedures for estimating the cost for diesel fuel.

$$C_{diesel} = M_{wood\_gasif} * \rho_{wood} * FC_{shredder} * €_{diesel\_unit} \quad [€] \quad \text{F. 10}$$

where ρ_{wood} is set equal to $500\ kg\ m^{-3}$ as biomass is obtained from prunings and other green wood waste [368] ; the Fuel Consumption of the wood shredder is set equal to $FC_{shredder} = 0.56\ l_{diesel}\ m^{-3}_{biomass}$ [367], the unit price for diesel fuel $€_{diesel\_unit} = 1.677\ €\ l^{-1}$ [369].

Appendix F.3. Energy revenues

Evaluation of revenues from the sale of electricity and thermal energy, Eqs. F. 11 and Eqs. F. 12.

$$R_{electrical} = E_{e\_gasif} * T_{ope} * €_{E_e} * \%_{tax} \quad [€] \quad \text{F. 11}$$

where $T_{ope} = 8000\ h\ y^{-1}$ and $€_{E_e}$ is the average price of "dedicated retirement" (an Italian way for power producers to trade energy and feed it into the electric grid) during the first six months of 2023, Table 34. The year 2022 is excluded as reference due to significant and unusual price fluctuations in the energy market.

$$R_{thermal} = E_{t\_gasif} * T_{ope} * €_{E_t} * \%_{tax} \quad [€] \quad \text{F. 12}$$

Appendix F.4. New biomass to be sourced

Biomass missing quantity can be calculated as shown in Eq. F. 13.

$$M_{biomass\_new} = M_{wood\_gasif} - M_{biomass\_extra} \quad [kg] \quad \text{F. 13}$$

where $M_{biomass\_extra}$ is the excess of biomass not used in the composting process, calculated according to Eq. F. 14.

$$M_{biomass\_extra} = M_{biomass} - (2 * M_{OFMSW} * 20\%) \quad [kg] \quad \text{F. 14}$$

Appendix F.5. Installation of a 1000 kWe gasifier & biochar production

The amount of Organic mix given by Eq. F. 15.

$$M_{mix\_biochar} = \frac{M_{biochar\_gasif}}{3\%} \quad [kg] \quad \text{F. 15}$$

The amount of Organic mix not treated with biochar is obtained with Eq. F. 16:

$$M_{mix} = M_{organic\_mix} - M_{mix\_biochar} \quad [kg] \quad \text{F. 16}$$

Appendix F.6. Compost revenues

Revenues from the sale of standard compost are calculated with Eq. F. 17. All data are reported in Table 34.

$$R_{compost} = €_{comp\_unit} * M_{compost} \quad [€] \quad \text{F. 17}$$

Appendix F.7. Cash flow and payback time

$$NPV = \sum_{t=0}^{n} \frac{Tot_{income\_y} - Tot_{outgoings\_y}}{(1 + WACC)^t} \quad [y] \quad \text{F. 18}$$

Appendix F.8. Carbon footprint and carbon credit revenue (VERRA standard)

The amount of removed GHGs in one year $ER_{PS,y}$, is calculated through Eq. F. 19:

$$ER_{PS,y} = \left(CC_y * \frac{44}{12}\right) - PE_{PS,y} \quad [\text{tons } CO_2\text{e y}^{-1}] \quad \text{F. 19}$$

where CC_y is the content of fixed carbon in biochar, see the Eq. F. 20; $\frac{44}{12}$ is the conversion fraction of fixed carbon to CO_2eq; $PE_{PS,y}$ are the project emissions during the thermo-conversion phase, see Eq. F. 21.

$$CC_y = M_y * FC_p * PR_{de} \quad [\text{tons } CO_2e\ y^{-1}] \quad \text{F. 20}$$

where M_y is the amount of biochar added to the organic mix, FC_p is the carbon content of biochar ($FC_p = 0.72$) and PR_{de} is an adjustment factor for carbon permanence due to biochar decay, set at 0.89 as suggested by VERRA. In all scenarios was adopted the most conservative carbon content FC_p value between BioDea biochar, used in S1 and equal to 72%, and SynCraft biochar, used in S2, S3, S4, FULL and equal to 80%. This assumption is necessary both to compare all scenario from a carbon credit point of view, and to present a cautionary analysis.

$$PE_{PS,y} = (PE_{D,y} + PE_{P,y} + PE_{C,y}) * \frac{M_y}{M_x} \quad [\text{tons } CO_2e\ y^{-1}] \quad \text{F. 21}$$

where $PE_{D,y}$, $PE_{P,y}$ e $PE_{C,y}$ are respectively the emissions of biomass pretreatment, biomass conversion, and energy use for the allothermic treatments. M_x Is the mass of biochar produced in the facility and M_y is the biochar mass applied in the final use. Here $M_x = M_y$.

The emission impact of diesel fuel for wood shredding operations, in terms of CO_2eq, is calculated thorough Eq. F. 22. $PE_{D,y}$ is required during the calculations of the VERRA standard.

$$PE_{D,y} = M_{wood\_gasif} * \rho_{wood} * FC_{shredder} * E_{unit_{diesel}} \quad [\text{tons } CO_2e\ y^{-1}] \quad \text{F. 22}$$

where E_{unit_Diesel} is the emission factor for the diesel fuel equal to $2697.49\ \text{kg } CO_2e\ m^{-3}$ [7,16].

In this case study, the avoided emissions of CH_4 and N_2O during the composting process, thanks the biochar addition as reported extensively in this thesis and in literature, were ignored in the calculation of carbon credits. Setting $1\ \text{Carbon Credit} = 1\ \text{ton } CO_2e$, it follows that $N_{\text{Carbon credit}} = ER_{PS,y}$, and the calculation of revenue from the sale of carbon credits comes from Eq. F. 23:

$$R_{\text{Carbon credit}} = N_{\text{Carbon credit}} * €_{\text{Carbon credit}} \quad [€] \quad \text{F. 23}$$

where $€_{\text{Carbon credit}} = 91\ € \ (\text{Carbon credits})^{-1}$ (Q2-2023) [402].

The emissions from the composting process are calculated through Eq. F. 24.

$$EC_{CO_2e} = \left(M_{organic_{mix}} * EF_{CH_4} + M_{mix_{biochar}} * EF_{CH_4} * (1 - 0.45) \right) * GWP_{CH_4} \quad [\text{tons } CO_2e\ y^{-1}] \qquad \text{F. 24}$$

where $M_{organic\_mix}$ is the Organic mix without biochar (in S1 and S2 is zero), $M_{mix\_biochar}$ is the biochar aided Organic mix and $GWP_{CH_4} = 28$ is the CH_4 global warming potential factor (GWP) [7].

List of Figures

List of Tables

References

[1] The Atmosphere: Getting a Handle on Carbon Dioxide – Climate Change: Vital Signs of the Planet n.d. https://climate.nasa.gov/news/2915/the-atmosphere-getting-a-handle-on-carbon-dioxide/ (accessed November 29, 2023).

[2] ESA - Eduspace IT - Home - Interferenza atmosferica 2010.

[3] File:Atmosfaerisk spredning.png - Wikimedia Commons n.d. https://commons.wikimedia.org/wiki/File:Atmosfaerisk_spredning.png (accessed November 30, 2023).

[4] US Department of Commerce NGML. Global Monitoring Laboratory - Carbon Cycle Greenhouse Gases n.d.

[5] Global Monitoring Laboratory - Carbon Cycle Greenhouse Gases n.d. https://gml.noaa.gov/ccgg/trends_n2o/ (accessed November 30, 2023).

[6] Muralikrishna I V., Manickam V. Air Pollution Control Technologies. Environ Manage, Elsevier; 2017, p. 337–97. https://doi.org/10.1016/B978-0-12-811989-1.00014-2.

[7] Calvin K, Dasgupta D, Krinner G, Mukherji A, Thorne PW, Trisos C, et al. IPCC, 2023: Climate Change 2023: Synthesis Report. Contribution of Working Groups I, II and III to the Sixth Assessment Report of the Intergovernmental Panel on Climate Change [Core Writing Team, H. Lee and J. Romero (eds.)]. IPCC, Geneva, Switzerland. 2023. https://doi.org/10.59327/IPCC/AR6-9789291691647.

[8] Masson-Delmotte V, P. Zhai, A. Pirani, S.L. Connors, C. Péan, S. Berger, et al. IPCC, 2021: Climate Change 2021: The Physical Science Basis. Contribution of Working Group I to the Sixth Assessment Report of the Intergovernmental Panel on Climate Change. Cambridge University Press; 2023. https://doi.org/10.1017/9781009157896.

[9] Nakicenovic N, Lempert RJ, Janetos AC. A Framework for the development of new socio-economic scenarios for climate change research: Introductory essay: A forthcoming special issue of Climatic Change. Clim Change 2014;122:351–61. https://doi.org/10.1007/S10584-013-0982-2/METRICS.

[10] Intergovernmental Panel on Climate Change. Climate Change 2021 – The Physical Science Basis. Climate Change 2021 – The Physical Science Basis 2023. https://doi.org/10.1017/9781009157896.

[11] O'Neill BC, Kriegler E, Riahi K, Ebi KL, Hallegatte S, Carter TR, et al. A new scenario framework for climate change research: The concept of shared socioeconomic pathways. Clim Change 2014;122:387–400. https://doi.org/10.1007/S10584-013-0905-2/TABLES/2.

[12] van Vuuren DP, Edmonds J, Kainuma M, Riahi K, Thomson A, Hibbard K, et al. The representative concentration pathways: An overview. Clim Change 2011;109:5–31. https://doi.org/10.1007/S10584-011-0148-Z/TABLES/4.

[13] Pielke R, Burgess MG, Ritchie J. Plausible 2005–2050 emissions scenarios project between 2 °C and 3 °C of warming by 2100. Environmental Research Letters 2022;17:024027. https://doi.org/10.1088/1748-9326/AC4EBF.

[14] Paris Agreement on climate change - Consilium n.d. https://www.consilium.europa.eu/en/policies/climate-change/paris-agreement/ (accessed December 12, 2023).

[15] Masson-Delmotte V, P. Zhai, A. Pirani, S.L. Connors, C. Péan, S. Berger, et al. Technical Summary. In Climate Change 2021: The Physical Science Basis. Contribution of Working Group I to the Sixth Assessment Report of the Intergovernmental Panel on Climate Change. Cambridge University Press, Cambridge, United Kingdom and New York, NY, USA, pp. 33−144, Cambridge University Press; 2021, p. 35–144. https://doi.org/10.1017/9781009157896.002.
[16] Livingston JE, Rummukainen M. Taking science by surprise: The knowledge politics of the IPCC Special Report on 1.5 degrees. Environ Sci Policy 2020;112:10–6. https://doi.org/10.1016/J.ENVSCI.2020.05.020.
[17] Döhlen Wedin A. Understanding Feasibility of Climate Change Goals and Actions. Ethics Policy Environ 2023. https://doi.org/10.1080/21550085.2023.2180254.
[18] Patterson JJ, Thaler T, Hoffmann M, Hughes S, Oels A, Chu E, et al. Political feasibility of 1.5°C societal transformations: the role of social justice. Curr Opin Environ Sustain 2018;31:1–9. https://doi.org/10.1016/J.COSUST.2017.11.002.
[19] Reisinger A, Geden O. Temporary overshoot: Origins, prospects, and a long path ahead. One Earth 2023. https://doi.org/10.1016/J.ONEEAR.2023.11.008.
[20] Climate Change: Global Temperature | NOAA Climate.gov n.d. https://www.climate.gov/news-features/understanding-climate/climate-change-global-temperature (accessed December 14, 2023).
[21] Global Climate Highlights 2023 | Copernicus n.d. https://climate.copernicus.eu/global-climate-highlights-2023 (accessed January 15, 2024).
[22] Professor Ed Hawkins MBE – Climate Scientist n.d. https://edhawkins.org/ (accessed December 15, 2023).
[23] CittàClima_2022 n.d. https://cittaclima.it/mappa/ (accessed December 15, 2023).
[24] Summary for Policymakers. Global Warming of 15°C 2022:1–24. https://doi.org/10.1017/9781009157940.001.
[25] All People on 1 Page 2023. https://www.worldometers.info/watch/world-population/ (accessed November 24, 2023).
[26] Transforming our world: the 2030 Agenda for Sustainable Development | Department of Economic and Social Affairs 2015. https://sdgs.un.org/2030agenda (accessed November 24, 2023).
[27] THE 17 GOALS | Sustainable Development 2023. https://sdgs.un.org/goals (accessed November 24, 2023).
[28] FOOD WASTE INDEX REPORT 2021. 2021.
[29] Renewable Energy and Agri-food Systems: Advancing Energy and Food Security towards Sustainable Development Goals. IRENA and FAO; 2021. https://doi.org/10.4060/cb7433en.
[30] IEA. Global electricity demand by scenario, 2010-2030 – Charts – Data & Statistics 2023. https://www.iea.org/data-and-statistics/charts/global-electricity-demand-by-scenario-2010-2030 (accessed November 27, 2023).
[31] Renewable energy statistics - Statistics Explained 2023. https://ec.europa.eu/eurostat/statistics-explained/index.php?title=Renewable_energy_statistics (accessed November 27, 2023).

[32] Il 2 agosto è l'Earth overshoot day 2023 | WWF Italia 2023. https://www.wwf.it/pandanews/societa/mondo/il-2-agosto-e-learth-overshoot-day-2023/ (accessed November 24, 2023).
[33] M. Pathak, R. Slade, P.R. Shukla, J. Skea, R. Pichs-Madruga, D. Ürge-Vorsatz. Mitigation of Climate Change Climate Change 2022 Working Group III contribution to the Sixth Assessment Report of the Intergovernmental Panel on Climate Change. 2022.
[34] IPCC. Annex I: Glossary. Global Warming of 15°C 2022:541–62. https://doi.org/10.1017/9781009157940.008.
[35] Smith P, Porter JR. Bioenergy in the IPCC Assessments. GCB Bioenergy 2018;10:428–31. https://doi.org/10.1111/GCBB.12514.
[36] Möllersten K, Yan J, Moreira JR. Potential market niches for biomass energy with CO2 capture and storage—Opportunities for energy supply with negative CO2 emissions. Biomass Bioenergy 2003;25:273–85. https://doi.org/10.1016/S0961-9534(03)00013-8.
[37] Even C, Hadroug D, Boumlaik Y, Simon G. Microalgae-based Bioenergy with Carbon Capture and Storage quantified as a Negative Emissions Technology. Energy Nexus 2022;7:100117. https://doi.org/10.1016/J.NEXUS.2022.100117.
[38] Basu P. Biomass gasification and pyrolysis: Practical design and theory. Biomass Gasification and Pyrolysis: Practical Design and Theory 2010:1–365. https://doi.org/10.1016/C2009-0-20099-7.
[39] Santos VO, Guimarães MN, Colpani D, Araujo RO, Chaar JS, de Souza LKC. Biomass Conversion By Pyrolysis Process. Reference Module in Earth Systems and Environmental Sciences 2023. https://doi.org/10.1016/B978-0-323-93940-9.00023-2.
[40] Wang H, Li H, Han X, Zeng Y, Xu CC. Biomass Conversion by Hydrothermal Liquefaction Technology. Reference Module in Earth Systems and Environmental Sciences 2023. https://doi.org/10.1016/B978-0-323-93940-9.00033-5.
[41] Joseph S, Cowie AL, Van Zwieten L, Bolan N, Budai A, Buss W, et al. How biochar works, and when it doesn't: A review of mechanisms controlling soil and plant responses to biochar. GCB Bioenergy 2021;13:1731–64. https://doi.org/10.1111/GCBB.12885.
[42] Agyekum EB, Nutakor C. Recent advancement in biochar production and utilization – A combination of traditional and bibliometric review. Int J Hydrogen Energy 2024;54:1137–53. https://doi.org/10.1016/J.IJHYDENE.2023.11.335.
[43] Reichle DE. Carbon, climate change, and public policy. The Global Carbon Cycle and Climate Change 2020:253–87. https://doi.org/10.1016/B978-0-12-820244-9.00012-3.
[44] What is the Kyoto Protocol? | UNFCCC n.d. https://unfccc.int/kyoto_protocol (accessed December 20, 2023).
[45] Puro.earth - carbon removal standard and registry n.d. https://puro.earth/ (accessed December 20, 2023).
[46] Methodology for Biochar Utilization in Soil and Non-Soil Applications - Verra n.d. https://verra.org/methodologies/methodology-for-biochar-utilization-in-soil-and-non-soil-applications/ (accessed December 20, 2023).
[47] What is REDD+? | UNFCCC n.d. https://unfccc.int/topics/land-use/workstreams/redd/what-is-redd (accessed December 20, 2023).

[48] DIRECTIVE 2003/87/EC OF THE EUROPEAN PARLIAMENT AND OF THE COUNCIL of 13 October 2003 establishing a scheme for greenhouse gas emission allowance trading within the Community and amending Council Directive 96/61/EC (Text with EEA relevance). n.d.
[49] Wilson B, Wilson B, Williams N, Liss B. A Comparative Assessment of Commercial Technologies for Conversion of Solid Waste to Energy. 2013.
[50] Stand di motori e gasogeni Deutz nel padiglione della meccanica alla Fiera Campionaria di Milano del 1936 - Archivio Fondazione Fiera Milano n.d. https://archiviostorico.fondazionefiera.it/oggetti/4844-stand-di-motori-e-gasogeni-deutz-nel-padiglione-della-meccanica-alla-fiera-campionaria-di-milano-del-1936 (accessed December 22, 2023).
[51] Ingenjörsvetenskapsakademien (Sweden), National Renewable Energy Laboratory (U.S.). Generator gas : the Swedish experience-gas 1939-1945. Biomass Energy Foundation; 1998.
[52] Vaasa Bio-gasification Power Plant - Renewable Technology n.d. https://www.renewable-technology.com/projects/vaasa-bio-gasification-power-plant/ (accessed December 22, 2023).
[53] Gasification applications in existing infrastructures for the production of sustainable value-added products | Bioenergy n.d. https://www.ieabioenergy.com/blog/publications/gasification-applications-in-existing-infrastructures-for-the-production-of-sustainable-value-added-products/ (accessed December 22, 2023).
[54] Higman C. Gasification process technology. Advances in Clean Hydrocarbon Fuel Processing: Science and Technology 2011:155–85. https://doi.org/10.1533/9780857093783.2.155.
[55] Ram M, Mondal MK. Biomass gasification: a step toward cleaner fuel and chemicals. Biofuels and Bioenergy: Opportunities and Challenges 2022:253–76. https://doi.org/10.1016/B978-0-323-85269-2.00008-3.
[56] Sikarwar VS, Zhao M. Biomass Gasification. Encyclopedia of Sustainable Technologies 2017:205–16. https://doi.org/10.1016/B978-0-12-409548-9.10533-0.
[57] Bermudez JM, Fidalgo B. Production of bio-syngas and bio-hydrogen via gasification. Handbook of Biofuels Production: Processes and Technologies: Second Edition 2016:431–94. https://doi.org/10.1016/B978-0-08-100455-5.00015-1.
[58] Guangul FM, Sulaiman SA, Ramli A. Study of the effects of operating factors on the resulting producer gas of oil palm fronds gasification with a single throat downdraft gasifier. Renew Energy 2014;72:271–83. https://doi.org/10.1016/J.RENENE.2014.07.022.
[59] Hendriyana H. Effect of Equivalence Ratio on the Rice Husk Gasification Performance Using Updraft Gasifier with Air Suction Mode. Jurnal Bahan Alam Terbarukan 2020;9:30–5. https://doi.org/10.15294/JBAT.V9I1.23527.
[60] Higman C, Van der Burgt M. Gasification. Gasification 2008:1–435. https://doi.org/10.1016/B978-0-7506-8528-3.X0001-6.
[61] Sansaniwal SK, Pal K, Rosen MA, Tyagi SK. Recent advances in the development of biomass gasification technology: A comprehensive review. Renewable and Sustainable Energy Reviews 2017;72:363–84. https://doi.org/10.1016/J.RSER.2017.01.038.

[62] Klass DL. Chapter 12 - Microbial Conversion: Gasification. Elsevier; 1998.
[63] Ahrenfeldt Jesper, Knoef Harrie, GasNet. Handbook biomass gasification 2005:378.
[64] ALL Power Labs n.d. https://www.allpowerlabs.com/ (accessed January 10, 2024).
[65] Su G, Ong HC, Mofijur M, Mahlia TMI, Ok YS. Pyrolysis of waste oils for the production of biofuels: A critical review. J Hazard Mater 2022;424:127396. https://doi.org/10.1016/J.JHAZMAT.2021.127396.
[66] Hoang AT, Ong HC, Fattah IMR, Chong CT, Cheng CK, Sakthivel R, et al. Progress on the lignocellulosic biomass pyrolysis for biofuel production toward environmental sustainability. Fuel Processing Technology 2021;223:106997. https://doi.org/10.1016/J.FUPROC.2021.106997.
[67] Piskorz J, Scott DS, Radlein D. Composition of oils obtained by fast pyrolysis of different woods. ACS Symposium Series 1988:167–78. https://doi.org/10.1021/BK-1988-0376.CH016.
[68] Diebold JP, Bridgwater A V. Overview of Fast Pyrolysis of Biomass for the Production of Liquid Fuels. Developments in Thermochemical Biomass Conversion 1997:5–23. https://doi.org/10.1007/978-94-009-1559-6_1.
[69] Lee M, Ko H, Oh S. Pyrolysis of Solid Recovered Fuel Using Fixed and Fluidized Bed Reactors. Molecules 2023, Vol 28, Page 7815 2023;28:7815. https://doi.org/10.3390/MOLECULES28237815.
[70] Safdari MS, Amini E, Weise DR, Fletcher TH. Heating rate and temperature effects on pyrolysis products from live wildland fuels. Fuel 2019;242:295–304. https://doi.org/10.1016/J.FUEL.2019.01.040.
[71] Shen Q, Wu H. Rapid pyrolysis of biochar prepared from slow and fast pyrolysis: The effects of particle residence time on char properties. Proceedings of the Combustion Institute 2023;39:3371–8. https://doi.org/10.1016/J.PROCI.2022.07.119.
[72] Sun J, He F, Pan Y, Zhang Z. Effects of pyrolysis temperature and residence time on physicochemical properties of different biochar types. Acta Agric Scand B Soil Plant Sci 2017;67:12–22. https://doi.org/10.1080/09064710.2016.1214745.
[73] Tomczyk A, Sokołowska Z, Boguta P. Biochar physicochemical properties: pyrolysis temperature and feedstock kind effects. Rev Environ Sci Biotechnol 2020;19:191–215. https://doi.org/10.1007/S11157-020-09523-3/TABLES/3.
[74] Ippolito JA, Laird DA, Busscher WJ. Environmental Benefits of Biochar. J Environ Qual 2012;41:967–72. https://doi.org/10.2134/JEQ2012.0151.
[75] Giorcelli M, Bartoli M, Sanginario A, Padovano E, Rosso C, Rovere M, et al. High-Temperature Annealed Biochar as a Conductive Filler for the Production of Piezoresistive Materials for Energy Conversion Application. ACS Appl Electron Mater 2021;3:838–44. https://doi.org/10.1021/ACSAELM.0C00971/SUPPL_FILE/EL0C00971_SI_001.MP4.
[76] Safarian S. Performance analysis of sustainable technologies for biochar production: A comprehensive review. Energy Reports 2023;9:4574–93. https://doi.org/10.1016/J.EGYR.2023.03.111.
[77] Danesh P, Niaparast P, Ghorbannezhad P, Ali I. Biochar Production: Recent Developments, Applications, and challenges. Fuel 2023;337:126889. https://doi.org/10.1016/J.FUEL.2022.126889.

[78] Lehmann J, Gaunt J, Rondon M. Bio-char sequestration in terrestrial ecosystems - A review. Mitig Adapt Strateg Glob Chang 2006;11:403–27. https://doi.org/10.1007/S11027-005-9006-5/METRICS.
[79] International Biochar Initiative. Standardized Product Definition and Product Testing Guidelines for Biochar That Is Used in Soil - IBI Biochar Standards, Version 2.1 n.d.
[80] Glaser B, Haumaier L, Guggenberger G, Zech W. The "Terra Preta" phenomenon: A model for sustainable agriculture in the humid tropics. Naturwissenschaften 2001;88:37–41. https://doi.org/10.1007/S001140000193/METRICS.
[81] Steiner C, Teixeira WG, Woods WI, Zech W. Indigenous knowledge about terra preta formation. Amazonian Dark Earths: Wim Sombroek's Vision 2009:193–204. https://doi.org/10.1007/978-1-4020-9031-8_9/COVER.
[82] Ippolito JA, Laird DA, Busscher WJ. Environmental Benefits of Biochar. J Environ Qual 2012;41:967–72. https://doi.org/10.2134/JEQ2012.0151.
[83] Lehmann J. Bioenergy: carbon neutral (reduces emissions from fossil fuels). n.d.
[84] Lehmann J, Joseph S. Biochar for Environmental Management: Science and Technology. Earthscan; 2009. https://doi.org/10.1016/J.FORPOL.2009.07.001.
[85] Wang J, Wang S. Preparation, modification and environmental application of biochar: A review. J Clean Prod 2019;227:1002–22. https://doi.org/10.1016/J.JCLEPRO.2019.04.282.
[86] Wang J, Liao Z, Ifthikar J, Shi L, Du Y, Zhu J, et al. Treatment of refractory contaminants by sludge-derived biochar/persulfate system via both adsorption and advanced oxidation process. Chemosphere 2017;185:754–63. https://doi.org/10.1016/J.CHEMOSPHERE.2017.07.084.
[87] Yoo S, Kelley SS, Tilotta DC, Park S. Structural Characterization of Loblolly Pine Derived Biochar by X-ray Diffraction and Electron Energy Loss Spectroscopy. ACS Sustain Chem Eng 2018;6:2621–9. https://doi.org/10.1021/ACSSUSCHEMENG.7B04119/SUPPL_FILE/SC7B04119_SI_001.PDF.
[88] Hansen V, Müller-Stöver D, Munkholm LJ, Peltre C, Hauggaard-Nielsen H, Jensen LS. The effect of straw and wood gasification biochar on carbon sequestration, selected soil fertility indicators and functional groups in soil: An incubation study. Geoderma 2016;269:99–107. https://doi.org/10.1016/J.GEODERMA.2016.01.033.
[89] Reguyal F, Sarmah AK, Gao W. Synthesis of magnetic biochar from pine sawdust via oxidative hydrolysis of FeCl2 for the removal sulfamethoxazole from aqueous solution. J Hazard Mater 2017;321:868–78. https://doi.org/10.1016/J.JHAZMAT.2016.10.006.
[90] Wiedner K, Rumpel C, Steiner C, Pozzi A, Maas R, Glaser B. Chemical evaluation of chars produced by thermochemical conversion (gasification, pyrolysis and hydrothermal carbonization) of agro-industrial biomass on a commercial scale. Biomass Bioenergy 2013;59:264–78. https://doi.org/10.1016/J.BIOMBIOE.2013.08.026.
[91] van Zwieten L, Kimber S, Morris S, Chan KY, Downie A, Rust J, et al. Effects of biochar from slow pyrolysis of papermill waste on agronomic performance and soil fertility. Plant Soil 2010;327:235–46. https://doi.org/10.1007/S11104-009-0050-X/TABLES/6.

[92] Fellet G, Marchiol L, Delle Vedove G, Peressotti A. Application of biochar on mine tailings: Effects and perspectives for land reclamation. Chemosphere 2011;83:1262–7. https://doi.org/10.1016/J.CHEMOSPHERE.2011.03.053.
[93] Wiedemeier DB, Abiven S, Hockaday WC, Keiluweit M, Kleber M, Masiello CA, et al. Aromaticity and degree of aromatic condensation of char. Org Geochem 2015;78:135–43. https://doi.org/10.1016/J.ORGGEOCHEM.2014.10.002.
[94] Mia S, Dijkstra FA, Singh B. Long-Term Aging of Biochar: A Molecular Understanding With Agricultural and Environmental Implications. Advances in Agronomy, vol. 141, Academic Press Inc.; 2017, p. 1–51. https://doi.org/10.1016/bs.agron.2016.10.001.
[95] Nguyen BT, Lehmann J, Hockaday WC, Joseph S, Masiello CA. Temperature sensitivity of black carbon decomposition and oxidation. Environ Sci Technol 2010;44:3324–31. https://doi.org/10.1021/ES903016Y/SUPPL_FILE/ES903016Y_SI_001.PDF.
[96] Adriana Downie, Alan Crosky, Paul Munroe. Physical Properties of Biochar | 9 | Biochar for Environmental Managem, 2009.
[97] More RB, Bokros JC. Biomaterials: Carbon. Encyclopedia of Medical Devices and Instrumentation 2006. https://doi.org/10.1002/0471732877.EMD023.
[98] Leng L, Huang H, Li H, Li J, Zhou W. Biochar stability assessment methods: A review. Science of The Total Environment 2019;647:210–22. https://doi.org/10.1016/J.SCITOTENV.2018.07.402.
[99] Adhikari S, Moon E, Paz-Ferreiro J, Timms W. Comparative analysis of biochar carbon stability methods and implications for carbon credits. Science of The Total Environment 2023:169607. https://doi.org/10.1016/J.SCITOTENV.2023.169607.
[100] Han L, Sun K, Yang Y, Xia X, Li F, Yang Z, et al. Biochar's stability and effect on the content, composition and turnover of soil organic carbon. Geoderma 2020;364:114184. https://doi.org/10.1016/J.GEODERMA.2020.114184.
[101] Spokas KA. Review of the stability of biochar in soils: Predictability of O:C molar ratios. Carbon Manag 2010;1:289–303. https://doi.org/10.4155/CMT.10.32/SUPPL_FILE/SUPPL_TABLE.DOC.
[102] Lehmann J, Rillig MC, Thies J, Masiello CA, Hockaday WC, Crowley D. Biochar effects on soil biota – A review. Soil Biol Biochem 2011;43:1812–36.
[103] Wang L, Gao C, Yang K, Sheng Y, Xu J, Zhao Y, et al. Effects of biochar aging in the soil on its mechanical property and performance for soil CO2 and N2O emissions. Sci Total Environ 2021;782. https://doi.org/10.1016/J.SCITOTENV.2021.146824.
[104] Fearnside PM. WHY A 100-YEAR TIME HORIZON SHOULD BE USED FOR GLOBAL WARMING MITIGATION CALCULATIONS. 2002.
[105] Sidik F, Lawrence A, Wagey T, Zamzani F, Lovelock CE. Blue carbon: A new paradigm of mangrove conservation and management in Indonesia. Mar Policy 2023;147. https://doi.org/10.1016/j.marpol.2022.105388.
[106] Lefebvre D, Fawzy S, Aquije CA, Osman AI, Draper KT, Trabold TA. Biomass residue to carbon dioxide removal: quantifying the global impact of biochar. Biochar 2023;5:1–17. https://doi.org/10.1007/S42773-023-00258-2/FIGURES/8.
[107] Ippolito JA, Laird DA, Busscher WJ. Environmental Benefits of Biochar. J Environ Qual 2012;41:967–72. https://doi.org/10.2134/jeq2012.0151.
[108] Lehmann J. Bio-energy in the black. Front Ecol Environ 2007;5:381–7. https://doi.org/10.1890/1540-9295(2007)5[381:BITB]2.0.CO;2.

[109] Joseph S, Husson O, Graber ER, Van Zwieten L, Taherymoosavi S, Thomas T, et al. The Electrochemical Properties of Biochars and How They Affect Soil Redox Properties and Processes. Agronomy 2015, Vol 5, Pages 322-340 2015;5:322–40. https://doi.org/10.3390/AGRONOMY5030322.
[110] Kwon JH, Park SB, Ayrilmis N, Oh SW, Kim NH. Effect of carbonization temperature on electrical resistivity and physical properties of wood and wood-based composites. Compos B Eng 2013;46:102–7. https://doi.org/10.1016/J.COMPOSITESB.2012.10.012.
[111] Prévoteau A, Ronsse F, Cid I, Boeckx P, Rabaey K. The electron donating capacity of biochar is dramatically underestimated. Scientific Reports 2016 6:1 2016;6:1–11. https://doi.org/10.1038/srep32870.
[112] Sun T, Levin BDA, Guzman JJL, Enders A, Muller DA, Angenent LT, et al. Rapid electron transfer by the carbon matrix in natural pyrogenic carbon. Nature Communications 2017 8:1 2017;8:1–12. https://doi.org/10.1038/ncomms14873.
[113] Ippolito JA, Cui L, Kammann C, Wrage-Mönnig N, Estavillo JM, Fuertes-Mendizabal T, et al. Feedstock choice, pyrolysis temperature and type influence biochar characteristics: a comprehensive meta-data analysis review. Biochar 2020;2:421–38. https://doi.org/10.1007/S42773-020-00067-X/TABLES/6.
[114] Fryda L, Visser R. Biochar for Soil Improvement: Evaluation of Biochar from Gasification and Slow Pyrolysis. Agriculture 2015, Vol 5, Pages 1076-1115 2015;5:1076–115. https://doi.org/10.3390/AGRICULTURE5041076.
[115] Antal MJ, Grønli M. The Art, Science, and Technology of Charcoal Production†. Ind Eng Chem Res 2003;42:1619–40. https://doi.org/10.1021/IE0207919.
[116] Bagreev A, Bandosz TJ, Locke DC. Pore structure and surface chemistry of adsorbents obtained by pyrolysis of sewage sludge-derived fertilizer. Carbon N Y 2001;39:1971–9. https://doi.org/10.1016/S0008-6223(01)00026-4.
[117] Zhang X, Han R, Liu Y, Li H, Shi W, Yan X, et al. Porous and graphitic structure optimization of biomass-based carbon materials from 0D to 3D for supercapacitors: A review. Chemical Engineering Journal 2023;460:141607. https://doi.org/10.1016/J.CEJ.2023.141607.
[118] Leng L, Xiong Q, Yang L, Li H, Zhou Y, Zhang W, et al. An overview on engineering the surface area and porosity of biochar. Science of The Total Environment 2021;763:144204. https://doi.org/10.1016/J.SCITOTENV.2020.144204.
[119] Yang H, Huan B, Chen Y, Gao Y, Li J, Chen H. Biomass-Based Pyrolytic Polygeneration System for Bamboo Industry Waste: Evolution of the Char Structure and the Pyrolysis Mechanism. Energy and Fuels 2016;30:6430–9. https://doi.org/10.1021/ACS.ENERGYFUELS.6B00732/SUPPL_FILE/EF6B00732_SI_001.PDF.
[120] Brunauer S, Emmett PH, Teller E. Adsorption of Gases in Multimolecular Layers. J Am Chem Soc 1938;60:309–19. https://doi.org/10.1021/JA01269A023/ASSET/JA01269A023.FP.PNG_V03.
[121] Palansooriya KN, Wong JTF, Hashimoto Y, Huang L, Rinklebe J, Chang SX, et al. Response of microbial communities to biochar-amended soils: a critical review. Biochar 2019 1:1 2019;1:3–22. https://doi.org/10.1007/S42773-019-00009-2.
[122] Lebrun M, Nandillon R, Miard F, Bourgerie S, Morabito D. Biochar assisted phytoremediation for metal(loid) contaminated soils. Assisted Phytoremediation 2022:101–30. https://doi.org/10.1016/B978-0-12-822893-7.00010-0.

[123] Cheng CH, Lehmann J, Engelhard MH. Natural oxidation of black carbon in soils: Changes in molecular form and surface charge along a climosequence. Geochim Cosmochim Acta 2008;72:1598–610. https://doi.org/10.1016/J.GCA.2008.01.010.
[124] Suliman W, Harsh JB, Abu-Lail NI, Fortuna AM, Dallmeyer I, Garcia-Perez M. Influence of feedstock source and pyrolysis temperature on biochar bulk and surface properties. Biomass Bioenergy 2016;84:37–48. https://doi.org/10.1016/J.BIOMBIOE.2015.11.010.
[125] Roshan A, Ghosh D, Maiti SK. How temperature affects biochar properties for application in coal mine spoils? A meta-analysis. Carbon Research 2023;2:1–17. https://doi.org/10.1007/S44246-022-00033-1/TABLES/2.
[126] Gomez-Eyles JL, Moreno-Jiménez E, Sizmur T. The potential of biochar amendments to remediate contaminated soils n.d. https://doi.org/10.13140/2.1.1074.9448.
[127] Adhikari S, Mahmud MAP, Nguyen MD, Timms W. Evaluating fundamental biochar properties in relation to water holding capacity. Chemosphere 2023;328:138620. https://doi.org/10.1016/J.CHEMOSPHERE.2023.138620.
[128] Adhikari S, Timms W, Mahmud MAP. Optimising water holding capacity and hydrophobicity of biochar for soil amendment – A review. Science of The Total Environment 2022;851:158043. https://doi.org/10.1016/J.SCITOTENV.2022.158043.
[129] Batista EMCC, Shultz J, Matos TTS, Fornari MR, Ferreira TM, Szpoganicz B, et al. Effect of surface and porosity of biochar on water holding capacity aiming indirectly at preservation of the Amazon biome. Scientific Reports 2018 8:1 2018;8:1–9. https://doi.org/10.1038/s41598-018-28794-z.
[130] Singh B, Dolk MM, Shen Q, Camps-Arbestain M. Biochar pH, electrical conductivity and liming potential, CSIRO PUBLISHING; n.d.
[131] Baronti S, Vaccari FP, Miglietta F, Calzolari C, Lugato E, Orlandini S, et al. Impact of biochar application on plant water relations in Vitis vinifera (L.). European Journal of Agronomy 2014;53:38–44. https://doi.org/10.1016/J.EJA.2013.11.003.
[132] Rezaei A, Kamali B, Kamali AR. Correlation between morphological, structural and electrical properties of graphite and exfoliated graphene nanostructures. Measurement 2020;150:107087. https://doi.org/10.1016/J.MEASUREMENT.2019.107087.
[133] Allesina G, Pedrazzi S, Allegretti F, Morselli N, Puglia M, Santunione G, et al. Gasification of cotton crop residues for combined power and biochar production in Mozambique. Appl Therm Eng 2018;139:387–94. https://doi.org/10.1016/J.APPLTHERMALENG.2018.04.115.
[134] Zhu X, Chen B, Zhu L, Xing B. Effects and mechanisms of biochar-microbe interactions in soil improvement and pollution remediation: A review. Environmental Pollution 2017;227:98–115. https://doi.org/10.1016/J.ENVPOL.2017.04.032.
[135] dos Santos Sousa EDT, de Queiroz DM, de Freitas Coelho AL, Valente DSM. Development of signal analysis algorithm for apparent soil electrical conductivity sensor. Biosyst Eng 2021;211:183–91. https://doi.org/10.1016/J.BIOSYSTEMSENG.2021.09.007.

[136] Reguera G, McCarthy KD, Mehta T, Nicoll JS, Tuominen MT, Lovley DR. Extracellular electron transfer via microbial nanowires. Nature 2005;435:1098–101. https://doi.org/10.1038/NATURE03661.
[137] Chen S, Rotaru AE, Shrestha PM, Malvankar NS, Liu F, Fan W, et al. Promoting Interspecies Electron Transfer with Biochar. Scientific Reports 2014 4:1 2014;4:1–7. https://doi.org/10.1038/srep05019.
[138] Marinho B, Ghislandi M, Tkalya E, Koning CE, de With G. Electrical conductivity of compacts of graphene, multi-wall carbon nanotubes, carbon black, and graphite powder. Powder Technol 2012;221:351–8. https://doi.org/10.1016/J.POWTEC.2012.01.024.
[139] Researchers discover high-def electron pathways in soil | Cornell Chronicle n.d. https://news.cornell.edu/stories/2017/03/researchers-discover-high-def-electron-pathways-soil (accessed January 9, 2024).
[140] Kocsis T, Ringer M, Biró B. Characteristics and Applications of Biochar in Soil–Plant Systems: A Short Review of Benefits and Potential Drawbacks. Applied Sciences 2022, Vol 12, Page 4051 2022;12:4051. https://doi.org/10.3390/APP12084051.
[141] Mukherjee S, Sarkar B, Aralappanavar VK, Mukhopadhyay R, Basak BB, Srivastava P, et al. Biochar-microorganism interactions for organic pollutant remediation: Challenges and perspectives. Environmental Pollution 2022;308:119609. https://doi.org/10.1016/J.ENVPOL.2022.119609.
[142] Semida WM, Beheiry HR, Sétamou M, Simpson CR, Abd El-Mageed TA, Rady MM, et al. Biochar implications for sustainable agriculture and environment: A review. South African Journal of Botany 2019;127:333–47. https://doi.org/10.1016/J.SAJB.2019.11.015.
[143] Graber ER, Harel YM, Kolton M, Cytryn E, Silber A, David DR, et al. Biochar impact on development and productivity of pepper and tomato grown in fertigated soilless media. Plant Soil 2010;337:481–96. https://doi.org/10.1007/S11104-010-0544-6.
[144] Agegnehu G, Srivastava AK, Bird MI. The role of biochar and biochar-compost in improving soil quality and crop performance: A review. Applied Soil Ecology 2017;119:156–70. https://doi.org/10.1016/J.APSOIL.2017.06.008.
[145] Gholamahmadi B, Jeffery S, Gonzalez-Pelayo O, Prats SA, Bastos AC, Keizer JJ, et al. Biochar impacts on runoff and soil erosion by water: A systematic global scale meta-analysis. Science of The Total Environment 2023;871:161860. https://doi.org/10.1016/J.SCITOTENV.2023.161860.
[146] Neogi S, Sharma V, Khan N, Chaurasia D, Ahmad A, Chauhan S, et al. Sustainable biochar: A facile strategy for soil and environmental restoration, energy generation, mitigation of global climate change and circular bioeconomy. Chemosphere 2022;293:133474. https://doi.org/10.1016/J.CHEMOSPHERE.2021.133474.
[147] Escuer O, Karp K, Escuer-Gatius J, Raave H, Teppand T, Shanskiy M. Hardwood biochar as an alternative to reduce peat use for seed germination and growth of Tagetes patula. Acta Agric Scand B Soil Plant Sci 2021;71:408–21. https://doi.org/10.1080/09064710.2021.1903986.
[148] Godlewska P, Schmidt HP, Ok YS, Oleszczuk P. Biochar for composting improvement and contaminants reduction. A review. Bioresour Technol 2017;246:193–202.

[149] Li R, Wang Q, Zhang Z, Zhang G, Li Z, Wang L, et al. Nutrient transformation during aerobic composting of pig manure with biochar prepared at different temperatures. Environ Technol 2015;36:815–26. https://doi.org/10.1080/09593330.2014.963692.
[150] Thomas Bachmann R, A Husni MH, W SA. Characterization of local mill rice husk charcoal and its effect on compost properties. n.d.
[151] Zhang J, Chen G, Sun H, Zhou S, Zou G. Straw biochar hastens organic matter degradation and produces nutrient-rich compost. Bioresour Technol 2016;200:876–83. https://doi.org/10.1016/j.biortech.2015.11.016.
[152] Chen Y-X, Huang X-D, Han Z-Y, Huang X, Hu B, Shi D-Z, et al. Effects of bamboo charcoal and bamboo vinegar on nitrogen conservation and heavy metals immobility during pig manure composting. Chemosphere 2010;78:1177–81. https://doi.org/10.1016/j.chemosphere.2009.12.029.
[153] Cayuela ML, Sánchez-Monedero MA, Roig A, Hanley K, Enders A, Lehmann J. Biochar and denitrification in soils: when, how much and why does biochar reduce N2O emissions? Scientific Reports 2013 3:1 2013;3:1–7. https://doi.org/10.1038/srep01732.
[154] Sánchez-Monedero MA, Cayuela ML, Sánchez-García M, Vandecasteele B, D'Hose T, López G, et al. Agronomic Evaluation of Biochar, Compost and Biochar-Blended Compost across Different Cropping Systems: Perspective from the European Project FERTIPLUS. Agronomy 2019, Vol 9, Page 225 2019;9:225. https://doi.org/10.3390/AGRONOMY9050225.
[155] Khan N, Clark I, Sánchez-Monedero MA, Shea S, Meier S, Qi F, et al. Physical and chemical properties of biochars co-composted with biowastes and incubated with a chicken litter compost. Chemosphere 2016;142:14–23. https://doi.org/10.1016/j.chemosphere.2015.05.065.
[156] Antonangelo JA, Sun X, Zhang H. The roles of co-composted biochar (COMBI) in improving soil quality, crop productivity, and toxic metal amelioration. J Environ Manage 2021;277. https://doi.org/10.1016/j.jenvman.2020.111443.
[157] Cao Y, Wang X, Bai Z, Chadwick D, Misselbrook T, G. Sommer S, et al. Mitigation of ammonia, nitrous oxide and methane emissions during solid waste composting with different additives: A meta-analysis. J Clean Prod 2019;235:626–35. https://doi.org/10.1016/J.JCLEPRO.2019.06.288.
[158] Sonoki T, Furukawa T, Jindo K, Suto K, Aoyama M, Sánchez-Monedero MÁ. Influence of biochar addition on methane metabolism during thermophilic phase of composting. J Basic Microbiol 2013;53:617–21. https://doi.org/10.1002/jobm.201200096.
[159] Nguyen BT, Trinh NN, Bach QV. Methane emissions and associated microbial activities from paddy salt-affected soil as influenced by biochar and cow manure addition. Applied Soil Ecology 2020;152:103531. https://doi.org/10.1016/J.APSOIL.2020.103531.
[160] Wang C, Lu H, Dong D, Deng H, Strong PJ, Wang H, et al. Insight into the effects of biochar on manure composting: Evidence supporting the relationship between N2O emission and denitrifying community. Environ Sci Technol 2013;47:7341–9. https://doi.org/10.1021/ES305293H/SUPPL_FILE/ES305293H_SI_001.PDF.
[161] Vandecasteele B, Sinicco T, D'Hose T, Vanden Nest T, Mondini C. Biochar amendment before or after composting affects compost quality and N losses, but

not P plant uptake. J Environ Manage 2016;168:200–9. https://doi.org/10.1016/j.jenvman.2015.11.045.
[162] Sánchez-García M, Alburquerque JA, Sánchez-Monedero MA, Roig A, Cayuela ML. Biochar accelerates organic matter degradation and enhances N mineralisation during composting of poultry manure without a relevant impact on gas emissions. Bioresour Technol 2015;192:272–9. https://doi.org/10.1016/j.biortech.2015.05.003.
[163] Dong W, Walkiewicz A, Bieganowski A, Oenema O, Nosalewicz M, He C, et al. Biochar promotes the reduction of N2O to N2 and concurrently suppresses the production of N2O in calcareous soil. Geoderma 2020;362:114091. https://doi.org/10.1016/J.GEODERMA.2019.114091.
[164] Yin Y, Yang C, Li M, Zheng Y, Ge C, Gu J, et al. Research progress and prospects for using biochar to mitigate greenhouse gas emissions during composting: A review. Science of the Total Environment 2021;798:149294. https://doi.org/10.1016/j.scitotenv.2021.149294.
[165] Baral KR, McIlroy J, Lyons G, Johnston C. The effect of biochar and acid activated biochar on ammonia emissions during manure storage. Environmental Pollution 2023;317:120815. https://doi.org/10.1016/J.ENVPOL.2022.120815.
[166] Sahin U, Cakmakci T, Yerli C. Biochar and mycorrhiza enhance soil carbon storage and reduce CO2 emissions in wastewater-irrigated turf. Journal of Water and Climate Change 2023;14:3280–92. https://doi.org/10.2166/WCC.2023.270.
[167] Wang J, Xiong Z, Kuzyakov Y. Biochar stability in soil: meta-analysis of decomposition and priming effects. GCB Bioenergy 2016;8:512–23. https://doi.org/10.1111/GCBB.12266.
[168] Minasny B, Malone BP, McBratney AB, Angers DA, Arrouays D, Chambers A, et al. Soil carbon 4 per mille. Geoderma 2017;292:59–86. https://doi.org/10.1016/J.GEODERMA.2017.01.002.
[169] Zimmerman AR, Gao B, Ahn MY. Positive and negative carbon mineralization priming effects among a variety of biochar-amended soils. Soil Biol Biochem 2011;43:1169–79. https://doi.org/10.1016/J.SOILBIO.2011.02.005.
[170] Chen G, Fang Y, Van Zwieten L, Xuan Y, Tavakkoli E, Wang X, et al. Priming, stabilization and temperature sensitivity of native SOC is controlled by microbial responses and physicochemical properties of biochar. Soil Biol Biochem 2021;154:108139. https://doi.org/10.1016/J.SOILBIO.2021.108139.
[171] Fang Y, Singh B, Singh BP. Effect of temperature on biochar priming effects and its stability in soils. Soil Biol Biochem 2015;80:136–45. https://doi.org/10.1016/J.SOILBIO.2014.10.006.
[172] World Business Council for Sustainable Development, South Pole. Removing carbon responsibly A guide for business on carbon removal adoption. n.d.
[173] SYNCRAFT® - Das Holzkraftwerk n.d. https://en.syncraft.at/ (accessed January 11, 2024).
[174] Home - PYREG GmbH n.d. https://pyreg.com/ (accessed January 11, 2024).
[175] Carbofex - Carbofex n.d. https://carbofex.fi/ (accessed January 11, 2024).
[176] Technology | Eco n.d. https://www.glock-ecotech.com/en/technology (accessed January 11, 2024).
[177] CharTainer - Pilot Unit - ALL Power Labs n.d. https://www.allpowerlabs.com/chartainer (accessed January 11, 2024).

[178] Fit for 55: reform of the EU emissions trading system - Consilium 2023. https://www.consilium.europa.eu/en/infographics/fit-for-55-eu-emissions-trading-system/ (accessed November 23, 2023).
[179] Guan P, Prasher SO, Afzal MT, George S, Ronholm J, Dhiman J, et al. Removal of Escherichia coli from lake water in a biochar-amended biosand filtering system. Ecol Eng 2020;150. https://doi.org/10.1016/J.ECOLENG.2020.105819.
[180] Mamera M, van Tol JJ, Aghoghovwia MP. Treatment of faecal sludge and sewage effluent by pinewood biochar to reduce wastewater bacteria and inorganic contaminants leaching. Water Res 2022;221:118775. https://doi.org/10.1016/J.WATRES.2022.118775.
[181] Razzaghi F, Obour PB, Arthur E. Does biochar improve soil water retention? A systematic review and meta-analysis. Geoderma 2020;361:114055. https://doi.org/10.1016/J.GEODERMA.2019.114055.
[182] Puglia M, Pedrazzi S, Allesina G, Morselli N, Tartarini P. Carbonization of Residual Biomass from River Maintenance Using Waste Heat from Gasification Power Plants, Copenhagen 2018: EtaFlorence; 2018, p. 1127–30.
[183] European Committee for Standardization. CEN/TS 15439:2006 - Biomass gasification - Tar and particles in product gases - Sampling and analysis n.d. https://standards.iteh.ai/catalog/standards/cen/868fa730-a77f-4a6c-8e28-e135fa7962a4/cen-ts-15439-2006 (accessed January 24, 2024).
[184] ASTM. Standard Test Method for Ash in Biomass. 2010.
[185] Basso AS, Miguez FE, Laird DA, Horton R, Westgate M. Assessing potential of biochar for increasing water-holding capacity of sandy soils. GCB Bioenergy 2013;5:132–43. https://doi.org/10.1111/GCBB.12026.
[186] Giupponi L, Leoni V, Carrer M, Ceciliani G, Sala S, Panseri S, et al. Overview on Italian hemp production chain, related productive and commercial activities and legislative framework. Italian Journal of Agronomy 2020;15:194–205. https://doi.org/10.4081/IJA.2020.1552.
[187] Summers HM, Sproul E, Quinn JC. The greenhouse gas emissions of indoor cannabis production in the United States. Nature Sustainability 2021 4:7 2021;4:644–50. https://doi.org/10.1038/s41893-021-00691-w.
[188] Net Zero by 2050: A Roadmap for the Global Energy Sector. International Energy Agency. 2021. n.d.
[189] Shukla PR, Skea J, Slade R. Working Group III Contribution to the Sixth Assessment Report of the Intergovernmental Panel on Climate Change n.d.
[190] Smith P. Soil carbon sequestration and biochar as negative emission technologies. Glob Chang Biol 2016;22:1315–24.
[191] Woolf D, Amonette J, Street-Perrott F, al. et. Sustainable biochar to mitigate global climate change. Nat Commun 2010;1:56.
[192] Abd Alla S, Bianco V, Scarpa F, Tagliafico LA. Electrification of the residential heat demand: An analysis of the power market potential to accommodate heat pumps. Thermal Science and Engineering Progress 2022;27:101173. https://doi.org/10.1016/j.tsep.2021.101173.
[193] Naumann G, Schropp E, Gaderer M. Life Cycle Assessment of an Air-Source Heat Pump and a Condensing Gas Boiler Using an Attributional and a Consequential Approach. Procedia CIRP 2022;105:351–6. https://doi.org/10.1016/j.procir.2022.02.058.

[194] Song M, Deng S, Dang C, Mao N, Wang Z. Review on improvement for air source heat pump units during frosting and defrosting. Appl Energy 2018;211:1150–70. https://doi.org/10.1016/j.apenergy.2017.12.022.
[195] Kim B-J, Jo S-Y, Jeong J-W. Energy performance enhancement in air-source heat pump with a direct evaporative cooler-applied condenser. Case Studies in Thermal Engineering 2022;35:102137. https://doi.org/10.1016/j.csite.2022.102137.
[196] Cheng X. Integrated Energy System in a Green Energy Lab. In: Wang R, Zhai X, editors. Handbook of Energy Systems in Green Buildings, Berlin, Heidelberg: Springer Berlin Heidelberg; 2017, p. 1–40.
[197] Raymond J, Mercier S, Nguyen L. Designing coaxial ground heat exchangers with a thermally enhanced outer pipe. Geothermal Energy 2015;3:7. https://doi.org/10.1186/s40517-015-0027-3.
[198] Go G-H, Lee S-R, Yoon S, Kim M-J. Optimum design of horizontal ground-coupled heat pump systems using spiral-coil-loop heat exchangers. Appl Energy 2016;162:330–45. https://doi.org/10.1016/j.apenergy.2015.10.113.
[199] Cui Y, Zhu J, Twaha S, Chu J, Bai H, Huang K, et al. Techno-economic assessment of the horizontal geothermal heat pump systems: A comprehensive review. Energy Convers Manag 2019;191:208–36. https://doi.org/10.1016/J.ENCONMAN.2019.04.018.
[200] Hou G, Taherian H, Song Y, Jiang W, Chen D. A systematic review on optimal analysis of horizontal heat exchangers in ground source heat pump systems. Renewable and Sustainable Energy Reviews 2022;154:111830. https://doi.org/10.1016/j.rser.2021.111830.
[201] Florides G, Theofanous E, Iosif-Stylianou I, Tassou S, Christodoulides P, Zomeni Z, et al. Modeling and assessment of the efficiency of horizontal and vertical ground heat exchangers. Energy 2013;58:655–63. https://doi.org/10.1016/j.energy.2013.05.053.
[202] Maghrabie HM, Abdeltwab MM, Tawfik MHM. Ground-source heat pumps (GSHPs): Materials, models, applications, and sustainability. Energy Build 2023;299:113560. https://doi.org/10.1016/j.enbuild.2023.113560.
[203] Wan R, Kong D, Kang J, Yin T, Ning J, Ma J. The experimental study on thermal conductivity of backfill material of ground source heat pump based on iron tailings. Energy Build 2018;174:1–12. https://doi.org/10.1016/j.enbuild.2018.06.010.
[204] Bernier MA, Chahla A, Pinel P. Long-term ground-temperature changes in geo-exchange systems. ASHRAE Trans 2008;114:342+.
[205] Zimmerman RW. Thermal conductivity of fluid-saturated rocks. J Pet Sci Eng 1989;3:219–27. https://doi.org/10.1016/0920-4105(89)90019-3.
[206] Rashid FL, Dhaidan NS, Hussein AK, Al-Mousawi FN, Younis O. Ground heat exchanger in different configuration: Review of recent advances and development. Geoenergy Science and Engineering 2023;227:211872. https://doi.org/10.1016/j.geoen.2023.211872.
[207] Bortoloni M, Bottarelli M, Su Y. A study on the effect of ground surface boundary conditions in modelling shallow ground heat exchangers. Appl Therm Eng 2017;111:1371–7. https://doi.org/10.1016/j.applthermaleng.2016.05.063.

[208] Usowicz B, Lipiec J, Łukowski M, Bis Z, Usowicz J, Latawiec AE. Impact of biochar addition on soil thermal properties: Modelling approach. Geoderma 2020;376. https://doi.org/10.1016/J.GEODERMA.2020.114574.
[209] Liu W, Li R, Wu T, Shi X, Zhao L, Wu X, et al. Simulation of soil thermal conductivity based on different schemes: An empirical comparison of 13 models. International Journal of Thermal Sciences 2023;190:108301. https://doi.org/10.1016/J.IJTHERMALSCI.2023.108301.
[210] Livello delle acque sotterranee n.d. https://webbook.arpae.it/indicatore/Livello-delle-acque-sotterranee-00001/?id=19a0fc0d-7558-11e4-8845-11c9866a0f33 (accessed January 26, 2024).
[211] Patwa D, Bordoloi U, Dubey AA, Ravi K, Sekharan S, Kalita P. Energy-efficient biochar production for thermal backfill applications. Science of The Total Environment 2022;833:155253.
[212] Dresden L-MG. guarded hot plate apparatus lambda-Meter EP500e - Characteristics n.d.
[213] Kline SJ, McClintock FA. Analysis of experimental data. Experimental methods for engineers, Chapter 3, pages 45–56., 1953.
[214] MIIPAF. Decreto legislativo 29 aprile 2010, n.75 - riordino e revisione della disciplina in materia di fertilizzanti, a norma dell'articolo 13 della legge 7 luglio 2009, n. 88. Gazzetta Ufficiale della Repubblica Italiana, p. 126. 2010.
[215] Homepage - URBAS Energietechnik und Stahlbau n.d. https://www.urbas.at/en/ (accessed January 22, 2024).
[216] Lane KS, Washburn DE, Krynine DP. CAPILLARITY TESTS BY CAPILLARIMETER AND BY SOIL FILLED TUBES. Highway Research Board Proceedings 1947;26.
[217] Lu N, Likos WJ. Rate of Capillary Rise in Soil. Journal of Geotechnical and Geoenvironmental Engineering 2004;130:646–50. https://doi.org/10.1061/(ASCE)1090-0241(2004)130:6(646).
[218] Liu Q, Yasufuku N, Miao J, Ren J. An approach for quick estimation of maximum height of capillary rise. Soils and Foundations 2014;54:1241–5. https://doi.org/10.1016/j.sandf.2014.11.017.
[219] ECH2O EC-5 - Meter Group n.d. https://metergroup.com/products/ech20-ec-5-soil-moisture-sensor/ (accessed January 26, 2024).
[220] Abu-Hamdeh NH. Thermal Properties of Soils as affected by Density and Water Content. Biosyst Eng 2003;86:97–102.
[221] EU Carbon Permits - Price - Chart - Historical Data - News n.d. https://tradingeconomics.com/commodity/carbon (accessed January 26, 2024).
[222] Household energy consumption for space heating per m2 — European Environment Agency n.d. https://www.eea.europa.eu/data-and-maps/daviz/unit-consumption-of-space-heating#tab-chart_1 (accessed January 26, 2024).
[223] Musurmonov M. Experimental Analysis of Geothermal heat pump. 2021.
[224] Gervasio H, Dimova S. Environmental benchmarks for buildings. EFIResources: resource efficient construction towards sustainable design. LU: Publications Office; 2018.
[225] Ravenni G, Sárossy Z, Ahrenfeldt J, Henriksen UB. Activity of chars and activated carbons for removal and decomposition of tar model compounds – A review. Renewable and Sustainable Energy Reviews 2018;94:1044–56. https://doi.org/10.1016/j.rser.2018.07.001.

[226] Chen Y, Syed-Hassan SSA, Li Q, Deng Z, Hu X, Xu J, et al. Effects of temperature and aspect ratio on heterogeneity of the biochar from pyrolysis of biomass pellet. Fuel Processing Technology 2022;235:107366. https://doi.org/10.1016/j.fuproc.2022.107366.
[227] Karimi M, Aminzadehsarikhanbeglou E, Vaferi B. Robust intelligent topology for estimation of heat capacity of biochar pyrolysis residues. Measurement 2021;183:109857. https://doi.org/10.1016/j.measurement.2021.109857.
[228] Lehmann J, Joseph S. Biochar for environmental management: science, technology and implementation. Second edition. London ; New York: Routledge, Taylor & Francis Group; 2015.
[229] Shahbaz M, AlNouss A, Ghiat I, Mckay G, Mackey H, Elkhalifa S, et al. A comprehensive review of biomass based thermochemical conversion technologies integrated with CO2 capture and utilisation within BECCS networks. Resour Conserv Recycl 2021;173:105734. https://doi.org/10.1016/j.resconrec.2021.105734.
[230] Shen Y. Preparation of renewable porous carbons for CO2 capture – A review. Fuel Processing Technology 2022;236:107437. https://doi.org/10.1016/J.FUPROC.2022.107437.
[231] Zhao Y, Wang X, Yao G, Lin Z, Xu L, Jiang Y, et al. Advances in the Effects of Biochar on Microbial Ecological Function in Soil and Crop Quality. Sustainability 2022;14:10411. https://doi.org/10.3390/su141610411.
[232] Zhu X, Mao L, Chen B. Driving forces linking microbial community structure and functions to enhanced carbon stability in biochar-amended soil. Environ Int 2019;133:105211. https://doi.org/10.1016/J.ENVINT.2019.105211.
[233] Roden EE, Kappler A, Bauer I, Jiang J, Paul A, Stoesser R, et al. Extracellular electron transfer through microbial reduction of solid-phase humic substances. Nature Geoscience 2010 3:6 2010;3:417–21. https://doi.org/10.1038/ngeo870.
[234] Singh DK, Garg A. A review on hydrothermal pretreatment of sewage sludge: Energy recovery options and major challenges. Advanced Organic Waste Management: Sustainable Practices and Approaches 2022:297–314. https://doi.org/10.1016/B978-0-323-85792-5.00040-X.
[235] Light TS. CONDUCTIMETRY AND OSCILLOMETRY. Encyclopedia of Analytical Science, Elsevier; 2005, p. 217–26.
[236] Celzard A, Marêché JF, Payot F, Furdin G. Electrical conductivity of carbonaceous powders. Carbon N Y 2002;40:2801–15. https://doi.org/10.1016/S0008-6223(02)00196-3.
[237] Park W, Kim H, Park H, Choi S, Hong SJ, Bahk Y-M. Biochar as a low-cost, eco-friendly, and electrically conductive material for terahertz applications n.d.;11:18498. https://doi.org/10.1038/s41598-021-98009-5.
[238] Parfen'eva LS, Orlova TS, Kartenko NF, Smirnov BI, Smirnov IA, Misiorek H, et al. Structure, electrical resistivity, and thermal conductivity of beech wood biocarbon produced at carbonization temperatures below 1000°C n.d.;53:2398–407. https://doi.org/10.1134/S1063783411110230.
[239] Rhim Y-R, Zhang D, Fairbrother DH, Wepasnick KA, Livi KJ, Bodnar RJ, et al. Changes in electrical and microstructural properties of microcrystalline cellulose as function of carbonization temperature. Carbon N Y 2010;48:1012–24. https://doi.org/10.1016/j.carbon.2009.11.020.

[240] Liu S, Zhang Y, Tuo K, Wang L, Chen G. Structure, electrical conductivity, and dielectric properties of semi-coke derived from microwave-pyrolyzed low-rank coal. Fuel Processing Technology 2018;178:139–47. https://doi.org/10.1016/j.fuproc.2018.05.028.
[241] Enders A, Hanley K, Whitman T, Joseph S, Lehmann J. Characterization of biochars to evaluate recalcitrance and agronomic performance n.d.;114:644–53. https://doi.org/10.1016/j.biortech.2012.03.022.
[242] Rafiq MK, Bachmann RT, Rafiq MT, Shang Z, Joseph S, Long R. Influence of Pyrolysis Temperature on Physico-Chemical Properties of Corn Stover (Zea mays L.) Biochar and Feasibility for Carbon Capture and Energy Balance n.d.;11:e0156894. https://doi.org/10.1371/journal.pone.0156894.
[243] Berek AK, Hue N V. IMPROVING SOIL PRODUCTIVITY WITH BIOCHARS 2013.
[244] Raghavendra SC, Raibagkar RL, Kulkarni AB. Dielectric properties of fly ash. Bulletin of Materials Science 2002;25:37–9. https://doi.org/10.1007/BF02704592.
[245] Usevičiūtė L, Baltrėnaitė-Gedienė E. Dependence of pyrolysis temperature and lignocellulosic physical-chemical properties of biochar on its wettability. Biomass Convers Biorefin 2021;11:2775–93. https://doi.org/10.1007/s13399-020-00711-3.
[246] Canımkurbey B. Investigation dielectric and morphological properties of fly ash collected from thermal power plant. Asia-Pacific Journal of Chemical Engineering 2020;15. https://doi.org/10.1002/apj.2437.
[247] Hoffmann V, Rodriguez Correa C, Sautter D, Maringolo E, Kruse A. Study of the electrical conductivity of biobased carbonaceous powder materials under moderate pressure for the application as electrode materials in energy storage technologies. GCB Bioenergy 2019;11:230–48. https://doi.org/10.1111/gcbb.12545.
[248] Kane S, Ulrich R, Harrington A, Stadie NP, Ryan C. Physical and chemical mechanisms that influence the electrical conductivity of lignin-derived biochar. Carbon Trends 2021;5:100088. https://doi.org/10.1016/j.cartre.2021.100088.
[249] Gabhi RS, Kirk DW, Jia CQ. Preliminary investigation of electrical conductivity of monolithic biochar. Carbon N Y 2017;116:435–42. https://doi.org/10.1016/J.CARBON.2017.01.069.
[250] Kennedy LJ, Vijaya JJ, Sekaran G. Electrical conductivity study of porous carbon composite derived from rice husk. Mater Chem Phys 2005;91:471–6. https://doi.org/10.1016/j.matchemphys.2004.12.013.
[251] Quosai P, Anstey A, Mohanty AK, Misra M. Characterization of biocarbon generated by high- and low-temperature pyrolysis of soy hulls and coffee chaff: for polymer composite applications. R Soc Open Sci 2018;5. https://doi.org/10.1098/RSOS.171970.
[252] Duba A. Electrical conductivity of coal and coal char☆. Fuel 1977;56:441–3. https://doi.org/10.1016/0016-2361(77)90074-6.
[253] Nan N. Development of polyvinyl alcohol/wood-derived carbon thin films: Influence of processing parameters on mechanical, thermal, and electrical properties. Graduate Theses, Dissertations, and Problem Reports 2016. https://doi.org/https://doi.org/10.33915/etd.6289.

[254] Jiang J, Zhang L, Wang X, Holm N, Rajagopalan K, Chen F, et al. Highly ordered macroporous woody biochar with ultra-high carbon content as supercapacitor electrodes. Electrochim Acta 2013;113:481–9. https://doi.org/10.1016/j.electacta.2013.09.121.
[255] Debevc S, Weldekidan H, Snowdon MR, Vivekanandhan S, Wood DF, Misra M, et al. Valorization of almond shell biomass to biocarbon materials: Influence of pyrolysis temperature on their physicochemical properties and electrical conductivity. Carbon Trends 2022;9:100214. https://doi.org/10.1016/J.CARTRE.2022.100214.
[256] Kane S, Warnat S, Ryan C. Improvements in methods for measuring the volume conductivity of electrically conductive carbon powders. Advanced Powder Technology 2021;32:702–9. https://doi.org/10.1016/j.apt.2021.01.016.
[257] Rey-Raap N, Calvo EG, Bermúdez JM, Cameán I, García AB, Menéndez JA, et al. An electrical conductivity translator for carbons. Measurement 2014;56:215–8. https://doi.org/10.1016/j.measurement.2014.07.003.
[258] Allesina G, Pedrazzi S. Barriers to Success: A Technical Review on the Limits and Possible Future Roles of Small Scale Gasifiers. Energies (Basel) 2021;14:6711. https://doi.org/10.3390/en14206711.
[259] Binulal BR, Rajan A, Unnikrishnan M, Kochupillai J. Experimental determination of time lag due to phase shift on a flexible pipe conveying fluid. Measurement 2016;83:86–95. https://doi.org/10.1016/j.measurement.2016.01.037.
[260] Kalina M, Sovova S, Hajzler J, Kubikova L, Trudicova M, Smilek J, et al. Biochar Texture—A Parameter Influencing Physicochemical Properties, Morphology, and Agronomical Potential. Agronomy 2022;12:1768. https://doi.org/10.3390/agronomy12081768.
[261] Zhang Y, Ghaly A, Li B-X. Physical properties of rice residues as affected by variety and climatic and cultivation conditions in three continents. Am J Appl Sci 2012;9:1757–68. https://doi.org/10.3844/ajassp.2012.1757.1768.
[262] Sánchez-González J, MacÍas-García A, Alexandre-Franco MF, Gómez-Serrano V. Electrical conductivity of carbon blacks under compression. Carbon N Y 2005;43:741–7. https://doi.org/10.1016/J.CARBON.2004.10.045.
[263] Al-Wabel MI, Al-Omran A, El-Naggar AH, Nadeem M, Usman ARA. Pyrolysis temperature induced changes in characteristics and chemical composition of biochar produced from conocarpus wastes. Bioresour Technol 2013;131:374–9. https://doi.org/10.1016/j.biortech.2012.12.165.
[264] Rehrah D, Reddy MR, Novak JM, Bansode RR, Schimmel KA, Yu J, et al. Production and characterization of biochars from agricultural by-products for use in soil quality enhancement. J Anal Appl Pyrolysis 2014;108:301–9. https://doi.org/10.1016/j.jaap.2014.03.008.
[265] Barroso-Bogeat A, Alexandre-Franco M, Fernández-González C, Macías-García A, Gómez-Serrano V. Electrical conductivity of activated carbon–metal oxide nanocomposites under compression: a comparison study. Physical Chemistry Chemical Physics 2014;16:25161–75. https://doi.org/10.1039/C4CP03952A.
[266] Dixit A, Gupta S, Pang SD, Kua HW. Waste Valorisation using biochar for cement replacement and internal curing in ultra-high performance concrete. J Clean Prod 2019;238:117876. https://doi.org/10.1016/j.jclepro.2019.117876.

[267] Patwardhan SB, Pandit S, Kumar Gupta P, Kumar Jha N, Rawat J, Joshi HC, et al. Recent advances in the application of biochar in microbial electrochemical cells. Fuel 2022;311:122501. https://doi.org/10.1016/j.fuel.2021.122501.
[268] Saravanan A, Kumar PS. Biochar derived carbonaceous material for various environmental applications: Systematic review. Environ Res 2022;214:113857. https://doi.org/10.1016/J.ENVRES.2022.113857.
[269] Holm R. Elektrische Kontakte in Meßgeräten. teme 1950;168–179:233–40. https://doi.org/10.1524/teme.1950.168179.jg.233.
[270] Euler KJ. The conductivity of compressed powders. A review. J Power Sources 1978;3:117–36. https://doi.org/10.1016/0378-7753(78)80011-1.
[271] Pantea D, Darmstadt H, Kaliaguine S, Summchen L, Roy C. Electrical conductivity of thermal carbon blacks Influence of surface chemistry 2001.
[272] Janerka K, Jezierski J, Stawarz M, Szajnar J. Method for Resistivity Measurement of Grainy Carbon and Graphite Materials. Materials 2019;12:648. https://doi.org/10.3390/ma12040648.
[273] Yemata TA, Ye Q, Zhou H, Kyaw AKK, Chin WS, Xu J. Conducting polymer-based thermoelectric composites. Hybrid Polymer Composite Materials, Elsevier; 2017, p. 169–95.
[274] Lou XF, Nair J. The impact of landfilling and composting on greenhouse gas emissions – A review. Bioresour Technol 2009;100:3792–8. https://doi.org/10.1016/j.biortech.2008.12.006.
[275] Elango D, Thinakaran N, Panneerselvam P, Sivanesan S. Thermophilic composting of municipal solid waste. Appl Energy 2009;86:663–8. https://doi.org/10.1016/J.APENERGY.2008.06.009.
[276] Parliament EU. Directive (EU) 2018/844 of the European Parliament and of the Council of 30 May 2018 amending Directive 2010/31/EU on the energy performance of buildings and Directive 2012/27 - EU on energy efficiency (2018). EU Directive 2018.
[277] Stylianou E, Pateraki C, Ladakis D, Cruz-Fernández M, Latorre-Sánchez M, Coll C, et al. Evaluation of organic fractions of municipal solid waste as renewable feedstock for succinic acid production. Biotechnol Biofuels 2020;13:1–16. https://doi.org/10.1186/S13068-020-01708-W/FIGURES/9.
[278] Di Maria F, Sisani F, Contini S. Are EU waste-to-energy technologies effective for exploiting the energy in bio-waste? Appl Energy 2018;230:1557–72. https://doi.org/10.1016/J.APENERGY.2018.09.007.
[279] Casini D, Barsali T, Rizzo AM, Chiaramonti D. Production and characterization of co-composted biochar and digestate from biomass anaerobic digestion. Biomass Convers Biorefin 2021;11:2271–9. https://doi.org/10.1007/S13399-019-00482-6/TABLES/8.
[280] Kumar M, Dutta S, You S, Luo G, Zhang S, Show PL, et al. A critical review on biochar for enhancing biogas production from anaerobic digestion of food waste and sludge. J Clean Prod 2021;305:127143. https://doi.org/10.1016/J.JCLEPRO.2021.127143.
[281] Kumar M, Xiong X, Sun Y, Yu IKM, Tsang DCW, Hou D, et al. Critical Review on Biochar-Supported Catalysts for Pollutant Degradation and Sustainable Biorefinery. Adv Sustain Syst 2020;4:1900149. https://doi.org/10.1002/ADSU.201900149.

[282] Kumar M, Xiong X, Wan Z, Sun Y, Tsang DCW, Gupta J, et al. Ball milling as a mechanochemical technology for fabrication of novel biochar nanomaterials. Bioresour Technol 2020;312:123613. https://doi.org/10.1016/J.BIORTECH.2020.123613.
[283] Sanchez-Monedero MA, Cayuela ML, Roig A, Jindo K, Mondini C, Bolan N. Role of biochar as an additive in organic waste composting. Bioresour Technol 2018;247:1155–64. https://doi.org/10.1016/j.biortech.2017.09.193.
[284] Zhou S, Kong F, Lu L, Wang P, Jiang Z. Biochar — An effective additive for improving quality and reducing ecological risk of compost: A global meta-analysis. Science of The Total Environment 2022;806:151439. https://doi.org/10.1016/J.SCITOTENV.2021.151439.
[285] Wei L, Shutao W, Jin Z, Tong X. Biochar influences the microbial community structure during tomato stalk composting with chicken manure. Bioresour Technol 2014;154:148–54. https://doi.org/10.1016/J.BIORTECH.2013.12.022.
[286] Zhang Y, Sun Q, Jiang Z, Wang J, Cao B, Zhang S, et al. Evaluation of the effects of adding activated carbon at different stages of composting on metal speciation and bacterial community evolution. Science of The Total Environment 2022;806:151332. https://doi.org/10.1016/j.scitotenv.2021.151332.
[287] Li H, Zhang T, Tsang DCW, Li G. Effects of external additives: Biochar, bentonite, phosphate, on co-composting for swine manure and corn straw. Chemosphere 2020;248:125927. https://doi.org/10.1016/j.chemosphere.2020.125927.
[288] Khoshnevisan B, Duan N, Tsapekos P, Awasthi MK, Liu Z, Mohammadi A, et al. A critical review on livestock manure biorefinery technologies: Sustainability, challenges, and future perspectives. Renewable and Sustainable Energy Reviews 2021;135:110033. https://doi.org/10.1016/J.RSER.2020.110033.
[289] Zheng X, Xu W, Dong J, Yang T, Shangguan Z, Qu J, et al. The effects of biochar and its applications in the microbial remediation of contaminated soil: A review. J Hazard Mater 2022;438:129557. https://doi.org/10.1016/J.JHAZMAT.2022.129557.
[290] Awasthi SK, Kumar M, Sarsaiya S, Ahluwalia V, Chen H, Kaur G, et al. Multi-criteria research lines on livestock manure biorefinery development towards a circular economy: From the perspective of a life cycle assessment and business models strategies. J Clean Prod 2022;341:130862. https://doi.org/10.1016/J.JCLEPRO.2022.130862.
[291] Wang X, Zhao Y, Wang H, Zhao X, Cui H, Wei Z. Reducing nitrogen loss and phytotoxicity during beer vinasse composting with biochar addition. Waste Management 2017;61:150–6. https://doi.org/10.1016/J.WASMAN.2016.12.024.
[292] Pandit NR, Schmidt HP, Mulder J, Hale SE, Husson O, Cornelissen G. Nutrient effect of various composting methods with and without biochar on soil fertility and maize growth. Arch Agron Soil Sci 2020;66:250–65. https://doi.org/10.1080/03650340.2019.1610168.
[293] Teodoro M, Trakal L, Gallagher BN, Šimek P, Soudek P, Pohořelý M, et al. Application of co-composted biochar significantly improved plant-growth relevant physical/chemical properties of a metal contaminated soil. Chemosphere 2020;242:125255. https://doi.org/10.1016/J.CHEMOSPHERE.2019.125255.
[294] Ravindran B, Karmegam N, Awasthi MK, Chang SW, Selvi PK, Balachandar R, et al. Valorization of food waste and poultry manure through co-composting amending saw dust, biochar and mineral salts for value-added compost

production. Bioresour Technol 2022;346:126442. https://doi.org/10.1016/J.BIORTECH.2021.126442.
[295] Li L, Guo X, Zhao T, Li T. Green waste composting with bean dregs, tea residue, and biochar: Effects on organic matter degradation, humification and compost maturity. Environ Technol Innov 2021;24:101887. https://doi.org/10.1016/J.ETI.2021.101887.
[296] Haug RT. The Practical Handbook of Compost Engineering. 1st ed. Routledge; 2018.
[297] Arrigoni JP, Paladino G, Garibaldi LA, Laos F. Inside the small-scale composting of kitchen and garden wastes: Thermal performance and stratification effect in vertical compost bins. Waste Management 2018;76:284–93. https://doi.org/10.1016/J.WASMAN.2018.03.010.
[298] He X, Yin H, Han L, Cui R, Fang C, Huang G. Effects of biochar size and type on gaseous emissions during pig manure/wheat straw aerobic composting: Insights into multivariate-microscale characterization and microbial mechanism. Bioresour Technol 2019;271:375–82. https://doi.org/10.1016/j.biortech.2018.09.104.
[299] Malinowski M, Wolny-Koładka K, Vaverková MD. Effect of biochar addition on the OFMSW composting process under real conditions. Waste Management 2019;84:364–72. https://doi.org/10.1016/J.WASMAN.2018.12.011.
[300] Awasthi MK, Wang M, Chen H, Wang Q, Zhao J, Ren X, et al. Heterogeneity of biochar amendment to improve the carbon and nitrogen sequestration through reduce the greenhouse gases emissions during sewage sludge composting. Bioresour Technol 2017;224:428–38. https://doi.org/10.1016/j.biortech.2016.11.014.
[301] Wang Q, Awasthi MK, Ren X, Zhao J, Li R, Wang Z, et al. Combining biochar, zeolite and wood vinegar for composting of pig manure: The effect on greenhouse gas emission and nitrogen conservation. Waste Management 2018;74:221–30. https://doi.org/10.1016/J.WASMAN.2018.01.015.
[302] Czekała W, Malińska K, Cáceres R, Janczak D, Dach J, Lewicki A. Co-composting of poultry manure mixtures amended with biochar – The effect of biochar on temperature and C-CO2 emission. Bioresour Technol 2016;200:921–7. https://doi.org/10.1016/j.biortech.2015.11.019.
[303] Steiner C, Das KC, Melear N, Lakly D. Reducing Nitrogen Loss during Poultry Litter Composting Using Biochar. J Environ Qual 2010;39:1236–42. https://doi.org/10.2134/jeq2009.0337.
[304] Awasthi MK, Wang Q, Ren X, Zhao J, Huang H, Awasthi SK, et al. Role of biochar amendment in mitigation of nitrogen loss and greenhouse gas emission during sewage sludge composting. Bioresour Technol 2016;219:270–80. https://doi.org/10.1016/j.biortech.2016.07.128.
[305] Bolan N, Hoang SA, Beiyuan J, Gupta S, Hou D, Karakoti A, et al. Multifunctional applications of biochar beyond carbon storage. International Materials Reviews 2022;67:150–200. https://doi.org/10.1080/09506608.2021.1922047.
[306] Wu H, Lai C, Zeng G, Liang J, Chen J, Xu J, et al. The interactions of composting and biochar and their implications for soil amendment and pollution remediation: a review. Crit Rev Biotechnol 2017;37:754–64. https://doi.org/10.1080/07388551.2016.1232696.

[307] Smith MM, Aber JD. Energy recovery from commercial-scale composting as a novel waste management strategy. Appl Energy 2018;211:194–9. https://doi.org/10.1016/J.APENERGY.2017.11.006.
[308] Mason IG, Milke MW. Physical modelling of the composting environment: A review. Part 1: Reactor systems. Waste Management 2005;25:481–500. https://doi.org/10.1016/J.WASMAN.2005.01.015.
[309] Xi B-D, He X-S, Wei Z-M, Jiang Y-H, Li M-X, Li D, et al. Effect of inoculation methods on the composting efficiency of municipal solid wastes. Chemosphere 2012;88:744–50. https://doi.org/10.1016/j.chemosphere.2012.04.032.
[310] Bruni C, Akyol C, Cipolletta G, Eusebi AL, Caniani D, Masi S, et al. Decentralized Community Composting: Past, Present and Future Aspects of Italy. Sustainability 2020, Vol 12, Page 3319 2020;12:3319. https://doi.org/10.3390/SU12083319.
[311] ISPRA-CNR. Sludge analytical methods - Book N.64 1985.
[312] Environment Department Piedmont Region. Compost analytical methods 1998.
[313] American Public Health Association. Standard Methods for the Examination of Water and Wastewater 2005;21st Edition.
[314] MIIPAF. MIIPAF, 1991. Official Methods of Analysis of Fertilizers - Supplement N. 2. Official Gazette n, 29 of 04 February 1991. 1991.
[315] Rynk R. The Composting Handbook. A how-to and why manual for farm, municipal, institutional and commercial composters. vol. 1. Elsevier Inc.; 2022.
[316] Leton TG, Stentiford EI. Control of aeration in static pile composting. Waste Management & Research 1990;8:299–306. https://doi.org/10.1016/0734-242X(90)90005-8.
[317] Ghaly A, Snow F. Thermal balance of invessel composting of tomato plant residues 2006.
[318] Shaw CM, Stentiford EI. Heat Transfer in Composting Systems. The Science of Composting 1996:1331–4. https://doi.org/10.1007/978-94-009-1569-5_170.
[319] 1412i - LumaSense Technologies A/S n.d. https://innova.lumasenseinc.com/manuals/1412i/ (accessed January 22, 2024).
[320] Pedersen AR, Petersen SO, Schelde K. A comprehensive approach to soil-atmosphere trace-gas flux estimation with static chambers. Eur J Soil Sci 2010;61:888–902. https://doi.org/10.1111/j.1365-2389.2010.01291.x.
[321] Petersen SO, Hoffmann CC, Schäfer C-M, Blicher-Mathiesen G, Elsgaard L, Kristensen K, et al. Annual emissions of CH4 and N2O, and ecosystem respiration, from eight organic soils in Western Denmark managed by agriculture. Biogeosciences 2012;9:403–22. https://doi.org/10.5194/bg-9-403-2012.
[322] Brewer SK, Costello TA. In situ measurement of ammonia volatilization from broiler litter using an enclosed air chamber. Transactions of the ASAE 1999;42:1415–22. https://doi.org/10.13031/2013.13305.
[323] Denmead OT. Chamber Systems for Measuring Nitrous Oxide Emission from Soils in the Field. Soil Science Society of America Journal 1979;43:89–95. https://doi.org/10.2136/SSSAJ1979.03615995004300010016X.
[324] Bach PD, Nakasaki K, Shoda M, Kubota H. Thermal balance in composting operations. Journal of Fermentation Technology 1987;65:199–209. https://doi.org/10.1016/0385-6380(87)90165-8.
[325] Robinzon R, Kimmel E, Avnimelech Y. ENERGY AND MASS BALANCES OF WINDROW COMPOSTING SYSTEM. Transactions of the ASAE 2000;43:1253–9. https://doi.org/10.13031/2013.3019.

[326] Klejment E, Rosiński M. Testing of thermal properties of compost from municipal waste with a view to using it as a renewable, low temperature heat source. Bioresour Technol 2008;99:8850–5. https://doi.org/10.1016/J.BIORTECH.2008.04.053.
[327] Agyarko-Mintah E, Cowie A, Van Zwieten L, Singh BP, Smillie R, Harden S, et al. Biochar lowers ammonia emission and improves nitrogen retention in poultry litter composting. Waste Management 2017;61:129–37. https://doi.org/10.1016/j.wasman.2016.12.009.
[328] Liang Y, Leonard JJ, Feddes JJ, McGill WB. A SIMULATION MODEL OF AMMONIA VOLATILIZATION IN COMPOSTING. Transactions of the ASAE 2004;47:1667–80. https://doi.org/10.13031/2013.17609.
[329] Bagdonienė I, Bleizgys R. Ammonia emissions from dairy cattle manure under variable ventilation rates. Annals of Animal Science 2014;14:141–51. https://doi.org/10.2478/aoas-2013-0084.
[330] Awasthi MK, Duan Y, Awasthi SK, Liu T, Zhang Z. Effect of biochar and bacterial inoculum additions on cow dung composting. Bioresour Technol 2020;297:122407. https://doi.org/10.1016/j.biortech.2019.122407.
[331] Jiang T, Ma X, Tang Q, Yang J, Li G, Schuchardt F. Combined use of nitrification inhibitor and struvite crystallization to reduce the NH3 and N2O emissions during composting. Bioresour Technol 2016;217:210–8. https://doi.org/10.1016/j.biortech.2016.01.089.
[332] Liu N, Zhou J, Han L, Ma S, Sun X, Huang G. Role and multi-scale characterization of bamboo biochar during poultry manure aerobic composting. Bioresour Technol 2017;241:190–9. https://doi.org/10.1016/j.biortech.2017.03.144.
[333] Zhang P, Sun H, Ren C, Min L, Zhang H. Sorption mechanisms of neonicotinoids on biochars and the impact of deashing treatments on biochar structure and neonicotinoids sorption. Environmental Pollution 2018;234:812–20. https://doi.org/10.1016/j.envpol.2017.12.013.
[334] Sánchez-Monedero MA, Roig A, Paredes C, Bernal MP. Nitrogen transformation during organic waste composting by the Rutgers system and its effects on pH, EC and maturity of the composting mixtures. Bioresour Technol 2001;78:301–8. https://doi.org/10.1016/S0960-8524(01)00031-1.
[335] Zhang L, Sun X. Changes in physical, chemical, and microbiological properties during the two-stage co-composting of green waste with spent mushroom compost and biochar. Bioresour Technol 2014;171:274–84. https://doi.org/10.1016/j.biortech.2014.08.079.
[336] IPCC. Climate Change 2014 Part A: Global and Sectoral Aspects. 2014.
[337] Sayara T, Sánchez A. Gaseous Emissions from the Composting Process: Controlling Parameters and Strategies of Mitigation. Processes 2021;9:1844. https://doi.org/10.3390/pr9101844.
[338] Liu W, Huo R, Xu J, Liang S, Li J, Zhao T, et al. Effects of biochar on nitrogen transformation and heavy metals in sludge composting. Bioresour Technol 2017;235:43–9. https://doi.org/10.1016/j.biortech.2017.03.052.
[339] Malińska K, Zabochnicka-Świątek M, Dach J. Effects of biochar amendment on ammonia emission during composting of sewage sludge. Ecol Eng 2014;71:474–8. https://doi.org/10.1016/j.ecoleng.2014.07.012.
[340] REGULATION (EU) 2019/1009. Regulation EU "1009 of the European Parliament and of the Council of 5 June 2019 Laying down Rules on the Making Available on

the Market of EU Fertilising Products and Amending Regulations (EC) No 1069/2009 and (EC) No 1107/2009 and Repealing Regulation (EC) No 2003/2003. 2019." J Eur Union 170 (2019): 1-114 2019;2019:114.
[341] López-Cano I, Roig A, Cayuela ML, Alburquerque JA, Sánchez-Monedero MA. Biochar improves N cycling during composting of olive mill wastes and sheep manure. Waste Management 2016;49:553–9. https://doi.org/10.1016/j.wasman.2015.12.031.
[342] Prost K, Borchard N, Siemens J, Kautz T, Séquaris J-M, Möller A, et al. Biochar Affected by Composting with Farmyard Manure. J Environ Qual 2013;42:164–72. https://doi.org/10.2134/jeq2012.0064.
[343] Hua L, Chen Y, Wu W, Ma H. Microorganism communities and chemical characteristics in sludge-bamboo charcoal composting system. Environ Technol 2011;32:663–72. https://doi.org/10.1080/09593330.2010.510534.
[344] Steiner C, Melear N, Harris K, Das K. Biochar as bulking agent for poultry litter composting. Carbon Manag 2011;2:227–30. https://doi.org/10.4155/cmt.11.15.
[345] Yoshizawa S, Tanaka S, Ohata M, Mineki S, Goto S, Fujioka K, et al. Promotion effect of various charcoals on the proliferation of composting microorganisms. 2006;224:261–5. https://doi.org/10.7209/tanso.2006.261.
[346] Hagemann N, Joseph S, Schmidt H-P, Kammann CI, Harter J, Borch T, et al. Organic coating on biochar explains its nutrient retention and stimulation of soil fertility. Nat Commun 2017;8:1089. https://doi.org/10.1038/s41467-017-01123-0.
[347] Liu H, Wang L, Lei M. Positive impact of biochar amendment on thermal balance during swine manure composting at relatively low ambient temperature. Bioresour Technol 2019;273:25–33. https://doi.org/10.1016/J.BIORTECH.2018.10.033.
[348] ISRPA. Rapporto rifiuti urbani - Ed 2021. 2021.
[349] Cao X, Williams PN, Zhan Y, Coughlin SA, McGrath JW, Chin JP, et al. Municipal solid waste compost: Global trends and biogeochemical cycling. Soil & Environmental Health 2023;1:100038. https://doi.org/10.1016/j.seh.2023.100038.
[350] Agenzia Nazionale per la Protezione dell'Ambiente (ANPA). Il recupero di sostanza organica dai rifiuti per la produzione di ammendanti di qualità. 2002.
[351] Visconti D, Ventorino V, Fagnano M, Woo SL, Pepe O, Adamo P, et al. Compost and microbial biostimulant applications improve plant growth and soil biological fertility of a grass-based phytostabilization system. Environ Geochem Health 2023;45:787–807. https://doi.org/10.1007/s10653-022-01235-7.
[352] Bhattarai R, Kalita PK, Yatsu S, Howard HR, Svendsen NG. Evaluation of compost blankets for erosion control from disturbed lands. J Environ Manage 2011;92:803–12. https://doi.org/10.1016/j.jenvman.2010.10.028.
[353] Isaka T, Clark S, Meyer J. Compost Functions as Effective Replacement for Peat-Based Potting Media in Organic Greenhouse Transplant Production. J (Basel) 2021;4:394–403. https://doi.org/10.3390/j4030030.
[354] Ren X, Zeng G, Tang L, Wang J, Wan J, Wang J, et al. The potential impact on the biodegradation of organic pollutants from composting technology for soil remediation. Waste Management 2018;72:138–49. https://doi.org/10.1016/j.wasman.2017.11.032.

[355] Xia Guo X, Tao Liu H, Zhang J. The role of biochar in organic waste composting and soil improvement: A review. Waste Management 2020;102:884–99. https://doi.org/10.1016/j.wasman.2019.12.003.
[356] Das SK, Ghosh GK, Avasthe R, Kundu MC, Choudhury BU, Baruah K, et al. Innovative biochar and organic manure co-composting technology for yield maximization in maize-black gram cropping system. Biomass Convers Biorefin 2023;13:7797–809. https://doi.org/10.1007/s13399-021-01519-5.
[357] Li Y, Kumar Awasthi M, Sindhu R, Binod P, Zhang Z, Taherzadeh MJ. Biochar preparation and evaluation of its effect in composting mechanism: A review. Bioresour Technol 2023;384:129329. https://doi.org/10.1016/J.BIORTECH.2023.129329.
[358] Nguyen MK, Lin C, Hoang HG, Sanderson P, Dang BT, Bui XT, et al. Evaluate the role of biochar during the organic waste composting process: A critical review. Chemosphere 2022;299:134488. https://doi.org/10.1016/J.CHEMOSPHERE.2022.134488.
[359] European Biochar Foundation (EBC). European Biochar Certificate - Guidelines for a Sustainable Production of Biochar, Version 10.1 n.d.
[360] Hai T, Dhahad HA, Zhou J, Attia EA, Kh TI, Shamseldin MA, et al. The novel integration of biomass gasification plant to generate efficient power, and the waste recovery to generate cooling and freshwater: A demonstration of 4E analysis and multi-criteria optimization. Sustainable Energy Technologies and Assessments 2022;53:102588. https://doi.org/10.1016/J.SETA.2022.102588.
[361] Montiel-Bohórquez ND, Pérez JF. Energy valorization strategies of fallen leaves and woody biomass in a based downdraft gasification-engine power plant. Sustainable Energy Technologies and Assessments 2022;49:101749. https://doi.org/10.1016/j.seta.2021.101749.
[362] George OS, Dennison MS, Yusuf AA. Characterization and energy recovery from biomass wastes. Sustainable Energy Technologies and Assessments 2023;58:103346. https://doi.org/10.1016/j.seta.2023.103346.
[363] Yadav K, Jagadevan S, Yadav K, Jagadevan S. Influence of Process Parameters on Synthesis of Biochar by Pyrolysis of Biomass: An Alternative Source of Energy. Recent Advances in Pyrolysis 2019. https://doi.org/10.5772/INTECHOPEN.88204.
[364] Garcia B, Alves O, Rijo B, Lourinho G, Nobre C. Biochar: Production, Applications, and Market Prospects in Portugal. Environments 2022, Vol 9, Page 95 2022;9:95. https://doi.org/10.3390/ENVIRONMENTS9080095.
[365] Sistek M. Life Cycle Assessment of biochar, electricity, and heat from a wood gasification plant. University of Applied Sciences Vorarlberg, 2021.
[366] Wei L, Pordesimo LO, To SDF, Herndon CW, Batchelor WD. Evaluation of Micro-Scale Syngas Production Costs through Modeling. Trans ASABE 2009;52:1649–59. https://doi.org/10.13031/2013.29116.
[367] Spinelli R, Magagnotti N. Determining long-term chipper usage, productivity and fuel consumption. Biomass Bioenergy 2014;66:442–9. https://doi.org/10.1016/j.biombioe.2014.04.016.
[368] Kowaluk G, Szymanowski K, Kozlowski P, Kukula W, Sala C, Robles E, et al. Functional Assessment of Particleboards Made of Apple and Plum Orchard Pruning. Waste Biomass Valorization 2020;11:2877–86. https://doi.org/10.1007/s12649-018-00568-8.

[369] Statistiche energetiche e minerarie - Ministero dell'ambiente e della sicurezza energetica n.d. https://dgsaie.mise.gov.it/ (accessed January 29, 2024).
[370] GSE n.d. https://www.gse.it/ (accessed January 29, 2024).
[371] Teleriscaldamento - Gruppo Hera n.d. https://www.gruppohera.it/gruppo/attivita/energia/teleriscaldamento (accessed January 29, 2024).
[372] Duc Bui V, Phuong Vu H, Phuong Nguyen H, Quang Duong X, Tuyen Nguyen D, Tuan Pham M, et al. Techno-economic assessment and logistics management of biomass in the conversion progress to bioenergy. Sustainable Energy Technologies and Assessments 2023;55:102991. https://doi.org/10.1016/j.seta.2022.102991.
[373] Zheng Y, Jenkins BM, Kornbluth K, Kendall A, Træholt C. Optimal design and operating strategies for a biomass-fueled combined heat and power system with energy storage. Energy 2018;155:620–9. https://doi.org/10.1016/j.energy.2018.05.036.
[374] EU Commission. COMMUNICATION FROM THE COMMISSION TO THE EUROPEAN PARLIAMENT, THE COUNCIL, THE EUROPEAN ECONOMIC AND SOCIAL COMMITTEE AND THE COMMITTEE OF THE REGIONS A new Circular Economy Action Plan For a cleaner and more competitive Europe. 2020.
[375] EU PARLIAMENT. DECISIONS DECISION (EU) 2022/591 OF THE EUROPEAN PARLIAMENT AND OF THE COUNCIL of 6 April 2022 on a General Union Environment Action Programme to 2030. 2022.
[376] EUROPEAN PARLIAMENT AND COUNCIL. REGULATION EU 2023/857 - Amending Regulation (EU) 2018/842 on binding annual greenhouse gas emission reductions by Member States from 2021 to 2030 contributing to climate action to meet commitments under the Paris Agreement, and Regulation (EU) 2018/1999 2023.
[377] ISPRA-Istituto Superiore per la Protezione e la Ricerca Ambientale. n.d.
[378] EUROPEAN PARLIAMENT AND COUNCIL. DIRECTIVE (EU) 2016/ 2284 on the reduction of national emissions of c ertain atmospheric pollutants, amending. Directive 2003/ 35/ EC and rep ealing Directive 2001/ 81/ EC. 2016.
[379] Agegnehu G, Bass AM, Nelson PN, Bird MI. Benefits of biochar, compost and biochar–compost for soil quality, maize yield and greenhouse gas emissions in a tropical agricultural soil. Science of The Total Environment 2016;543:295–306. https://doi.org/10.1016/j.scitotenv.2015.11.054.
[380] Portejoie S, Martinez J, Guiziou F, Coste CM. Effect of covering pig slurry stores on the ammonia emission processes. Bioresour Technol 2003;87:199–207. https://doi.org/10.1016/S0960-8524(02)00260-2.
[381] Fdez-Sanromán A, Pazos M, Rosales E, Sanromán MA. Unravelling the Environmental Application of Biochar as Low-Cost Biosorbent: A Review. Applied Sciences 2020, Vol 10, Page 7810 2020;10:7810. https://doi.org/10.3390/APP10217810.
[382] Quispe JIB, Campos LC, Mašek O, Bogush A. Use of biochar-based column filtration systems for greywater treatment: A systematic literature review. Journal of Water Process Engineering 2022;48:102908. https://doi.org/10.1016/J.JWPE.2022.102908.

[383] Zhang Y, Wang J, Feng Y. The effects of biochar addition on soil physicochemical properties: A review. Catena (Amst) 2021;202:105284. https://doi.org/10.1016/J.CATENA.2021.105284.
[384] Paul D, Hall SG. Biochar and zeolite as alternative biofilter media for denitrification of aquaculture effluents. Water (Switzerland) 2021;13:2703. https://doi.org/10.3390/W13192703/S1.
[385] Deng S, Chen J, Chang J. Application of biochar as an innovative substrate in constructed wetlands/biofilters for wastewater treatment: Performance and ecological benefits. J Clean Prod 2021;293:126156. https://doi.org/10.1016/J.JCLEPRO.2021.126156.
[386] EN 13725:2022. Stationary source emissions - Determination of odour concentration by dynamic olfactometry and odour emission rate 2022.
[387] GAZZETTA UFFICIALE DELLA REPUBBLICA ITALIANA. Ordinary supplement n. 90 to the GAZZETTA UFFICIALE of 18-04-2016 - Attachment X. vol. 18. 2016.
[388] GAZZETTA UFFICIALE DELLA REPUBBLICA ITALIANA. Ordinary supplement n. 90 to the GAZZETTA UFFICIALE of 18-04-2016 - Attachment I / Part A.. 2016.
[389] Turin Chamber of Commerce Industry Crafts and Agriculture. Assets price list - 16/03/2023. 2023.
[390] Schans DA van der, Bleeker PO, Molendijk LPG, Plentinger MC, Weide RY van der, Lotz LAP, et al. Practical weed control in arable farming and outdoor vegetable cultivation without chemicals. Lelystad: Applied Plant Research; 2006.
[391] Bauer M V., Marx C, Bauer F V., Flury DM, Ripken T, Streit B. Thermal weed control technologies for conservation agriculture—a review. Weed Res 2020;60:241–50. https://doi.org/10.1111/WRE.12418.
[392] Martelloni L, Frasconi C, Sportelli M, Fontanelli M, Raffaelli M, Peruzzi A. The Use of Different Hot Foam Doses for Weed Control. Agronomy 2019, Vol 9, Page 490 2019;9:490. https://doi.org/10.3390/AGRONOMY9090490.
[393] Andersen J. Experimental Trials and Modelling of Hydrogen and Propane Burners for Use in Selective Flaming. Biological Agriculture & Horticulture 1997;14:207–19. https://doi.org/10.1080/01448765.1997.9754811.
[394] Panwar NL, Rathore NS, Kurchania AK. Experimental investigation of open core downdraft biomass gasifier for food processing industry. Mitig Adapt Strateg Glob Chang 2009;14:547–56. https://doi.org/10.1007/S11027-009-9173-X/TABLES/6.
[395] Gunarathne DS, Mellin P, Yang W, Pettersson M, Ljunggren R. Performance of an effectively integrated biomass multi-stage gasification system and a steel industry heat treatment furnace. Appl Energy 2016;170:353–61. https://doi.org/10.1016/J.APENERGY.2016.03.003.
[396] Milne TA, Evans RJ, Abatzaglou N. Biomass Gasifier "'Tars'": Their Nature, Formation, and Conversion. Constraints 1998:v. https://doi.org/10.2172/3726.
[397] Wernet G, Bauer C, Steubing B, Reinhard J, Moreno-Ruiz E, Weidema B. The ecoinvent database version 3 (part I): overview and methodology. International Journal of Life Cycle Assessment 2016;21:1218–30. https://doi.org/10.1007/S11367-016-1087-8/FIGURES/7.
[398] Morselli N, Boccaletti S, Meglioraldi S, Puglia M, Pedrazzi S, Allesina G. Biomass-powered thermal weeding in wine farms: An environmental and economic assessment. J Clean Prod 2023;385:135684. https://doi.org/10.1016/J.JCLEPRO.2022.135684.

[399] Miller FC, Finstein MS. Materials balance in the composting of wastewater sludge as affected by process control strategy. Journal of Water Pollution Control Federation 1985.
[400] Cengel Y. Introduction To Thermodynamics and Heat Transfer : Yunus Cengel : 9780071287739 2010:670–2.
[401] Ahn HK, Sauer TJ, Richard TL, Glanville TD. Determination of thermal properties of composting bulking materials. Bioresour Technol 2009;100:3974–81. https://doi.org/10.1016/J.BIORTECH.2008.11.056.
[402] EU Emissions Trading System (EU ETS) - European Commission n.d. https://climate.ec.europa.eu/eu-action/eu-emissions-trading-system-eu-ets_en (accessed January 29, 2024).
[403] Radiative Forcing | MIT Climate Portal n.d. https://climate.mit.edu/explainers/radiative-forcing (accessed November 30, 2023).